TRINITY COLLEGE DUBLIN

The Effects of Low-Dose Methotrexate on Metabolism in Primary Human PBMCs.

Laura O'Farrell

A dissertation submitted to the University of Dublin in candidature

for the degree of Doctor of Philosophy

July 2017

Supervisor:

Prof. Gavin Davey

Declaration

I declare that this thesis has not been submitted as an exercise for a degree at this or any other university and it is entirely my own work.

I agree to deposit this thesis in the University's open access institutional repository or allow the library to do so on my behalf, subject to Irish Copyright Legislation and Trinity College Library conditions of use and acknowledgement.

_____

Laura O'Farrell

2017

Summary

Low-dose Methotrexate (MTX) is a powerful anti-arthritic drug used in the treatment of a variety of inflammatory diseases. It is an economical drug and is easily administered, but incomplete knowledge into its mechanism of action limits its therapeutic capability. As an anti-folate drug, MTX has been shown to have a variety of effects including effects on the one-carbon metabolism pathway, including purine and thymidine nucleotide synthesis. MTX has also been shown to reverse the aberrant glycosylation patterns in Rheumatoid arthritis (RA) patients. It is not known exactly which effect of MTX has therapeutic potential nor is it known which aspect of this anti-folate is responsible. Elucidating new effects of MTX and whether purine and thymidine inhibition is the mechanism by which these effects occur, would provide new insight into the workings of this drug and expand its therapeutic potential. Using a model of activated T cells, the effects of MTX on a variety of biochemical processes were investigated and compared to unactivated PBMCs to see if MTX could preferentially affect activated PBMCs, such as the over-active T cells in RA.

Flow cytometric analysis revealed that MTX displayed activation-dependent effects on cell viability, proliferation, transferrin receptor expression and blastogenesis, but dissipated the mitochondrial inner-membrane potential ($\Delta\Psi_m$) in both activated and unactivated PBMCs. The MTX-mediated effects were either partially or completely reversed upon purine and thymidine rescue, which indicated that insults to this biosynthesis pathway were the mechanism in which these effects occurred.

No direct effect of low-dose MTX on cellular glycosylation has ever been shown. In this study, flow cytometry was also employed to quantify ManNAz incorporation on the-cell-surface, using click chemistry and was used to show how changes to surface sialylation can occur during activation which can thus be used to evaluate the effects of drug treatment that limit cellular activation. MTX was found to significantly affect cell-surface sialylation, which was reversed by purine and thymidine rescue.

In the absence of extensive metabolic profiling upon low-dose MTX treatment, HPLC was used to quantify any changes to intracellular nucleotides and sugar-nucleotides in both unactivated and anti-CD3-activated PBMCs. MTX inhibited CDP and NAD/NADH

nucleotides in activated PBMCs but no changes were found in the sugar-nucleotides detected. NAD/NADH did not increase during activation, which suggested that MTX could exert effects which were activation-independent. Purine and thymidine inhibition was also shown to be the mechanism in which MTX reduced the levels of NAD/NADH nucleotides.

Combined, the findings shown here suggest that the MTX-mediated inhibition of purine and thymidine synthesis has far-reaching consequences, encompassing effects on cellular activation and on cell-surface sialylation. A state of folate-deficiency was found under these MTX-treated conditions, illustrating the powerful effect of this anti-folate, even at low-doses. This finding has implications for any future effects shown by MTX whereby a consequence of folate-deficiency would have to be disproven.

Therapeutically, these results highlight a new link between the anti-proliferative effect of MTX and the altered glycosylation patterns found in RA patients treated with MTX. Although the therapeutic value of these insults by MTX was not measured, the global effects of purine and thymidine inhibition strengthen the anti-proliferative effect as a potent mechanism of action.

For Andy

Acknowledgements

First and foremost, I would like to thank Dr. Anne Molloy for her encouragement, support and guidance over the last two years, without which this thesis would never have been possible. It is impossible to put into words how much I learned, but I can say that I was blessed to have you as a mentor. I only hope this thesis does all your help justice, Anne.

The second person who deserves a mention is Dr. Jerrard Hayes for the 4 years of work you put in helping me with this project (the last year doesn't count). Your unpolished advice and expertise saw me through the first three years. I hope you realise what your help meant, because I will never forget.

Thanks to Dr. Olga Abramczyk, whose technical expertise got me my final results chapter and made me eligible for this doctoral degree.

A special thanks goes to Barry Moran, the flow cytometry expert, whose help was gladly given for the entirety of this project and who has taught me everything I know about flow cytometry. I hope I can return the favour in the future.

To Dr. Cliona O'Farrelly, Dr. Amir Khan and Dr. Jean Fletcher. I want to thank each and every one of you for the help and advice you gave at a time when I really needed it.

To all the PhD students in the fifth-floor reading room,; thank you for always being there, for the amazing science conversations at lunch, for the great laughs we had, for being the astounding people I have gotten to know and for hopefully being some of my future life-long friends (if you'll have me). In particular, to Darren, Aisling, Natalie, Niki, Ryan and Andy, it's been an absolute blast! A second (I may regret this later), thanks to Jer for all our arguments over a pint!! I wouldn't trade them for anything.

To my parents Jacinta and Martin, who have put up with me and more importantly, have given me the strength and support I needed to continue over the past five years. I hope you enjoy reading this thesis; you've most certainly earned it.

A special thank you to my supervisor, Prof. Gavin Davey for funding this project for the past 5 years and taking a chance on me as a PhD student, for which I am very grateful.

Contents

Abbreviations

5-FU	5-flurouracil
7-OH-MTX	7-hydroxymethotrexate
DAPA	Diamino-2, 4-N-10-methylpteroic acid
ACN	Acetonitrile
ACPA	Anti-citrullinated protein antibody
ADA	Adenosine deaminase
ADP	Adenosine diphosphate
AICD	Activation induced cell death
AICAR	Amino-imidazolecarboxamide ribosyl-5-phosphate
AICARFT	AICAR formyltransferase
AMP	Adenosine monophosphate
AO	Aldehyde oxidase
APRT	Adenine phosphoribosyltransferase
APS	Ammonium persulfate
ATP	Adenosine triphosphate
BER	Base-excision repair
BSA	Bovine serum albumin
CA	*Candida albicans*
CAD	Caspase-activated deoxyribonuclease
CFSE	Carboxyfluorescein succinimidyl ester
CHO	Chinese hamster ovary
CIA	Collagen induced arthritis
CMP NeuAc	Cytidine monophosphate neuraminic acid
CNT	Concentrative nucleoside transporters
cSHMT	Cytoplasmic serine hydroxymethyltransferase
CTP	Cytidine triphosphate
DAMPA	Diamino-2, 4-N-10-methylpteroic acid
DC	Dendritic cell
DHF	Dihydrofolate
DHFR	Dihydrofolate reductase
DMG	Dimethylglycine
DMSO	Dimethyl sulfoxide
DNA	Deoxyribonucleic acid
dTMP	Deoxythymidine monophosphate (thymidylate)
dTTP	Deoxythymidine triphosphate
dUMP	Deoxyuridine monophosphate
dUTPase	Deoxyuridine triphosphate nucleotidohydrolase
ENT	Equilibrative nucleoside transporters
ETC	Electron transport chain
FA	Folic acid
FACS	Fluorescence activated cell sorting
Fab	Fragment antigen binding
FBS	Foetal calf serum
Fc	Fragment crystallisable region

FCCP	Carbonyl cyanide 4-(trifluoromethoxy)phenylhydrazone
FCS	Foetal bovine serum
FDH	10-formyl THF dehydrogenase
FITC	Fluorescein isothiocyanate
FPGS	Folylpolyglutamate synthase
FR	Folate receptor
FSC	Forward scatter
FTHFS	10-formyl THF synthase
GalNAc	N-acetylgalactosamine
GAR	Glycinamide ribonucleotide
GARFT	GAR formyltransferase
GCS	Glycine cleavage system
GDP fucose	Guanosine diphosphofucose
GDP mannose	Guanosine diphosphomannose
GGH	γ-glutamyl hydrolase
GlcNAc	N-acetylglucosamine
GTP	Guanosine triphosphate
Hcy	Homocysteine
Hep-2	Human laryngeal squamous carcinoma cells
HGPRT	Hypoxanthine-guanine phosphoribosyltransferase
HLA	Human leukocyte antigen
HPLC	High-performance liquid chromatography
HRP	Horse radish peroxidase
Hx	Hypoxanthine
iBMDM	Immortalised bone marrow derived macrophages
ICAM-1	Intercellular adhesion molecule 1
ICMT	Isoprenylcysteine carboxymethyltransferase
Ig	Immunoglobulin
IMP	Inosine monophosphate
JC-1	5,5'6,6'-tetrachloro-1,1'3,3'-tetraethylbenzimidazolylcarbocyanine iodide
LPS	Lipopolysaccharide
ManNAc	*N*-acetylmannosamine
MAPK	Mitogen-activated protein kinase
MAT	Methionine adenosyltransferase
MEFs	Mouse embryonic fibroblasts
MFT	Mitochondrial folate transporter
MHC	Major-histocompatibility complex
MMR	Mismatch repair
MS	Methionine synthase
mSHMT	Mitochondrial serine hydroxymethyltransferase
MTHFC	Methenyl THF cyclohydrolase
MTHFD	MethenylTHF dehydrogenase
MTHFR	5, 10-methylenetetrahydrofolate reductase
mTOR	Mammalian target of rapamycin
MTX	Methotrexate

MTXPG	Methotrexate polyglutamate
NAC	N-acetyl-L-cysteine
NADH	Nicotinamide adenine dinucleotide
NADPH	Nicotinamide adenine dinucleotide phosphate
NeuAc	Neuraminic acid
NF-kB	Nuclear factor-kappa B
NK	Natural Killer cell
NTDs	Neural tube defects
NS	Non-significant
OCM	One carbon metabolism
ODC	Ornithine decarboxylase
PBL	Peripheral blood lymphocytes
PBMC	Peripheral blood mononuclear cell
PBS	Phosphate buffered saline
PCFT	Proton-coupled folate transporter
PFA	Paraformaldehyde
PHA	Phytohaemagglutinin
PI	Propidium iodide
PKC	Protein kinase C
PMA	phorbyl myristate acetate
PRPP	phosphoribosyl pyrophosphate
PS	Phosphatidyl serine
RA	Rheumatoid arthritis
RBC	Red blood cell
RFC	Reduced folate carrier
ROS	Reactive oxygen species
RPMI	Roswell Park Memoria Institute 1640 medium
RNA	Ribonucleic acid
SAH	S-adenosyl homocysteine
SAM	S-adenosyl methionine
SF	Synovial fluid
SHMT	Serine hydroxymethyltransferase
Siglecs	Sialic acid immunoglobulin-type lectins
SSC	Side scatter
SLC	Solute carrier
TCR	T cell receptor
TT	Tetanus toxoid
Th	Helper T-lymphocyte
THF	Tetrahydrofolate
Thy	Thymidine
TLD	Thymineless death
TLR	Toll-like receptor
TNF	Tumour necrosis factor
Treg	Regulatory-T-lymphocyte
TS	Thymidylate synthase
UDP	Uridine diphosphate

UDP-Gal   Uridine diphosphate galactose
UDP-GalNAc   Uridine diphosphate N-acetylgalactosamine
UDP-Glc   Uridine diphosphate glucose
UDP GlcNAc   Uridine diphosphate N-acetylglucosamine

Chapter 1:

General Introduction

1.1 Rheumatoid Arthritis

Rheumatoid Arthritis (RA) is a chronic inflammatory disease characterised by inflammation of the joints and overlying synovium (Rossi et al., 2015). RA affects approximately 1% of the population, particularly the elderly, however early onset can occur with some patients presenting symptoms in their mid-twenties (McInnes and Schett, 2007). Left untreated, the inflammation can destroy the cartilage and underlining bone, causing suffering to the individual.

The aggravated synovial joint is infiltrated by a complex network of mononuclear cells, cytokines and chemokines, which exert both localised and systemic effects (Shinde et al., 2014). The RA joint contains plasma cells, mast cells, activated macrophages, as well as B and T cells (Brennan and McInnes, 2008). Autoantibodies including rheumatoid factor and anti-citrullinated protein antibody (ACPA), are present in 60% of cases (Bax et al., 2014). Citrullination is a post-translational modification of proteins occurring under a variety of conditions, including inflammation (Makrygiannakis et al., 2006). In autoimmune conditions, immune responses are mounted to these modified proteins, called ACPA's. The acute inflammation perpetuates the generation of these auto-reactive antibodies by causing tissue and bone destruction thereby exposing self-particulates not usually exposed to the immune system. These neo-antigens, can be degraded further into multiple neo-antigens, with each capable of activating an inflammatory response.

The cause of RA is still unknown. Individuals that contain a common amino acid motif (QKRAA) in the human leukocyte antigen (HLA)-DRB1 locus, encoding the major histocompatibility complex (MHC) proteins which present antigen to the T cell at the onset of an immune response, are susceptible to the disease. The role of T cells in the perpetuation of RA is also well established. Autoreactive T cells against citrullinated self-proteins have been identified (McInnes and Schett, 2011). Alterations in T cell subsets, which include the $CD4^+$ T helper cells and the $CD8^+$ cytotoxic T cells have been found alongside differences in the synovial fluid compared to peripheral blood from patients with RA (Duke et al., 1983). The frequency of naïve $CD4^+$ T cells were shown to be reduced in early RA due to the commitent differentiation into other T cell subsets, following exposure to the inflammatory milieu (Ponchel et al., 2014). A subset of $CD8^+$ T cells containing a Natural Killer (NK) cell-surface marker, Leu7 was increased in the

synovial fluid mononuclear cells (Burns et al., 1992). Another CD8^{+} T cell subset, containing a naïve surface maker, CD45RA, was shown to be decreased in both the synovial fluid and peripheral blood of RA patients (Kremer et al., 2016). The frequency of naturally occurring regulatory T cells was also reduced in early RA (Ponchel et al., 2014). Certain T cell subsets have a direct involvement in RA pathogenesis. Correlations have recently been shown between disease activity and CD4^{+}CD29^{+} memory T cells (Kremer et al., 2016). A particular type of T helper cell, Th17 was shown to instigate much of the inflammation through the secreted cytokine IL-17 (McInnes and Schett, 2011).

1.2. Low-dose Methotrexate

Methotrexate (MTX) is often used as a chemotherapeutic drug. High doses of MTX exert anti-cancer effects by perturbing purine and thymidine incorporation into DNA, killing highly active cancerous cells (Wessels et al., 2008). Low-dose MTX is now the frontline treatment in RA and psoriatic arthritis. However, disparities exist as to what constitutes low-dose MTX. The concentration of MTX considered to be low-dose was originally based on the final serum concentration of MTX in patients. Variation in the methods used to accurately detect and measure MTX in serum samples, as well as inter-patient variability in renal clearance of the drug, led to discrepancies in the literature as to what was considered low-dose therapy. In addition, the wide range of treatment (5 mg-25 mg per week) considered low-dose MTX, potentiated this variability (Cronstein, 2005). The reported low-dose concentration in serum was also dependent on the time samples were taken after administration of MTX. Ingestion of a 20 mg MTX tablet was shown to lead to plasma concentrations of ~0.5 µM after 1 h and ~0.1 µM after 10 h (Spurlock et al., 2011). At 52 h, serum concentrations were found to be less than one hundredth the original value measured 5 h after ingestion (0.58 µM to 0.005 µM) (Kremer et al., 1986). Leeb et al,1989, the most widely cited study in this regard, found that serum concentrations ranged from 0.1 nM- 1 µM (Paillot et al., 1998, Annussek et al., 2014). Other reports found that the lowest serum concentrations were found to be 1.3 nM (Seideman et al., 1993).

However, intracellular red blood cell (RBC) [MTX] was found to be more indicative of therapeutic efficacy as they reflected cellular retention of the drug and thus the final

working concentration. These concentrations ranged from 50 nM-340 nM over the course of 9 days, an average of 180 nM (Kremer et al., 1986).

The current consensus is that low-dose treatment is considered to be ~1 μM for at least 24 h (Cohen and Wolff, 2013). However, much research has been conducted using 1 mg/ml of MTX, which corresponds to 2.2 μM thought to be considered low-dose treatment at the time of study. Although this is now considered high-dose treatment, these studies highlight possible mechanisms of action of MTX, in which parallels can be drawn with low-dose treatment. Indeed, it was acknowledged that there may be overlapping mechanisms of action of high-dose MTX used in chemotherapy and low-dose used in RA (Blits et al., 2013). For this reason, the effects of MTX in this region have been included in this study. Furthermore, it was suggested that the duration of treatment was a more important measurement of efficacy than concentration as severe toxicity was found during high-dose MTX treatment, when 8 g MTX was given for 48 h but not when 20 g MTX was given over the course of 24 h (Cohen and Wolff, 2013). This finding potentiates the need to include these higher-than-low-dose-concentrations of MTX, which are still far from the high-doses used in chemotherapy (1-5 g/week) (Cronstein, 2006).

1.2.1 Cellular uptake of MTX

In serum, MTX is metabolised to 7-hydroxy-MTX (7-OH-MTX) and diamino-2, 4-N-10-methylpteroic acid (DAMPA) with the former comprising 3-12% of MTX in circulation (Cutolo et al., 2001). Each metabolite of MTX can compete for cellular uptake. Both metabolites are less effective inhibitors of DHFR and have an increased affinity for the folate transporters as well as FPGS, which means their accumulation minimises MTX-induced toxicity. 7-OH-MTX was also found to be a less efficacious catabolite in rat adjuvant arthritis than MTX (Baggott and Morgan, 2009).

It was suggested that at high concentrations, MTX could be taken up into the cell by passive diffusion, however, this was later shown to be negligible (Genestier et al., 2000). Cellular uptake of MTX was found to be mediated by the same transporters that recognise folate,-the reduced folate carrier (RFC) as well as the proton-coupled folate transporter (PCFT) (Genestier et al., 2000, Walling, 2006, Assaraf, 2007). The folate receptors (FR) were shown to be a third mechanism of uptake, but were found to be cell type specific, with the FRβ expressed predominantly in macrophages (Blits et al., 2013). Oral MTX

was shown to be taken up by the PCFT in particular as the receptor was found to function optimally at the acidic pH of the small intestine (Blits et al., 2013).

1.2.2 Polyglutamation of MTX

Cellular uptake was shown to result in the addition of glutamate residues (polyglutamation) to MTX by folylpolyglutamate synthase (FPGS) which increased the intracellular retention (Walling, 2006). In serum, degradation occurred between 8-15 h or between 8-10 h following administration (van Ede et al., 1998, Patane et al., 2013). It was undetectable in serum after 24 h (Chan and Cronstein, 2013). However, a significant proportion of the MTXglu-4 and MTXglut-5 residues were found 24 h after removal of MTX (Genestier et al., 2000). The same authors showed that the extent of glutamation influenced retention, as a significant fraction of MTX containing 2 and 3 glutamate residues were lost. Thus, MTX can either be metabolised or polyglutamated which increases the cellular retention and resultant half-life (Fig 1.1A).

1.2.3 An overview of the mechanism of action of MTX

The mechanism of action of MTX is still unclear. Part of its anti-inflammatory action is thought to stem from the fact that it is a folate antagonist, by virtue of the fact that it is similar in structure to folate (Fig 1.1B). MTX has been shown to exert effects on a variety of immunomodulatory processes including the inhibition of chemotaxis of monocytes and the reduction in adhesion molecules as well as cytokine expression, specifically the inflammatory cytokine TNF (Chan and Cronstein, 2010). It has also been shown to increase adenosine concentrations, and cause the apoptosis of T cells as well as inhibiting lymphocyte proliferation (Bird, 2014). Both MTX and its polyglutamated form (MTXGlu) have been shown to exert toxicity on the cellular processes requiring folate cofactors encompassing One-carbon (1C) metabolism. Polyglutamation of MTX increased the affinity of MTX for folate binding enzymes, potentiating its anti-folate action (Fig 1.2).
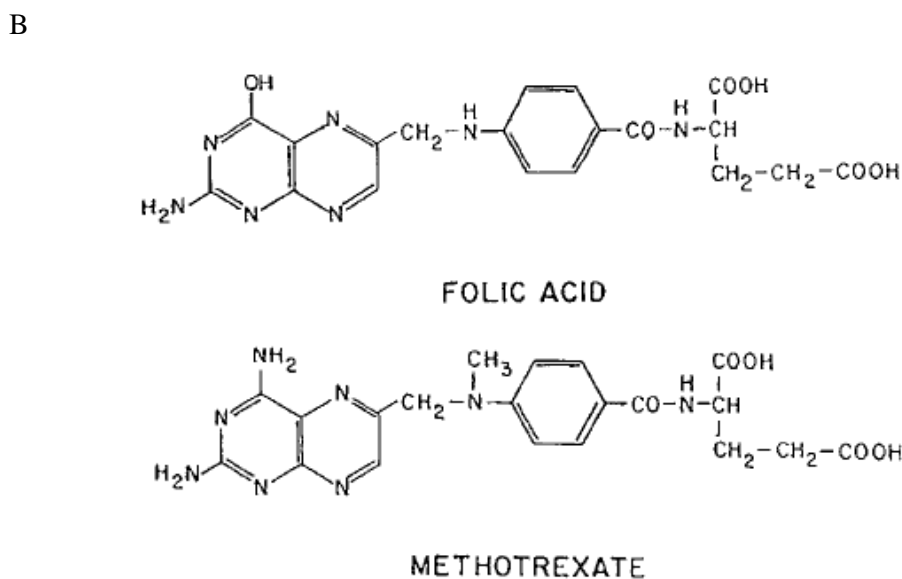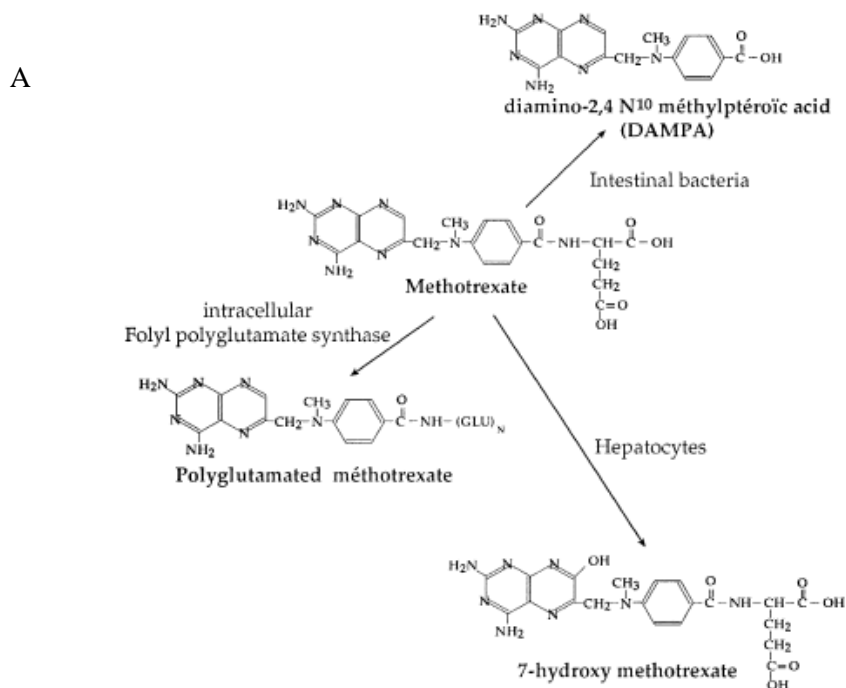
Figure 1.1 The structure of MTX, its metabolites and folic acid.

(A) Extracellularly MTX is degraded to two metabolites, DAMPA and 7-OH-MTX; the latter by the action of liver aldehyde oxidase. Intracellularly, MTX can be polyglutamated to increase its cell retention. Taken from Genestier et al. (2000). (B) The antagonistic effects of MTX on folate metabolism are in part due to the fact that MTX is a structural analog. Taken from Morgan et al. (2004).
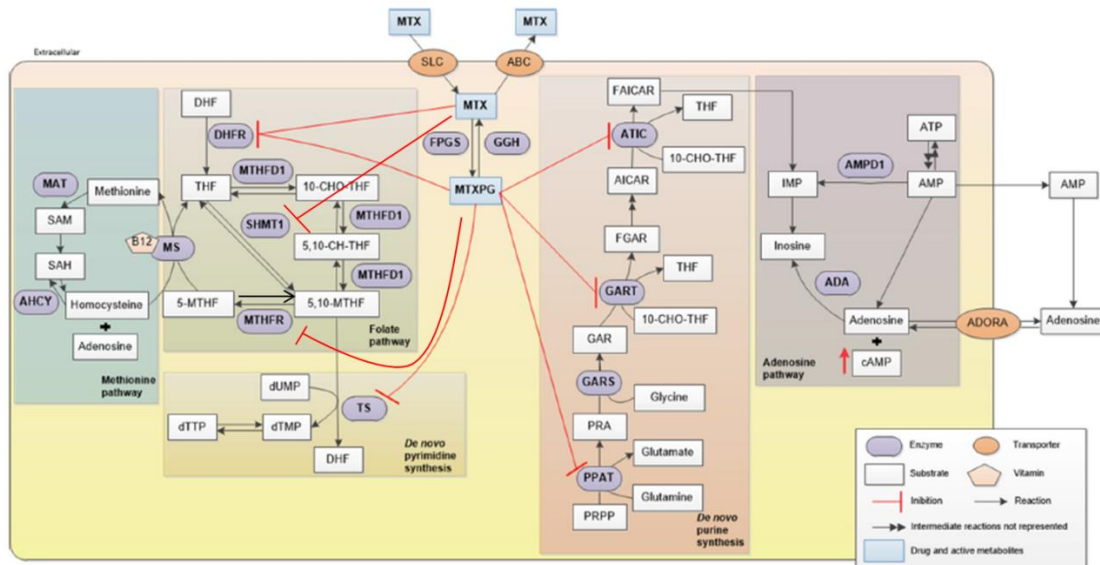
Figure 1.2 An overview of the action of MTX which depends on both uptake and intracellular retention.

Uptake of MTX is mainly mediated by solute carriers (SLCs), part of the family of RFC and efflux occurs by adenosine triphosphate (ATP)-binding cassette (ABCs) transporters. Retention of MTX is dependent on the sum of the addition of glutamate molecules, mediated by FPGS and their removal by γ-glutamylhydrolase (GGH). MTX and its polyglutamated derivative (MTXPG) inhibit multiple enzymes involved in folate metabolism. These include enzymes involved in de novo thymidylate (dTTP) and purine synthesis as well as methionine synthesis, inhibiting nucleotide production and effecting methylation reactions. As a result of purine inhibition, adenosine also increases. MTX inhibits DHFR, reducing the availability of reduced folates (THF). MTX also inhibits serine-hydroxymethyltransferase (SHMT), inhibiting the formation of the 1C donor, 5,10-methylene-THF (5, 10-MTHF). MTXPG inhibit methylene-THF-reductase (MTHFR), which also prevents the synthesis of: 5,10-methylene-THF from 5-methyl-THF (5-MTHF). This reduction in 5,10-methylene-THF, affects the other folate derivatives 5,10, methenyl-THF (5, 10-CH-THF) and 10-formyl-THF (10-CHO-THF), the latter crucial to purine synthesis. This inhibition of MTHFR also affects 5-methyl-THF from 5,10-methylene-THF, the activated folate carrier for methionine synthesis and methylation reactions by way of the universal methyl donor, S-adenosylmethionine (SAM). Methionine inhibition raises the levels of the methionine precursor, homocysteine. MTXPG also inhibits de novo purine synthesis by way of AICAR-formyl-transferase (AICARFT) and glycinamide-aicar-formyl-transferase (GARFT), the former denoted by the dual enzyme complex, 5-aminoimidazole- 4-carboxamide ribonucleotide transformylase (ATIC). The resultant increase in the undepleted substrate, AICAR, inhibits two enzymes in the salvage purine synthesis pathway, adenosine deaminase (ADA) degrading adenosine to inosine and AMP deaminase (AMPD1) converting AMP to IMP. The conversion of AMP to adenosine contributes to the increase in adenosine. MTXPG also inhibits phosphoribosyl pyrophosphate amidotransferase (PPAT), the first committed step in de novo purine synthesis. Adapted from Romao et al. (2014).

1.3 Folate

Folate is the general name for soluble vitamin B9 and its derivatives which are provided in the diet from leafy vegetables (Danenberg et al., 2016). The main dietary natural folate is 5-methyl-THF and is also the main folate found in blood (Visentin et al., 2012). These 'natural folates' are composed of a pteridine ring, a p-aminobenzoic acid and a glutamate moiety (Fig 1.3) (Assaraf, 2007). They are converted to the functional reduced folates that are utilised in biochemical pathways by the action of dihydrofolate reductase (DHFR) (Wibowo et al., 2013).

There are a variety of receptors responsible for uptake of both the oxidised (folic acid) and reduced (tetrahydrofolate moieties) forms of folate. The RFC also known as the folate-binding protein is the main carrier for reduced folates which binds and exchanges these folates for organic phosphates such as adenine nucleotides (Walling, 2006, Assaraf, 2007). The RFC has a much lower affinity for oxidised folate (K_m of 200-400 μM) compared to reduced folates, (K_m of 1-3 μM) and thus preferentially takes up the oxidised form. The RFC are highly expressed in a variety of tissues including peripheral blood leukocytes (Inoue and Yuasa, 2014). Oxidised and reduced folates are taken up by the PCFT also called SLC46A1, which is a member of the SLC family and plays a pivotal role in folate uptake as loss of function leads to hereditary folate-malabsorption (Inoue and Yuasa, 2014). The folate receptors (FRs) also mediate folate uptake via receptor-mediated endocytosis but are only expressed on certain cells (Assaraf, 2007).

Folates are present in the blood at ~10-50 nM (Assaraf, 2007). Intracellularly, folate is present at a much higher concentration of 1-10 μM (Walling, 2006). This is achieved following its polyglutamation by FPGS (Blits et al., 2013). In this reaction, successive glutamate molecules are added at the γ-carboxyl moiety to form a peptide chain with up to eight glutamate molecules, resulting in increased intracellular retention (Visentin et al., 2012).

The reactions that utilise folate and their derivatives, called one-carbon metabolism (1C metabolism) include a variety of metabolic processes from nucleotide synthesis, to methylation of DNA and RNA and the synthesis of methionine, as well as the degradation of a variety of amino acids. Of these, 6 reduced folate-derivatives, each with different
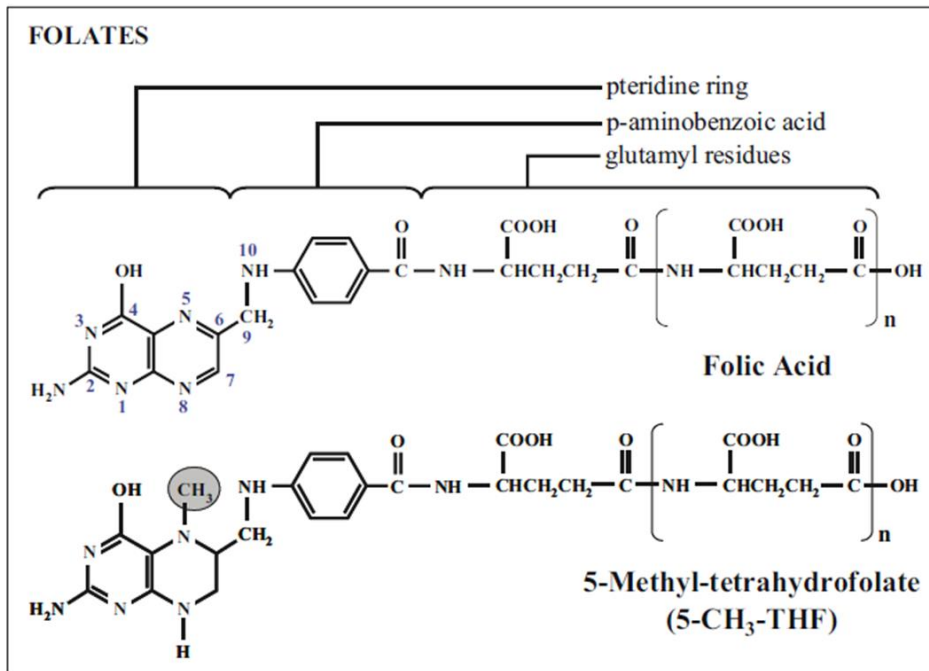
Figure 1.3 The basic structure of the oxidised form of folate, folic acid, and the reduced folate, 5-methyl-THF.

Folic acid contains a pteridine ring attached to a p-aminobenzoic acid moiety which is attached to a variety of glutamyl residues. 5-methyl-THF (5-CH₃-THF) contains an additional methyl group on the C6 of the pteridine ring. Taken from Assaraf (2007).

substituents at the 6 carbon have different functions within these pathways (Fig 1.4). As such folate-deficiency, either diet or drug-induced has far reaching consequences.

1.4 Folate and MTX

In the clinic, folate supplementation, either folinic acid or folic acid proved effective in lowering the MTX-induced side effects (Ortiz Z, 2009, Shea et al., 2014). In addition, it also prevented the discontinuation of treatment (Chladek et al., 2008). In one study it was shown to extend the course of treatment to 48 weeks for 83% of patients compared to 62% on MTX treatment alone (Whittle and Hughes, 2004). Folate supplementation could also increase the dose of MTX used (Cohen and Wolff, 2013). As a result, folate supplementation is now widely used with both low- and high-dose MTX.

Two forms of folate supplements were given during treatment;-the unreduced folate, folic acid, and the reduced form, folinic acid or 5-formyl-THF. Traditionally, folic acid was given to all patients on MTX treatment to offset the side effects and folinic acid in cases of MTX overdose, to rescue haematological toxicity (Whittle and Hughes, 2004). Folic acid, as an unreduced folate was shown to displace MTX from DHF binding sites, and increase the small pool of THF (van Ede et al., 1998). However, because complete enzyme inhibition of DHFR has only been shown at high concentrations of MTX, DHF binding of the few available sites on DHFR at low MTX concentrations, can maintain the small pool of THF. Thus, it is not known whether folic acid can have a significant effect on the already existing pools of THF. Folinic acid was also shown to replenish THF levels by bypassing the MTX-induced inhibition of DHFR (Genestier et al., 2000). However, it is also unclear what effect folinic acid would have on the depleted, yet existing THF pool.
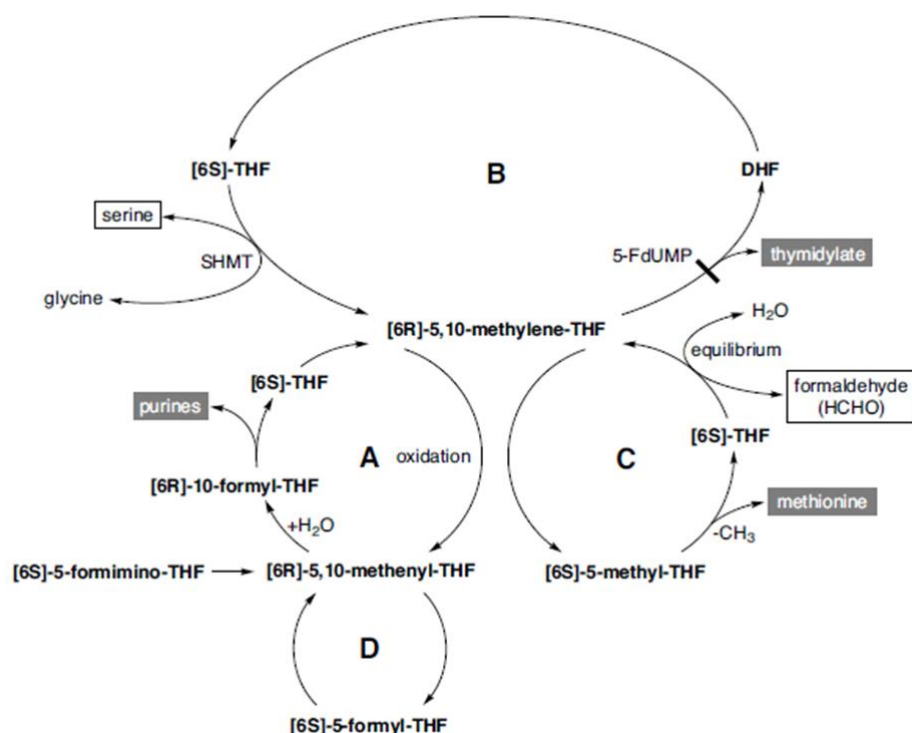
Figure 1.4. The direct and indirect involvement of tetrahydrofolate-derivatives in 1C metabolism.

[6R]-10-formyl-THF is involved in purine synthesis (cycle A) of which two moles are required for each purine ring synthesised (Tibbetts and Appling, 2010). [6R]-5,10-methylene-THF is involved in thymidylate synthesis (cycle B); [6S]-5-methyl-THF is involved in methionine synthesis (cycle C). The THF-derivatives not directly involved in biosynthetic pathways, but are crucial for the interconversion of folate intermediates are [6S]-5-formimino-THF, [6R]-5,10-methenyl-THF, and [6S]-5-formyl-THF (cycle D) Taken from Danenberg et al. (2016).

A putative role for folic acid in increasing efficacy of MTX was a result of the competitive inhibition demonstrated for aldehyde oxidase (AO) which catabolises MTX to 7-OH- MTX, a less efficacious catabolite in rat adjuvant arthritis than MTX (Baggott and Morgan, 2009). This suggested that folic acid could increase MTX efficacy by preventing its oxidative degradation. Folinic acid, as a reduced form of folate was thought to work by displacing MTX from THF binding sites. In theory, rescuing the reactions using reduced folate cofactors which include the majority of the folate-dependent pathways would seem to have a greater impact on the anti-folate, if competitive enzyme inhibition was a mechanism of action. However, most studies have found no differential effect of folic acid or folinic acid rescue in reducing the side effects of MTX treatment (Ortiz Z, 2009). This would suggest that perhaps folate rescue is not mediated by overcoming the MTX mediated enzyme inhibition, but rather competition for cellular uptake of MTX by these folates. Indeed, the folate receptor (FR) was shown to have a much lower affinity for MTX than both reduced folates and folic acid (Walling, 2006). Overall, this would suggest that the main mechanism of action of folate rescue is lowering the effective dose of MTX. In practise, this is achieved by adjusting the dose of folate to levels where side effects are reduced, whilst efficacy is still maintained.

It was originally hypothesised that inhibition of proliferation was not critical to the therapeutic effect of MTX because folate rescue overcame the side effects of MTX treatment, which occurred in highly proliferating tissues, but did not affect efficacy of treatment (Cronstein, 1996, Chan and Cronstein, 2013). However, later reports demonstrated a reduction in MTX efficacy following folate rescue. This hypothesis assumed that the dividing cells where these side effects occurred contained the same amount of MTX as the over-active T cells in RA, a finding that was never shown. It also assumed that the rate of proliferation was the same for both cell types. Indeed differing rates of proliferation may mean differential uptake of MTX due to different cellular requirements. Differential uptake of MTX may occur anyway due to differential folate influx and efflux receptor expression as well as differential polyglutamation and excretion in different cells (see **Section 1.3**). Furthermore, the salvage capacity of cells to withstand the anti-folate effects of MTX is very much cell-dependent. Thus, because the intracellular MTX concentration was not determined, it is possible that in some cases, the

proliferation of some cells were rescued, minimising side effects whilst others were susceptible to the effects of MTX, maintaining efficacy.

The only real evidence supporting this hypothesis was reports that found no diminution in T cell count in RA patients on MTX treatment, suggesting that MTX was not exerting an anti-proliferative effect. One such report found no change in circulatory T cell counts following MTX treatment (Olsen et al., 1987). Other reports found that treatment with a CD4 monoclonal antibody, which depleted CD4 cell numbers, did not correlate with therapeutic efficacy when given as monoclonal therapy or in conjunction with MTX treatment (Moreland et al., 1995, van der Lubbe et al., 1995). This suggested that a reduction in $CD4^+$ T cell numbers in those studies were not associated with therapeutic efficacy, however, the effect of MTX alone was not investigated. A frequently cited report which demonstrated that long term treatment with MTX actually increased the proportion of $CD3^+$ and $CD4^+$ T cells in circulation further confused the matter (Chan and Cronstein, 2002). However, these authors failed to report an inherent contradiction in this increase in $CD4^+$ T cells as the $CD8^+$ T cell numbers did not increase nor was there a change in the ratio of CD4:CD8 T cells. Furthermore, many reports cite the absence of a reduction in the proliferative responses of T cells from MTX treated RA patients following mitogenic activation ex vivo, as evidence that the efficacy of MTX is not linked to the anti-proliferative effect (Olsen et al., 1987, Furst and Kremer, 1988). One such study measured thymidine incorporation on mitogen-stimulated lymphocyte proliferation after a 2 yr MTX treatment, a finding that implicates the activation state of cells more than the anti-proliferative capacity of MTX (Weinblatt et al., 1988).

Wascher et al, as cited by Cronstein (1996), provided evidence supporting a reduction in T and B cell counts following short-term MTX therapy. Numerous studies have demonstrated inhibitory effects of MTX *in vitro* and *in vivo* on neutrophils as well as monocytes/macrophages, which have a crucial role in the synovitis and pathophysiology of RA (Cutolo et al., 2001). More recently, a long term trial conducted using low-dose MTX showed a reduction in memory helper $CD4^+$ T cells following MTX treatment as well as correlations with T cell counts and disease activity (Kremer et al., 2016). There is also ample evidence to suggest that low-dose MTX exerts an anti-inflammatory effect in dividing cells *in vitro*, with varied doses (see **Section 1.8**). Thus it was finally realised that MTX acts as both an anti-proliferative and anti-inflammatory agent in RA (Shinde et al., 2014).

There are reports documenting cases of folate over-rescue and cases of reduced efficacy, incorrectly cited as over-rescue with high-dose MTX but are now what is understood as low-dose treatment (Cohen, 2013). Folinic acid was shown to normalise 5-Aminoimidazole-4-carboxamide (AICA) urine levels following low-dose MTX treatment suggesting that it had prevented the MTX-mediated inhibition of aica-ribotide-formyl-transferase (AICARFT) (Morgan et al., 2004). It was also shown to reverse the ability of MTX to lower the levels of RF (Chan and Cronstein, 2010). Folic acid also demonstrated antagonistic effects. It reduced intracellular red blood cell (RBC) MTXGlu and plasma homocysteine levels (Chladek et al., 2008, Hazra et al., 2010). Cases of over-rescue were also found with folinic acid supplementation (Ortiz Z, 2009). This was explained as competition of folinic acid with MTX for uptake for the same folate transporter (Visentin et al., 2012).

Because it is not known whether folate supplementation acts by competing for uptake of MTX or limiting the effects of folate antagonism, experiments involving folate rescue from the inhibitory effects of MTX do not offer any clear explanation as to how MTX is exerting these differential effects. Competition for uptake could also explain how folate reduces side effects whilst maintaining efficacy in some cells because of differential intracellular concentrations of MTX. Thus, since cases of reduced efficacy and over-rescue have been reported, the anti-proliferative effect of MTX may be crucial to its anti-inflammatory action.

1.5 Anti-CD3-activation of T cells-a model of RA

In the literature, the effect of MTX on a variety of activators such as antigens, mitogens, or endogenous activators such as CD28 and anti-CD3, have been investigated. However, studies have yielded different findings using artificial stimuli compared to those using endogenous stimuli (Johnston et al., 2005). To evaluate the effect of MTX it is important that the model chosen is fitting for those physiological conditions. Except for the evaluation of cytokines, using LPS, a known TLR4 agonist to induce cytokine production, the use of antigenic-stimulation does not seem appropriate to delineate the mechanism of MTX in inflammatory diseases such as RA.

Some studies have looked at universal activation of cells, using phorbol myristate acetate (PMA), a cell permeable molecule, that directly activates protein kinase C, inducing signalling events resulting in universal cellular activation (Suzawa et al., 1984). Ionomycin, a calcium ionophore is used alongside PMA, converging on this same signalling pathway (Voet, 1990). Other activators such as phytohaemagglutinin (PHA) or concavalin A, both plant lectins, cause select cellular-activation through cross-linking of glycans on TCRs, or immunoglobulins which are present on certain cell types. Indeed the number of *N*-glycosylation sites on the TCRαβ chains and on the γδ are extensive and the *O*-glycosylation sites on the T cell co-receptor, CD8 are also well characterised, reviewed in Hounsell and Davies (1993). Finally, superantigens can activate antigen presenting cells (APC) as well as the T cell it is presented to, causing polyclonal activation (Li et al., 1999). However this is not the best model of the inflammation characterising RA. The inflammation in RA is mainly attributed to overly-activated T cells, which recognise self-antigen. Thus, the use of PMA to universally activate all cells does not seem fitting in this study.

In vivo, in the absence of an ongoing immune response, like those in healthy individuals, most of the T cells isolated from blood are naïve or resting T cells (Kleiveland, 2015). T cell-activation is achieved following binding of the CD3 receptor complex to the APC-complex of antigen-bound major histocompatibility complex (MHC), and ligation of the CD28 costimulatory molecule to CD80/86 on the APC. These signals initiate an ordered sequence of events activating the transcription factors, nuclear factor of activated T cells (NFAT) and activating protein-1 (AP-1) (Hogan, 2017). These transcription factors regulate IL-2 and IFN-γ production, and the induction of a variety of other processes including T cell proliferation and transferrin (CD71) receptor expression (Fig 1.5). The expression of receptors for IL-2 is an early event, occurring between 6 h and 9 h after activation and maximal transferrin receptor transcription occurs 48 h after activation (Goronzy et al., 1987). Transferrin receptor expression can be inhibited by blocking the IL-2 signal, indicating that IL-2 also regulates iron uptake in activated T cells (Lum et al., 1986). Other surface receptors expressed include the early T cell-activation marker, CD69 and the late expression of CD25 and HLA-DR (Reddy et al., 2004). The increase in the cytoplasmic volume, called 'blast formation' is also characteristic of T cell-activation, as a result of increased uptake of metabolic precursors for incorporation into daughter cells (Darzynkiewicz et al., 1976).

A
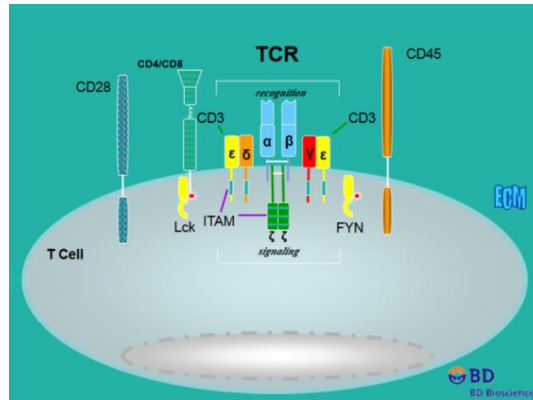
B
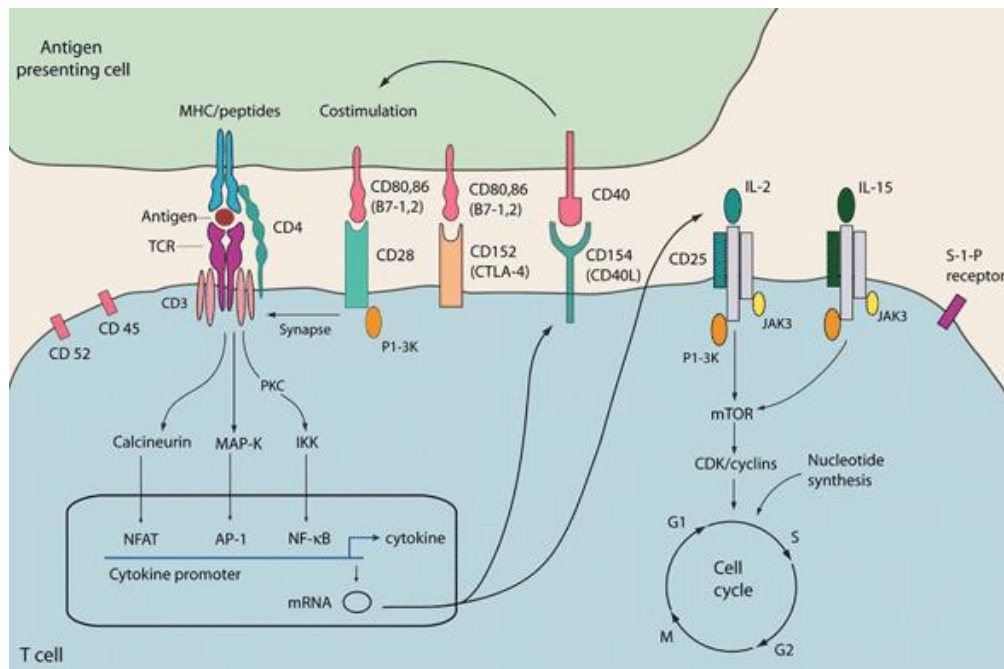
Figure 1.5. Signalling pathways leading to the induction of T cell-activation.

(A) The TCR synapse. (B) The signalling pathways initiated upon ligation of the TCR. The TCR ligates the antigen-bound antigen-presenting cells and the CD28 receptor ligates the CD80/86 ligand on the antigen-presenting cell. This binding transduces activation through calcineurin, RAS-mitogen-activated protein kinase (MAP-K), and protein kinase C (PKC) signalling pathways, leading to the activation of NFAT, AP-1 and the nuclear factor-kappa B (NF-kB). These transcription factors transcribe genes involved in other activation-dependent processes such as IL-2 production. The upregulation of receptors for IL-2 allows for this third signal to orchestrate cell proliferation through the induction of mammalian target of rapamycin (mTOR). Taken from (A) (P.Weller) and (B) Hunt and Haddad (2008).

In vitro, this process is mimicked through artificial ligation of the CD3 receptor, part of the T cell receptor (TCR) complex and the CD28 receptor by supplying the reciprocal antibodies, anti-CD3 and CD80/86 respectively (Goronzy et al., 1987). However, the concentrations of anti-CD3 used (1 µg/ml) induce polyclonal T cell-activation, whereby nearly 100% of T cells are activated (Kleiveland, 2015). Thus, anti-CD3-activation amplifies what happens on a physiological level. Even reducing concentrations of anti-CD3 to induce sub-optimal activation is not conducive to *in vivo* conditions as the presentation of antigen to one T cell induces the select proliferation of that specific T cell, recognising that particular antigen. Despite this limitation, the use of anti-CD3 was the preferred activator for this study.

Activation of a mixed population of immune cells, such as those within the PBMC cohort, negates the need to supply the co-stimulatory molecule, which is already provided by the antigen-presenting cells present. It is also more representative of conditions *in vivo*. Within the PBMC population, activation with anti-CD3 occurs in cells carrying a CD3 receptor, of which ~60% of the PBMC cohort are $CD3^+$ T cells, comprising $CD4^+$ T cells and $CD8^+$ T cells in a 2:1 ratio (Kleiveland, 2015). Following activation, a program of differentiation into distinct subsets of $CD4^+$ T cells can be initiated in the presence of exogenous polarising cytokines, such as IL-4, IL-12 or IFN- γ, to differentiate these $CD4^+$ T cells, into Th2 or Th1 respectively (Zhu et al., 2010). Even the production of endogenous cytokines by these T cells or other cells in the PBMC population could contribute to partial polarisation into either a Th1 or a Th2 phenotype (Swain, 1995). For this study however, only activation of T cells was required so PBMCs were activated in the absence of polarising cytokines (Th0). The effect, if any of endogenous cytokines on the differentiation into effector T cells was thus not a concern.

1.6 One-Carbon metabolism

One-carbon metabolism (1C metabolism) encompasses a wide range of reactions that involve the movement of methyl groups in the nucleus, cytoplasm and mitochondrial compartments. These methyl groups are donated by one-carbon donors, such as serine, glycine, formate (tryptophan degradation), choline and betaine, which contain methyl groups in their molecules. The reactions of 1C metabolism are intricately linked to folate metabolism. Reduced folates are required as carriers for these methyl groups and a

component of 1C metabolism, specifically methionine synthesis acts to replenish the levels of the free reduced-folate, from 5-methyl-THF, the most abundant form of folate in serum (van Ede et al., 1998). 1C metabolism includes the synthesis of DNA and RNA precursors, S-adenosylmethionine (SAM), the universal methyl donor for methylation reactions and also serves to metabolise the amino acids serine, glycine, tryptophan, histidine as well as choline.

A schematic of the interplay of 1C pathways of the cytoplasm, mitochondria and nucleus is shown in Fig 1.6. It is an intricate pathway comprising three compartments, connected only by select one-carbon donors and sharing one fundamental reaction. Each compartment has its own de novo thymidylate synthesis pathway-via thymidylate synthase (TS) and its substrate, 5,10-methylene-THF, itself synthesised by compartment-specific isozymes of serine- hydroxymethyltransferase (SHMT). In the mitochondria this was found to be SHMT2 and was localised to the mitochondrial matrix (Anderson et al., 2011). This was discovered when isolated nuclei from mouse liver synthesized thymidylate, following the addition of dUMP, NADPH and serine (Anderson and Stover, 2009). Isolated mitochondria were also found to have de novo thymidylate synthesis enzymatic capability when CHO cells also produced thymidylate when provided with serine and NADPH (Anderson et al., 2011). The reduction of unreduced folate precursors is also a commonality between compartments, mediated by dihydrofolate reductase (DHFR).

Not all 1C reactions take place in every compartment; the mitochondria is the only site for the regeneration of serine from glycine, known as the glycine cleavage system (GCS). This reaction controls glycine levels and is one of the pathways for serine synthesis, a major source of 1C units. The mitochondria is also the major pathway utilising the one-carbon donors from serine via SHMT (Yoshida and Kikuchi, 1970, Kikuchi, 1973). It is also the only entry point for the methyl groups from sarcosine and dimethylglycine, into the folate cycle. In addition, it is the site of formyl-methionine RNA synthesis. As of yet, the only connection between the compartmental-specific pathways is the passage of the one-carbon donors, formate, serine and glycine. Formate is known to enter intact mitochondria, as evidenced by swelling assays (Cybulski and Fisher, 1977). Serine uptake was demonstrated in isolated mitochondria taken from rat liver, and this serine was then shown to be oxidised to formate (Barlowe and Appling, 1988). The same authors showed release of this serine-derived formate from the mitochondria. Formate efflux from the

Figure 1.6. The interplay of 1C donors (blue) and THF-derivatives (green) for methionine, thymidylate and purine synthesis between the cytoplasm, nucleus and mitochondria.

Reduced folate (THF) is synthesised from DHFR and unreduced folate, reaction 13. Formate enters the 1C metabolism pathway in both the cytoplasm and mitochondria, generating the one-carbon donor 5,10-methylene-THF (CH_2-THF) by reactions 1-3; catalyzed by 10-formyl-THF synthase, 5,10-methenyl-THF (CH^+-THF) cyclohydrolase, and 5,10-methylene-THF dehydrogenase, respectively. This substrate is also synthesised from the one-carbon donor glycine by the mitochondrial glycine cleavage system (GCS); reaction 5. Dimethylglycine (DMG) derived from the betaine precursor, choline via betaine-homocysteine methyltransferase, reaction 14; and sarcosine are also sources of 5,10-methylene-THF via dimethylglycine dehydrogenase and sarcosine dehydrogenase; reactions 8 and 9 respectively. This one-carbon donor is also generated by serine, via serine hydroxymethyltransferase (SHMT) in each compartment, with the nuclear and mitochondrial compartments denoted by n and m, respectively. Thymidylate synthase (TS) synthesises thymidylate using 5,10-methylene-THF and dUMP in the de novo thymidylate synthesis pathway in each compartment. 5,10-methylene-THF can be converted to 5-methyl-THF via 5,10-methylene-THF reductase, reaction 6. This one-carbon donor is utilized by methionine synthase for the synthesis of methionine from homocysteine (Hcy), reaction 7. Methionine is the precursor for *S*-adenosylmethionine (AdoMet) which is interconverted to *S*-adenosylhomocysteine (AdoHcy). Free THF is regenerated from 10-formyl-THF by 10-formyl-THF dehydrogenase, reaction 11 and methylene-THF dehydrogenase, (MTHFD1L), reaction 1m and methionyl-tRNA formyltransferase, reaction 12. End products of one-carbon metabolism are in red. Taken from Tibbetts and Appling (2010).

18

mitochondria has also been shown in yeast and in vitro (Barlowe and Appling, 1988, Garcia-Martinez and Appling, 1993). Glycine was also taken up by the mitochondria as demonstrated by 1-^{14}C labelling experiments and converted to CO_2 (Hampson et al., 1983). Choline uptake in the mitochondria precedes DMG uptake, thus choline levels are indicative of the levels of the one-carbon donors DMG and sarcosine (Porter et al., 1992).

The flux of one-carbon donors was originally thought to be the sole communication between compartments. Treatment with the DHFR inhibitor, trimethotrexate, showed a decrease in THF and increase in DHF in the cytosol, without any corresponding changes in the mitochondria of leukemic cells, suggesting that there was no exchange of mitochondrial folates with the cytosol (Trent et al., 1991). However, isolated mitochondria were shown to synthesise thymidylate *de novo* and the isozyme DHFRL1 was found localised to the mitochondrial matrix, suggesting that some form of unreduced folate traversed the membrane (Anderson et al., 2011). Although this isozyme showed lack of activity, it is now accepted that folate can traverse the mitochondrial membrane, through a carrier mediated process using the mitochondrial folate transporter (MFT) (Wang et al., 1967). This was demonstrated in CHO cells so it is unclear whether this is cell-type-dependent (Titus and Moran, 2000). There is also conflicting evidence regarding the form of folate that crosses this membrane; some reports found that the reduced folate, tetrahydrofolate was not transported across isolated rat liver mitochondria as loss of DHFR activity in the mitochondria could not replenish THF levels in the mitochondria (Cybulski and Fisher, 1981, Anderson et al., 2011). However, evidence for the transport of reduced folates within compartments was demonstrated by the presence of a reduced folate carrier localised to the mitochondria in human leukaemia cell lines (Trippett et al., 2001). In rat liver mitochondria, uptake of the reduced folates, 5-methyl-THF and 5-formyl-THF was faster than the unreduced folates (Horne et al., 1992). Although it is not clear whether the reduced or unreduced form of folate crosses the mitochondrial membrane it has been established that it is a folate monoglutamate since polyglutamates could not enter the mitochondria in CHO cells (Lin and Shane, 1994). Polyglutamates could not be detected in the mitochondria in folylpolyglutamate synthase (FPGS)-deficient CHO cells expressing only the cytosolic FPGS isoform (Lawrence et al., 2014). The activity of the mitochondrial isozyme, FPGS was also required for folate accumulation in the mitochondria, suggesting that monoglutamate forms are transported into the mitochondria (Chen et al., 1996). Finally, it was shown that the human FPGS

gene had two isoforms, one containing a mitochondrial leader sequence, which directed its fate to the mitochondria, affirming the impermeability of the mitochondria to polyglutamates (Lawrence et al., 2014).

The importance of adequate function of the 1C pathway, in particular the mitochondrial compartment, is demonstrated when deficiencies in this pathway can cause neural tube defects (NTDs). Inactivating mutations in the GCS, an enzyme localised to the mitochondria is a predisposition for neural tube defects, demonstrating the importance of glycine as a provider of 5,10-methylene-THF (Brosnan et al., 2015). These defects were prevented by replenishing the methyl donors, specifically formate which normalized the folate profile and prevented neural tube defects (Pai et al., 2015). Although the defects could not be completely reversed, as glycine levels in the plasma and urine were still elevated, it illustrates how important the 1C donors are, of which the mitochondria is the main receiver. These 1C donors and the reactions of their metabolism, have roles in DNA synthesis, and the synthesis of methionine, the precursor to the universal methyl donor SAM for reactions involving RNA, DNA, proteins, phospholipids and amino acids (Cronstein, 1996). Methylation is also crucial for polyamine synthesis, the proteins involved in cell proliferation, regulation, differentiation, protein synthesis and immune mediated cell reactions (van Ede et al., 1998). As such, perturbations of this 1C metabolism can have major consequences on cellular function.

1.7 The anti-folate MTX affecting 1C metabolism

MTX inhibits many aspects of 1C metabolism (Table 1.1). MTX (0.3, 1 and 3 µM) was shown to inhibit 50% of [^{14}C]formate uptake into DNA, RNA and protein reflecting permeation of MTX through the 1C metabolism pathway (White et al., 1975). Much of the inhibition of MTX is because it is a folate analog and as such, can affect any enzyme which relies on both unreduced and reduced folate cofactors. This permeation has even been shown for the mitochondrial 1C pathway. MTX was found to be transported into the matrix by a carrier mediated mechanism (Cybulski and Fisher, 1981). Although this transporter has not been identified, it seems likely that MTX enters the mitochondria using the same transporter as folate, like it does entering the plasma membrane. Further evidence of MTX traversing the mitochondrial membrane was demonstrated when MTX

was able to inhibit thymidylate production from isolated mitochondria in CHO cells (Anderson et al., 2011). Thus, the MTX-mediated effect on purine, thymidylate and methionine synthesis, as well as methylation reactions via the reduction of the methyl donor, SAM could permeate every 1C metabolism compartment.

Table 1.1. The effects of low-dose MTX on 1C metabolism

	Direct effects	Indirect effects
Inhibition of purine synthesis	10-formyl-THF depletion (inhibition of amidophosphoribsyltransferase, GARFT and AICARFT)	AICAR mediated inhibition of salvage (adenine deaminase and AMP deaminase)
Inhibition of thymidylate synthesis	Partial depletion of TS substrate 5, 10-methylene-THF (via inhibition of SHMT)	Partial depletion of TS substrate, 5, 10-methylene-THF (DHFGlu mediated inhibition of 5, 10- methylene-THF cyclohydrolase)
	Inhibition of TS	DHFGlu inhibiton of TS
Inhibition of methionine synthesis	Inhibition of methylene-THF-reductase (converting 5,10-methylene-THF to 5-methyl-THF)	DHF inhibition of MS DHFGlu inhibition of methylene THF reductase (converting 5,10-methylene-THF to 5-methyl-THF)
	Inhibition of MAT	S-adenosylhomocysteine inhibition of methyltransferases such as ICMT

1.7.1 The effect of MTX on methionine synthesis

MTX as well its polyglutamate derivative, MTXGlu, inhibit methionine synthesis by reducing the levels of the 1C donor, 5-methyl-THF required for its synthesis. This has implications for cellular methylation, including polyamine synthesis and cell function. By inhibiting DHFR, MTX depletes the reduced folate THF, and the subsequent activated 1C donor carrier, 5-methyl-THF, inhibiting the formation of methionine from homocysteine (Cronstein, 2005). The increasing levels of DHF, were also shown to inhibit methionine synthase (MS) (Baggott et al., 1986). MTXGlu's were shown to inhibit 5,10 methylene-THF reductase, required for the conversion of 5,10-methylene-THF to 5-methyl-THF. Although it has also been suggested that MTX could inhibit MS directly, little has been shown in this regard (van Ede et al., 1998).

This inhibition of methionine synthesis reduces levels of the universal methyl donor, SAM, involved in methylation reactions. In addition to depleting levels of the precursor to SAM, MTX was also shown to directly inhibit a key enzyme in SAM synthesis, methionine s-adenosyltransferase (MAT). MTX treatment was also shown to lead to changes in methylation patterns and resultant changes in gene expression (Neradil et al.,

2012). It was also shown to have consequences on polyamine synthesis, which have multiple roles in proliferation and cell function (Cronstein, 1996).

Additional insults to cell methylation by MTX arise from the concurrent increase in homocysteine, which had not been depleted for methionine synthesis. Homocysteine has been shown to form s-adenosylhomocysteine (SAH), which is an inhibitor of methyltransferases including isoprenylcysteine carboxyl methyltransferase (ICMT), involved in the methylation of RAS, a crucial G protein involved in cell growth signalling pathways. Indeed, MTX (10 µM) caused a 90% reduction in Ras methylation in DK0B8 cells (Winter-Vann et al., 2003). Even artificially increasing SAH, by incubating cells with homocysteine and adenosine in the presence of adenosine deaminase inhibitor was shown to inhibit lymphocyte and mononuclear cell function (Cronstein, 1996).

1.7.2 The effect of MTX on thymidylate synthesis

MTX (1µM) was shown to reduce TS activity by 20% but there was only a partial reduction in the TS substrate, 5,10-methylene-THF, which suggested that other mechanisms of inhibition were in place (Genestier et al., 2000). Inhibition of de novo thymidylate synthesis by MTX was thus found to be a multifactorial process, which included TS inhibition by both polyglutamated DHF (DHFGlu) and MTXGlu as well as partial-substrate depletion (Genestier et al., 2000). DHF which accumulated in response to DHFR inhibition, inhibited TS (Baggott et al., 1986). MTXGlu blocked TS, with the degree of binding increasing with polyglutamation. The Ki for MTX with one glutamate residue was found to be 13 µM, but for two and five glutamate residues it decreased to 0.17 µM and 0.047 µM respectively (Allegra et al., 1985a).

MTX was shown to deplete the substrate, 5,10-methylene-THF for TS in a variety of ways. Inhibition of DHFR by pentaglutamated MTX with a (Ki 0.004 nM) was found to deplete THF levels, on which 5,10-methylene-THF is formed and inhibition of SHMT, depleted 5,10-methylene-THF (Sant et al., 1992, Walling, 2006, Tibbetts and Appling, 2010). The interconversion of 10-formyl-THF to 5,10-methylene-THF, by the mitochondrial isozyme, 5,10-methylene-THF cyclohydrolase was also shown to be inhibited by DHFGlu, (Baggott et al., 1986). This reduced the levels of 5,10-methylene-THF for the synthesis of thymidylate, for incorporation into DNA (Fig 1.7).
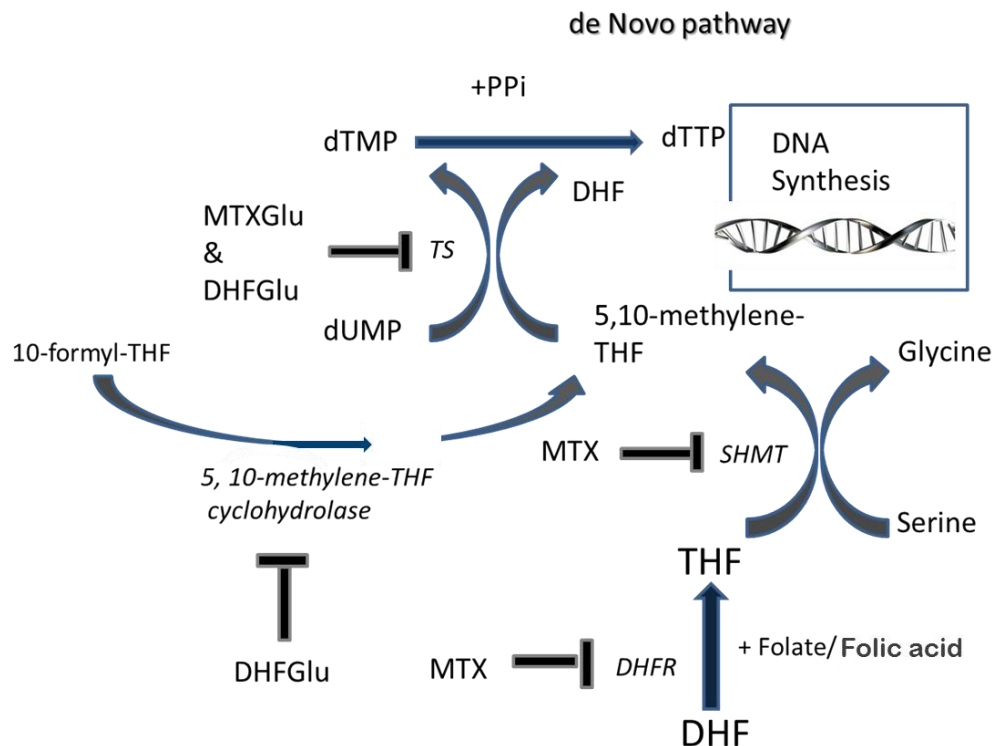
Figure 1.7. MTX enzyme inhibition and substrate depletion results in the inhibition of de novo thymidylate synthesis.

MTX inhibits dihydrofolate reductase, (DHFR*)* and serine hydroxymethyltransferase (SHMT)*,* depleting THF and 5,10-methylene-THF, substrate levels. The inhibition of DHFR, increases DHF concentrations, whose glutamate form (DHFGlu) has a greater affinity for TS. DHFGlu inhibits 5,10-methylene-THF cyclohydrolase which interconverts 10-formyl-THF to 5,10-methenyl-THF before synthesis of 5,10-methylene-THF, potentiating this inhibition. MTX polyglutamates (MTXGlu) also have a greater affinity for TS inhibiting thymidylate (dTTP) synthesis.

The importance of the one-carbon folate carrier 5,10-methylene-THF for TS was clear by its numerous carbon sources (Barlowe and Appling, 1988, Garcia-Martinez and Appling, 1993). Serine was found to be a major source of 5,10-methylene-THF, both for methionine synthesis as well as for thymidylate synthesis. C-13 labelled serine provided nearly all of the methyl groups required for homocysteine remethylation to methionine, via the interconversion of 5,10-methylene-THF to 5-methyl-THF (Brosnan et al., 2015). Knockdown of SHMT2, was found to prevent the generation of 5,10-methylene-THF from serine and diminished thymidylate levels (Anderson et al., 2011). Glycine was also shown to generate 5,10-methylene-THF via the GCS in the mitochondria (Hampson et al., 1983). The 1C donors sarcosine and dimethylglycine were also shown to be sources of 5,10-methylene-THF via sarcosine dehydrogenase and dimethylglycine dehydrogenase, respectively (Mitoma and Greenberg, 1952, Lewis et al., 1978, Barlowe and Appling, 1988).

1.7.2.1 The regulatory role of thymidylate

The MTX-mediated inhibition of de novo thymidylate synthesis was also found to affect the regulatory role exerted by thymidylate. Thymidylate levels are self-regulated by controlling both the *de novo* and salvage synthesis pathways of its precursor, dUMP. dUMP can be formed by (i) phosphorylation of deoxyuridine by thymidine kinase, (ii) reduction of UDP to dUDP by ribonucleotide reductase, and (iii) the deamination of dCMP by deoxycytidylate deaminase reaction. These negative feedback mechanisms in place on each enzyme, ensures that both the de novo and salvage pathway is switched off in the presence of excess thymidine. This is not only important to conserve resources, but also because excess thymidine is toxic, causing growth inhibition in Novikoff hepatoma cells. Indeed, the addition of thymidine (40 μM) inhibited deoxyuridine synthesis in DNA in N1s1 cells by more than 90% (Jackson, 1978). It was shown that the mechanism of thymidine induced toxicity was a deficiency in dCTP synthesis, when the growth of Human T-leukemic Lymphocytes was rescued from excess thymidine upon the addition of deoxycytidine (Fox et al., 1980). The deamination of dCMP was shown to be the main pathway for dUMP production as the activity of deoxycytidylate deaminase was high in proliferating tissues (Jackson, 1978, Goulian et al., 1980a). Furthermore, thymidine (13

µM and 100 µM) exerted maximal negative feedback on this pathway, reducing dCTP levels by 80% and causing 50% inhibition of deoxycytidylate deaminase, respectively. Thymidylate was also shown to inhibit CDP reductase, upstream of dCMP preventing an increase in dCMP levels (Jackson, 1978).

1.7.3 The effect of MTX on uracil

This waning in the negative feedback mechanisms normally exerted by thymidylate leads to an increase in dUMP and other uracil moieties, such as deoxyuridine or uridine. MTX (10 µM) treatment caused deoxyuridine levels to increase ~10^3 fold and also caused an increase in dUMP concentration in cultured human lymphoblasts (Goulian et al., 1980b, 1980a). However, there is also evidence found where MTX did not lead to an increase in dUMP (FitzGerald and Wick, 1987). Although normal cell processes seek to minimise dUTP levels by the actions of UTPase, which hydrolyses dUTP to dUMP, increasing dUMP levels, the MTX-mediated increase in dUTP was suggested to outcompete the maximal workings of the dUTPase to keep dUTP levels low. Even at the rate of hydrolysis of UTPase equal to the rate of formation of dUTP, MTX treatment was suggested to lead to a gradual increase in dUTP levels (Goulian et al., 1980a).

1.7.3.1 The correlation of uridine moieties in circulation with uracil incorporation in DNA

It was thought that an increase in uracil in circulation, for instance, dUTP, would correspond to an increase in uracil content of the DNA because of the unspecific nature of the DNA polymerase, choosing a base depending on the strength of binding of the base to the opposite strand (Voet, 1990). This meant that either thymidine or uridine could base pair to the adenine nucleobase in the parent strand. However, there are conflicting reports of whether this increase in dUMP or its dephosphorylated form deoxyuridine, reflect an increase in uracil content in DNA since the unspecific nature of the DNA polymerase has recently been questioned. The addition of both uridine and deoxyuridine, or folate-deficiency leading to a reduction in thymidine levels, was not found to increase the uracil concentration in HeLa cell-DNA (Martiniova et al., 2015). The same authors showed that 30 times more deoxyuridine than uridine was incorporated in DNA in Hela cells

indicating that preferential uptake of deoxyuridine had occurred. The group found that this was not because plasma uridine concentrations did not reflect the increase in uridine or deoxyuridine in the diet, as plasma levels of these nucleosides significantly increased. Other evidence was provided by depleting thymidine levels in mouse embryonic fibroblasts (MEF) using thymidylate synthase inhibitors, 5-flurouracil (5-FU) (1 µM) and 5-fluro-deoxyuridine (5-FdUrd) (50 nM), which resulted in a high dUMP:dTTP ratio, but did not lead to an increase in uracil content of DNA (Nielsen et al., 2007). Studies have also investigated whether folate treatment can reduce uracil incorporation in DNA, however, the level of uracil misincorporation in white blood cells was not reduced compared to those without supplementation (Hazra et al., 2010).

However, there are reports where increasing uracil concentrations have led to an increase in uracil incorporation in DNA. Deoxyuridine accumulated in mitochondrial DNA following impaired de novo dTMP synthesis (Anderson et al., 2011). The addition of deoxyuridine also increased uracil incorporation in HeLa cells, grown in folate-deficient or replete media (Duthie and McMillan, 1997). Elevated uracil in DNA has also been shown to occur in cells starved of folate, akin to incubation in the anti-folate drug MTX. At folate concentrations found in the human plasma of folate-deficient individuals, (12 nM), CD4$^+$ and CD8$^+$ T cells had significantly increased uracil content in DNA as compared to folate-replete cells (Courtemanche et al., 2004). Incubating human lymphocytes in folate-deficient media also increased the level of incorporated uracil (Duthie and McMillan, 1997).

The presence of uracil in DNA can occur spontaneously through the deamination of cytosine already present or through misincorporation. Although one molecule of dUMP is incorporated into DNA for every 10^5 dTMP in normal human lymphoblasts, the presence of uracil in DNA is dependent on the efficiency of the uracil removal repair mechanisms in place (Goulian et al., 1980a).

This excision repair machinery, collectively known as Uracil-DNA-glycosylases (UDG), include Uracil (Ung), Single-strand monofunctional uracil- (Smug1), Thymine mismatch (Tdg) and methyl CpG binding domain one (Mbd4/med 1) DNA glycosylases (Andersen et al., 2005). The highly conserved Ung is the most widely distributed UDG (Aravind and Koonin, 2000). Knockdown of Ung-/-, one of the Uracil-DNA glycosidases, in MEFs, resulted in an increase in both uracil and AP sites after treatment with the cytotoxic drugs.

It is possible that in certain cell types, this removal mechanism is more efficient and thus can withstand elevated uracil levels in circulation, preventing a build-up in DNA.

1.7.4 The inhibitory effect of MTX on purine synthesis

Some of the first evidence of MTX-mediated inhibition of de novo purine synthesis, was the reported increase in the purine nucleotide precursor, PRPP (Sawyer et al., 1989). This was shown to be a result of the MTX-mediated inhibition of amidophosphoribosyltransferase, the first step in de novo purine synthesis (Genestier et al., 2000). The reduction in the purine-dependent folate derivative, 10-formyl-THF as a result of reduced THF pools was not shown to be the main mechanism of the MTX-inhibition of purine synthesis as intracellular levels of 10-formyl-THF were maintained at 80% during DHFR inhibition (Neradil et al., 2012). Complete DHFR inhibition and complete depletion of THF pools were only possible at high concentrations of MTX because a few available DHFR binding sites were found to be enough to maintain a small amount of the THF pool (Assaraf, 2007). MTXGlu was later shown to block two enzymes in the de novo purine salvage pathway; MTX with 5 glutamate residues (Pentaglutamated MTX) was shown to inhibit glycinamide-aicar-formyl-transferase (GARFT) with a Ki of 2.5 µM (Sant et al., 1992). Pentaglutamated MTX also inhibited aica-ribotide-formyl-transferase (AICARFT), an enzyme upstream of de novo purine synthesis with a Ki of 56 nM (Walling, 2006). This prevented the synthesis of nucleotides downstream, such as IMP, AMP, GMP and their analogs. Inhibition of AICARFT by pentaglutamated MTX resulted in elevated levels of urinary AICAR metabolites in RA patients (Chan and Cronstein, 2010). In animals, a 2-3 fold increase in splenocyte AICAR levels occurred upon injection with MTX (Morabito et al., 1998). These AICAR metabolites (aica riboside being the cell permeable nucleoside which can be converted to aica ribotide, also known as ZMP) potentiated the damage to the purine synthesis pathway (Fig 1.8). AICA ribotide was found to inhibit AMP deaminase, which normally degraded AMP to IMP (Morgan et al., 2004). AICA riboside also inhibited adenosine deaminase (ADA), which normally converts adenosine to inosine in the purine salvage pathway (Yanagimachi et al., 2011). In this way MTXGlu indirectly potentiated the reduction in the IMP precursor for purine nucleotides (Fig 1.8). Additionally, inhibition of ADA was also shown to increase deoxyadenosine and deoxyadenosine triphosphate (dATP) levels,
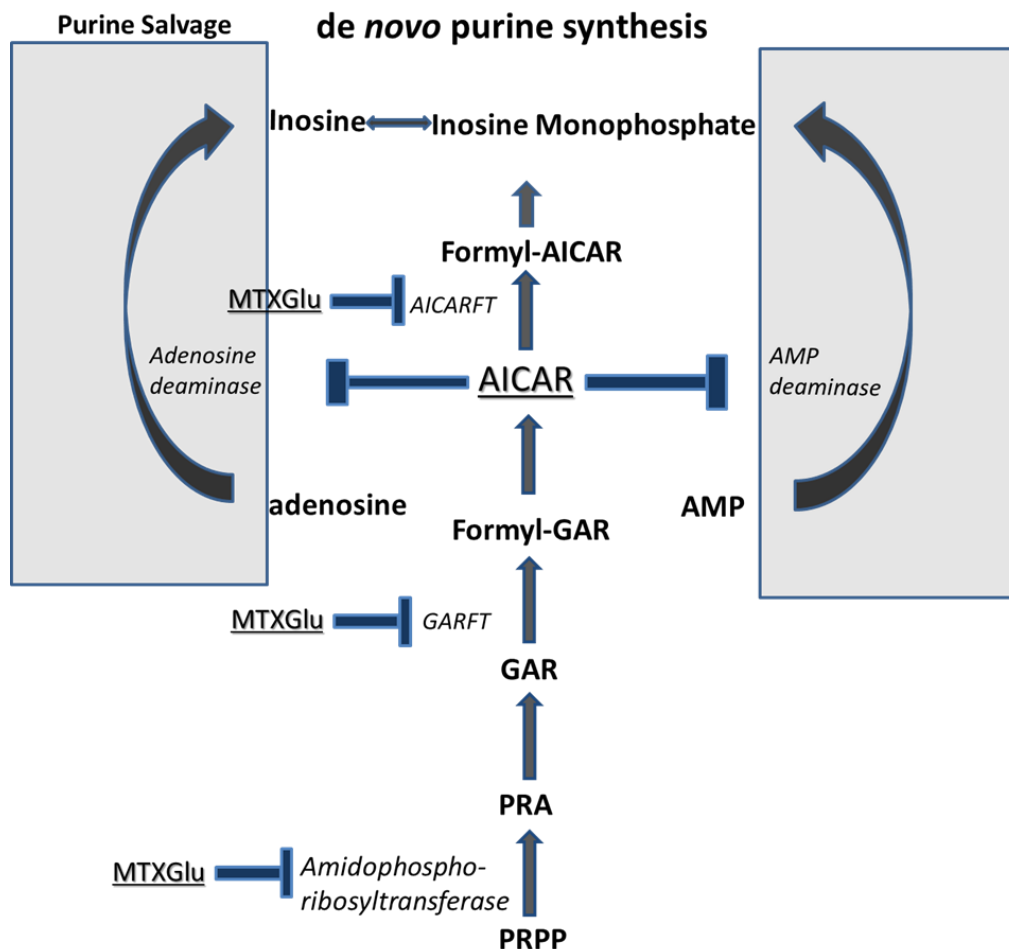
Figure 1.8. MTX polyglutamates inhibit de novo purine synthesis, whilst AICAR metabolites inhibit the salvage pathway of purine synthesis.

MTXGlu inhibits the first step in de novo purine synthesis by inhibiting the conversion of PRPP to PRA, via amidophosphoribosyltransferase. MTXGlu also inhibit GARFT, converting GAR to formyl-GAR in the de novo purine pathway. The MTXGlu inhibition of AICARFT raises AICAR metabolites which exert inhibitory effects on purine synthesis. AICA ribotide was found to inhibit AMP deaminase, which normally degraded AMP to IMP. The other AICAR metabolite, AICA riboside inhibited adenosine deaminase (ADA), which normally converts adenosine to inosine, in the purine salvage pathway. This reduced inosine as well as inosine monophosphate levels, limiting both the salvage and de novo purine synthesis pathway.

which have been shown to inhibit ribonucleotide reductase, necessary for DNA synthesis (van Ede et al., 1998).

1.7.5 Enzyme inhibition by unreduced folate

Folate antagonism by the anti-folate, MTX is partly mediated by the antagonism of the unreduced (DHF) folate pool which increases following treatment. These unreduced folates with dihydro or oxidised pteridine rings were shown to inhibit TS, GARFT, MS, 5 forminotetrahydrofolate cyclodeaminase, 5, 10 methenyltetrahydrofolate cyclohydrolase and methylenetetrahydrofolate reductase (Baggott et al., 1986, Blits et al., 2013). Treatment of human MCF-7 breast cancer cells with MTX (1 µM) increased DHFGlu to about 20% of the total folate pool (Sant et al., 1992). Polyglutamation was shown to endow these unreduced folates with further inhibitory properties. DHFGlu was also shown to inhibit AICARFT (Allegra et al., 1985b). However, when DHF levels had built up, these unreduced folates were shown to antagonise the effects of MTX by competing for binding for the few available binding sites of DHFR needed to maintain THF cofactor pools within cells (Visentin et al., 2012).

1.8 The anti-proliferative effect of MTX

Purine and thymidine inhibition, following treatment with MTX resulting in inhibition of cellular proliferation has been shown in a variety of cell types and following activation with a variety of stimuli. MTX (20 nM-20 µM) inhibited the proliferation of PHA-stimulated T lymphocytes (Fairbanks et al., 1999). MTX (1 µM) was also found to halt cellular proliferation in T lymphocytes (Quemeneur et al., 2003). High-dose MTX (10 µM) reduced the proliferation in concavalin A-stimulated PBMCs (Tohyama et al., 2013). Even stimulation with non-mitogenic stimuli following MTX treatment, inhibited the proliferation of T cells indicating that T cells proliferate upon activation, in a mitogen-independent manner. The proliferation induced following flu-antigen-stimulation was also inhibited by MTX (20 nM) (Collinge et al., 2010). Proliferation induced by Superantigens or conventional antigens acting on CD4^{+} T cells was also decreased with MTX (1 µM) (Sigmundsdottir et al., 2004). This anti-proliferative capacity of MTX (10 nM) was also demonstrated in B cell growth factor and anti-Ig stimulated B lymphocytes,

where both the number of antibody forming cells and a corresponding decrease in antibody production was found (Rosenthal et al., 1988). However, there has been a report which shows that low-dose MTX treatment has no anti-proliferative effect. This was shown following MTX (0.05 µM or 1 µM) treatment with concavalin A for 4 days (Tohyama et al., 2013).

MTX also inhibited the proliferation of immortalised cell lines. AML 193 human myeloid leukemic cells stimulated with the growth factor, GM-CSF, showed an increase in inhibition from 49-89% following MTX (2.2 µM) treatment (Ciaiolo et al., 1988). The growth of Erlich tumour ascites was also inhibited by MTX (2 µM) (Li and Kaminskas, 1984). So too was the growth of Human Leukemic-T lymphoblasts CCRF-CEM cell line and Human Jurkat T lymphoblasts inhibited by MTX (100 nM) (da Silva et al., 1996).

The anti-proliferative effect of folate-deprivation has also been shown in cells cultured in folate-deficient media. Human mononuclear cells that were stimulated with IL-2 and PHA showed a dose-dependent reduction in proliferation when folate was reduced from (12 nM- 6 nM) (Courtemanche et al., 2004). Lymphocytes also failed to proliferate in response to stimulation with 0.5% PHA following a 6 day folate-deficient media incubation (Duthie and McMillan, 1997).

The inhibition of cell division does not necessarily prevent the increase in cytoplasmic volume accompanying the increased intake of cellular building blocks. This unbalanced cell growth leads to an increase in cell size and fragmented DNA, if the cells cannot divide. Indeed, MTX treatment of monocytes led to enhanced cellular fusion and the formation of multiple nucleated giant cells upon phorbol esters stimulation (Tian and Cronstein, 2007).

1.8.1 Megaloblastic anaemia

Megaloblastic anaemia is a clinical manifestation of both cobalamin and folate-deficiency (John Lindenbaum, 1994). It is characterised by the presence of megaloblasts in the bone marrow and neutrophil hypersegmentation, clinically defined as having more than 5% five-lobed or any six-lobed cell per 100 granulocytes (John Lindenbaum, 1994) (Fig 1.9). Macrocytosis, an increase in the mean corpuscular volume also occurs due to continued
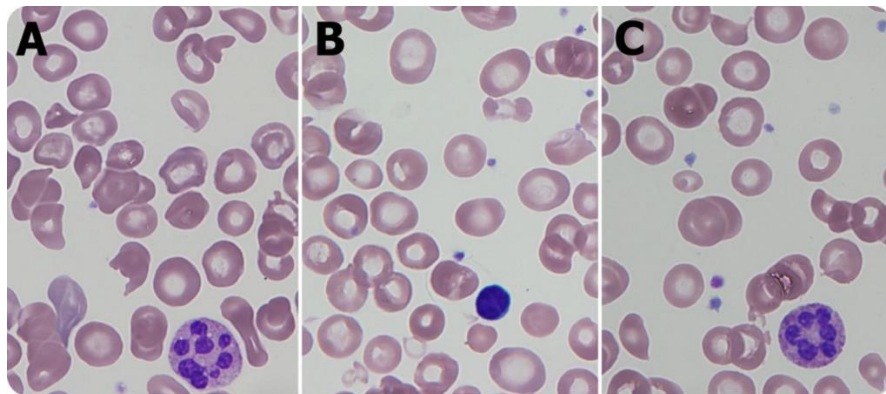
Figure 1.9. The clinical manifestations of folate or cobalamin deficiency.

(A&C); a blood smear demonstrating hypersegmented neutrophils and red blood cell fragments. (B), macrocytes. Taken from Li and Sieff (2016).

cell growth without division. It is thought to occur as a result of a disturbance of DNA synthesis in the bone marrow (Hoffbrand, 1973). Although defects usually occur in the bone marrow, chromosome breaks have been observed in both bone marrow cells and leukocytes from patients with megaloblastic anaemia (Keller and Norden, 1967).

The anti-folate, MTX induces a state of folate-deficiency. As such, megaloblastic anaemia has been reported during low-dose MTX treatment in RA patients. The mean corpuscular volume was also found to increase in patients on low-dose MTX treatment. Low-dose MTX treatment has also been shown to result in DNA fragmentation (see Section 1.10.1) (Weinblatt and Fraser, 1989). However, megaloblastic anaemia was not shown to occur due to the reduction in thymidylate following folate-deficiency, as PHA-stimulated lymphocytes from untreated megaloblastic anaemic patients were not found to have decreased thymidylate concentrations (Hoffbrand, 1973). This suggested that megaloblast formation following low-dose MTX treatment may be due to a different consequence of folate-deficiency.

1.9 The apoptotic effect of MTX

The extent of apoptosis induced by MTX has been shown to depend on the activating stimulus, the growth phase of the cell and the dose and duration of MTX treatment. In immortalised cell lines it is generally accepted that MTX causes cell death but at various doses. MTX (100 nM) caused significant cell death in Human Leukemic T lymphoblasts and Jurkat T lymphoblasts (da Silva et al., 1996). MTX (1 µM) significantly reduced cell viability in A549 cells (Huang et al., 2011). MTX (2 µM) caused significant cell death in Ehrlich ascites tumour cells (Li and Kaminskas, 1984). Higher doses of MTX were required to cause cell death in Jurkat T cells as MTX (0.1 µM) did not significantly increase cell death after 48 h (Spurlock et al., 2011). 48 h also proved too short a duration in CaSki and NRK cells, as treatment with MTX (1 µM) did not induce cell death after this time (Mazur et al., 2009).

For primary cells the extent of cell death is also cell-type-dependent and varies with different stimuli but the most important factor is that the cells are dividing. MTX (2.2 µM), higher than low-dose treatment (<1 µM), was shown to cause significant apoptosis in anti-CD3- and CD28-activated CD4^{+} and CD8^{+} T cells in comparison to the untreated

control (Strauss et al., 2002). The same concentration of MTX caused (30% and 60%) apoptosis in PMA- and ionomycin-activated PBMCs (Quemeneur et al., 2003). MTX (0.05 μM) also caused significant increases in cell death after 4 days treatment of PBMCs cultured in concavalin A or PHA (Tohyama et al., 2013). Up to 1 μM MTX was shown to induce apoptosis in PBMCs already activated with PHA (Herman et al., 2003, Swierkot et al., 2004). Folate-deficiency also increased the apoptosis of CD4^{+} and CD8^{+} T cells activated with PHA (Courtemanche et al., 2004).

The differential cytotoxic effect of MTX in non-dividing verses dividing cells was verified, when PBMCs stimulated with tetanus toxin (TT) or candida albicans (CA) showed no increase in apoptosis in non-dividing cells. In dividing cells however, an increase in the proportion of apoptotic cells was found following high-dose MTX (22 μM) treatment (Nielsen et al., 2007). This was also the case for dividing T-helper cells, stimulated with TT or CA, whereby MTX treatment caused a six-fold increase in the proportion of apoptotic cells (Herman et al., 2005). Further evidence was shown when peripheral blood lymphocytes (PBL) activated with either PHA or concavalin A underwent apoptosis following MTX (1 μM) treatment, but not in the resting lymphocytes (Genestier et al., 1998). The same authors also showed that lymphocytes exposed to MTX (1 μM) treatment following activation with anti-CD3, or PMA and ionomycin, also induced apoptosis but not in the resting lymphocytes. However, one report was found where MTX had no effect on cell viability which was more than 95% after whole blood-activation with CD28 and anti-CD3 (Haroon et al., 2008). A possible explanation for these findings is that these cultures were isolated from RA patients on low-dose MTX treatment, which may have become desensitised to the effects of MTX.

1.9.1 DNA damage in response to MTX

The reduction in thymidylate, following culture in folate-deficient media or media supplemented with uracil moieties, leading to an increase in uracil has been shown to result in DNA strand breaks. CD4^{+} and CD8^{+} T cells cultured in low levels of folate-conditioned media, had elevated uracil incorporation in DNA and were stuck in the S phase of the cell cycle (Courtemanche et al., 2004). Patients with folate-deficiency had increased incorporation of uracil and chromosome breakage in whole blood DNA (Blount

et al., 1997). Human hepatoma HepG2 cells also showed DNA fragmentation preceding apoptosis following folate-deficiency (Huang et al., 1999). Supplementation with deoxyuridine (100 µM) significantly increased the DNA damage in HeLa cells cultured in folate-replete conditions, suggesting that uracil moieties could damage even healthy cells (Duthie and McMillan, 1997).

MTX treatment was also shown to lead to DNA fragmentation (Jackson, 1978). MTX (2 µM) led to DNA strand breaks in NIH 3T3R cell and in Ehrlich ascites tumour cells (Li and Kaminskas, 1984, Lorico et al., 1988). MTX (1µM) induced DNA strand breaks in PHA-activated PBLs (Genestier et al., 1998). MTX (60 nM) was also found to induce DNA fragmentation in rat intestinal epithelial cells (Papaconstantinou et al., 2001).

However, DNA fragmentation does not necessarily correspond to cytotoxic effects on cell viability or proliferation. Uridine supplementation resulted in DNA fragmentation but did not correlate to cytotoxic effects on cell proliferation (Martiniova et al., 2015). The addition of deoxyuridine (100 µM) had no effect on cell proliferation in HeLa cells cultured in folate-replete conditions (Duthie and McMillan, 1997). A higher dose of deoxyuridine (10 mM) also had no effect on proliferation in mouse lung fibroblast CCL39 cells (Ingraham et al., 1986). Treatment with TS inhibitors 5-FU and 5 FrUrd, increased uracil in the DNA of Ung -/- MEFs leading to a reduction in cell proliferation but had no effects on cell viability (Andersen et al., 2005).

Indeed one form of uracil, deoxyuridine has even been shown to be protective. Deoxyuridine administered to folic acid-deficient mice, rescued these mice from neural tube defects (NTDs) resulting from DNA fragmentation (Martiniova et al., 2015). This was shown to be a result of increasing plasma folate levels as deoxyuridine supplementation raised folate levels compared to control mice. Indeed, deoxyuridine was shown to replenishing dUMP levels via thymidine kinase and thus enter the de novo pathway of thymidylate synthesis (Garavito et al., 2015).

The toxicity shown by uracil has in some cases been shown to be due to the removal, not the presence of uracil in DNA. Since the ability to excise uracil varies among human cell lines, it is possible that this also contributes to the differential effects of MTX in different cell types (Visnes et al., 2008). Removal of uracil residues 12 base pairs apart on opposite plasmid DNA strands was shown to produce double strand breaks (Duthie and McMillan, 1997). Unwound DNA, which occurs during the repair process, was shown to leave the

DNA vulnerable to nucleases. Thus the apurigenic sites or DNA strand breaks induced by the repair mechanism were found to be toxic. Little difference was found in the cytotoxicity incurred in DNA repair knockouts compared to healthy controls. One such study treated MEFs with the thymidylate synthase inhibitor, 5-flurouracil (5-FU) (5 µM) and found only a slight difference in growth inhibition in Ung-/- compared to WT MEFs despite the increase in the levels of uracil in the genome (Andersen et al., 2005). Apoptosis following a 24 hr MTX (100 µM) treatment occurred more frequently in MMR-competent Hela cells and the human colon tumour cell line, HCT116 compared to those unable to remove uracil (Frouin et al., 2001). Cytotoxicity upon removal of uracil has been observed for several cytotoxic drugs, including alkylating and methylating agents as well as platinum compounds (Frouin et al., 2001). Even in bacteria, the toxicity of thymine starvation was reduced when the Uracil-DNA glycosylase was impaired (Ingraham et al., 1986). Of further note, supplementation with Uracil-DNA-glycosylase, significantly increased the DNA damage of lymphocytes cultured under folate-deficient conditions (Duthie and McMillan, 1997).

However, it is impossible to study the toxic effect of uracil alone, as it is still unclear how much uracil toxicity is attributed to the toxicity induced by thymidine-deprivation.

The positive and negative effects of low-dose MTX are interlinked. The mechanisms in which MTX acts therapeutically are probably the same ones which cause the side effects in healthy cells. Even the putative role of adenosine production, (see Section 1.16) shown to have a high anti-inflammatory potential, occurs alongside inhibition of purine synthesis, and could thus potentiate toxicities in healthy dividing cells. It is also possible that some inhibitory effects of MTX on 1C metabolism are less potent than others, because of the presence of compensatory-biosynthetic processing pathways. The other route of methionine synthesis via betaine-homocysteine methyltransferase (BHMT), using betaine, is one such pathway (Sunden et al., 1997). This may suggest that the therapeutic effects of MTX are attributable to inhibitory effects on specific 1C metabolism pathways. However, because these pathways are linked, partial inhibition could still contribute to the effects of MTX.

1.10 Mitochondrial function

The pathways of one-carbon metabolism (1C) and ATP synthesis by the electron transport chain (ETC) are interdependent. 1C metabolism was shown to fuel the ETC by supplying 50% of the NADPH reductive equivalents via the mitochondrial SHMT. This was shown to occur using the mitochondrial isozyme, methylene-THF dehydrogenase (MTHD2) which can produce either NADH/NADPH during the conversion of 5,10-methylene-THF to 5,10-methenyl-THF. The malic enzyme and the pentose phosphate pathway accounted almost equally for the remaining 50% (Brosnan et al., 2015). Adequate flux of these one-carbon donors in the mitochondria was shown to be dependent on the respiratory state of the mitochondria, maintained by the ETC (Garcia-Martinez and Appling, 1993). This process was found to be dependent on an adequate mitochondrial inner-membrane potential and a proton gradient to drive the synthesis of ATP from the ATP synthase (Fig 1.10) (Voet, 1990).

1.10.1 The mitochondrial inner-membrane potential and MTX

The importance of a functioning mitochondrial inner-membrane potential ($\Delta\Psi_m$) is demonstrated by the toxic effects of compounds that affect this potential. Dissipation of the $\Delta\Psi_m$ is one of the first steps preceding apoptosis, prior to cytochrome c release. Protonophores that dissipate this $\Delta\Psi_m$ uncouple ATP synthesis from oxygen consumption, so that the cell cannot utilise the energy contained in the reductive equivalents to make ATP. Matrix condensation, a step in the apoptotic pathway, can even be induced in mitochondria isolated from healthy cells, by either denying oxidisable substrates or by protonophores that dissipate the $\Delta\Psi_m$ (Gottlieb et al., 2003). Oligomycin, an ATP synthase inhibitor, prevents the utilisation of this $\Delta\Psi_m$, by hyperpolarising the $\Delta\Psi_m$ and dissipating cellular respiration, inhibiting the workings of the cell (Jeremy M.Berg, 2007).

In light of the interdependence of these processes, insults to 1C metabolism, drug- or damage-induced, can reflect changes in mitochondrial function; in particular the $\Delta\Psi_m$, limiting energetic output and impeding cellular function. In addition to affecting 1C metabolism, MTX was also shown to affect the $\Delta\Psi_m$. PHA-activated PBL treated with MTX (1 μM) had a reduced $\Delta\Psi_m$ (Genestier et al., 1998). The same dose significantly reduced the $\Delta\Psi_m$ in HL-60 cells as well as IEC-6 cells isolated from the rat jejunum crypt
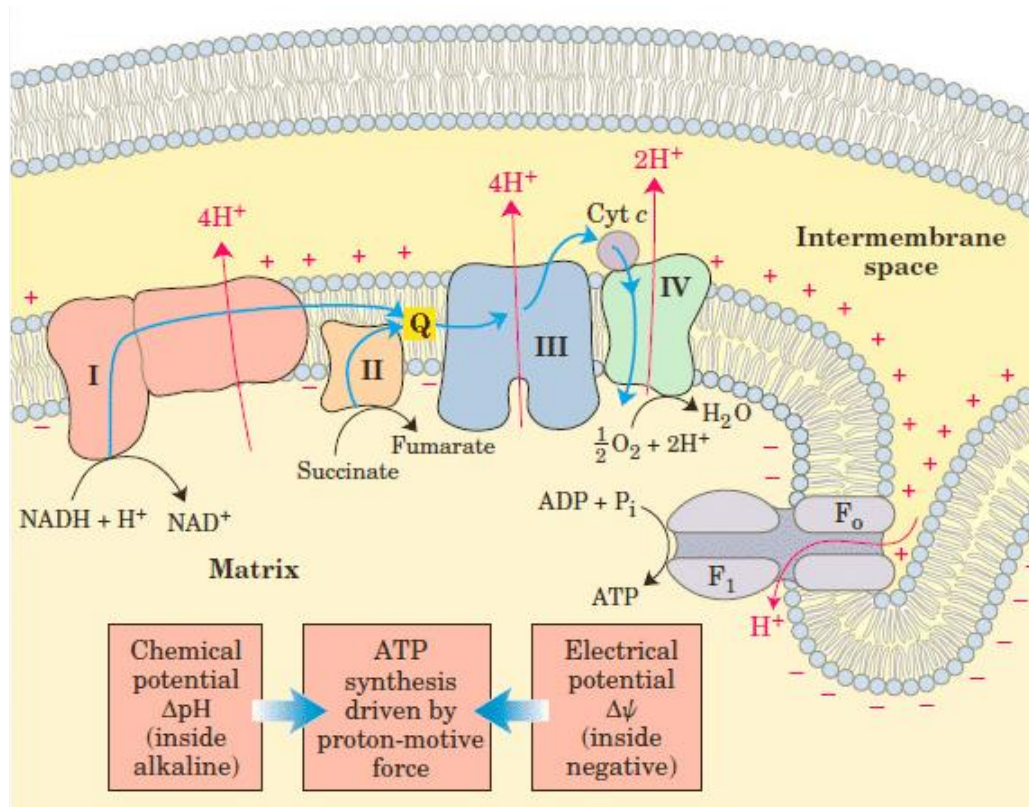
Figure 1.10. Electron transport and the production of ATP by the electron transport chain.

Oxidation of substrates malate and succinate result in the reduction of the cofactors, producing NADH and FADH$_2$ whose electrons enter the ETC at complex I and II. The electrons are transferred between complexes (arrows), promoting proton (H$^+$) transport from the matrix to the intermembrane space. This creates an electrical and chemical gradient, called the mitochondrial inner-membrane potential $\Delta\Psi_{\mathrm{m}}$, used to drive the synthesis of ATP as protons flow down this gradient, through ATP synthase (complex V) converting ADP to ATP. Electrons having passed through the complexes are then used to reduce molecular oxygen to water at complex IV. Taken from Crisóstomo (2013).

(Huang et al., 2005, Chang, 2013). Folate-deprivation depolarised the $\Delta\Psi_m$ in cultured embryonic cortical neurons and in DRG neurons (Ho et al., 2003, Tjiattas et al., 2004). Another study investigated the effect of MTX on the $\Delta\Psi_m$ of peripheral lymphocytes from South African RA patients, using the dimeric-potential dependent dye, JC-1 (Moodley et al., 2008). However, their results have not been taken into consideration since neither the concentration of JC-1, nor the wavelength used to measure the monomeric/aggregate fluorescence of JC-1 was stated. No papers have been found regarding the effect of MTX on the $\Delta\Psi_m$ in both activated and unactivated PBMCs to investigate if this contributes to the anti-inflammatory effect.

1.10.2 ROS

Loss of mitochondrial function can also be assessed by measuring changes in the rate of ROS production. ROS (Reactive Oxygen Species) is the collective name for oxygen radicals and their non-radical derivatives such as hydrogen peroxide or singlet oxygen. Single electrons which exit the ETC prior to the reduction of molecular oxygen to water can be transferred to molecular oxygen, creating superoxide, and other ROS such as hydrogen peroxide, upon the action of superoxide dismutase (SOD). Electron leakage can occur at complex I and III, but other mitochondrial enzymatic complexes are also sources of ROS including the dihydrolipomide dehydrogenase containing FAD-linked pyruvate and α-ketoglutarate dehydrogenase complexes (Starkov et al., 2004). The flavoenzyme α-glycerophosphate dehydrogenase was also shown to be a source of ROS as well as the electron-transferring flavoprotein:Q oxidoreductase (ETFQOR) of fatty acid β-oxidation (St-Pierre et al., 2002, Tretter et al., 2007).

Electron leakage at complex I occurs at two sites where the transfer of electrons takes place, first on to the flavin mononucleotide site and after electrons have passed down a chain of iron-sulphur centres to the ubiquinone binding site. At both these sites, electrons react with molecular oxygen, forming superoxide within the matrix (Kussmaul and Hirst, 2006, Hirst et al., 2008). Leakage of electrons from complex III is thought to occur when ubiquinol binds to the ubiquinone site, where its electrons can bypass their normal transfer in the ubiquinone cycle and react directly with oxygen to form superoxide. However, the contribution of ROS production under conditions of uninhibited complex

III, is thought to be minor (Murphy, 2009). In addition, the membrane-bound NADPH oxidase and xanthine oxidase are also sources of superoxide (Cross and Templeton, 2006).

In addition to ROS, other types of reactive species exist including Reactive Nitrogen Species (RNS). These are nitric oxide radicals, formed from the oxidation of one of the terminal guanido-nitrogen atoms of L-arginine by nitric oxide synthase (NOS), and can be converted into other RNS including the nitrosonium cation (NO1), nitroxyl anion (NO2) or peroxynitrite (Stowe and Camara, 2009).

Loss of mitochondrial function, via dissipation of the $\Delta\Psi_m$, can also induce changes in ROS production. Damage to the components of the ETC, such as complex I or II, which provide the electrons from substrates to the ETC to pump protons into the intermembrane space, creating the electrochemical potential, can dissipate the $\Delta\Psi_m$. In this case, damage to complex I or III, results in reduced rates of ATP synthesis and electron transfer between the different complexes, increasing the chance of electron leakage from complex I and III. Uncoupling ATP synthesis to respiration following treatment with protonophores, such as FCCP, can dissipate the $\Delta\Psi_m$ and reduce electron leakage from complexes I and III, because electron transfer is not limited by ATP production, a process analogus to the effects of uncoupling proteins (Brand and Esteves, 2005). Thus, insults to mitochondrial function are interlinked and the measurement of both the $\Delta\Psi_m$ and ROS production can provide some insight into how mitochondrial function has been affected.

ROS are dynamic molecules with a variety of cellular functions including the induction of cell death, cell signalling and activation, as well as in disease pathogenesis. These diverse effects are mediated by alterations in the concentration, duration and location of ROS production. ROS has also been shown to have both anti-inflammatory and inflammatory effects. ROS are implicated in RA disease pathogenesis, in particular in proliferative synovitis (Mirshafiey and Mohsenzadegan, 2008). Neutrophils and lymphocytes isolated from the peripheral blood of synovial fluid of RA patients had higher levels of cellular ROS, which coincided with an increase in NADPH oxidase activity (Kundu et al., 2012, Mateen et al., 2016). These high levels of intracellular ROS were matched with a decrease in synovial fluid and serum antioxidants (Mirshafiey and Mohsenzadegan, 2008). However, ROS levels have also been found to be decreased in CD4^{+} T cells from

RA patients (Yang et al., 2013). This suggests that ROS has differential effects even in RA disease pathogenesis. These differential effects may even be anti-inflammatory. A reduced capacity to produce ROS, following a polymorphism in the respiratory-burst oxidase component neutrophil cytosolic-factor 1 (Ncf1), increased RA disease severity in rats by the activation of arthritrogenic T cells. Other defects in the oxidative burst, leading to a lowered burst capacity, were found in more severe collagen-induced arthritis animal models (Mirshafiey and Mohsenzadegan, 2008).

These diverse roles of ROS in inflammation are paralleled with the differing effects of ROS on cell death. ROS has been shown to induce cell death at high concentrations and inhibit cell cycle progression via the expression of the cell cycle inhibitor p21 (DROGE, 2002). However, ROS can also prevent the induction of apoptosis (Cross and Templeton, 2006). These different roles could be explained by the main instigator of ROS in RA, TNFα which has been shown to induce both cell death and survival responses via ROS. The mechanism behind ROS production was found to be the activation of the NADPH oxidases in both leukocytes and fibroblasts (DROGE, 2002). TNFα-induced apoptosis was found to be mediated in part by mitochondrial ROS, as well as the activation of caspases and DNA fragmentation. TNFα- induced cell survival was shown to be mediated by the ROS-activation of NF-kB and increased expression of genes such as BCL-2 and superoxide dismutase (Mirshafiey and Mohsenzadegan, 2008).

Interestingly, it was suggested that bi-directional regulation could be in place as pre-treatment of cells with N-acetylcysteine (NAC), or the antioxidant, cysteine to prevent ROS production was shown to inhibit the TNFα-induced activation of NF-kB (DROGE, 2002, Cross and Templeton, 2006). This also suggested that ROS had a crucial role in signalling. Specifically, mitochondrial-derived ROS was shown to have roles in signalling, as disruption of the ETC interfered with this TNFα signalling process (Cross and Templeton, 2006). Mitochondrial ROS, via complex III was found to be crucial for the NF-AT-induced activation of CD4^{+} T cells (Sena et al., 2013). This modulation by ROS was shown to be via the redox-responsive signalling cascades; in particular the reversible oxidation of cysteine residues (Cross and Templeton, 2006). Indeed, oxidative modification of conserved cysteines has been shown to regulate the activities of the transcription factors NF-kB, AP-1, p53, HIF-1α, and c-Myc. In synovial T lymphocytes, ROS was found to alter functional characteristics of the TCR, specifically cell-surface

thiols, to influence T cell signalling. This increase in cell-surface thiols directly increased T cell-activation and proliferation, potentiating the inflammatory response (Mirshafiey and Mohsenzadegan, 2008).

However, the role of ROS in T cell-activation was found to be concentration-dependent. Low concentrations (10 µM) of hydrogen peroxide enhanced IL-2 production during T lymphocyte activation, but high concentrations (100 µM) completely inhibited IL-2 (DROGE, 2002). Elsewhere, ROS has also been shown to suppress T cell-activation. Oxidative conditions, following the artificial reduction in intracellular glutathione levels (GSH) mediated by BSO or after prolonged exposure to oxidative stress, impaired the anti-CD3-mediated release of IL-2 following T cell-activation (Gringhuis et al., 2000, DROGE, 2002). Both reports also showed that this suppression of T cell-activation was reversed by NAC, indicating that ROS was responsible. ROS affected the proliferation of anti-CD3/CD28 activated synovial fluid (SF)-T lymphocytes as the partial restoration of proliferation was achieved upon NAC treatment (Maurice et al., 1997). In Jurkat T cells, pre-exposure to hydrogen peroxide before TNF activation led to a reduction in NF-kB transcription (Lahdenpohja et al., 1998). The hypoxic environment of the synovial joint was also shown to have suppressive effects. T cells isolated from the SF were less responsive and displayed complete absence of phosphorylation of LAT, a crucial step in the signalling pathway towards IL-2 production, when activated with anti-CD3, compared to those from the peripheral blood of RA patients and healthy controls. Indeed, the suppressive effect of ROS on T cell activity was shown to be due to the redox-sensitive subcellular localization of LAT (Flescher et al., 1994).

MTX has been shown to directly affect the cellular redox state by increasing ROS production by increasing products of ROS oxidation, such as lipid peroxidation, or by reducing ROS scavengers. Jurkats and U937 monocytes exhibited marked increases in peroxide with up to MTX (1 µM) treatment (Phillips et al., 2003). Even at the lower dose of MTX (0.1 µM) an increase in ROS production in Jurkat T cells was found (Herman et al., 2005). Primary T cells activated with PHA, also showed a significant increase in cellular peroxide levels, after 4 h and 16 h with MTX (1 µM) treatment (Phillips et al., 2003). Folate-deprivation also increased ROS production. Culture for 2 h in folate-depleted conditions was shown to increase intracellular ROS in cultured embryonic murine cortical neurons, differentiated SH-SY-5Y human neuroblastoma cells and DRG neurons, as well as after 3 weeks in Hep G2 cells (Chern et al., 2001, Ho et al., 2003,

Elango et al., 2014). However, MTX has also been found to reduce ROS production in some studies. MTX (1 µM) reduced the superoxide production in neutrophils primed with LPS or TNF (Okuda et al., 1997). Another study showed that MTX 1 µg/ml (2.2 µM) reduced ROS production in fibroblast like-synoviocytes (Ji-Yeon Sung a et al., 2000).

Overall, most studies suggest that MTX increases ROS by a variety of mechanisms. The main mechanism has been suggested to be inhibition of the reduction of dihydropterin to tetrahydropterin, a nitro oxide precursor, as the addition of tetrahydrobiopterin, prevented the MTX (1 µM) induced ROS production in Jurkat cells (Spurlock et al., 2011). A reduction in glutathione levels were shown to be responsible for the MTX-induced increase in ROS in both cultured embryonic murine cortical neurons, differentiated SH-SY-5Y human neuroblastoma cells, as well as Jurkat and U937 monocytes (Ho et al., 2003, Phillips et al., 2003). The MTX-induced increase in homocysteine was also thought to be responsible for the rise of ROS production in folate-deficient Hep G2 cells as the levels of homocysteine increased as ROS production increased (Chern et al., 2001). Interestingly, the reduction in the one-carbon donors THF and 5-methyl-THF upon MTX treatment could also contribute to the MTX-induced increase in ROS, as both have been shown to be potent antioxidants (Rezk et al., 2003). It has not yet been explored whether depletion of these key 1C intermediates is also responsible for the increase in ROS production by MTX.

1.10.3 ROS as a mechanism of MTX-induced cell death

ROS production is associated with cell death in both folate-deficient and MTX-treated conditions. The increased intracellular ROS following culture in folate-depleted conditions was shown to cause DNA fragmentation and phosphatidylserine (PS) externalisation, indicating apoptotic death in both cultured embryonic murine cortical neurons and differentiated SH-SY-5Y human neuroblastoma cells (Ho et al., 2003). Following MTX treatment, an increase in ROS has been shown to accompany apoptosis with caspase 3 activation in tissues from psoriatic arthritis patients (Elango et al., 2014). The prevention of MTX-induced cell death upon the addition of ROS scavengers was definitive proof that ROS was a mechanism of MTX-induced cell death. The cytotoxicity of MTX (1 µM) in IEC-6 cells was reduced by a natural ROS scavenger, lutein (Chang,

2013). ROS scavengers also reduced the MTX (1 µM)-induced apoptosis in HL-60 cells (Huang et al., 2005). The MTX (0.1 µM)-induced growth arrest in U937 monocytes was also prevented by the anti-oxidant, NAC (Phillips et al., 2003). NAC also prevented the apoptosis of Jurkat T cells following MTX (0.1 µM) treatment as well as the cell death induced by both MTX (0.1 µM) and the ligation of the death receptor FAS, using anti-FAS (Spurlock et al., 2011).

1.11 Signalling pathways activated by MTX

The mechanism in which low-dose MTX has been shown to activate cell death is both dose- and cell type-dependent. Cell death following high dose MTX (2.2 µM) treatment of anti-CD3/CD28-activated $CD4^+$ and $CD8^+$ T cells was shown to be accelerated by FAS-FAS-ligand-mediated apoptosis (Strauss et al., 2002). But in T cells from mice, low-dose MTX caused cell death which was found to be FAS-independent (Izeradjene et al., 2001). Apoptosis was prevented using a caspase inhibitor z-VAD-fmk in HL-60 cells, demonstrating that MTX (1 µM) induced caspase-dependent cell death in this cell line (Huang et al., 2005). Caspase 9, 2 and 3 were induced in rat intestinal epithelial cells following MTX (60 nM) treatment and caspase 9 in the JAR carcinoma cell line following a higher concentration of MTX (220 nM) (Papaconstantinou et al., 2001, Chen et al., 2009). This activation of caspase 9 was followed by loss of the mitochondrial membrane potential and up-regulation of BAX and BCL-2 expression. In other cell types, MTX (10 nM and 2.2 µM) induced cell death via PARP cleavage in MMR defective Hec59 cells and in CA or TT stimulated PBMCs, respectively (Nielsen et al., 2007, Martin et al., 2009). Jun, a JNK target gene was increased in the blood of RA patients on MTX treatment (Spurlock et al., 2011). In vitro, MTX (0.1 µM) also induced JNK activation followed by expression of p53 in PBMCs, Jurkat T cells and anti-CD3-activated T cells but not in fibroblast-like synoviocytes (FLS) (Spurlock et al., 2011, 2014, 2015). This p53-dependent cell death induced by MTX was also found in the immortalised A549 and Hep-2 cell lines with MTX (1 µM and 50 nM), respectively (Kraljevic Pavelic et al., 2008, Huang et al., 2011).

There are mixed reports with regard to the effect of MTX on NF-kB. MTX (0.1 µM) was shown to inhibit NF-kB activation in TNFα-stimulated Jurkat and primary T cells but not

in FLS (Spurlock et al., 2014, 2015). The MTX (1 µM)-mediated inhibition of TNFα-induced NF-kB was not observed in either HeLa or Jurkat cells, except at high doses (>5 µM) (Majumdar and Aggarwal, 2001).

1.12 Nucleotide salvage

There are reports where extracellular nucleotides have been shown to potentiate drug-induced toxicities. However, it is understood that in most cases, salvage pathways of both purine and pyrimidine synthesis minimise insults to de novo pathways from drugs or nutrient starvation, by repleting nucleotide levels. These salvage pathways rely on phospho-ribosyl-pyrophosphate (PRPP) and both intracellular as well as extracellular nucleosides and bases such as those present in human sera (Chong et al., 2010). Every cell has some salvage capacity, but most cell types use a combination of de novo and salvage pathways (Budzik et al., 2000). However, these differential nucleotide requirements can change during cellular activation. It was shown that activated T cells are totally dependent on de novo pyrimidine synthesis (Evans and Guy, 2004). PHA-activated human $CD4^+$ and $CD8^+$ T cells were shown to contain 8-fold more pyrimidines and only 2-fold more purine nucleotides (Fairbanks et al., 1995). MTX, however was also found to inhibit an enzyme involved in nucleotide salvage, specifically deoxycytidine kinase responsible for phosphorylating the preformed nucleosides, deoxyadenosine, deoxyguanosine and deoxycytidine into their monophosphate forms, (Uga et al., 2006). This suggests that salvage cannot completely circumvent MTX-inhibition and may explain why the effects of MTX at the same concentration vary for different cell types.

1.12.1 Pyrimidine salvage

Mammalian cells possess transport mechanisms for both purine and pyrimidine nucleosides and bases (Pickard and Kinsella, 1996). The principle salvage pathways for pyrimidines however, involve conversion of nucleosides to nucleotides (Mathews, 2015). The extent to which nucleobases can be salvaged in mammalian cells is still unclear (Garavito et al., 2015). Uptake of both pyrimidine- and purine- nucleobases as well as

nucleosides, has been shown for a variety of different organisms, which replenish nucleotide levels through various pathways (Fig.1.11).

1.12.2 Purine salvage

Purine salvage pathways also work to minimise imbalances in purine homeostasis. Similar to pyrimidine salvage, pathways exist to synthesise nucleotides and nucleosides from free base precursors (Fig 1.12.). In humans, hypoxanthine is the principle salvageable purine nucleobase in the bloodstream and is transported by various nucleobase transporters and ENT 2 (Kong and Wang, 2003). In order for any drug-induced toxicity to occur, these salvage precursors, including PRPP, must be depleted. 20-fold more thymidine was needed in LA9 cells deficient in cytoplasmic TK than in control cells upon MTX (10 µM) treatment (Bogenhagen and Clayton, 1976). Limiting these salvage precursors was only achieved with high-dose MTX (10 µM) in human embryo fibroblast cell lines (Pickard and Kinsella, 1996). Salvage pathways are so pertinent for cellular homeostasis that they have even been targeted by inhibitors of nucleoside transport to potentiate the toxicity of anti-metabolites (Kong and Wang, 2003). Tumour cells were also found to exploit these pathways to resist chemotherapeutic drugs (Pickard and Kinsella, 1996). The salvage pathways were even shown to limit the effects of thymidylate synthesis inhibition on mitochondrial DNA (mtDNA) as uracil levels only increased by 40% in SHMT-/- CHO cells. However, the workings of the salvage pathway were not absolute, as salvage thymidylate synthesis was not found to be sufficient to sustain mtDNA replication (Anderson et al., 2011).
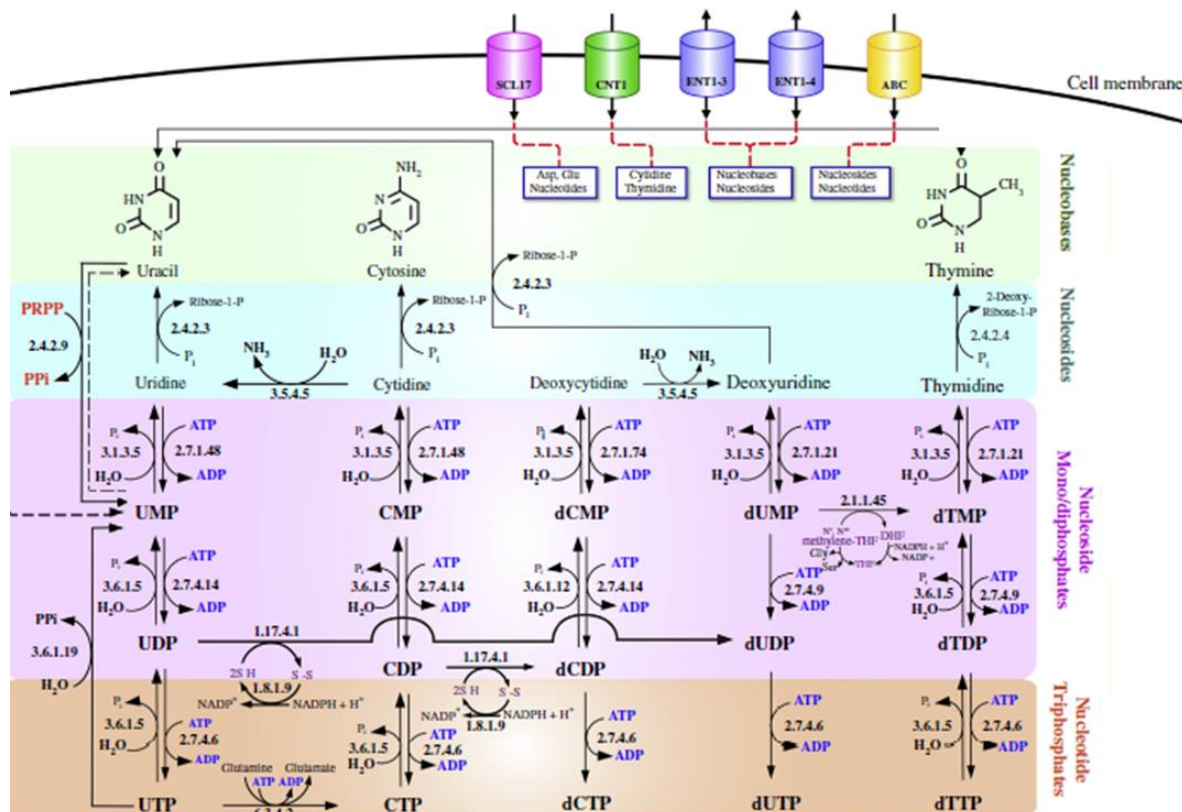
Figure 1.11. Uptake of pyrimidine nucleobases, nucleosides or nucleotides and their interconversion in a variety of organisms.

The solute carrier family (SCL17) takes up both amino acids (aspartate and glutamate) and nucleotides; the equilibrative nucleoside transporters (ENTs) can transport nucleosides while the ABC transport family imports nucleotides and nucleosides into the cell. Nucleobases are taken up by the concentrative nucleoside transporters (CNT1) and the ENT. The purine salvage pathways include nucleotide synthesis from uptake of either nucleobases or nucleosides. These nucleobases are converted to nucleotides via PRPP. Nucleobases can also be converted to nucleosides by specific phosphoribosyl-transferases (cyan). These nucleosides may be phosphorylated to form nucleoside monophosphates, diphosphates and triphosphates by nucleoside kinases. Nucleoside diphosphates can then be transformed into deoxynucleosides by the ribonucleotide reductase system. Salvage is also apparent at the interconversion of nucleosides with different bases. The principal salvage pathways for pyrimidines include conversion of the nucleosides to nucleotides. Adapted from Garavito et al. (2015).
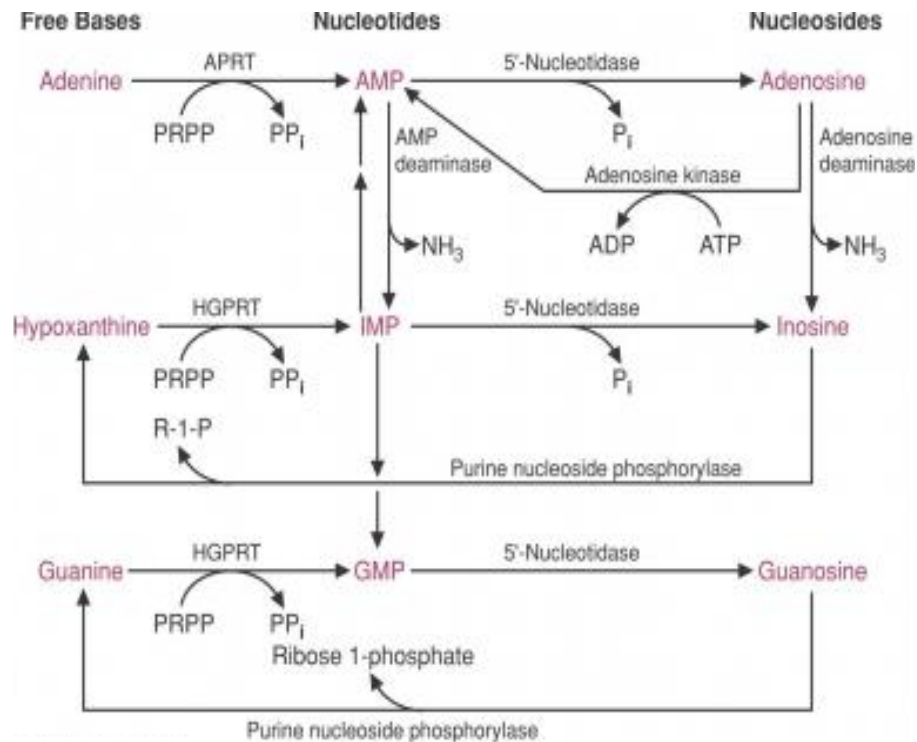
Figure 1.12. The interconversion of purine nucleobases, nucleosides, and nucleotides.

Purines (hypoxanthine and guanine) and adenine can be converted to their corresponding nucleotides using hypoxanthine-guanine phosphoribosyltransferase (HGPRT) and adenine phosphoribosyltransferase (APRT), respectively. Purine nucleotides can be converted to their corresponding nucleosides using extracellular 5'-nucleotidases. Adenine and hypoxanthine-based nucleotides can replenish each purine nucleotide. Adenosine feeds into the inosine pathway for the phosphorylase-catalysed conversion into the free base, regenerating ribose 1-phosphate. Guanosine nucleosides are also degraded to the free base and ribose 1 phosphate. Taken from (studydroid).

1.13 Thymidine rescue from MTX

In vitro the effects of MTX can be circumvented by exploiting the salvage pathways through the addition of thymidine and hypoxanthine. The addition of thymidine can replenish thymidylate levels through thymidine kinase (TK) (Fig 1.13). This overrides the MTX-inhibition of *de novo* thymidylate synthesis, preventing cell death. The addition of thymidine was shown to rescue cells in the S phase of the cell cycle from MTX-induced apoptosis (Paillot et al., 1998). Thymidine was found to prevent the apoptosis induced by MTX (1 µM and 2 µM) in NIH 3T3R cells (Genestier et al., 1998, Lorico et al., 1988). Thymidine was also shown to prevent the peripheral elimination of a specific subset of T cells, Vb8^{+} T cells (Izeradjene et al., 2001).
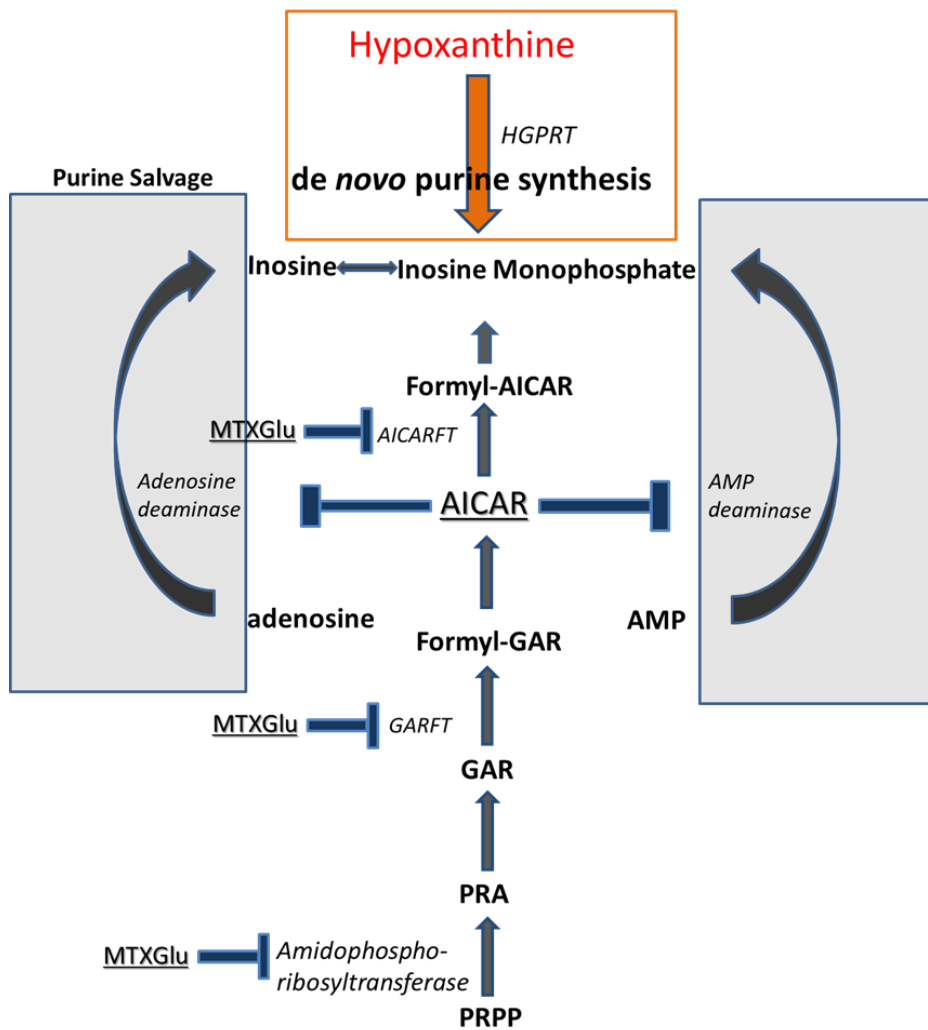
1.14 Purine rescue from MTX

In vitro, rescue of purine synthesis is achieved by the addition of the end stage nucleotide, hypoxanthine. This nucleotide feeds into pathways from which the purine nucleotides GMP and AMP can be synthesised (Fig 1.14). However, different cells have differential requirements for thymidine and hypoxanthine for maintaining cellular homeostasis and/or during proliferation. Hypoxanthine or adenine (but not thymidine) restored the cellular proliferation of B cells stimulated with anti-Ig and B-cell growth factor, following MTX (100 nM) treatment (Rosenthal et al., 1988). The same authors showed that proliferation could not be restored with the addition of guanine because guanine does not replenish the levels of AMP or IMP. In most cases, rescue from MTX treatment has been shown to require both thymidine and hypoxanthine to replete nucleotide levels. Thymidine and hypoxanthine, (but not hypoxanthine alone), rescued the growth of the human T cell line CEM, following MTX (1 µM) treatment (Budzik et al., 2000).
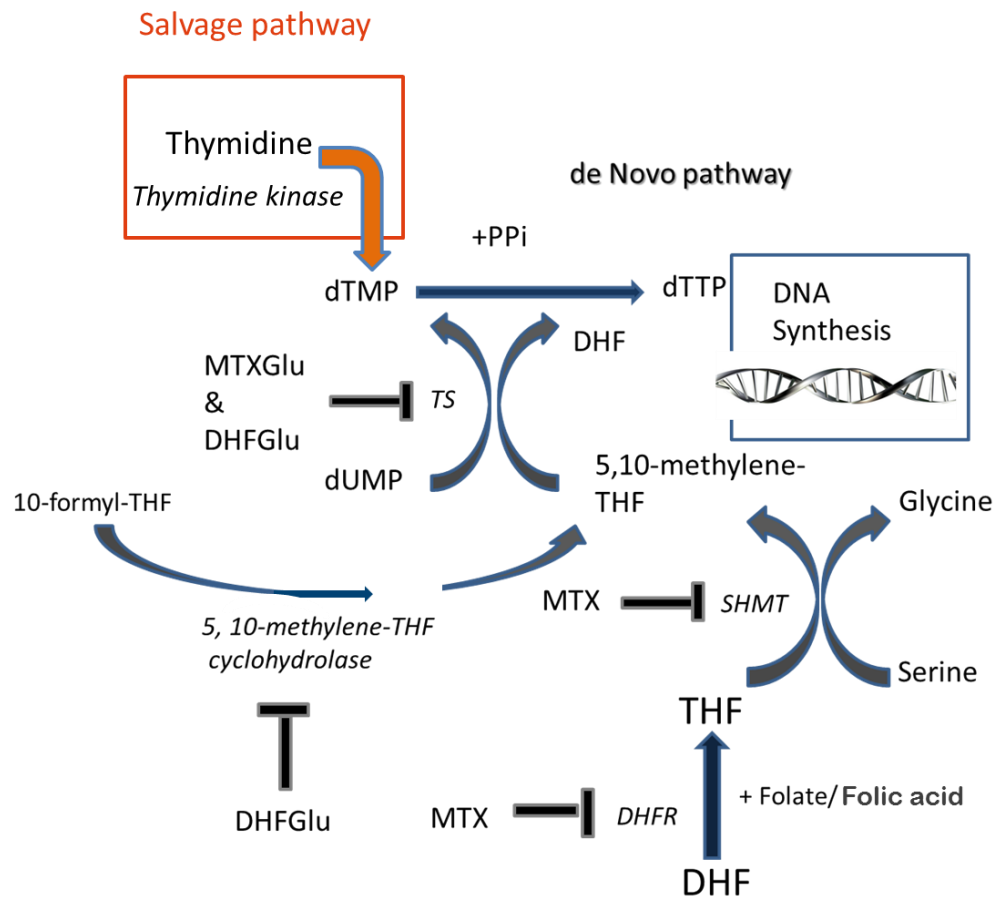
Figure 1.13. Recovery of thymidylate from MTX and MTXGlu inhibition.

The addition of thymidine feeds through the salvage pathway through thymidine kinase, replenishing thymidylate levels after MTX and MTXGlu-mediated inhibition of the 1C metabolism pathway shown.

**Figure 1.14. Recovery of purine nucleotides from MTX-inhibition.**

The addition of hypoxanthine can recover IMP levels, through the actions of HGPRT. IMP can then feed into the salvage GMP and AMP synthesis pathways.

1.15 Folate rescue from MTX

Replenishing folate intermediates has also been shown to rescue MTX-induced cell death and inhibition of proliferation. Folinic acid (5-formyl THF) was shown to rescue the MTX (1 µM)-mediated inhibition of cell proliferation of pokeweed-stimulated PBMCs and rescued activated T cells from cell death (Nesher and Moore, 1990, Genestier et al., 1998). Folinic acid reversed the high-dose MTX (22 µM)-induced apoptosis in PHA-stimulated CD4$^+$ T cells and CD8$^+$ T cells. Folic acid was also shown to offset some effects of MTX. Folic acid prevented CA-activated CD4$^+$ T cells from MTX (22 µM)-induced apoptosis (Nielsen et al., 2007). Folic acid rescue also reversed the anti-proliferative effect of MTX (1 µM) in PHA-stimulated PBMCs and Hec59 cells from MTX-induced cell death (Olsen and Murray, 1989, Martin et al., 2009). Folate-repletion was also shown to restore proliferation and prevented cell death of CD4$^+$ and CD8$^+$ T cells in folate-deficient conditions (Courtemanche et al., 2004). The same authors showed that folate-repletion reduced uracil incorporation in CD4$^+$ and CD8$^+$ T cells following culture in folate-deficient media. Treatment with high-dose MTX (50 µM) inhibited the cell growth of CCRF-CEM cells which was rescued by both 5-methyl THF and 5-formyl THF (Nicholas P. B. Dudman, 1982). The interconversion of these folates may have rescued cells from the MTX-mediated effects, by repleting the activated folate carriers (Fig 1.15). Although both folic acid and folinic acid can compete for binding with MTX to DHFR, it is not known whether folic acid and folinic acid has any significant effect on THF pools, as although reduced, still exist under low-dose MTX conditions, as micromolar levels of MTX are required to inhibit DHFR and hence deplete THF synthesis (Visentin et al., 2012).

Other intermediates in the 1C metabolism pathway have also been shown to rescue the effects of MTX, indicating that the effects of MTX on cell proliferation or apoptosis are not just mediated by pyrimidines and purines, but other consequences of folate antagonism. The methyl donor, SAM reversed the MTX (8 nM)-induced growth-inhibition in FM3A cell lines (Kimura et al., 2004). Methionine or SAM also reversed the MTX-mediated inhibition of proliferation in pokeweed-stimulated PBMCs (Nesher and Moore, 1990). The same authors showed that the addition of polyamines could also recover these cells from the MTX (1 µM)-induced inhibition of proliferation. This rescue

Figure 1.15. Folate rescue of MTX-mediated purine and thymidine inhibition.
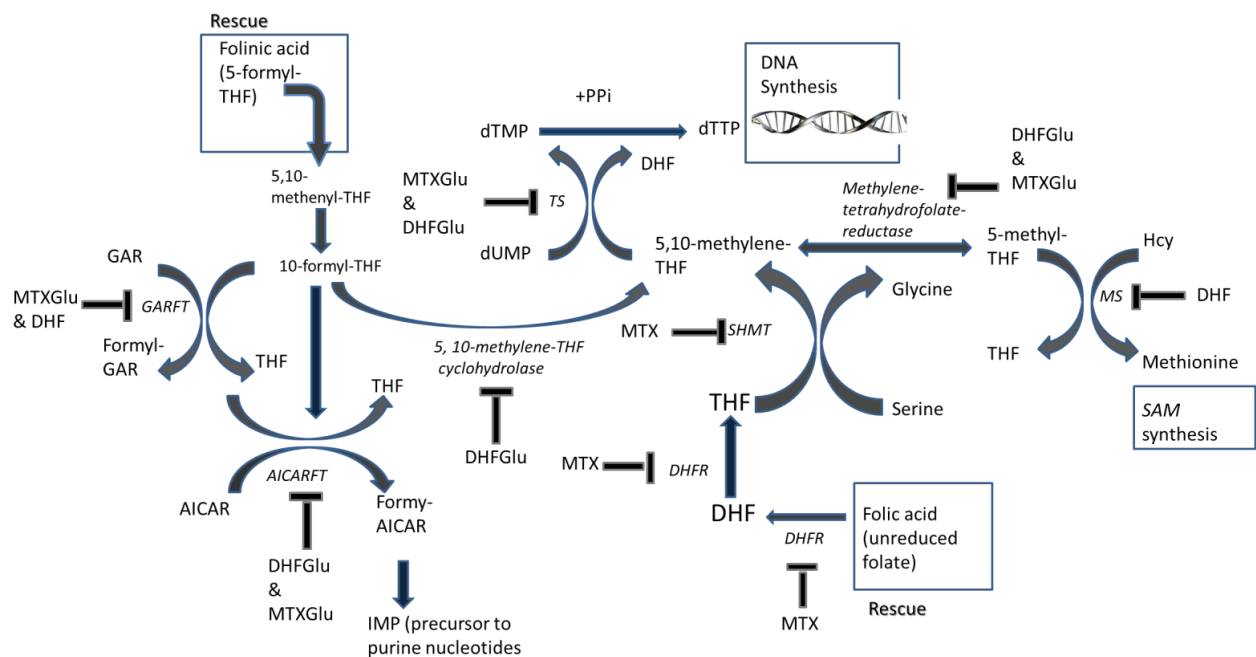
Folic acid competes for binding with MTX to DHFR. The significance on the minimal THF pool, already generated by the binding of DHF to the few available binding sites, is unknown. The addition of folinic acid (5-formyl-THF) was shown to bypass the MTX-mediated inhibition of DHFR and replenish reduced folate levels (Visentin et al., 2012). Folinic acid can be interconverted to other activated 1C carriers, further rescuing the pathway from MTX. Folinic acid is acid catalysed in the stomach to 5,10-methenyl-THF (Nicholas P. B. Dudman, 1982). This can be converted to 10-formyl-THF, which can compete with MTX for binding for AICARFT and GARFT, to salvage purine synthesis by supplying the critical 1C donor for purine synthesis. 10-formyl-THF can be converted to the activated 1C carrier, 5,10-methylene-THF, competing with MTX to bind to TS and thus, rescuing thymidylate synthesis. 5,10-methylene-THF can also be converted to 5-methyl-THF, the substrate for methionine synthesis.

following polyamine addition is explained by the fact that polyamines are also crucial for cell proliferation (van Ede et al., 1998).

1.16 MTX and immunosuppression by adenosine

The MTX inhibition of AICARFT and the subsequent inhibition of adenosine deaminase and AMP deaminase resulted in increased adenosine and AMP levels respectively (see **Section 1.7.4**). The extracellular conversion of these raised AMP levels to adenosine occurred via the enzyme ecto-5-nucleotidase (Morabito et al., 1998). This increase in adenosine was shown to exert an anti-inflammatory effect by binding to the adenosine receptor, A1, A2 or A3 on the surface of cells (Montesinos et al., 2000). On T-regs, extracellular dephosphorylation of ATP to adenosine by the cell-surface ectoenzymes, ectonucleoside triphosphate diphosphohydrolase 1 and ecto-5'-nucleotidase, also known as CD39 and CD73 respectively, have been associated with immunosuppression (Chan and Cronstein, 2010). Furthermore, administration of ATP or adenosine, which both act at the A2 receptor, attenuated rat adjuvant-induced arthritis (Green et al., 1991).

There is much evidence to show that the anti-inflammatory effect of MTX is mediated by adenosine release. Modulation of the anti-inflammatory effects of direct adenosine administration have not been possible as adenosine has a half-life of about 10 seconds in humans (Chan and Cronstein, 2013). Blocking adenosine synthesis has yielded interesting findings. One such study showed that levels of TNFα and leukocytes were reduced following MTX treatment in wild type but not in CD73-/- mice, who were unable to convert AMP to adenosine extracellularly (Montesinos et al., 2007). Children treated with MTX for leukaemia had higher adenosine concentrations in their cerebrospinal fluid, and upon the administration of adenosine antagonists, the effects of treatment were reversed (Chan and Cronstein, 2010). It was also shown that the activity of adenosine deaminase, which degrades adenosine, was significantly reduced in lymphocytes of RA patients being treated with MTX (Riksen et al., 2006). Even in murine studies, blocking adenosine by administration of an adenosine receptor antagonist and adenosine deaminase, which catabolizes adenosine, reversed the anti-inflammatory effects of MTX (Cronstein et al., 1993). However there is evidence that disprove the anti-inflammatory effect of adenosine. Adenosine antagonists administered alongside MTX did not weaken the anti-arthritic effect in some studies. In fact, one particular adenosine antagonist, R-PIA actually

reduced the arthritis, suggesting that adenosine is inflammatory (Andersson et al., 2000). It was also shown that patients receiving low-dose MTX displayed altered adenosine metabolism, yet this did not attenuate the RA disease severity (Cronstein, 2006).

1.17 Glycosylation

The addition of sugars to either lipids or proteins, termed glycosylation, is a post-translational modification that determines the structure and function of antibodies, secreted and endogenous glycoconjugates, and the surface glycans of the glycocalyx (Fuster and Esko, 2005). It involves the concerted action of glycosyltransferases, glycosidases and other glycan-modifying enzymes. Cell-surface-glycans have multiple-functions, with roles in cell-signalling, cell-adhesion and trafficking, in cell structural integrity and identity, as well as in modulating the stability and solubility of the glycoconjugate itself (Collins et al., 2013). The cell-signalling ability of glycans has implications in immune and non-immune functions. Specific surface-glycans serve as a marker of 'self' and relay information to specific lectins about the activation or differentiation state of immune cells and any insults occurring to the cell. It also serves as an autocrine process to send similar information to regulate cellular functions on cells containing that glycan.

1.17.1 The structure of glycans

There are two main types of glycans, *N*-linked and *O*-linked glycans; *N*-linked glycans are attached to a nitrogen atom in an asparagine residue in the protein or lipid, and *O*-linked are attached to an oxygen atom. There are eight core *O*-linked glycan structures, contributing to the vast diversity of *O*-linked glycans. *N*-linked glycans are thought to occur more often due to the frequent occurrence of the asparagine(asn)-x(any amino acid except proline)-serine(ser)/threonine(thr) sequence, following analysis of protein sequence databases (Varki et al., 1999). The nature of x in the amino acid sequence has been shown to influence glycosylation when it is acidic (glutamate or aspartate). The core structure is retained in *N*-linked glycans but the terminal residues differ (Fig 1.16). *N*-glycans can be classified into high mannose, hybrid or complex structures (Clark and Baum, 2012). The main class of sugars most commonly found in mammalian glycoconjugates are hexoses, six-carbon sugars. The six-carbon sugars can be rearranged
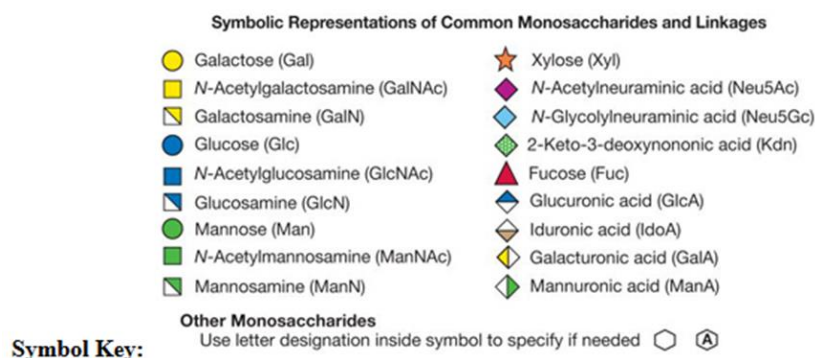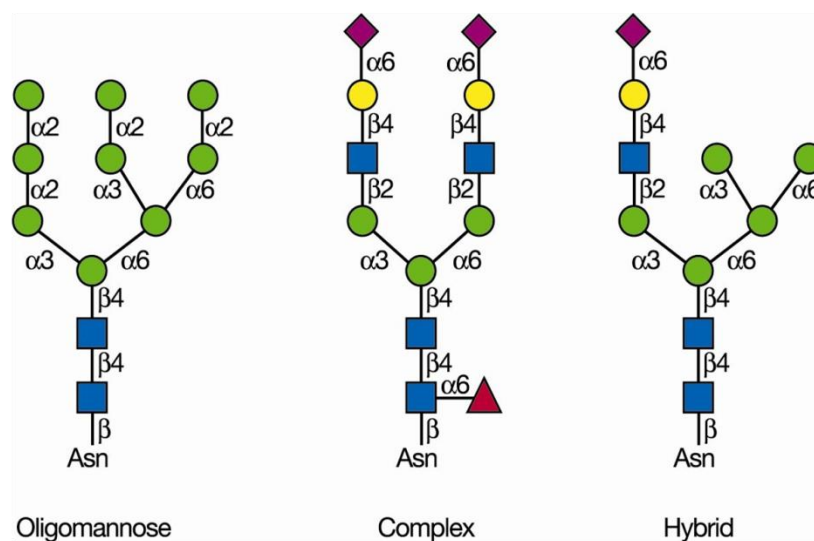
Figure 1.16. Structure of the three types of *N*-glycans containing a common core.

GlcNAc is first placed on an asparagine residue in an asn-x-ser/thr sequence. This is followed by another GlcNAc sugar and then mannose, arranged through the linkages shown. This core sequence, Manα1,–6(Manα1,–3)Manβ1,–4GlcNAcβ1,–4GlcNAcβ1-asn-x-ser/thr can then be modified creating oligomannose *N*-glycans, in which only mannose residues are attached to the core; complex *N*-glycans, in which branches initiated by *N*-acetylglucosaminyltransferases (GlcNAcTs) are attached to the core; and hybrid *N*-glycans, in which only mannose residues are attached to the Manα1,–6 arm of the core and one or two antennae are on the Manα1,–3 arm. Taken from Varki et al. (1999).

in different ways to create sixteen possible sugars. For instance, six-carbon glucose can be sterically rearranged to form galactose and mannose as well as substituted with an acetylated amino group for a 2-hydroxyl group to yield *N*-acetylglucosamine (GlcNAc) or *N*-acetylgalactosamine (GalNAc), for glucose or galactose, respectively. Loss of carbon-six generates xylose, which is a five-carbon sugar (pentose) and fucose is generated by loss of the 6-hydroxyl group from L-galactose. The sugars can be arranged in different combinations, sequentially or in a branched orientation, making multiple functionalities possible, termed glycoforms and forming a unique glycan profile. Indeed not all glycoforms are possible because of steric hindrance and other constraints imposed on the molecule. This is the case in the glycosylation site on asn 297 in IgG (Varki et al., 1999).

The synthesis of *N*-linked glycans, specifically in the late golgi, contributes to the variety of glycoforms possible. Formation of the 14-sugar scaffold and the remaining processes involved in the synthesis of *N*-linked glycans is extensively covered in Varki et al. (1999) and is summarised in this section (Fig 1.17-1.18). It begins with the transfer of GlcNAc-P to dolichol phosphate, (a lipid-scaffold on which the sugar is temporarily placed), catalysed by GlcNAc-1-phosphotransferase. This phosphate is transferred along with the sugar GlcNAc to provide the energy required later to cleave the 14-sugar from the lipid scaffold. An additional GlcNAc and five mannose residues are then attached before the dolichol-sugar is flipped across the membrane, facing the lumen of the ER, whereby four mannose residues and three glucose residues, donated by the sugar-donors, dol-P-Mannose and dol-P-glucose respectively, are attached. The 14-sugar glycan is then transferred to an acceptor containing an asn-x-ser/thr, following cleavage of the GlcNAc-P bond by oligosaccharyltransferase (OST).

This 14-sugar glycan then undergoes further processing en route through the ER and golgi (Fig 1.18). The initial steps are imperative to ensure correct folding of the glycoprotein, facilitated by chaperone proteins. It begins with the removal of one terminal glucose by α-glucosidase I, the two innermost glucose residues by α-glucosidase II, and the re-addition of the innermost glucose residue. A specific mannose residue may also be removed by ER α-mannosidase I after which point, misfolded proteins may be targeted for degradation by the ER degradation-enhancing α-mannosidase I–like protein (EDEM). In multicellular organisms, *N*-glycans with either eight or nine mannose residues, depending on whether they have been acted on by ER α-mannosidase I, exit the ER,
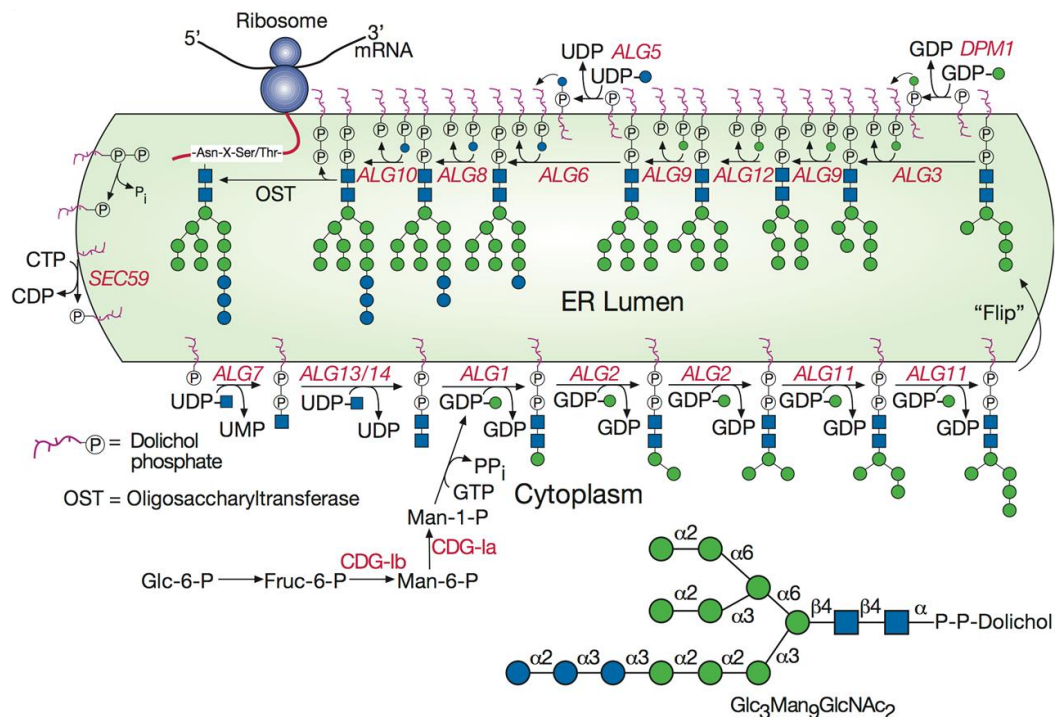
Figure 1.17. Synthesis of the dolichol phosphate scaffold containing 14 sugars for en bloc transfer to a protein/lipid acceptor.

GlcNAc-P is first transferred to dolichol-phosphate from UDP-GlcNAc on the cytoplasmic face of the ER membrane. This generates dolichol pyrophosphate *N*-acetylglucosamine (dol-P-P-GlcNAc) which is extended upon the sequential addition of GlcNAc and 5 mannose residues through the linkages shown. This newly formed dol-P-P-GlcNAc$_2$Man$_5$ is then flipped across the ER membrane to the luminal side and extended by 4 more mannose residues and three glucose residues. OST catalyses the transfer of these 14 sugars to an acceptor protein or lipid, upon cleavage of the GlcNAc-P high-energy bond. This releases dol-P-P and upon removal of the phosphate, regenerates the lipid scaffold dol-P. Taken from Varki et al. (1999).
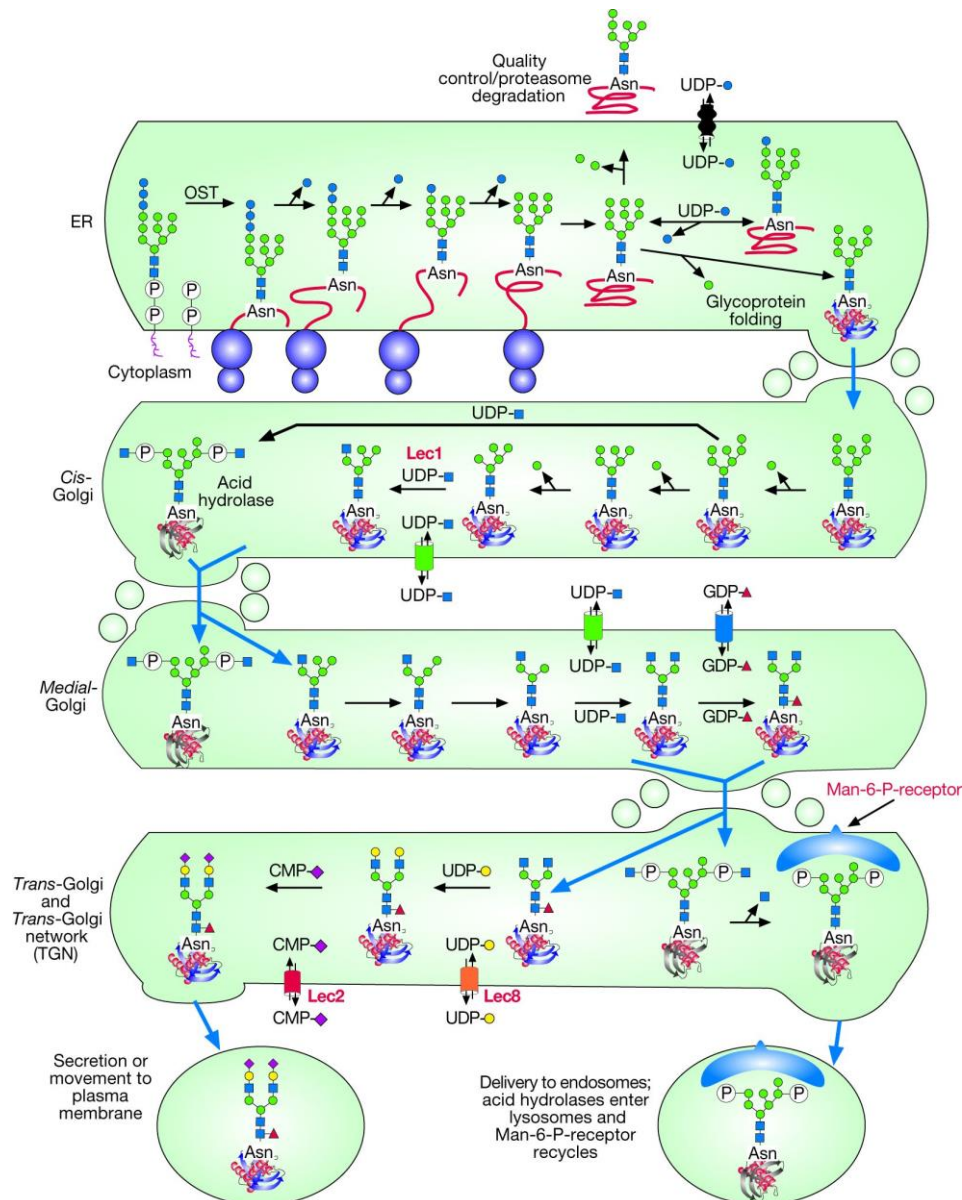
Figure 1.18. Processing of the 14-sugar acceptor towards the three common core *N*-linked glycans.

Removal of one terminal glucose by α-glucosidase I, the two innermost glucose residues by α-glucosidase II, precedes the re-addition of the innermost glucose residue. A specific mannose residue may also be removed by ER α-mannosidase I, after which misfolded proteins may be targeted for degradation by the EDEM. In multicellular organisms, *N*-glycans with either eight or nine mannose residues, depending on whether they have been acted on by ER α-mannosidase I, exit the ER, where further mannose residues are removed by α1,–2 mannosidases IA, IB, and 1C in the *cis*-Golgi to give Man$_5$GlcNAc$_2$. *N*-glycans fully processed to Man$_5$GlcNAc$_2$ then undergo remodelling to form hybrid and

complex structures in the *medial*-golgi. This begins with the transfer of a GlcNAc residue by *N*-acetylglucosaminyltransferase (GlcNAcT-I) to the carbon-2 of the core mannose $\alpha 1,-3$ of $Man_5GlcNAc_2$. Following this, two terminal mannose residues are removed, forming $Man_3GlcNAc_2$ and a second GlcNAc is added to carbon-2 of the core mannose $\alpha 1,-6$ by the action of GlcNAcT-II to yield the precursor for all biantennary, complex *N*-glycans. Hybrid *N*-glycans are formed if the mannose residues are not removed (Fig 1.17). Complex *N*-glycans are formed from two branches initiated by the addition of two terminal GlcNAc residues to $Man_3GlcNAc_2$. Further branches can be formed on the carbon-4/6 of the core mannose $\alpha 1,-3$ or carbon-6 of the core mannose $\alpha 1,-6$. A GlcNAc residue can also be attached to the β-mannose of the core complex and hybrid *N*-glycans. In the *trans*-Golgi, sugars are added to the core, or to extend the GlcNAc branches and to the end of branches, and is responsible for the extensive array of mature, complex *N*-glycans, the complexity of which is organism-dependent. After this final processing step, these glycans can be secreted or budded from the golgi in vesicles, destined for the cell-surface. Taken from Varki et al. (1999).

where further mannose residues are removed by $\alpha 1,-2$ mannosidases IA, IB, and 1C in the *cis*-Golgi to give $Man_5GlcNAc_2$.

N-glycans fully processed to $Man_5GlcNAc_2$, then undergo remodelling to form hybrid and complex structures in the *medial*-golgi. This begins with the transfer of a GlcNAc residue by *N*-acetylglucosaminyltransferase (GlcNAcT-I) to the carbon-2 of the core mannose $\alpha 1,-3$ of $Man_5GlcNAc_2$. Following this, two terminal mannose residues are removed, forming $Man_3GlcNAc_2$, to which a second GlcNAc is added to carbon-2 of the core mannose $\alpha 1,-6$ by GlcNAcT-II to yield the precursor for all biantennary, complex *N*-glycans. Hybrid *N*-glycans are formed if the mannose residues are not removed (Fig 1.17). Complex *N*-glycans are formed from two branches initiated by the addition of two terminal GlcNAc residues to $Man_3GlcNAc_2$. Tri- and tetra-antennary *N*-glycans are formed by creating branches at carbon-4 of the core mannose $\alpha 1,-3$ by GlcNAcT-IV or GlcNAcT-VI, carbon-6 of the core mannose $\alpha 1,-6$ by GlcNAcT-V or carbon-6 of the core mannose $\alpha 1,-3$ by GlcNAcT-IX also called GlcNAcT-Vb. Complex and hybrid *N*-glycans may carry a "bisecting" GlcNAc residue that is attached to the β-mannose of the core by GlcNAcT-III.

The extensive array of mature, complex *N*-glycans, whereby sugars are added to the core, or to extend the GlcNAc branches and to cap the end of branches depends on the organism and occurs mostly in the *trans*-Golgi. In vertebrates, the main core modification is the addition of fucose in an $\alpha 1,-6$ linkage to the GlcNAc adjacent to asn in the core. Elongated branches are made by the addition of a β-linked galactose residue to either the carbon-4 or carbon-5 of GlcNAc to produce the ubiquitous building block Galβ1,-4/5GlcNAc, referred to as *N*-acetyllactosamine or"LacNAc"sequence. This structure may be repeated upon the addition of sequential GlcNAc and galactose residues. Alternatively, β-linked GlcNAc can be added to GlcNAc instead of β-linked galactose, forming a GalNAcβ1,-4GlcNAc extension, referred to as ("LacdiNAc") extension. Sialic acid, fucose, galactose, GlcNAc, and sulphate can all be added, most commonly attached through an α-linkage as capping residues to the end of branches described in the preceding paragraph. After this final processing step, these glycans can be secreted or budded from the golgi in vesicles, destined for the cell-surface.

1.17.2 Sialic acids

Sialic acids, include the nine-carbon sugar *N*-acetylneuraminic acid (NeuAc), formed from pyruvate (Varki et al., 1999). Sialic acids are added to glycans at either α2,-3-, α2,-6-, or α2,-8- linkages by specific sialyltransferases (Zhuo and Bellis, 2011). The main sialyltransferases involved in the addition of sialic acids to the α2,-6-linkage, is β-galactosidase-2,-6-sialyltransferase (ST6Gal1). Sialic acids are the most abundant surface glycans on mammalian cells, with *N*-acetylneuraminic acid (Neu5Ac) and *N*-glycoylneuraminic acid (Neu5Gc) the predominant types (Boligan et al., 2015). The α2,-6-sialylated structures comprise the predominant type of *N*-glycans on CD4$^+$ and CD8$^+$ T cells (Zhuo and Bellis, 2011). Surface-sialic acids can affect the binding of other lectins to the same cell-surface, but can also act as ligands to sialic acid-immunoglobulin-type lectins. These sialic acid-immunoglobulin-type lectins (siglecs) relay signals following sialic acid or glycoprotein binding on the same cell-surface, or on the surface of other cells (Varki and Angata, 2006). These siglecs contain immune tyrosine-based immunomodulatory motifs (ITIMs) which have inhibitory effects on signalling.

The sialic acid, Neu5Ac is one of the end products of the synthesis of *N*-acetylmannosamine (ManNAc), formed from a variety of precursors including UDP-*N*-acetylglucosamine (UDP-GlcNAc) as well as the interconversion of another sugar, UDP-*N*-acetylgalactosamine (UDP-GalNAc) (Fig 1.19).
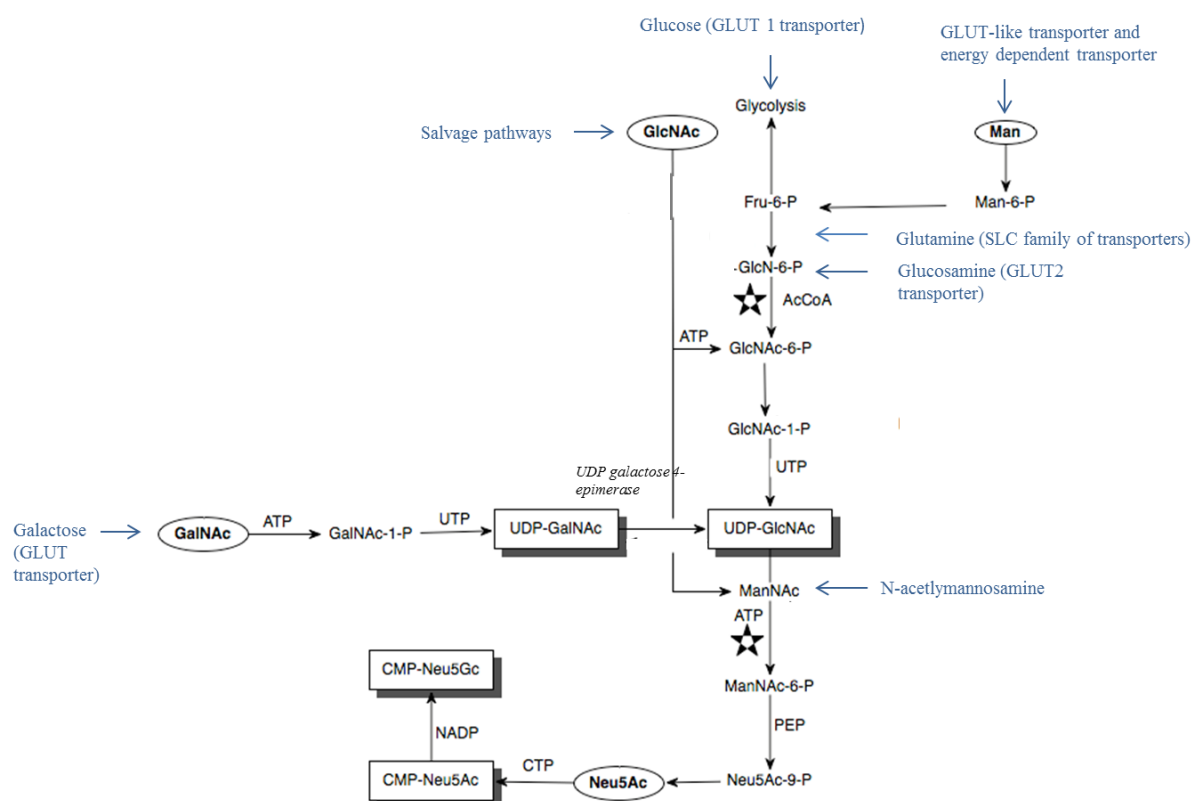
Figure 1.19. Processing of *N*-acetylmannosamine and its precursors for incorporation into CMP-*N*-acetylneuraminic acid (CMP-Neu5Ac).

ManNAc is synthesised from a variety of precursors (blue) including mannose; which is transported by a GLUT-like transporter and an energy-dependent transporter, glucosamine; which is transported by GLUT2 and glucose, by the GLUT family of transporters (Varki et al., 1999). Glutamine uptake is mediated by the SLC family of transporters. Mannose, glucose, glucosamine and glutamine all enter the hexokinase synthesis pathway at the points indicated for de novo synthesis of UDP-GlcNAc. Salvage pathways for *N*-acetylglucosamine (GlcNAc) also exist, with 80% of GlcNAc from glycoproteins degraded in liver lysosomes to UDP-GlcNAc (Varki et al., 1999). UDP-GalNAc, formed from GLUT mediated transport of galactose can be converted into UDP-*N*-acetylglucosamine (UDP-GlcNAc) by the enzyme UDP-galactose 4-epimerase. Externally added ManNAc has greater membrane permeability than sialic acid and has been shown to passively diffuse through the cell membrane in many cell types as well as tissues, at physiological pH (Gu and Wang, 1998). Adapted from Varki et al. (1999).

1.17.3 Methods used to determine surface-sialic acid expression

The functionality of these sialic acid-surface-glycans, has been delineated upon their removal by sialidases, however there are limitations to this method. Lectins, which bind these sialic acids demonstrate high specificity but have low affinity for single glycans (Varki and Angata, 2006). Many cell interactions are mediated by binding multiple ligands, which increases the avidity of binding. Thus, a lack of sialic acids could reduce steric interference affecting the binding of other lectins. These changes in the landscape upon sialic acid removal were also suggested to alter the biophysical properties of the cell membrane, resulting in changes in the net charge and hydrophilicity of the membrane, resulting in reduced charge repulsion between adjacent surface molecules and the elimination of ligands for endogenous receptors (Varki and Gagneux, 2012). Indeed, experimentally, the removal of cell-surface sialic acids using sialidases is often used to enhance cell-cell interactions by reducing negative charge repulsion (Varki and Angata, 2006). These indirect changes in the proximity to other cell-surfaces or the exposure of other glycans may contribute to the observed effects of sialic acid removal.

The expression of specific sialic acid linkages, α2,-3- and α2,-6- has been determined following binding via their respective ligands, Siglec-1 and CD22 (Varki and Angata, 2006). This has been achieved by virtue of the high specificity of these siglecs for their corresponding ligands, not shown for other siglecs, limiting the evaluation of the expression of other sialic acids. Knockdown of the main sialyltransferase (ST), β-galactosidase α2,-6-sialyltransferase, responsible for the addition of sialic acids on the α2,-6-position has also yielded interesting findings about the function of this α2,-6-linkage (Zhuo and Bellis, 2011). However, knockdown of ST6Gal1 does not deplete every α2,-6-linkage, thus the effect of the total α2,-6-sialic acid cohort cannot be assessed using this method. In addition, ST6Gal1 is specific for complex *N*-glycans, and T cells have been shown to express both high mannose, hybrid and complex *N*-glycan structures. Thus, experiments delineating the function of the α2,-6-linkage exclude those on high mannose or hybrid *N*-glycans. In addition, it was suggested that measuring the activity and expression levels of glycan-modifying enzymes does not reveal how or why modifications to glycans have occurred, as other factors like the competition of these glycosyltransferases for substrates in the Golgi and the expression of alternatively spliced isoforms can have a significant effect (Clark and Baum, 2012).

1.17.4 The Sialome

The array of sialic acids on the cell-surface, coined the 'sialome', relays signals of 'healthy self' and as such, is thought to exert an anti-inflammatory effect (Xiao et al., 2016). Hypersialylation was even shown to be a mechanism used by tumours to suppress the immune response (Boligan et al., 2015). In parallel, a reduction in sialic acid-expression, hyposialylation, was found in a variety of inflammatory conditions. The onset of RA was accompanied by decreased plasmablast-surface-expression of sialic acids (Pfeifle et al., 2016). Reduced sialylation of IgG was also found in RA patients and in mouse models of RA (Ohmi et al., 2016). Of these IgG, between 5 and 10% of IgG were mono-sialylated and less than 1% had two sialic acids (Troelsen et al., 2012). Importantly, since sialic acids commonly bind galactose residues, this reduction in sialic acids may in fact be a consequence of a reduction in galactose residues, previously discussed.

These reports of the anti-inflammatory activity of sialic acids have been met with contradictory reports. Sialic acid-expression was not reduced during inflammation, as indicated by the large numbers of Sn-(the ligand for α2,-6-linked sialic acids) positive macrophages found in the RA synovium. The reduction in sialic acid residues or an inability to respond to these glycans was shown to weaken the inflammatory process. ST6Gal sialyltransferase (ST6Gal1) null mice, lacking the sialic acid ligand for CD22 binding showed diminished B cell reactivity *in vitro* and *in vivo*. Mice with mutations in the V-set arginine residue required for sialic acid recognition, could not signal the presence of sialic acids and displayed reduced proliferation of B cells upon BCR ligation, indicating that the CD22 binding of sialic acid signalled activatory pathways (Varki and Angata, 2006). These discrepancies could partly be due to surface sialylation being a consequence of the environmental milieu which may not modulate the immune response in all cases. It was shown that inducers of inflammation, specifically IL-23-activated Th17 cells reduced the expression of sialyltransferase (ST6Gal1) in antibody-producing cells (Pfeifle et al., 2016).

Sialic acids may act by preventing the binding of other lectins by shielding the underlying sugar. The addition of α2,-6-sialyl linkages prevented the binding of a glycan binding protein, galectin-1 to β-galactosidase preventing galectin-induced apoptosis (Zhuo and

Bellis, 2011). Sialic acids also prevented galectin-1 binding in T cells, preventing T cell apoptosis (Cohen and Varki, 2010).

The presence of sialic acid residues was thus shown to modulate the immune response as Th2 cells expressed greater $\alpha 2$,-6-sialic acid linkages compared to Th1 and Th17 cells, leaving them less susceptible to galectin-induced cell death (Toscano et al., 2007). This modulation of sialic acids was shown to limit the immune response, as activated peripheral T cells were shown to undergo apoptosis mediated by galectin-1 binding (Clark and Baum, 2012). However, the anti- or inflammatory consequence of sialic acid-mediated protection from galectin binding is dependent on the cell type in which inhibition of apoptosis is prevented.

1.17.5 Siglecs

Sialic acids can also mediate a variety of different actions through the binding of sialic acid-immunoglobulin-type lectins (siglecs). These can bind individual glycoconjugates or clusters (Cohen and Varki, 2010). These signals can be transduced on the cell containing siglecs or on the same cell containing the sialic acid, via binding of the sialic acid in *cis* (Crocker et al., 2007). Most siglecs do have signalling capability and contain an immune-tyrosine-based inhibitory motif (ITIM) or can associate with a killer-cell activating receptor associated protein, containing an immune-tyrosine-based activatory motif (ITAM) (von Gunten and Bochner, 2008). As such they can initiate an activatory or inhibitory signal, which could have an inflammatory or anti-inflammatory response depending on the immune cell type containing the siglec.

There are many siglecs, categorised based on those which have been evolutionary conserved (siglec 1, 2, 4 and 15) or based on those rapidly evolving CD33-type siglecs (Angata et al., 2004). Most siglecs have a unique specificity for sialylated ligands, recognising the linkage to the underlying sugar, the carboxyl group, and the glycerol-like side chain at carbon-7 and 9, as well as the sia species (Powell et al., 1993, Powell and Varki, 1995, Collins et al., 1997a, 1997b, Barnes et al., 1999, Angata and Varki, 2000a, 2000b, Brinkman-Van der Linden and Varki, 2000). Except for siglec 6 and MAG, most siglecs are expressed on the haematopoietic and immune systems and the repertoire expressed also appear to be cell-specific (Crocker and Varki, 2001, 2007). T cells have

low siglec expression, with only a subset of CD8^{+} T cells expressing siglec 7 and 9 (Nicoll et al., 1999, Razi and Varki, 1999, Zhang et al., 2000, Ikehara et al., 2004).

Sialic acids also mediate a variety of non-immune related cell-signalling roles in part mediated by the sialic acid ligand, Siglec-1 (Naito-Matsui et al., 2014). α2,-6-sialylation altered the conformation and function of β1-intergrin, a molecule involved in cell-adhesion and migration. Sialic acid involvement was shown to enhance or reduce the signal in different cell types. Sialic acids were crucial for the clustering and cell-surface retention of PECAM in endothelial cells, but α2,-6-sialylation inhibited clustering of the CD45 tyrosine phosphatase in T cells and diminished the signal (Zhuo and Bellis, 2011). Sialic acids residing on the T cell glycoprotein CD45, keeping individual CD45 molecules separate, and preventing clustering were shown to increase T cell receptor signalling (Clark and Baum, 2012). Thus, sialic acids can have dual effects in mediating or inhibiting receptor clustering, enhancing or diminishing the signal.

1.17.6 The activation-dependence of glycosylation

Changes in both intracellular *N*-linked glycosylation and glycosylation of surface-glycans, including specific sialic acid linkages, have been shown following activation or differentiation. These changes are achieved by a vast number of proteins which regulate the expression of glycosyltransferases and glycosidases that dictate the final glycan array. Naïve T cells were shown to express α2,-6-surface glycans, the levels of which were shown to be decreased upon activation (Clark and Baum, 2012). This was due to decreased expression of ST6Gal1 in activated T cells (Zhuo and Bellis, 2011). However, changes to the α2,-8-linkage had not been investigated. Determining the expression of total sialic acids as well as the individual α2,-6- and α2,-3-linkage, revealed that surface sialic acid expression had increased in activated Th cells, due to an increase in α2,-8-sialyltransferases, despite a reduction in the α2,-6- and α2,-3-linkage (Villanueva-Cabello et al., 2015). These changes in sialylation upon activation were not reflected in mice, as α2,-6- as well as α2,-3-sialylation increased in anti-CD3-activated splenic T cells (Naito-Matsui et al., 2014). Changes to the expression of sialyltransferases as well as other glycosyltransferases have been shown during differentiation and activation. ST6Gal1

expression was shown to be downregulated following the differentiation of primary monocytes towards a macrophage phenotype (Dalziel et al., 1999). α1,-3-fucosyltransferase VII expression increased upon the anti-CD3/CD28 activation of splenic CD4^{+} T cells, and core 2 β1,-6-glucosaminyltranferase-1 (C2GlcNAcT-I) expression increased upon IL-12 polarization towards a Th1 response (White et al., 2001).

Changes in the glycosylation of the two most abundant glycoproteins on the CD4^{+} and CD8^{+} T cell-surface, CD45 and CD43, occurred during T cell-activation (Clark and Baum, 2012). The *N*-glycans on CD45 terminating in α2,-6-linked sialic acids were reduced upon activation (Varki and Angata, 2006, Clark and Baum, 2012). This was thought to render these activated T cells susceptible to the apoptotic effects of galectin-1 binding.

In addition to changes in the sialic acid linkage during activation of both surface-glycans and specific glycoproteins, changes to the sialic acid species may also occur. The major type of surface sialic acid expressed changed from *N*-glycolyneuraminic acid in resting B and T cells to *N*-acetylneuraminic acid following activation. Changes in these sialic acid species was also shown to have an inflammatory effect. Knockout of CMP-Neu5Ac hydroxylase (CMAH), which converts Neu5Ac to Neu5Gc, was shown to potentiate the anti-CD3-induced proliferation of splenic T cells (Naito-Matsui et al., 2014).

Activation or differentiation can also modify the expression or availability of siglecs, which can regulate the interaction with other immune cells. Maturation of dendritic cells (DCs) with LPS downregulated siglec 7 and 9, but monocytes retained their expression of siglecs when differentiated into macrophages or activated with LPS (Naito-Matsui et al., 2014). Following B cell-activation the CD22 siglec dissociated from binding to cis-ligands, enabling it to interact with other cell-surface sialic acids. Indeed B cells with an activated phenotype in the transitional and marginal zone of the spleen, had unmasked CD22, leaving CD22 available for binding (Varki and Angata, 2006).

1.17.7 Regulation of glycosylation

The overexpression of sialyltransferases in cancer is mediated by the proto-oncogenes c-Myc and Ras (Boligan et al., 2015). It is not known what controls the sialylation of *N*-glycans during activation. *O*-GlcNAcylation was shown to be regulated at the level of precursor uptake, as the transport of UDP-GlcNAc precursors, glutamine and glucose, were partially controlled by Notch and c-Myc during T cell-activation (Swamy et al., 2016). UDP-GlcNAc has been shown to be fed into the *N*-glycan sialic acid-processing pathway via ManNAc (Varki et al., 1999). Thus, it is possible that these transcription factors, c-Myc and Notch, could influence the *N*-glycan sialic pathway by modulating one of its precursors, UDP-GlcNAc. Cytokines are also thought to modulate surface glycosylation by controlling the expression of glycosylation enzymes. IL-6 was shown to regulate the hepatic expression of ST6Gal1 during the acute phase response (Dalziel et al., 1999). The increased expression of C2GlcNAcT-I upon splenic T cell-activation with anti-CD3/CD28, was shown to be mediated through cytokine-activated Stat4 signalling (White et al., 2001).

Substrate availability was also shown to direct the fate of the sugar into a specific pathway, by way of competition between glycosyltransferases for these substrates in the Golgi (Clark and Baum, 2012). Even in vitro, sialylation could be enhanced following the addition of nucleotide-sugar substrates. Substrate availability from indirect routes of ManNAc synthesis via UDP-GalNAc was also shown to be a contributing factor, as it was shown that a lack of galactosylation was a potential cause for the reduced sialic acid content in a recombinant Fc-fusion protein in CHO cells (Liu et al., 2015).

Epigenetic modification, leading to alternatively spliced isoforms of these glycosyltransferase enzymes, could also dictate the end glycan product (Clark and Baum, 2012). Indeed alternatively spliced isoforms of ST6Gal1 were shown to exhibit preferential types of sialylation (Luley-Goedl et al., 2016). These glycosylation enzymes were also shown to be compartment-specific, limiting the type of sugar that could be incorporated.

1.18 Antibodies

The glycans on the surface of protein structures called antibodies have an integral role in antigen recognition and the initiation of an immune response. They are categorised into five classes, IgG, IgA, IgD, IgE and IgM, and in the case of IgG and IgA, further

separated into subgroups, IgG1-4 and IgA1-2 respectively (Drickamer, 2003). The glycans on these antibodies, in particular IgG are highly variable. The majority (more than 92%) of human IgG Fc glycans are core fucosylated and are further divided into three classes, depending on the number of terminal galactose residues on the conserved *N*-glycosylation site at asparagine (asn) 297 in the Fc region of the IgG heavy chains (Fig 1.20). IgG G_O, G_1, and G_2 represent zero, one or two terminal galactose residues respectively (Varki et al., 1999). As such there are over 30 human glycoforms on a single IgG heavy chain that have been identified, 900 possible variants on each IgG molecule, because each consists of two heavy chains (Anthony, 2013).

The FcγR is broadly classified into three groups FccRI, FccRII, and FccRIII. Signalling occurs through either an ITAM for activating FccRI, FccRIIa, FccRIII or an ITIM, for inhibitory FccRIIb. Each FcγR contains at least two glycosylation sites with up to seven potential sites observed in the high affinity FccRIa (Hayes et al., 2014). Glycosylation data has been reported for recombinant soluble human FccRIIa and FccRIIIa (Takahashi et al., 1998, 2002). Glycosylation data have also been described for the family of recombinant receptors- FccRIa, FccRIIa, FccRIIb, FccRIIIa, and FccRIIIb expressed in the murine cell line NS0 (Cosgrave et al., 2013). Structurally these carbohydrate domains interact with the asn 297 glycosylation sites on a specific isotype of IgG, IgG1 lacking fucose residues (Ferrara et al., 2011). However, functionally, there have been mixed reports of the importance of the interaction between the glycosylation site on the Fc region at asn 297 and the FcγR. In the absence of glycosylation on this site, FcγRs expressed in E. coli and purified from inclusion bodies were found to retain the ability to bind IgG (Sondermann and Jacob, 1999, 2000, Maenaka et al., 2001). This suggested that the asn 297 glycosylation site was not imperative for binding to the FcγR. However, an homologous glycosylation site in IgE at an asn 275 was shown to be crucial for effector binding as a mutation of asn 275 was shown to eliminate binding to its cognate receptor FcεRI (Nettleton and Kochan, 1995).

Other glycosylation sites on the Fc region may be as important in regulating the interaction between specific FcγRs, specifically an α1,6-core linked fucose which when absent, was shown to enhance binding to activating FcγRs and improved ADCC (Shields et al., 2002, Okazaki et al., 2004, Niwa et al., 2005, Iida et al., 2006, Natsume et al., 2006, Satoh et al., 2006). Two *N*-linked sites of FccRIIIa have been shown to regulate the
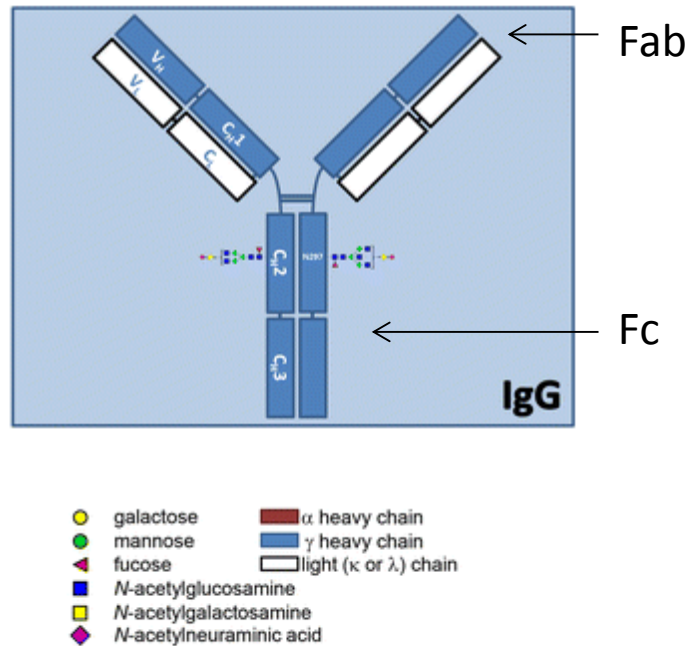
Figure 1.20. Schematic representation of immunoglobulin G (IgG) and the glycosylation sites at asparagine 297 on the Fc region.

Antigen binding occurs via the Fab region of the antibody molecule, and the Fc region binds a variety of receptors to initiate various responses. IgG antibodies, through their Fc region, can bind c-type lectins, complement receptors and various Fc receptors including the FcγR to induce phagocytosis, complement activation and antibody-dependent cell-mediated cytotoxicity (ADCC) (Hayes et al., 2014). IgG antibodies can also bind Fc receptors to induce non-immune related signalling. Binding to the neonatal Fc receptor termed FcRn, has an important role in recycling IgG and maintaining the serum concentrations of the antibody (Ward et al., 2003). FcRn is also involved in the transport of IgG to the foetus, transferring humoral immunity to the baby (Brambell, 1966, Morphis and Gitlin, 1970). Most research has been conducted on the binding of IgG to the Fc receptor, FcγR, which like its cognate antibody, also contains glycans as part of its structure. Adapted from Bondt et al. (2017).

binding of IgG. A glycan on asn 45 was shown to have an inhibitory role and negative effect on IgG binding, whereas glycosylation at asn 162, located at the IgG binding interface was found to increase IgG interaction and binding affinity (Ferrara et al., 2006, Shibata-Koyama et al., 2009, Ferrara et al., 2011).

The effector receptors can differ in their biological properties, functional location and ability to deal with different antigens (Karsten and Kohl, 2012). FccRIIIa exists as cell type-specific glycoforms on monocytes and macrophages with different affinities for IgG and different responses to an IgG stimulus due to the differently glycosylated FcγRs (Kimberly et al., 1989, Edberg et al., 1990, Edberg and Kimberly, 1997). To elicit the appropriate antigen-dependent response, many immune cells, including macrophages, dendritic cells, and neutrophils express both activatory and inhibitory FcγRs (Anthony, 2013). IgG antibodies will interact with many different receptors on the same cell, creating an extremely complex series of interactions and signalling pathways (Hayes et al., 2016).

1.18.1 Aberrant glycosylation patterns in IgG and serum proteins in RA

Parekh et al first detected aberrant galactosylation patterns in patients with RA (Arnold et al., 2007). In the case of RA, mutations in the glycan structure in the Fc region of the IgG molecule, alter the glycoprint normally recognised by self and is thus considered a foreign target on which an immune response is mounted. Specifically, the absence of terminal galactose residues was shown to eliminate some of the interactions that normally hold the glycan in the pocket of the Ch2 domains (Parekh et al., 1989, Krapp et al., 2003). This exposed a glycan to the immune system, which ordinarily is not present, creating autoantibodies against this Fc portion of the IgG molecule, known as Rheumatoid factor (Kunkel et al., 1961).

This aberrant IgG galactosylation, occurring mainly in autoantibodies, was found to begin prior to the onset of RA and was associated with disease activity in RA patients, especially in women. An association between the extent of agalactosylation of IgG *N*-glycan and the onset of adult and juvenile RA was then made (Parekh et al., 1989). Further evidence was discovered during pregnancy, during which RA patients went into remission. Levels of IgG-G_O were found to fall during remission of the disease and also during pregnancy (Rook et al., 1991). This association of agalactosylation and disease

extended to juvenile chronic arthritis, whereby the increase in agalactosylated IgG was proven to be a diagnostic marker (van Zeben et al., 1994, Lacki et al., 1996, Pasek et al., 2006, Gindzienska-Sieskiewicz et al., 2007, Ercan et al., 2010).

If this loss of galactose residues impacted an inflammatory disease, it suggested that the absence of galactose could be inflammatory. Indeed, in vitro agalactosylated IgG was shown to bind mannose binding lectin (MBL) and subsequently activate complement via the exposed mannose sugars (Malhotra et al., 1995) . However, this activation is isotype specific as IgG_2 failed to activate complement despite the presence of the exposed mannose sugar (Troelsen et al., 2012).

Further evidence that the absence of galactose leads to an inflammatory phenotype was demonstrated in vitro where the presence of galactose could inhibit complement activation. It was shown that galactose associated with the inhibitory receptor FccRIIB and a certain C-type lectin-like receptor, dectin-1, resulting in inhibition of the complement, C5a receptor (Anthony, 2013).

However, despite the fact that human studies confirm the anti-inflammatory nature of galactosylation there is in vitro evidence that this is not the case. One such study of a mouse model of RA found that removal of the terminal galactose on IgG did not increase ADCC (Anthony, 2013).

In addition to aberrant galactosylation, there are additional variabilities with regard to the glycan profile in RA patients. However, with regard to the level of GlcNAc or fucose residues, there have been conflicting reports as to whether they are altered in RA patients (Drickamer, 2003). Aberrant glycosylation also occurs in serum proteins, mirroring the aberrant glycosylation that takes place on immunoglobulins in disease. α-1-acid glycoprotein (AGP) is a serum acute phase protein, whose concentration raises several fold under chronic pathological conditions like RA (Collins et al., 2013). AGP is heavily glycosylated and its binding and immunomodulatory function seem to depend on this glycosylation. Changes in fucosylation on the glycan have also been reported in RA and different AGP glycoforms exist in different diseases. Transferrin is a negative acute phase protein which means that its concentration decreases with the acute phase response (Varki et al., 1999). Changes of branching, fucosylation, or sialylation of transferrin have been observed in many inflammatory diseases. In particular, in RA this increase in branching of transferrin glycans correlates with disease activity. Aberrantly fucosylated haptoglobin

is also found in high levels in RA patients. However elevation of these levels may not be disease-specific since they are also found in sero-negative patients (Gornik and Lauc, 2008). Thus, not only are there aberrant glycosylation patterns in IgG antibodies in RA patients, but other serum proteins whose levels fluctuate in response to environmental inflammatory factors.

1.18.2 MTX and the effect on glycosylation in IgG and serum proteins in RA

Most studies have evaluated the effects of combination therapy using both anti-TNF and MTX on glycosylation. There have been few reports on MTX monotherapy for the treatment of RA. Overall, these studies have shown that combined treatment of infliximab (anti-TNF) and MTX in RA increase galactosylated IgG levels (Anthony, 2013). One such study followed the galactosylation status of IgG from RA patients undergoing clinical treatment with MTX and a combination of MTX and anti-TNF. Out of 11 patients, 7 showed a reduction in agalactosylation that matched a reduction in CRP and ESR, other markers of disease progression, compared with the agalactosylation levels in healthy donors. However, only one patient out of this cohort was on MTX monotherapy, the other patients were on combined MTX/ anti-TNF treatment so it is difficult to evaluate the effect of MTX alone on the glycosylation profile (Pasek et al., 2006). Another report found there was a reduction in IgG-G_0 with a combination of MTX, anti-TNF and steroids, however again, the relevance to this study is minimal (Croce et al., 2007). Investigations were also conducted following 3 months of therapy, however , although the levels of agalactosylation were reduced, the levels were still aberrant, so the effectiveness of treatment in this regard is questionable (Ercan et al., 2012).

The few studies that have investigated the effectiveness of MTX monotherapy include one in which the total serum $G_0:G_1$ (agalactosylation versus monogalactosylation) profile was evaluated. The results are in keeping with the previous studies on combination treatment, where treatment correlated with a reduction in agalactosylated IgG. This reduction correlated with improvement in clinical scores for both MTX and anti-TNF (Ercan et al., 2012). In addition to the effects on IgG galactosylation, MTX is also capable of markedly inhibiting the fucosylation and sialylation of human serum α-acid-glycoprotein in RA patients (Croce et al., 2007). So although few studies have looked at MTX treatment alone, those that have, show an increase in both IgG galactosylation and

potentially of other serum glycan, possibly suggesting an effect on serum protein glycan patterns.

1.19 Aims of the project

The extent in which the anti-proliferative effect of MTX contributes to its anti-arthritic mechanism is still not fully understood. This study sought to investigate the extent in which nucleotide inhibition is the mechanism behind a range of MTX-induced effects. Although the effect of purine and thymidine rescue on certain parameters have been measured, as previously discussed, no study has been found which has measured the extent of purine and thymidine inhibition on cytotoxicity, on the inhibition of T cell-activation, on mitochondrial function, or on the cell-surface sialome and correlated these to changes in intracellular metabolites in order to determine if MTX exerts differential effects on unactivated and anti-CD3-activated PBMCs, all under the same conditions.

Nothing is known about the effects of MTX on the sialome or how it changes during activation. Given the complex signalling and functional role surface glycans play in immune and non-immune mediated reactions, elucidating the phenotypical changes that can occur is imperative in understanding this potent anti-folate.

Thus far, the effects of MTX on intracellular metabolites has been limited and no conclusive study has been found which examines the effect of MTX on a range of nucleotides and sugar-nucleotides in unactivated cells and whether this changes during activation. Understanding the extent in which this anti-folate permeates the sugar-nucleotide and nucleotide pathways could shed new light on this potent anti-arthritic drug.

Specifically the aims of the project are;

Aim 1: To compare the cytotoxic and cytostatic effects of MTX as well as effects on mitochondrial function in both unactivated and activated PBMCs to see if MTX exerts differential effects during cellular activation.

Aim 2: To investigate the effect of MTX on T cell-activation, including blastogenesis, proliferation and transferrin receptor expression and investigate whether these diverse effects of MTX are mediated by purine and thymidine inhibition and not another consequence of folate deprivation.

Aim 3: To develop a method to analyse the effect of MTX on cell-surface sialylation in unactivated and anti-CD3-activated PBMCs at different stages of activation.

Aim 4: To quantify any changes in flux through the entire nucleotide and sugar nucleotide pathway in unactivated and anti-CD3-activated PBMCs with MTX treatment.

Aim 5: To explore the extent in which sugar-nucleotides depend on nucleotide levels and to investigate the link between the MTX-mediated purine and thymidine inhibition and both cell-surface sialylation and the levels of intracellular sugar-nucleotides, to see if MTX could impact on glycosylation by affecting the levels of nucleotides and sugar-nucleotide donors.

Chapter 2

Materials and General Methods

2.1 General methods

2.1.1 Antibodies and reagents

Functional grade purified mouse IgG2a, kappa, anti-human CD3, clone OKT3, was purchased from eBioscience, cat no: 16-0037-85. The goat pAb to mouse IgG conjugated alexa fluor 594 cat no: 150116 was purchased from abcam.

The following FACS reagents were purchased from eBioscience; Ultracomp beads cat no: 01-2222-41, as well as the following fluorochrome-conjugated antibodies; mouse IgG2a, kappa CD3-PE-clone OKT3 cat no; 12-0037-42, CD4-APC clone OKT4 cat no; 17-0048-41, anti-human CD8-APC efluor 780 clone RPA-T8 cat no; 47-0088-42, CD19-Pe-Cyanine 7 clone HIB19 cat no; 25-0198-41, with the exception of CD11c-Brilliant violet 421 clone 3.9 cat no: 301628 which was purchased from MSC and FITC mouse anti-human CD71 which was purchased from BD Pharmingen, cat no: 561939.

The following nucleotides and sugar-nucleotides were purchased from Carbosynth; GDP fucose cat no: MG01912, UDP-*N*-acetylglucosamine cat no: MU07955, UDP-*N*-acetylgalactosamine cat no: MU04515, UDP-glucose cat no: MU08960, UDP-galactose cat no: MU31560, CMP-*N*-acetylneuraminic acid cat no: MC04391, GDP-mannose cat no: MG05610. CTP cat no: NC03860.

JC-1 and Pro-long Gold antifade reagent with DAPI was purchased from life technologies, Eugene, Oregon, USA.

Phosphatase inhibitor tablets protease inhibitor tablets along with DNase were supplied by Roche.

Lymphoprep cat no: 1114545 was purchased from eBioscience. RPMI with Glutamax, DMEM with glutamax, DCF-DA, alamar blue was purchased from Biosciences.

Potassium phosphate monobasic and dibasic along with Coomassie Bradford assay kit were purchased from Fisher.

All other reagents used including antimycin A, oligomycin, propidium iodide, thymidine, hypoxanthine, DMSO, trypan blue, ammonium persulphate, MTX, AMP, ATP, ADP,

UTP, GTP, FBS, PBS, Poly-D-Lysine, PS were purchased form Sigma Aldrich C.o., Poole, Dorset, UK.

2.1.2 Preparation of solutions

Reagents were weighed on a Mettler College Model analytical balance for weights above 5g or on a Mettler K7t top-loading balance for weights below 5g. All aqueous solutions were prepared using deionized water from a Millipore Elix advantage 10 water purification system. All solutions were adjusted to the required pH using a Corning pH meter, model 240 which was calibrated daily using standard buffer solution of pH 4.0, 7.0 and 10.0. Gilson pipettes were used to pipette volumes from 50 µl to 1ml.

MTX was dissolved in 1M sodium carbonate buffer, pH 9-9.5 and sterile filtered. Stock solutions were kept at -20°C and stored for 1 month.

2.1.3 Centrifugation

For volumes of 1.5 ml or less, an Eppendorf benchtop centrifuge 5414 was used. An Eppendorf centrifuge 5810R was used for larger volumes.

2.2 Statistical analysis

Statistical analysis was carried out using Graph pad Prism 5. Analysis of data from matched observations from the same donor was carried out using a two-tailed paired student T-test, with a confidence interval of 95%. An unpaired student T-test was conducted from unmatched observations such as the comparison of metabolites from the same donor after 24 h in unactivated PBMCs and 72 h in anti-CD3-activated PBMCs or the comparison of anti-CD3-activated to unactivated PBMCs, broken out in the last 24 h. For the analysis of two or more groups, such as the untreated PBMCs compared to PBMCs treated with both MTX and rescue, a one-way ANOVA repeated measures test assuming Gaussian distributions was employed. This was followed with a Tukey's post-test or for the analysis of varying concentrations of the same treatment, a test for a linear trend using Prism. All data was presented as the mean ± SEM unless otherwise stated. A P-value of 0.05 or less was deemed to be statistically significant.

2.3 Cell culture

All cell culture work was carried out under sterile conditions in a NUAIRE laminar flow hood. All cells were maintained at 37°C, in 95% humidity and 5% CO_2. Cell growth and viability was monitored visually using a Nikon Eclipse TS100 light microscope with 10X, 20X and 40X dry objectives.

Human monocytic, immortalised, THP-1 (ATCC, Manassas, VA, USA) cells were cultured in RPMI media with GlutaMAX, (Life Technologies) containing 10% v/v foetal bovine serum (FBS) and 1% v/v penicillin-streptomycin. Cells were counted using Trypan Blue exclusion dye on a Countess Automated Cell Counter (Life Technologies) and maintained in culture at $<1X10^6$/ml, every 48h.

THP-1 cells were differentiated using PMA (200 nM) for 72 h, detached by incubating with a 1X solution of Trypsin-EDTA for 5 min. This reaction was stopped by the addition of media, reducing the strength of Trypsin to 0.1X. The cells were then seeded at $5X10^6$/ml, left to rest for 72h before treatments.

iBMDMs were maintained in DMEM glutamax, supplemented with 10% FBS, 1% penicillin-streptomycin. Cells were counted using Trypan Blue exclusion dye on a haemocytometer and maintained in culture at $<5X10^5$/ml. Cells were passaged every 48 h.

2.3.1 Isolation of human PBMCs from whole blood

Healthy donor blood was obtained with informed consent using the TBSI ethically sourced donor system, using sterile 9 ml heparin-coated tubes. The blood was diluted 1 in 2 with sterile PBS and 30 ml was layered over 20 ml of Lymphoprep (Life technologies) before being centrifuged at 800 x g/ 20 mins/ 20°C/with the brake off to separate its components based on their relative densities. The PBMC layer was pipetted off using a sterile pasteur pipette into a 50 ml falcon containing 20 ml PBS, and then centrifuged at 720 x g for 10 mins. The pellet was then resuspended in 3 ml 0.88% sterile filtered-ammonium chloride for 10 min at 37°C to lyse the red blood cells. PBMCs were rescued upon the addition of 15 ml complete media and centrifuged at 200 x g for 7 min. The

supernatant was discarded and the pellet resuspended in 20 ml complete media, and centrifuged at 200 x g for 7 min to remove contaminating platelets. The supernatant was poured off, and the pellet resuspended in 20 ml complete media, before counting. For ELISA's, cells were seeded at $5X10^5$/ml, for JC-1 incubation and membrane potential determination, $1X10^6$/ ml cells were used.

Buffy coats were acquired for analysis of the intracellular metabolites because of the large number of cells required. An additional 1 in 4 dilution with PBS was performed before layering over 20 ml of Lymphoprep as before.

2.3.2 Extraction and culture of murine dendritic cells from femur and tibia of wild-type mice

Bone Marrow stromal stem cells were flushed from the femur and tibia with RPMI and glutamax, using a 23G needle, into a 70µm nylon mesh cell strainer (Fisher). Isolated cells were centrifuged for 3 min at 300 x g and the supernatant discarded. The pellet was suspended in (1 ml ammonium chloride (1.5%)), for 1 min to selectively lyse red blood cells. The suspension was made to 30 ml with culture medium to terminate osmotic stress and centrifuged at 1400 rpm for 3 min. Pelleted cells were resuspended in 30 ml culture medium and counted. Cells were seeded in culture flasks at (4 X 10^5cells/ml), in a total volume of 30 ml per flask, and differentiated using (20 ng/ml) GMCSF for a total of 10 days. On days 3 and 8, cells were fed with 30 ml RPMI with glutamax, On day 10, culture flasks were gently agitated and the cells counted before seeding at (5 X 10^5 cells/ml) for ELISA and Trypan blue viability assays.

2.3.3 Activation of CD3^{+} PBMCs using anti-CD3

Anti-CD3 antibody was let adhere to 6 well cell culture plates at 1µg/ml in PBS for 2 hours at 37°C before being washed twice with PBS, to remove any non-adherent antibody. Following this, PBMCs were then added to the anti-CD3-coated 6 well plate at $1X10^6$/ml, 3ml/well and left for 72 h, previously been found to be the optimum density based on clustering of T cells and the induction of significant proliferation (Fig 2.1). Optimising cell density for the activation required for individual experiments was

recommended as was a 48-72 h duration (eBioscience). No data can be found on whether the measured increase in proliferation under these conditions is in keeping with the data found elsewhere. The cells were then counted and used in subsequent experiments.
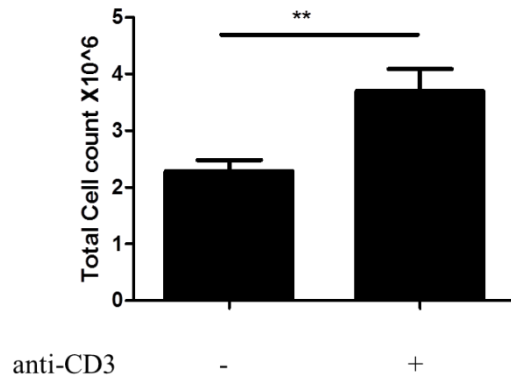
Figure 2.1. Anti-CD3-induced significant cellular proliferation of PBMCs after 72 h.

PBMCs were seeded at $1X10^{\wedge}6$/ml, 3ml/6well plate in the presence or absence of anti-CD3 (1 µg/ml) for 72 h. PBMCs were then counted following the addition of Trypan blue exclusion dye and the values compared to that of the unstimulated control. Data presented as mean ±SD, n=3; a paired student T-test was performed and significance is indicated by *P<0.05, **P<0.01, or ***P<0.001.

.

2.3.4 Use of FACS buffer

Complete RPMI (RPMI glutamax with 10% FBS and 1% PS) was diluted 1:5 with PBS for all flow cytometry experiments. This was important to maintain cell viability of these primary cells during incubations for all flow cytometry experiments.

However the use of 2% FACS buffer for spectrophotometric assays such as those measuring DCF-DA, gave high background readings which couldn't be removed. Thus, for the measurement of ROS production, Krebs buffer supplemented with 10 mM glucose was used. For this reason ROS levels produced may be higher because of the reduction in cell viability incurred in the absence of FBS.

Chapter 3:

The toxicity of low-dose Methotrexate in human PBMCs
associated with purine and thymidine inhibition

3.1 Introduction

Methotrexate has been shown to be both a cytotoxic and anti-proliferative drug- at both high and low concentrations. It is generally accepted that low-dose MTX has no cytotoxic effect in unactivated primary cells and non-mitogen-activated primary cells have also shown little susceptibility to these cytotoxic effects. However, cell death has been shown to occur in immortalised cell lines and proliferating primary cells, to varying degrees, because these cells are dividing. Following MTX treatment in vitro, folinic acid has been shown to recover cell proliferation (Rosenblatt et al., 1982). During MTX treatment, folinic acid was also shown to offset the side effects without negating the anti-arthritic effect of MTX. This was deemed evidence that the mechanism of action of MTX was not inhibition of cell proliferation (Chan and Cronstein, 2010). However recently, it has come to light that over-rescue using folinic acid can occur with low-dose treatment (Cohen, 2013). This over-rescue actually diminished the effects of treatment, to the extent where in some cases rescue had to be stopped. Other reports noted that in cases where the side effects were minimised, so too were the anti-arthritic effects (Tishler et al., 1988). Since folinic acid rescue can recover cell proliferation or completely reverse the therapeutic effect of MTX, it means that the anti-proliferative effect could still be a crucial mechanism to the anti-arthritic effect of MTX. This anti-proliferative effect, mediated by purine and thymidine inhibition has multiple effects on the one-carbon metabolism pathway, effecting nucleotide and metabolic precursors as well as cofactors. In addition, because MTX is known to inhibit mTOR mediated cellular activation, it was important to assess the effect of MTX on the morphological and metabolic changes that occur during cellular activation and assess whether these changes were related to purine and thymidine inhibition.

3.1.1 Antigen-dependent toxicity

A huge limitation to the study of MTX-induced toxicity is the variability in activation stimulus used during treatment, as the extent of activation varies dramatically for different stimuli in the same time frame (Collins, 2000). This means that comparing the effect of MTX using different activators is not only difficult, but highly inaccurate. One of the most important studies done in this regard were experiments comparing the

activation status of PBMCs following stimulation with PMA/ionomycin, anti-CD3/CD28, PHA and the superantigen SEB (Reddy et al., 2004). The authors evaluated expression of activation markers and cytokine secretion upon these antigenic or mitogenic stimuli, in parallel, and showed that the kinetics of activation depended on the stimuli in question. Results showed that activation marker expression of CD71 and CD65, amongst others, varied depending on the stimuli for the same induction time. Since these measurable parameters of cellular activation are the only way to determine the activation state of a cell, these results demonstrated that the same cells were at different activation states using different stimuli. Finally, the same study evaluated the effect of an inhibitor of early T cell-activation, dexamethasone, on the induction of activation markers and cytokine secretion with different stimuli. Unsurprisingly, this inhibitor showed differential effects with different stimuli. With regard to MTX, stimulus-dependent cytotoxicity, reflecting different states of activation has also been shown (Johnston et al., 2005). Thus, it is difficult to draw parallels of the cytotoxic effect of MTX across a broad range of antigenic and non-antigenic stimuli. This is because the extent of activation may influence how much MTX is taken up into the cell. Indeed, flow cytometric analysis conducted on PBMC cultures, unstimulated or stimulated with antigens CA or TT, showed that only stimulated cultures took up the FITC-labelled MTX (Nielsen et al., 2007).

3.1.2 Rescue from the apoptotic effects of MTX

Rescue from MTX-induced cell death has been achieved through a variety of different mechanisms in different cell types. This indicated that MTX exerted cytotoxic effects through different pathways. Reversal of the induction of apoptosis has been shown in platelets, upon the addition of the antioxidant, N-acetylcysteine (NAC), thus showing that reactive oxygen species (ROS) production was involved in the apoptotic pathway (Paul et al., 2015). It was also shown that NAC incubation alongside MTX (0.1 μM) for 48 h, followed by blocking of the cell death receptor, FAS, prevented the apoptosis in Jurkat T cells (Spurlock et al., 2011). ROS was also shown to be the mechanism of MTX (1 μM)-induced cytotoxicity in HL-60 cells when overexpression of ornithine decarboxylase, the first rate limiting enzyme in the polyamine pathway, which increases polyamine synthesis, including the free radical scavenger, prevented the MTX induced apoptosis (Ha et al., 1998, Huang et al., 2005). S-adenosylmethionine, involved in methylation

reactions, has also been shown to recover growth of suspension cell lines following MTX (8 nM) treatment (Kimura et al., 2004). This suggested that inhibition of methionine synthesis and its s-adenosylmethionine derivative was linked to the cytotoxic effects observed in this cell type. Thymidine and hypoxanthine rescue of cell viability following low-dose MTX has been shown in the CCRF-CEM leukemic cell line (Taylor and Tattersall, 1981). Finally this suggested that inhibition of purine and thymidine synthesis was linked to the cytotoxic effects observed in this cell type. No study has been found that demonstrates that rescue of proliferation subsequently rescues cell viability in human PBMCs. It is also not known what other MTX-mediated effects can be prevented by purine and thymidine rescue. Thus, the aim of this part of the study was to delineate the secondary effects of MTX-mediated purine and thymidine inhibition.

3.1.3 mTOR and T cell-activation

mTOR is a crucial serine/threonine kinase involved in metabolic sensing and the control of a variety of cellular processes involved in the cell cycle and anabolic pathways. Its downstream targets include the transcription factors, c-Myc and HIF-1α, which are thought to be responsible for controlling changes in cellular metabolism in the early and late stages of T cell-activation, respectively (Fernandez-Ramos et al., 2016). c-Myc is responsible for the activation-induced upregulation of glycolysis and glutamine metabolism in T cells (Wang et al., 2011a). c-Myc deletion prevented T cell growth and proliferation demonstrating that mTOR was indirectly controlling cellular proliferation via c-myc. This control of c-Myc by mTOR was strengthened when mTOR inhibition partially affected the activity of c-Myc transcription (Wang et al., 2011a). mTOR inhibition has been shown to occur during nutrient starvation, via the transcription factor AMPK (O'Neill and Hardie, 2013). Through increasing AMP and its analogue AICAR, (see **Section 1.7.4**) MTX mimics nutrient starvation and can potentiate the activation of AMPK and thus inhibit mTOR-dependent cellular activation (Beckers et al., 2006). To date, the effects of MTX have been shown on a range of characteristics of cellular activation, these include cytokine secretion, adhesion molecule or activation marker expression, such as CD69; granzyme B expression, enhancement of cytotoxic function, NF-kB activation or blast cell formation in immune cells, as well as antibody production (Nesher and Moore, 1990, Izeradjene et al., 2001, Gerards et al., 2003, Kremer, 2004, Quemeneur et al., 2004, Johnston et al., 2005, Torres-Alvarez et al., 2007, Spurlock et al.,

2015). However, the mechanism in which MTX has inhibited these activation parameters is unknown in most cases. No reports have been found which examine the effect of low-dose MTX on transferrin receptor expression and lymphoblast generation as a means of limiting cellular activation.

3.1.4 Mitochondrial toxicity

The MTX-mediated, potentiation of AMPK activation has been shown to have effects on mitochondrial biogenesis (Fernandez-Ramos et al., 2016). In light of this, it was important to determine how else MTX could affect the mitochondria. Since an adequate mitochondrial inner-membrane potential ($\Delta\Psi_m$) is required for optimal mitochondrial function, the effects of MTX on the $\Delta\Psi_m$ were examined. MTX has also been shown to increase ROS production. The inhibition of DHFR prevented the reduction of dihydrobiopterin to tetrahydrobiopterin, a cofactor to all nitric oxide synthases (Spurlock et al., 2015). Since mitochondrial generated ROS is the biggest source of cellular ROS in eukaryotes, the effect of MTX on intracellular ROS in these PBMCs was also investigated. Although, these insults to the mitochondria have been examined to a certain extent, with regard to limiting cellular activation, the contribution of purine and thymidine inhibition to both, has not been investigated. Neither have these insults been explored as a toxicity to normal cellular function.

3.2 Aims of the chapter

High dose MTX (>1 µM) exerts its chemotherapeutic effect by limiting cellular proliferation, although low-dose MTX (<1 µM) has also been shown to limit mitogen-induced proliferation, in a variety of cell types. Folinic acid treatment has been shown to undermine the efficacy of MTX in some cases which suggests that the anti-proliferative effect could be a crucial mechanism in which MTX exerts its therapeutic effect in inflammatory disease. The one-carbon metabolism pathway, including purine and thymidine synthesis, is also responsible for other biosynthetic precursors. Thus, it is possible that purine and thymidine inhibition via MTX have secondary implications on other anabolic pathways which could at least contribute to the anti-inflammatory effect of MTX. It could prove that the simplistic view of purine and thymidine-mediated inhibition of proliferation is in fact key to the success of MTX as an anti-inflammatory drug. To achieve these aims a variety of mechanisms were employed including flow cytometry. This enabled the exclusion of dead cells from any observed effects and eliminated the possibility that reversal of these effects by purine and thymidine rescue was simply rescuing cell viability.

The specific aims of the study are to;

1. Verify the anti-proliferative and cytotoxic effect of MTX treatment in dividing cells and determine if the cell death incurred could be reversed by purine and thymidine rescue.

2. Investigate whether MTX affected any other aspect of cellular activation, specifically transferrin expression and lymphoblast formation and determine if this inhibition could be reversed by purine and thymidine rescue.

3. Investigate whether the mitochondrial inner-membrane potential was affected by MTX treatment in unactivated and anti-CD3-activated PBMCs, and whether these effects could be reversed by purine and thymidine rescue.

4. Measure ROS production upon MTX treatment in PBMCs, unactivated and activated with anti-CD3 and see if these effects could be reversed by purine and thymidine rescue.

3.3 Methods

3.3.1 Cell viability assays

3.3.1.2 Immortalised cell lines

THP-1 cells were activated with PMA (200 nM) for 72 h. They were then trypsinised and seeded (5 X 10^4 cells/ml and 200 μl/well) in a 96 well plate for 72 h. Alamar blue was added at the time of MTX treatment (0.1, 1, 10,100 nM, 1 μM) and readings were taken at 570 nm and 600 nm 4 h later. The percent viability values are expressed as a percentage of the control, set at 100% viability.

iBMDMs (1.66 X 10^5 cells/ml and 180 μl/well) were seeded in a 96 well plate and were left to rest o/n before activation with LPS (100 ng/ml) and MTX (0.1, 1, 10, 100 nM, 1, 5, 10, 20, 50, 70, 80, 90, 100 and 125 μM) for 24 h. Alamar blue was added in the last 4 h of treatment and readings were taken at 570 nm and 600 nm. The percentage viability values are expressed as a percentage of the control, set at 100% viability.

3.3.1.3 Unactivated and LPS-activated human PBMCs and mouse DCs

PBMCs were isolated from human blood as described previously (see **Section 2.3.1**) and seeded (5 X 10^5 cells/ml and 200 μl/well) in a 96 well plate. MTX (0.1 nM-1 μM) and LPS (100 ng/ml) were added to cells where appropriate, for 24 h before the viability was assessed using trypan blue exclusion dye on an automated cell counter.

Mouse DCs were isolated from the mouse tibia and femur as described previously (see **Section 2.3.2**) and seeded (2 X 10^5 cells/ml and 200 μl/well) in 96 well plates o/n to rest. MTX (0.1 nM-1 μM) and LPS (1 ng/ml) were added to cells where appropriate, for 24 h before the viability was assessed using trypan blue exclusion dye on an automated cell counter.

3.3.1.4 Partially-activated PBMCs

PBMCs (1 X 10^6 cells/ml and 200,000 cells/well) were activated with anti-CD3 (1 μg/ml) for 72 h. MTX (0.1, 1, 10, 100 nM,1 μM) was added in the last 4, 6, 8 and 24 h of this 72 h activation or for the duration of the activation. Alamar blue was added in the last

4 h of activation. Absorbance values at 570 nm and 600 nm were taken after those times and viability of MTX treated cells expressed relative to controls, set at 100% viability.

3.3.2 Cell proliferation assays

3.3.2.1 Cell counts

PBMCs were seeded according to the basic set up conditions-(1 X $10^{\wedge}6$ cells/ml and 3 ml/well) ± anti-CD3 (1 μg/ml) ± MTX (at the indicated doses) ± thymidine and hypoxanthine (100 μM) for 72 h. Proliferation was assessed by comparing the total viable cell count after 72 h of the control cells, either anti-CD3-activated or unactivated PBMCs using trypan blue exclusion dye.

A growth curve of anti-CD3-activated PBMCs ± MTX 100 nM was generated by taking a 10 μl cell sample at specific times over the course of the activation and counting the viable cells manually on a haemocytometer, following trypan blue exclusion dye.

3.3.2.2 Carboxyfluorescein succinimidyl ester (CFSE) staining

PBMCs were isolated from fresh human blood as discussed previously (see **Section 2.3.1**) and were left to rest for an hour before CFSE incubation. PBMCs (3 million) were set aside as an unstained control that did not contain CFSE. A further (~25 million) were washed in unsupplemented RPMI with glutamax (10 ml) before resuspending in 2 ml of the same media at 1.2 X $10^{\wedge}7$ cells/ml. This 2 ml total volume was then added to a 2 ml solution of the same buffer, containing CFSE (2.7 μg/ml). The cells were incubated with CFSE for 10 min at 37°C before recovery with ~20 ml supplemented RPMI with glutamax media. PBMCs were finally centrifuged and resuspended in supplemented RPMI with glutamax and left to rest for one hour. 3 million CFSE stained PBMCs were left unactivated to measure basal proliferation. The remaining PBMCs were seeded (1 X $10^{\wedge}6$ cells/ml and 3 ml/well) with anti-CD3 (1 μg/ml) ± MTX (0.1, 1, 10, 100 nM, 1 μM) for 72 h. After this time PBMCs were counted on a haemocytometer and resuspended in 2% FACS buffer (1 X $10^{\wedge}7$ cells/ml). A sample of CFSE stained control cells and the unstained cells was left without antibody as a CFSE control. Two microliters of each antibody against the surface marker CD4, CD8, CD11c and CD19 was added to 100 μl of cells from each condition and incubated on ice for 40-60 min. After this time, cells were

centrifuged and the pellet resuspended in 600 µl 2% FACS buffer. This was repeated 3 times. PBMCs were then resuspended in 400 µl 2% FACS buffer for flow cytometric analysis. Single stained cells and compensation beads were ran for compensation controls. PI (1 µg/ml) was added to each condition. Cell debris was first excluded following gating against FS and SS measurements. Doublets were excluded following gating against FS and pulse width. Viable cells were determined as those cells negative for PI stain in the total population (% PI negative). These PI negative PBMCs were then gated using one of two strategies. The first on a histogram of CFSE with increasing peaks to the left reflecting loss of CFSE and the % proliferation measured after excluding the first peak. This statistical analysis was chosen because successive generations of cells could not always be identified (Roederer, 2011).

To analyse the proliferation of PBMC subsets, CD4$^+$ T cells and CD8$^+$ T cells were determined following gating against CD4 and CD8. Those cells positive for both CD4 and CD8 were considered dead cells and were not included. CD4$^+$ T cells or CD8$^+$ T cells were determined as those positive for either CD4 or CD8. Those cells negative for both CD4 and CD8 were then gated on CD19 and CD11c. CD19$^+$ or CD11c+ cells were determined as those positive for either CD19 or CD11c only. The proliferation of each cell subset was measured by analysing staining with CFSE as before.

3.3.3 Measurement of viability, transferrin receptor expression and lymphoblast formation

PBMCs were seeded as for the basic set up-(1 X 10^6 cells/ml and 3 ml/well) ± anti-CD3 (1 µg/ml) ± the concentrations of MTX indicated, with or without thymidine and hypoxanthine (100 µM). Unactivated PBMCs were broken out from frozen on the last day of activation, cultured for 1 h and left unactivated as a control.

Cells were counted on a haemocytometer and resuspended in 2% FACS buffer (1 X 10^7 cells/ml). A sample of the control cells was taken and divided into two, for an unstained and PI only control and single stains achieved using compensation beads as before. An antibody cocktail comprised of antibodies against the surface markers, CD4, CD8 and CD71 was added to cells and left to incubate on ice for 40-60 min. After this time, cells were centrifuged and the pellet resuspended in 600 µl 2% FACS buffer and this was repeated 3 times. PBMCs were then resuspended in 400 µl 2% FACS buffer for flow

cytometric analysis. PI (1 µg/ml) was added to cells. Cell debris was first excluded following gating against FS and SS measurements. Doublets were excluded following gating against FS and pulse width. Viable cells were determined as those cells negative for PI stain in the total population (% PI negative).The cells were then gated as follows;

For the determination of CD71 expression on both CD4$^+$ and CD8$^+$ T cell subsets. PBMCs were gated on CD4 positive and CD8 negative, or CD8 positive and CD4 negative. Populations that were positive for both CD4 and CD8 were dead cells and were excluded. The percentage of CD4$^+$CD71$^+$ T cells and CD8$^+$CD71$^+$ T cells were determined, following gating of either CD4 or CD8 with CD71.

For the determination of lymphoblast formation PBMCs were gated on either CD4 positive and CD8 negative, or CD8 positive and CD4 negative. Populations that were positive for both CD4 and CD8 were dead cells and were excluded. The size of those CD4$^+$T cells or CD8$^+$T cells was analysed by a histogram analysis of FS. Large T cells were found to be (>35k) in size, reflecting lymphoblast formation.

The viability of individual CD4$^+$ and CD8$^+$ T cell subsets was also determined following MTX treatment using a different gating strategy. Cell debris was first excluded following gating against FS and SS measurements. Doublets were excluded following gating against FS and pulse width. CD4$^+$ T cells were identified following gating on cells positive for CD4 expression and negative for CD8 expression. These cells were then backgated for those CD4$^+$ T cells negative for PI stain. CD8$^+$ T cells were identified following gating on cells positive for CD8 expression and negative for CD4 expression. These cells were then backgated for those CD8$^+$T cells negative for PI stain.

3.3.4 Measurement of $\Delta\Psi_m$ with JC-1

Activated PBMCs were seeded as for the basic set up-(1 X 10$^{\wedge}$6 cells/ml and 3 ml/well) in an anti-CD3 (1 µg/ml) coated 6 well plate $\pm$ MTX (100 nM) $\pm$ thymidine and hypoxanthine (100 µM). Unactivated PBMCs were seeded (1 X 10$^{\wedge}$6 cells/ml and 3 ml/well) $\pm$ MTX (100 nM) for 5 h. The mitochondrial membrane potential $\Delta\Psi_m$ of whole PBMCs was determined using JC-1 dye (5,5'6,6'-tetrachloro-1,1'3,3'-tetraethylbenzimidazolylcarbocyanine iodide) (Life Technologies) which exhibits potential-dependant accumulation in the mitochondria. Thus, in healthy cells, a high

membrane potential causes the JC-1 to aggregate and in cells containing depolarized mitochondria, the JC-1 accumulates in the cytosol. The JC-1 aggregate and monomeric form fluoresce at different wavelengths, excitation/emission $\lambda = 535/590 \pm 17.5$nm and $\lambda = 485/530 \pm 15$ nm respectively and the ratio of the emission of the aggregate to the monomeric form are indicative of mitochondrial health (Fig 3.1A). On a flow cytometer, the aggregate JC-1 is detected in the FL2 channel and the momomeric JC-1 in the FL1 channel.

After treatment cells were centrifuged and resuspended in 2% FACS buffer. A sample of the untreated cells was taken for the unstained and PI only controls. The remaining PBMCs were incubated in PBS containing JC-1 (4 µM) at (1 X $10^{\wedge}6$ cells/ml) for 15 min at 37°C. Cells were washed three times before resuspending in (400 µl 2% FACS buffer) for flow cytometric analysis.

PBMCs loaded with JC-1 that contained no MTX were split into 3 tubes, one left untreated and the other tubes treated with either antimycin A (250 nM) or oligomycin (1 µg/ml) for 15 min before $\Delta\Psi_m$ determination. A sample of the untreated cells containing JC-1 was first run and re-run after being treated with FCCP (500 nM) to identify the aggregate JC-1 (Fig 3.1B &C). FCCP had an uncoupling effect and reduced the aggregate population. This gate was then applied to all other samples. Although measurement of the percentage reduction of the aggregate was only semi-quantitative it was deemed the most accurate way to analyse the samples. The uncoupling of the $\Delta\Psi_m$ following FCCP (500 nM) treatment was more clearly shown by a reduction in the aggregate JC-1 (Fig 3.1E) rather than the ratio of the aggregate (575 nm)/monomeric JC-1 (530 nm), (Fig 3.1D).

The maintenance of these primary cells in 2% FACS buffer, containing FCS was important for the viability of the cell and maintenance of a healthy $\Delta\Psi_m$, containing a high % aggregate JC-1 (Fig 3.2).
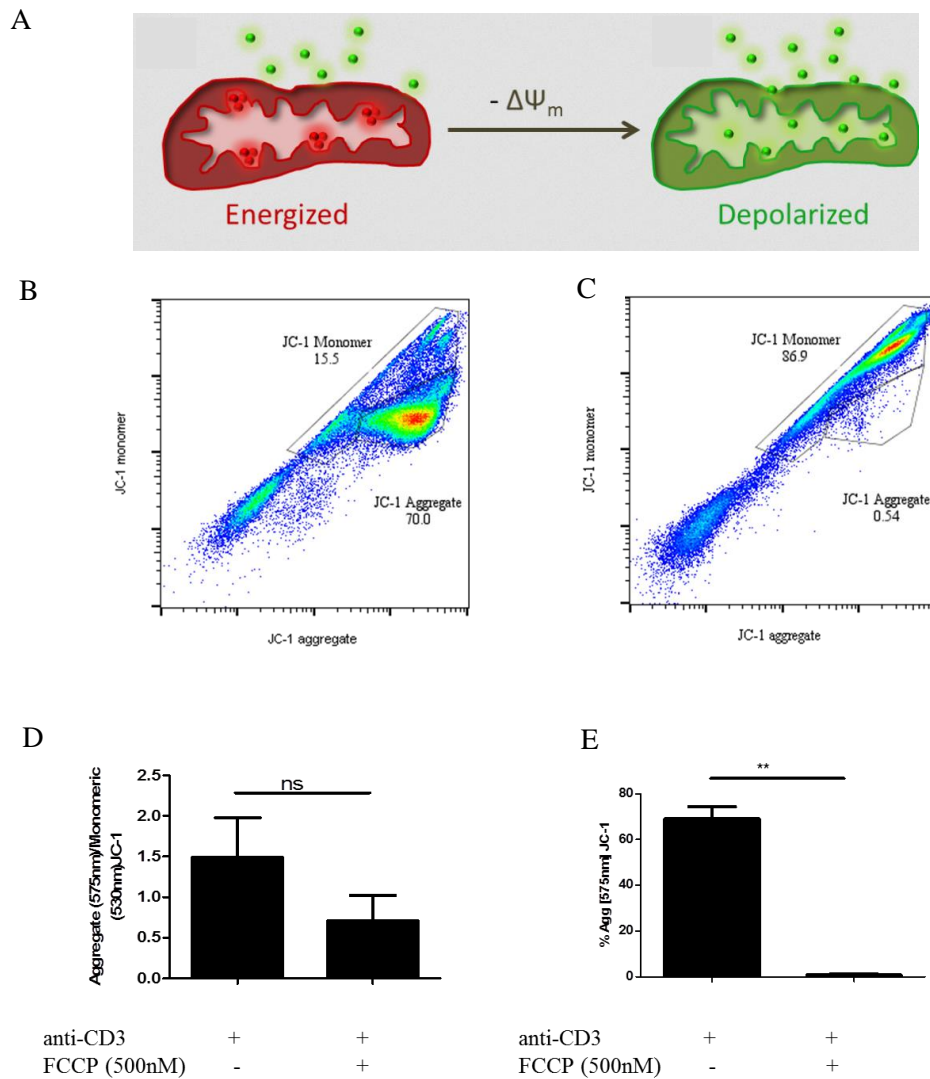
Figure 3.1. Semi-quantitative analysis of the $\Delta\Psi_m$ is achieved by measuring changes in the aggregate JC-1.

PBMCs ($1X10^{\wedge}6$/ml) were incubated with JC-1 (4 µM) for 15 min at 37 degrees. Flow cytometry was used to assess the $\Delta\Psi_m$. (A) Schematic of the high aggregate JC-1 in healthy cells, or a low aggregate/ high monomeric JC-1 in depolarised cells. The gate applied to identify the aggregate population. (B) The addition of FCCP (500 nM) (upper panel) depolarised the $\Delta\Psi_m$ and depleted the aggregate JC-1 population. (D) ratio of the aggregate (575nm) / monomeric JC-1 (530nm) upon the addition of FCCP (500 nM), (E) changes to the % aggregate (575nm) JC-1 upon the addition of FCCP (500 nM). (B&C) representative histograms of the identification of the JC-1 aggregate. (D&E) Data are presented as mean ± SD, n=3, a paired student T-test was performed with significance indicated by *P<0.05, **P<0.01. (A) Taken from (http://synentec.com).
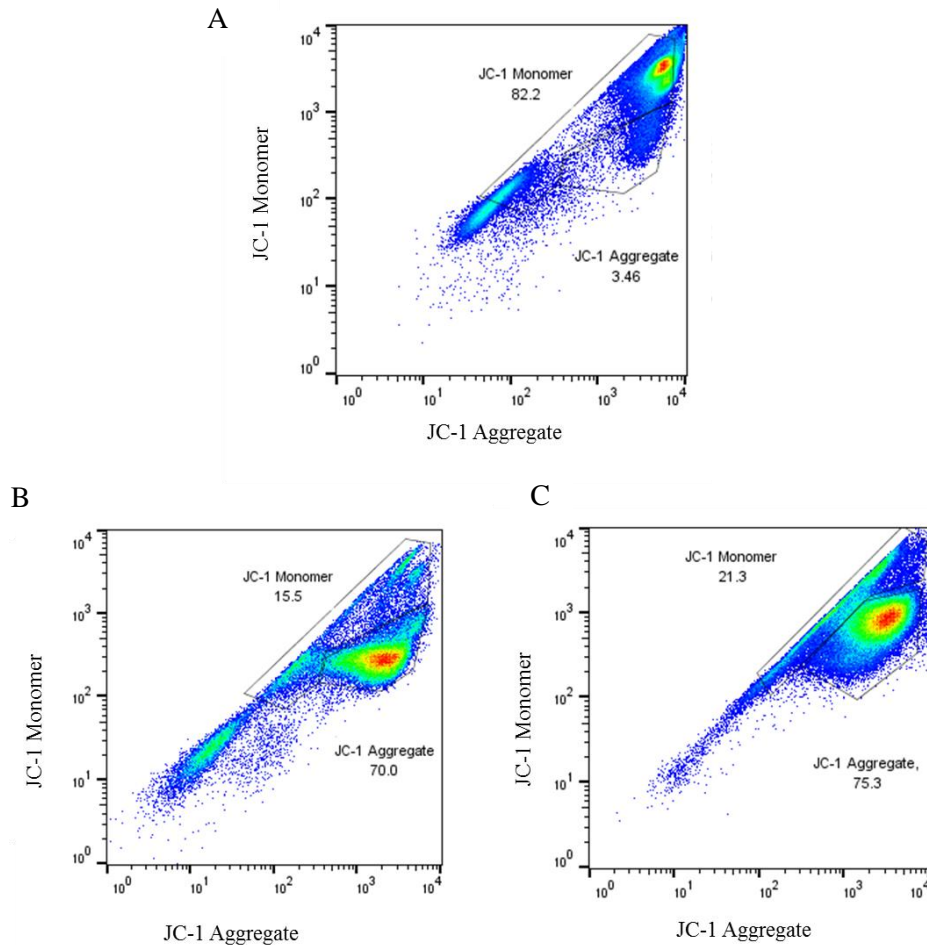
Figure 3.2. The addition of FCS is important in maintaining viable PBMCs, determined by having a higher $\Delta\Psi_m$ or high % aggregate JC-1.

PBMCs were incubated in either (RPMI with glutamax containing 0% FCS, diluted 1:5 with PBS (A), full media, diluted 1: 10 with PBS (B), or full media diluted 1:5 with PBS (C) as shown. They were then incubated with JC-1 (4 µM) for 15 min at 37degrees before analysis of their % aggregate JC-1 on flow cytometry. Dot plots shown display representative data of one experiment.

3.3.5 The measurement of cellular redox status using $H_2DCF-DA$

$H_2DCF-DA$ is a cell permeable, chemically reduced form of fluorescein which is oxidised in the presence of ROS. Oxidation cleaves the acetate groups and converts this non-fluorescent molecule into fluorescent 2',7'-dichlorodihydrofluorescein diacetate (DCF). There are limitations using this assay as DCF-DA is not a direct measure of hydrogen peroxide production, which is the type of ROS which leaves the mitochondria. However, DCF-DA can be used to measure a variety of reactive species including hydroxyl radicals and those formed following peroxynitrite decomposition (Klionsky et al., 2016). Hydroxyl radicals can be formed during the fenton reaction by superoxide and hydrogen peroxide which suggests that it can measure mitochondrial derived ROS, but cannot differentiate between mitochondrial and cytosolic-produced ROS such as that from NADPH oxidase. As a result the use of DCF-DA was used to measure cellular redox status, and an increase in oxidised DCF-DA fluorescence used to indicate a more oxidised environment, referred to in this study for simplistic reasons as an increase in ROS production. Optimum assay conditions for the measurement of cellular redox status/ ROS production using $H_2DCF-DA$ were determined as outlined (Fig 3.3). A range of PBMC cell numbers /well were tested to determine whether the cell numbers used were inside the linear range of detection using DCF-DA (A). A range of concentrations of DCF-DA were tested to ensure the concentration used was not limiting (B). DCF-DA (10 μM) measured maximal fluorescence using the PBMC cell numbers shown from (B) and was used to show that ROS production, derived from the mitochondria could be measured upon the addition of a positive control, antimycin A (C). Antimycin A is an inhibitor of complex III and has been shown to increase the rates of ROS production from the mitochondria (St-Pierre et al., 2002, Muller et al., 2004, Miwa and Brand, 2005).

Activated PBMCs were seeded as for the basic set up-(1 X $10^{\wedge}6$ cells/ml and 3 ml/well) in an anti-CD3 (1 μg/ml) coated 6 well plate ± MTX (100 nM) ± thymidine and hypoxanthine (100 μM). Unactivated PBMCs were seeded (1 X $10^{\wedge}6$ cells/ml and 3 ml/well) ± MTX (100 nM) for 5 h. PBMCs were counted using trypan blue exclusion dye, and resuspended in Krebs Buffer (3 mM KCL, 140 mM NaCL, 25 mM Tris-HCL, 2 mM $MgCl_2$, 2 mM $CaCl_2$, pH 7.4, supplemented with 10 mM glucose) before being seeded (6.66 X $10^{\wedge}5$ cells/ml and 100,000 cells/well) in a black 96 well plate. Controls for ROS production, including antimycin A (250 nM, 500 nM or 1 μM) or ethanol was added

A

B

C
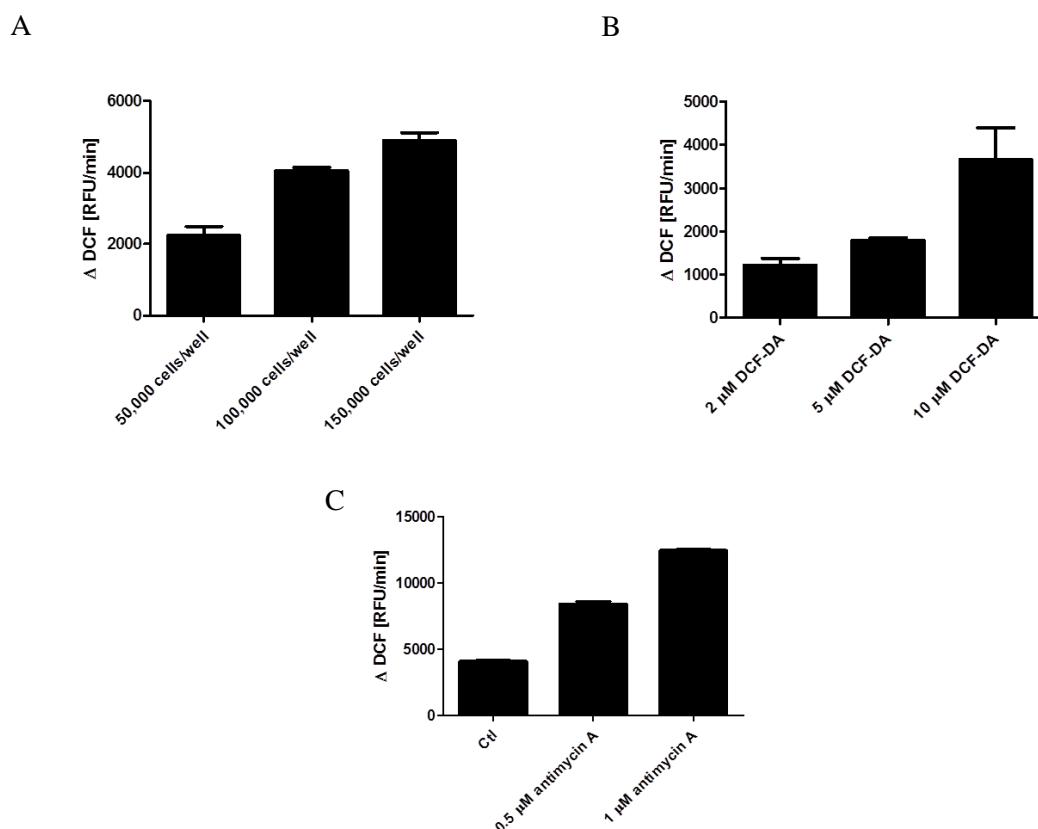
Figure 3.3. Determination of the optimum conditions for ROS detection in PBMCs.

(A) PBMCs (either 50,000/100,000/150,000 cells/well) were treated with DCF-DA (2 µM) to verify that the rate of DCF production was proportional to the number of cells. (B) PBMCs (100,000 cells/well) were treated with a dose response of DCF-DA (2 µM, 5 µM, 10 µM) to determine the concentration of DCF to measure maximal ROS production. (C) PBMCs (100,000 cells/well) were treated with DCF-DA (10 µM) and left untreated or treated with antimycin A (250 nM and 500 nM), a positive control for ROS production, to investigate the limits of sensitivity for DCF production. Data presented as mean ± SD, of one assay done in triplicate.

as indicated. DCF-DA was made up to a final concentration of (10 µM) and added to each well before fluorescence measurements (excitation 488 nm and emission 525nm) were taken every 30 s for 1 h. Rates were calculated by measuring the slope of the straight part of the curve, excluding the initial lag phase. The rate of ROS production, quantified by measuring the oxidised form of DCF-DA, DCF for each condition was then calculated by subtracting the blank rate.

3.4 Results

3.4.1 MTX has differential cytotoxic effects on immortalised cell lines compared to primary murine DCs or human PBMCs

Low-dose MTX (<1 µM) reduces the cell viability of PMA (200 nM) differentiated-THP-1 monocytic cells after 24 h (Fig 3.4A). MTX (100 nM) also caused cell death in iBMDMs co-cultured with LPS (100 ng/ml) (Fig 3.4B). The IC50 of iBMDMs activated with LPS was found to be 17.44 µM. However, low-dose MTX treatment (<1 µM) did not cause significant cell death in unactivated as well as LPS-activated primary human PBMCs or murine DCs (100 ng/ml or 1 ng/ml), respectively (Fig 3.6A) and Fig 3.6B).

The effect of MTX on mitogen-activated PBMCs at different stages of activation was then investigated. A range of concentrations of MTX added for the last 4, 6, 8 or 24 h of the 72 h anti-CD3 activation had no significant effect on cell viability (Fig 3.7). However, MTX (100 nM and 1 µM) significantly reduced the viable cell count for the duration of the anti-CD3 activation (Fig 3.8A). Co-culture in the same cells left unactivated showed no reduction in cellular viability. In order to investigate the reason for this loss in viable cells, a growth curve was conducted over the course of this 72 h activation (Fig 3.8B). After 48 h of anti-CD3 activation the same drop in viable cells was observed in both MTX treated and un-treated controls. After 72 h, there was a significant increase in viable cells in the un-treated compared to the MTX-treated cells, which began to plateau. Thus, it was clear that the difference in viable cell counts on the final day of the 72 h activation, was due to failure of the MTX-treated cells to proliferate. However, after 120 h the number of viable MTX-treated cells was at its lowest, indicating that cell death had occurred at this time.

In order to assess whether cell death had contributed to the reduction in viable cells observed after 72 h of the anti-CD3 activation, propidium iodide (PI), was added to the cells after this time. This verified that significant cell death had occurred in the MTX (100 nM and 1 µM) treated cells compared to the un-treated control (Fig 3.9). However, since cell viability was an acceptable ~75%, a 72 h activation period was used for subsequent experiments. Moreover, since the activation of CD3^{+} T cells was the main focus of this project, it was important to investigate what proportion of the viable cells were CD4^{+} and CD8^{+} T cells after anti-CD3 activation.
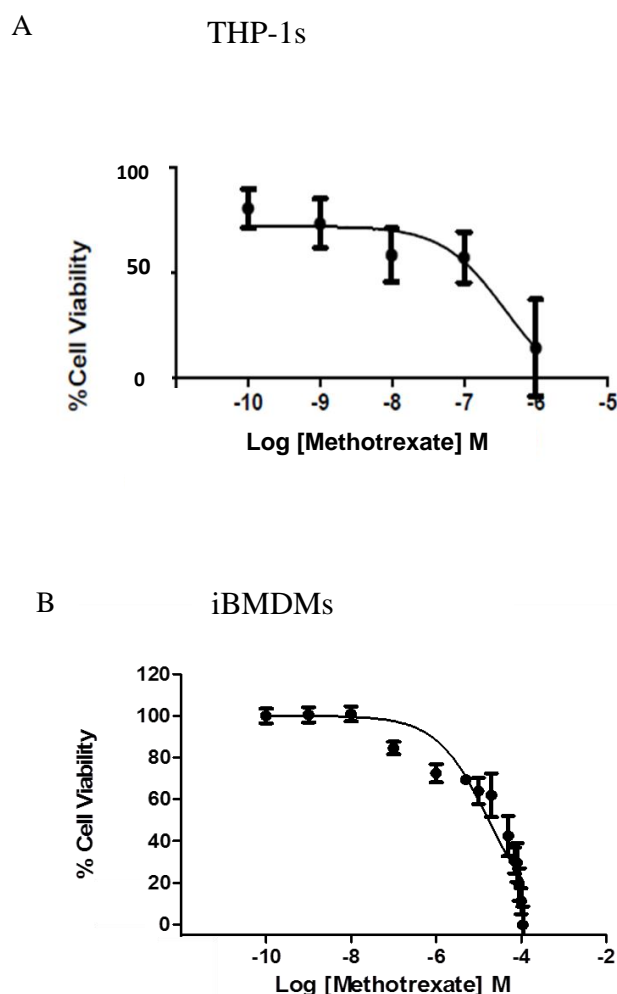
A　　　　　THP-1s

B　　　　　iBMDMs

Figure 3.4. Methotrexate induces cell death in PMA-differentiated THP-1 cells and LPS-activated iBMDMs.

(A) THP-1 cells were activated with PMA (200nM) for 72 h. They were then trypsinised and seeded (5 X $10^{\wedge}4$ cells/ml and 200 µl/well) in a 96 well plate for 72h before the addition of MTX (0.1, 1, 10,100 nM, 1 µM) for a further 4 h. (B) iBMDMs were seeded (1.66 X $10^{\wedge}5$ cells/ml and 180 µl/well) in a 96 well plate and were left to rest o/n. before activation with LPS (100 ng/ml) and MTX (0.1, 1, 10, 100 nM, 1, 5, 10, 20, 50, 70, 80, 90, 100 and 125 µM) for 24 h. Alamar blue was added in the last 4 h of treatment and readings were taken at 570 nm and 600 nm. Cell viability values are expressed as a percentage of the control. For LPS-activated iBMDMs, the IC50 was found to be 17.44 µM. Data are presented as (A) mean ± SEM, n=3 and (B) mean ±SEM, n=6.

A　　　　　　　　Human PBMCs
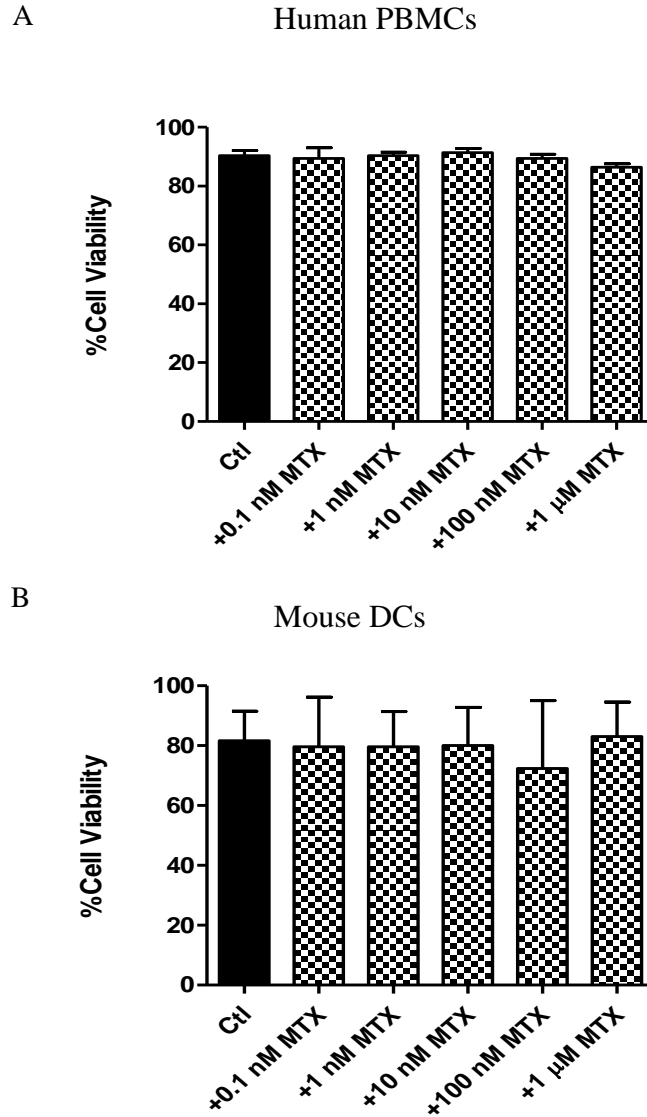
B　　　　　　　Mouse DCs

Figure 3.5. Methotrexate treatment had no effect on the cell viability of mouse DCs or human PBMCs.

(A) Human PBMCs were seeded (5 X 10^5 cells/ml and 200 µl/well) and (B) mouse DCs were seeded (2 X 10^5 cells/ml and 200 µl/well) in a 96well plate. Both mouse DCs and human PBMCs were treated with MTX (0.1, 1, 10, 100 nM, 1 µM) for 24 h. Cell viability was measured following cell counts after the additions of trypan blue exclusion dye. Data are presented as mean ±SEM, n=3.

A   Human PBMCs
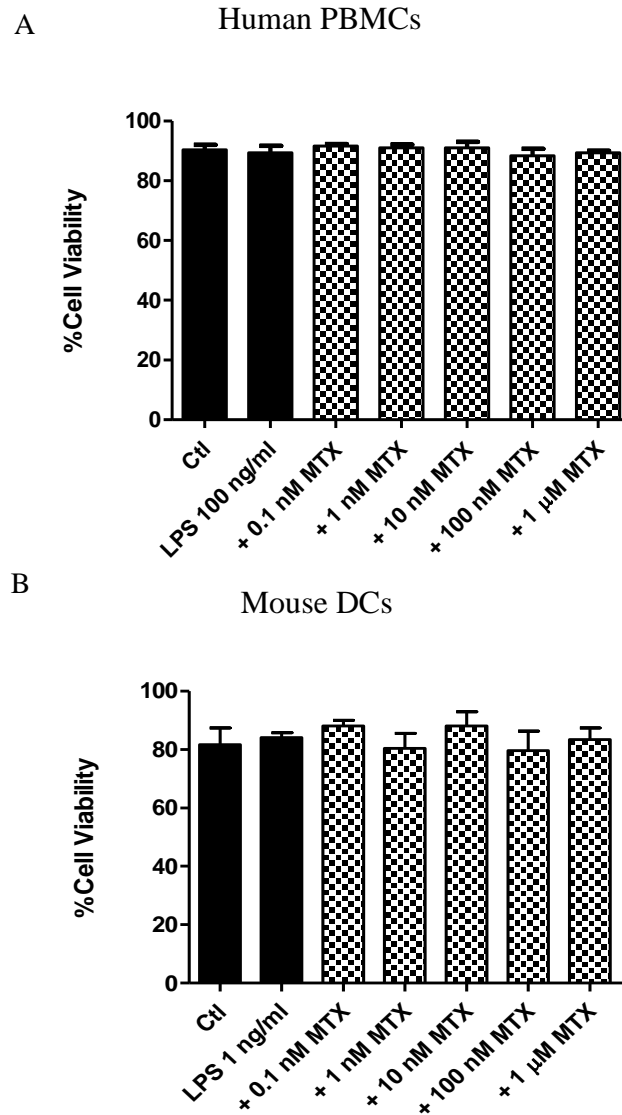
B   Mouse DCs

Figure 3.6. Methotrexate treatment had no effect on the cell viability of LPS-activated mouse DCs or human PBMCs.

(A) Human PBMCs were seeded (5 X $10^{\wedge}5$ cells/ml and 200 µl/well) in a 96well plate and before the addition of LPS (100 ng/ml) and MTX (0.1, 1, 10, 100nM, 1 µM) for 24 h. (B) Mouse DCs were seeded (2 X $10^{\wedge}5$ cells/ml and 200 µl/well) and left o/n before the addition of LPS (1 ng/ml) alongside MTX (0.1, 1, 10,100 nM, 1 µM) for 24 h. Cell viability was measured following cell counts after the additions of trypan blue exclusion dye. Data are presented as mean ±SEM, n=3.
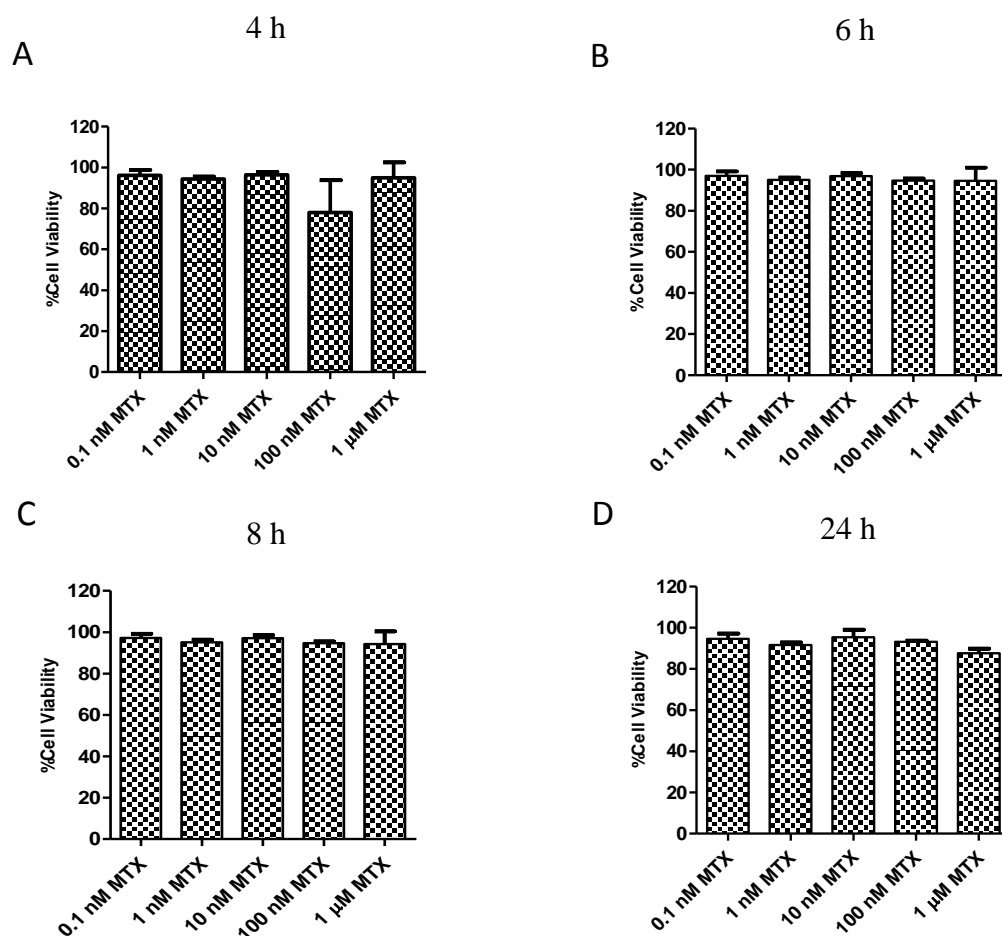
**Figure 3.7. Methotrexate treatment had no effect on the cell viability of partially-activated PBMCs.**

PBMCs were cultured in the presence of anti-CD3 (1μg/ml) for 2 days then seeded (1 X $10^{\wedge}6$ cells/ml and 3 ml/well) in an anti-CD3 coated 96 well plate and treated with a range of concentrations of MTX (0.1, 1, 10, 100 nM, 1 μM). Alamar blue was added at the time of treatments and readings at 570 nm and 600 nm were taken at (A) 4 h, (B) 6 h, (C) 8 h, and (D) 24 h. Cell viability is expressed as a percentage of the vehicle control and the Data are presented as mean ± SEM, n=3.

A

anti-CD3	-	-	-	+	+	+
MTX 100 nM	-	+	-	-	+	-
MTX 1 µM	-	-	+	-	-	+

B
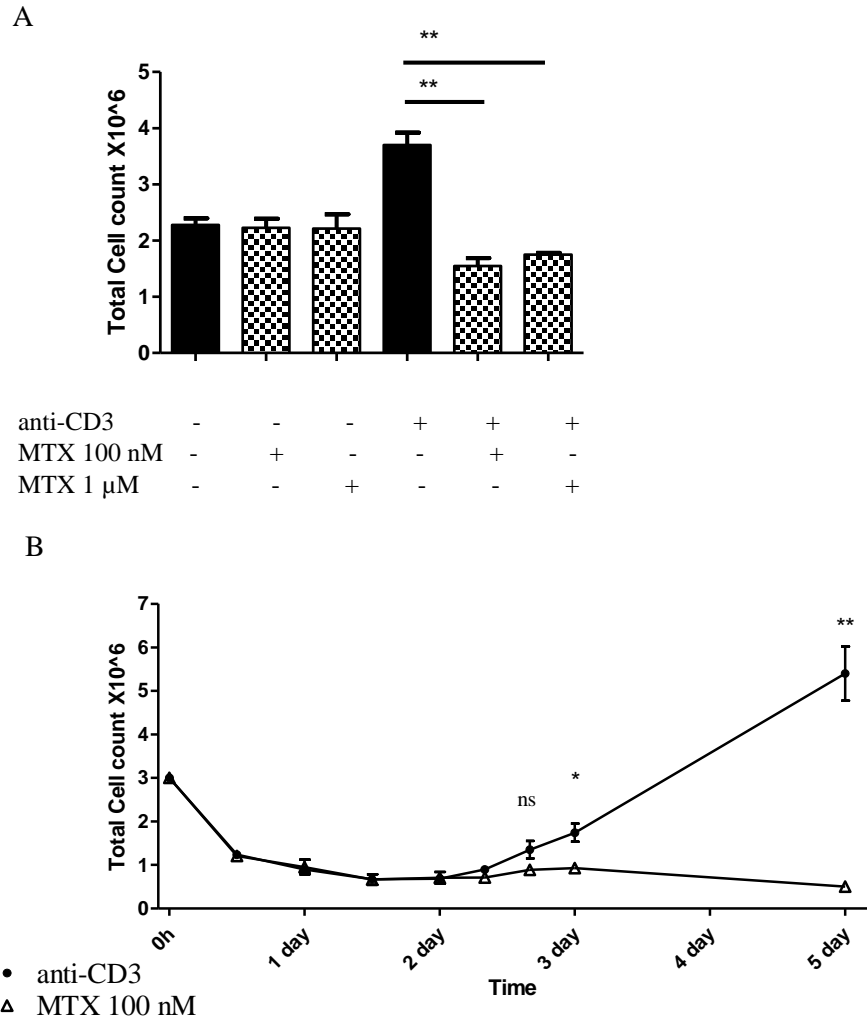
- • anti-CD3
- △ MTX 100 nM

Figure 3.8. Methotrexate reduces the PBMC cell count during anti-CD3-activation.

(A) PBMCs (1 X 10^6 cells /ml and 3 ml/well) were cultured in the presence or absence of anti-CD3 (1 µg/ml) with MTX (0, 100 nM and 1 µM) for 72 h at which time cell counts were taken following the addition of trypan blue exclusion dye. (B) PBMCs (1 X 10^6 cells /ml and 3 ml/well) were cultured in the presence of anti-CD3 (1 µg/ml) ± MTX (100 nM) and cell counts were measured at the times shown following the addition of Trypan blue exclusion dye. Data are presented as (A) mean ± SEM, n=3; a one-way ANOVA, followed by Tukey's multiple comparison test was performed and significance is indicated by *P<0.05, **P<0.01, or ***P<0.001. (B) mean ±SEM, n=3; an unpaired student T-test was performed and significance is indicated by *P<0.05, **P<0.01, or ***P<0.001.
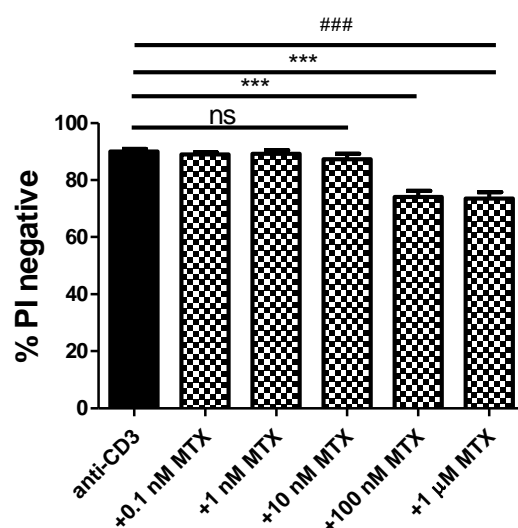
Figure 3.9. High doses of Methotrexate induce cell death in anti-CD3-activated PBMCs.

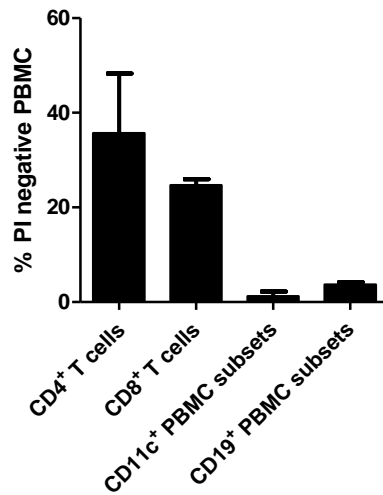PBMCs (1 X 10^6 cells /ml and 3 ml/well) were cultured in the presence of anti-CD3 (1 µg/ml) with MTX (0.1, 1, 10, 100 nM, 1 µM) for 72 h. Viable cells were determined using flow cytometry by determining those negative for propidium iodide stain (1 µg/ml) following exclusion of doublets and cell debris. Data are presented as mean ± SEM, n=5; a paired student T-test and a one-way ANOVA followed by a test for linear trend was performed with significance indicated with *P<0.05, **P<0.01,***P<0.001 or ### P<0.001 representing a significant linear trend.

Both $CD4^+$ and $CD8^+$ T cells accounted for more than half of the remaining cells (Fig 3.10). Back-gating on the entire population, revealed that MTX (100 nM and 1 µM) had a significant effect on both $CD4^+$ and $CD8^+$ T cell viability (Fig 3.11). Since MTX had both cytostatic and cytotoxic effects on these anti-CD3-activated PBMCs it was important to determine whether inhibition of cell proliferation predated cell death. Thymidine and hypoxanthine rescue of cell proliferation also reversed the cell death incurred by MTX (100 nM) (Fig 3.12). This suggested that cell death was linked to inhibition of cellular proliferation.

3.4.2 MTX exerts an anti-proliferative effect in anti-CD3-activated PBMCs

To verify this anti-proliferative effect of MTX, CFSE was employed as a method used to quantify the proliferation induced by anti-CD3 and to measure the changes in proliferation induced by MTX. Histograms of the CFSE dye with increasing peaks to the left reflect loss of CFSE labelled lysine residues following each round of cell division. Anti-CD3-activation resulted in the dilution of CFSE with each division. Treatment with MTX resulted in higher levels of CFSE and was comparable to the basal level of proliferation seen in the absence of anti-CD3 (Fig 3.13A). This anti-CD3-induced cell proliferation was significantly inhibited with increasing concentrations of MTX (Fig 3.13B).

PBMCs that didn't express a CD3 receptor were also found to proliferate (Fig 3.14). These $CD11c^+CD19^-$ PBMC subsets were found to proliferate, however the proliferation was less than that for the CD3 receptor-expressing cells (Fig 3.14). In light of this, it was important to determine whether these $CD11c^+CD19^-$ PBMC subsets were proliferating due to anti-CD3-activation or whether this was basal proliferation. There was no significant increase in the proliferation of these $CD11c^+CD19^-$ PBMC subsets in response to anti-CD3-activation compared to basal levels (Fig 3.15). However there was a significant increase in the proliferation of $CD19^+CD11c^-$ PBMC subsets in response to anti-CD3-activation just like that observed for $CD4^+$ and $CD8^+$ T cells. The anti-proliferative effects of MTX on these PBMC subsets was then determined. MTX (100 nM and 1 µM) significantly inhibited the proliferation of these $CD11c^+CD19^-$ PBMC subsets just like the $CD4^+$ and $CD8^+$ T cells (Fig 3.16). There was no significant anti-proliferative

Figure 3.10. CD4^{+} and CD8^{+} T cells are the predominant subsets in PBMCs following 72 h of anti-CD3-activation.

PBMCs (1 X 10^6 cells /ml and 3 ml/well) were cultured in the presence of anti-CD3 (1 μg/ml) for 72 h. PBMCs were then incubated in an antibody cocktail comprised of antibodies against the surface markers CD4, CD8, CD11c and CD19 for 30 min. Cell debris and doublets were excluded and propidium iodide (1 μg/ml) negative cells were then gated to identify the frequency of the cell cohorts using flow cytometry. Data are presented as mean ± SEM, n=3.
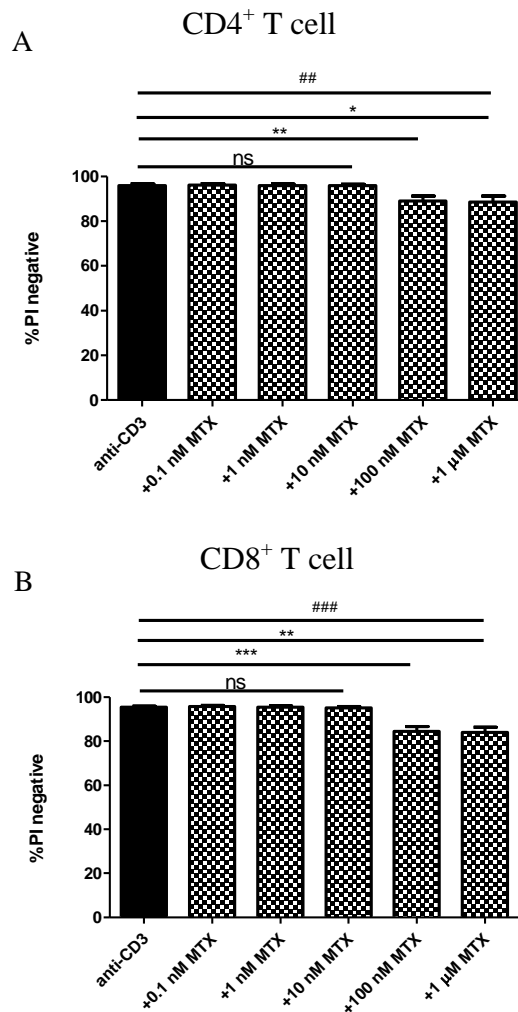
Figure 3.11 High doses of Methotrexate induce cell death in anti-CD3-activated CD4^{+} T cells and CD8^{+} T cells.

PBMCs (1 X 10^6 cells /ml and 3 ml/well) were cultured in the presence of anti-CD3 (1 μg/ml) with MTX (0.1, 1, 10, 100 nM, 1 μM) for 72 h. PBMCs were then incubated in an antibody cocktail comprised of antibodies against the surface markers CD4 and CD8 for 30 min. Cell debris and doublets were excluded and cells were gated on CD4^{+} T cells or CD8^{+} T cells using flow cytometry. They were then back-gated for T cells that were propidium iodide (1 μg/ml) negative. Data are presented as mean ± SEM, n=7; a paired student T-test or a one-way ANOVA, followed by a test for a linear trend was performed with significance indicated with *P<0.05, **P<0.01,***P<0.001 or ### P<0.001 representing a significant linear trend.
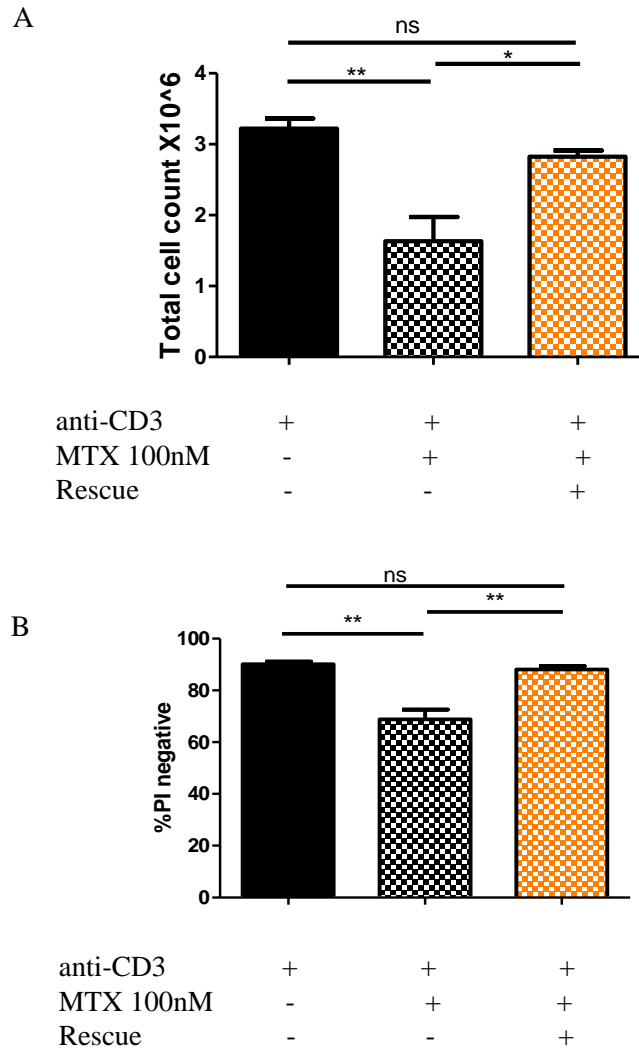
Figure 3.12. Hypoxanthine and thymidine restored cell proliferation and cell viability after Methotrexate treatment in anti-CD3-activated PBMCs.

PBMCs (1 X 10^6 cells /ml and 3 ml/well) were cultured in the presence of anti-CD3 (1 μg/ml) ± MTX (100 nM) ± hypoxanthine (100 μM) and thymidine (100 μM) for 72 h. (A) Cell proliferation was analysed as a change in viable cell count following staining with trypan blue exclusion dye. (B) Cell viability was measured using propidium iodide stain (1 μg/ml) following exclusion of doublets and cell debris using flow cytometry. Data are presented as mean ± SEM, n=4; a one-way ANOVA, followed by Tukey's multiple comparison test was performed and significant differences are indicated with *P<0.05, or **P<0.01.
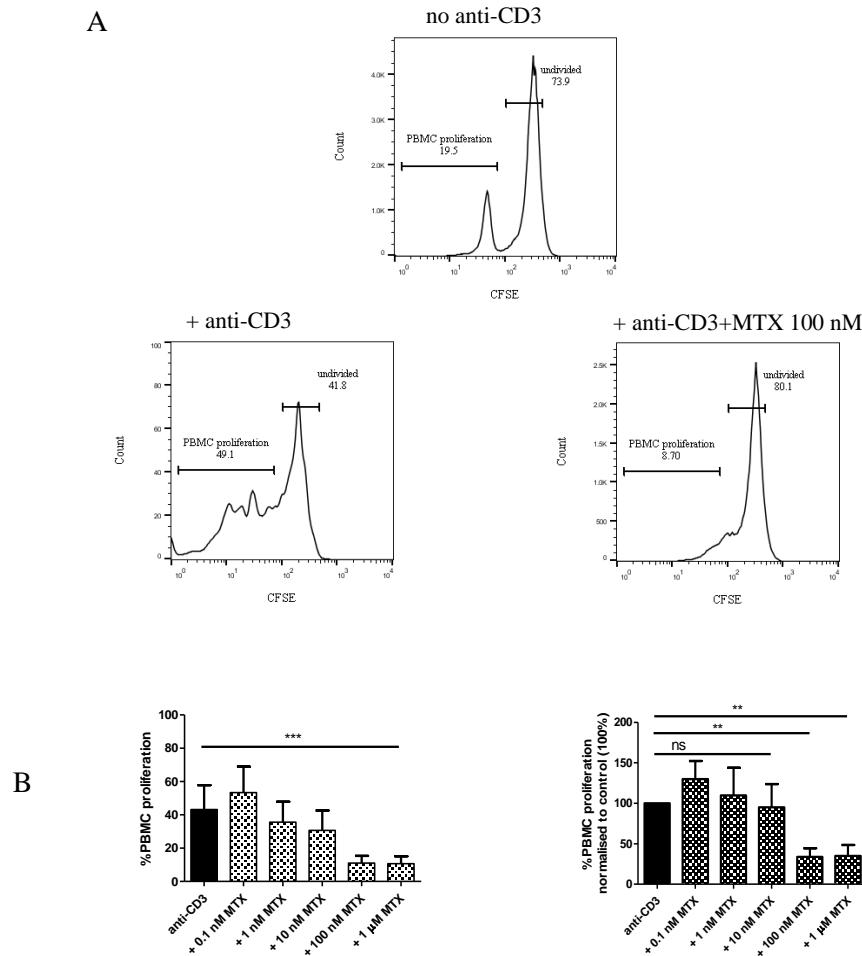
Figure 3.13. Low-dose Methotrexate prevents the anti-CD3-induced proliferation of PBMCs.

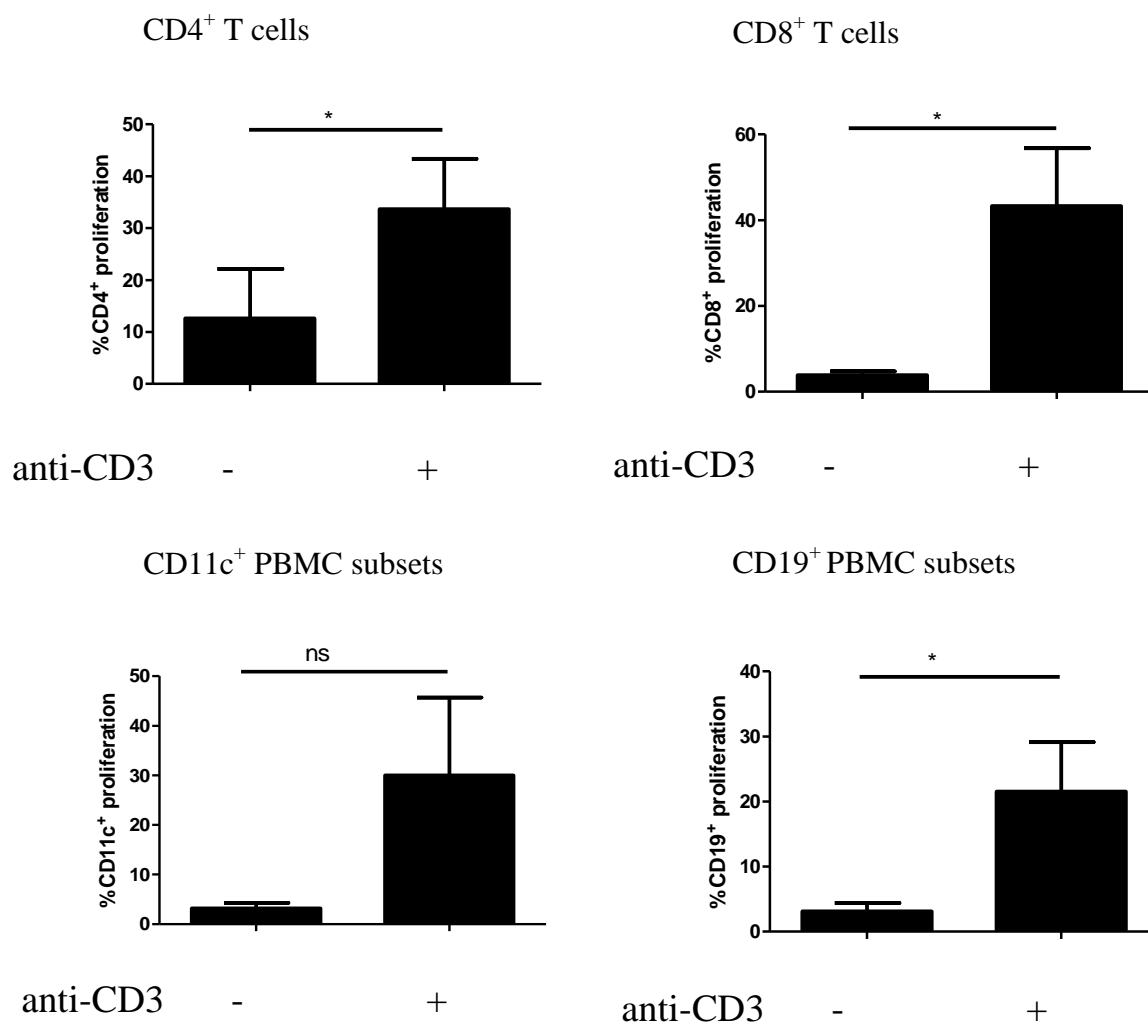The proliferation assay dye, CFSE was added to PBMCs for 10 mins and then seeded at $(1 \times 10^{\wedge}6$ cells /ml and 3 ml/well) ± anti-CD3 (1 µg/ml) with a range of concentrations of MTX (0, 0.1, 10, 100 nM and 1 µM) for 72 h. Flow cytometric analysis then assessed the effect of MTX treatment on the proliferation. (A) Representative histogram of MTX (100 nM) reversing the anti-CD3-induced proliferation of PBMCs to their unactivated levels. (B) A dose response with MTX shows significant trends in anti-CD3-induced proliferation inhibition and normalised values indicate that the highest concentrations of MTX (100 nM and 1 µM) induce significant effects. Data are presented as the mean ± SEM, n=5; (B left) a one-way ANOVA was performed followed by a test for linear trend (B right) a paired student T-test was performed and significant differences are indicated with *P<0.05 or **P<0.01.

A

B
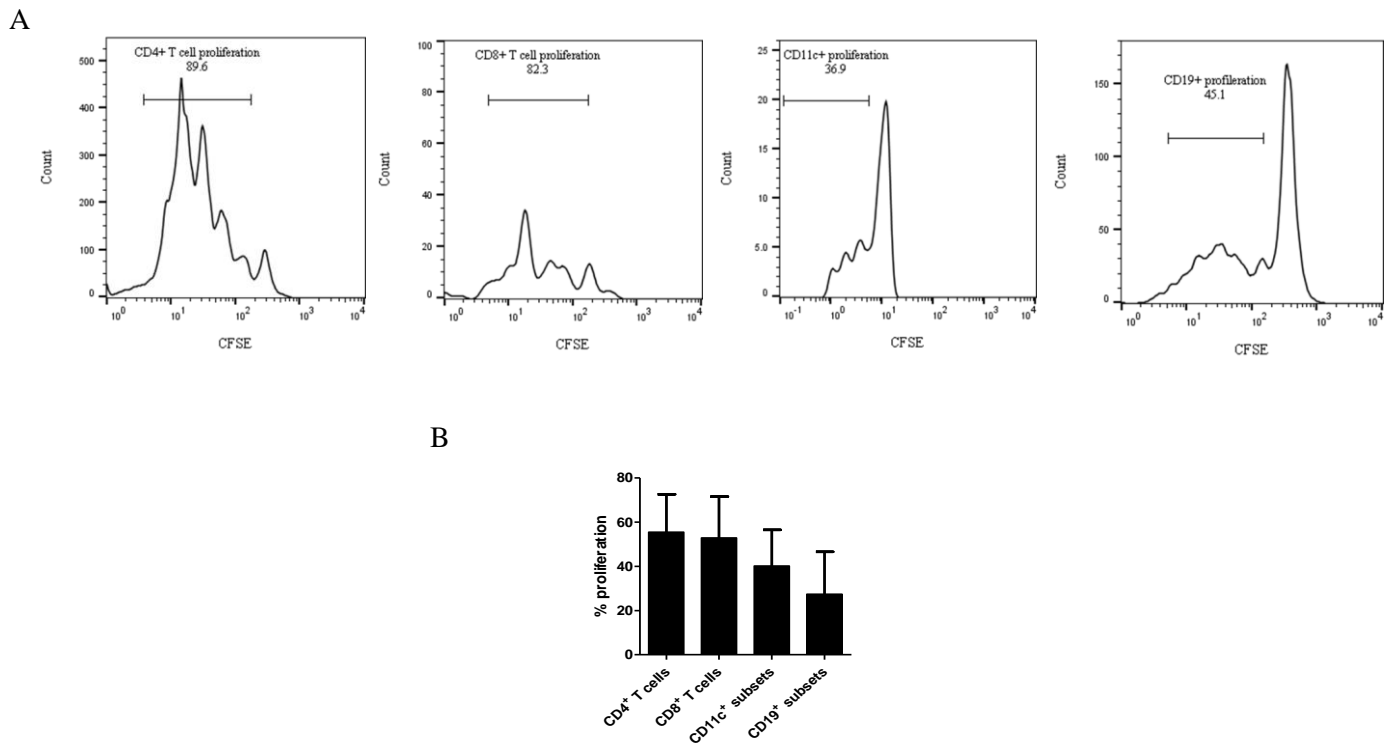
Figure 3.14. CD11c$^+$ and CD19$^+$ PBMC subsets proliferated following anti-CD3-activation.
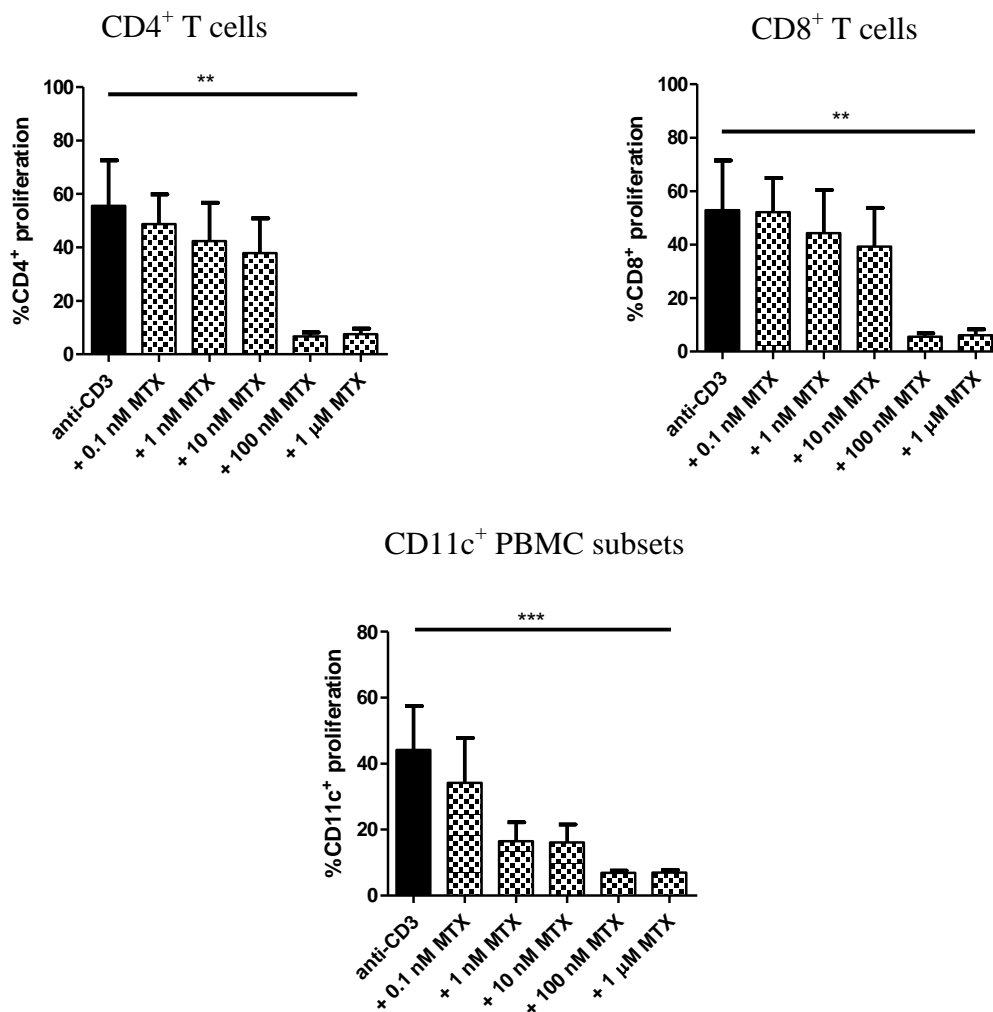
The proliferation assay dye, CFSE was added to PBMCs for 10 mins. They were then seeded (1 X 10^6 cells /ml and 3 ml/well) ± anti-CD3 (1 µg/ml) for 72 h. PBMCs were then incubated in an antibody cocktail comprised of antibodies against the surface markers CD4, CD8, CD11c and CD19 for 30 min. Flow cytometric analysis then assessed the proliferation of each subset. (A) Representative histograms of the proliferation of CD4$^+$ T cells, CD8$^+$ T cells, CD11c$^+$CD19$^-$ PBMC subsets and CD19$^+$CD11c$^-$ PBMC subsets (B) Quantitative analysis of the proliferation of these subsets presented as mean ± SEM, n=4.

Figure 3.15. CD19+ PBMC subsets did proliferate due to anti-CD3-activation.

The proliferation assay dye, CFSE was added to PBMCs for 10 mins or left untreated. They were then seeded (1 X $10^{\wedge}6$ cells /ml and 3 ml/well) ± anti-CD3 (1 µg/ml) for 72 h. PBMCs were then incubated in an antibody cocktail comprised of antibodies against the surface markers CD4, CD8, CD11c and CD19 for 30 min. Flow cytometric analysis then assessed the proliferation of each subset. CD11c+ PBMC subsets did not proliferate due to anti-CD3. CD4+ and CD8+T cells as well as CD19+ PBMC subsets proliferated in response to anti-CD3. CD11c+PBMC subsets did not proliferate in response to anti-CD3. Data are presented as (A) mean ± SEM, n=3; (B, C and D) mean ± SEM, n=6. A paired student T-test was performed with significant differences indicated with *P<0.05 or **P<0.01.

Figure 3.16. Methotrexate inhibited the proliferation of the dividing cells within this mixed population of anti-CD3-activated PBMCs.

The proliferation assay dye, CFSE was added to PBMCs for 10mins. They were then seeded (1 X 10^6 cells /ml and 3 ml/well) ± anti-CD3 (1ug/ml) with a range of concentrations of MTX (0, 0.1, 10, 100 nM and 1 µM) for 72 h. PBMCs were then incubated in an antibody cocktail comprised of antibodies against the surface markers CD4, CD8, CD11c and CD19 for 30 min. Flow cytometric analysis then assessed the effect of MTX treatment on the anti-CD3-induced proliferation of each subset. MTX (0.1 nM- 1 µM) significantly inhibited the proliferation of CD4+ and CD8+ T cells as well as CD11c+ PBMC subsets. Data are presented as mean ± SEM, n=5; a one-way ANOVA was performed, followed by a test for linear trend and significant differences are indicated with *P<0.05 or **P<0.01.

effect on CD19+CD11c- PBMCs (Fig 3.17). MTX (0.1 nM-10 nM) had no significant anti-proliferative effect in all four PBMC subsets.

3.4.3 MTX treatment of anti-CD3-activated PBMCs results in reduced levels of transferrin (CD71) receptor expression on CD4$^+$ and CD8$^+$ T cells

To see if MTX affected other aspects of cellular activation in addition to cellular proliferation, the effects on the iron receptor (CD71) were investigated. Upon anti-CD3-activation, it was found that CD71 receptor expression significantly increased in both CD4$^+$ and CD8$^+$ T cells, compared to unactivated cells (Fig 3.18). The highest doses of MTX (100 nM and 1 μM), significantly lowered the expression of the CD71 receptor on both CD4$^+$ and CD8$^+$ T cell subsets (Fig 3.19). The lower doses of MTX (0.1 nM-10 nM) had no observable effect on CD71 receptor expression in these cells. In order to determine whether these effects were related to purine and thymidine inhibition, the effects on CD71 receptor expression upon thymidine and hypoxanthine rescue were examined (Fig 3.20). Reflecting the ability to restore cell proliferation, thymidine and hypoxanthine also restored CD71 receptor expression.

3.4.4 MTX inhibits CD4$^+$ and CD8$^+$ T lymphoblast formation following anti-CD3-activation

Anti-CD3-activation is also characterised by lymphoblast formation. The percentage of blast CD4$^+$ and CD8$^+$ T cells (greater than 35k) significantly increased upon anti-CD3-activation (Fig 3.21). Thus, the effect of MTX on this parameter of cellular activation was investigated. MTX (100 nM and 1 μM) reduced the percentage of blast CD4$^+$ and CD8+ T cells (Fig 3.22&Fig 3.23). There was no significant reduction in the percentage of blast CD4$^+$ or CD8$^+$ T cells for MTX (<100 nM). The addition of hypoxanthine and thymidine (100 μM) significantly reversed the MTX (100 nM) mediated inhibition of lymphoblast formation in both CD4$^+$ and CD8$^+$ T cells (Fig 3.24).
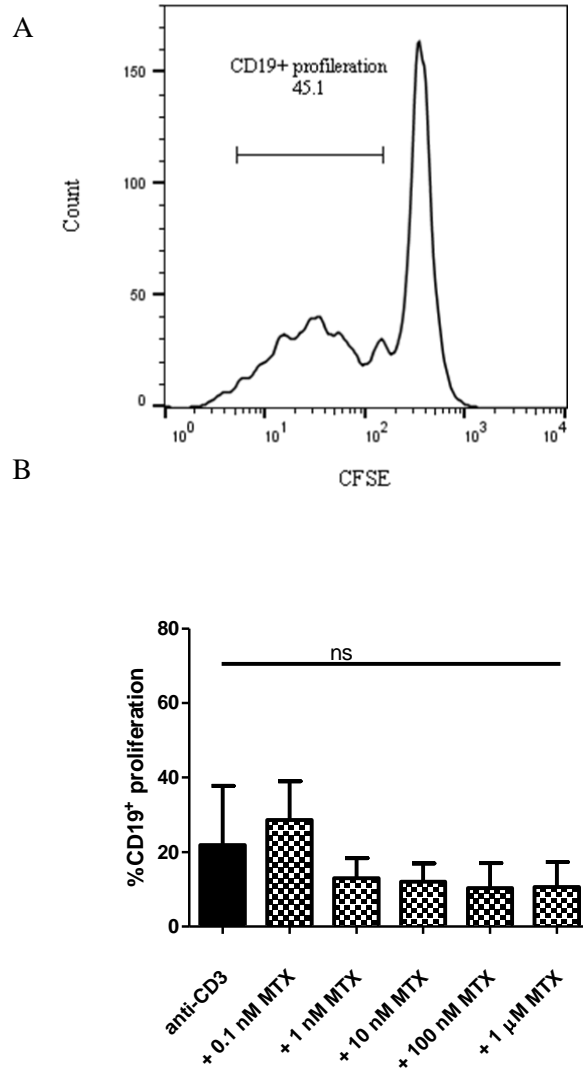
Figure 3.17. Methotrexate did not inhibit the proliferation of CD19$^+$ PBMC subsets

The proliferation assay dye, CFSE was added to PBMCs for 10 min. They were then seeded (1 X 10$^{\wedge}$6 cells /ml and 3 ml/well) ± anti-CD3 (1ug/ml) with a range of concentrations of MTX (0, 0.1, 10, 100 nM and 1 μM) for 72 h. PBMCs were incubated in an antibody cocktail comprised of antibodies against the surface markers CD4, CD8, CD11c and CD19 for 30 min. Flow cytometric analysis then assessed the effect of MTX treatment on the anti-CD3 proliferation of each subset. (A) Representative histograms of the anti-CD3-induced proliferation. (B) Quantitative analysis of the proliferation of these CD19$^+$ PBMC subsets. Data are presented as mean ± SEM, n=4; a one-way ANOVA was performed, followed by a test for linear trend and significant differences are indicated with *P<0.05 or **P<0.01.

A

CD4$^+$ T cells

anti-CD3   -   +

B
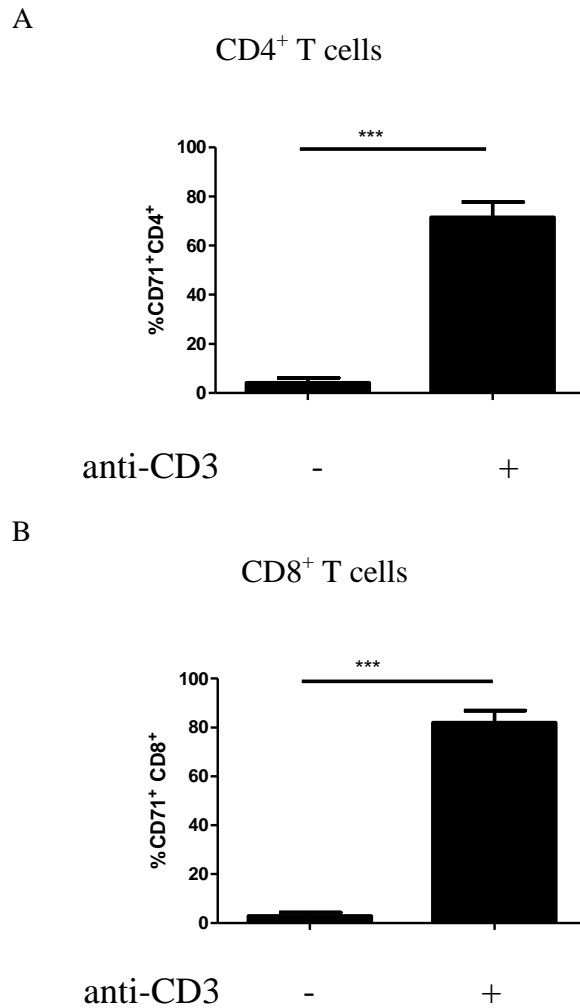
CD8$^+$ T cells

anti-CD3   -   +

Figure 3.18. CD4$^+$ and CD8$^+$ T cells upregulate transferrin (CD71) receptor expression upon anti-CD3-activation.

PBMCs were seeded (1 X 10$^{\wedge}$6 cells /ml and 3 ml/well) ± anti-CD3 (1 µg/ml) for 72 h. Unactivated PBMCs were broken out on day 3 and used in control experiments. Both unactivated and anti-CD3-activated PBMCs were then incubated in an antibody cocktail comprised of antibodies against the surface markers CD4, CD8 and CD71 for 30 min. Flow cytometric analysis then assessed the effect of anti-CD3-activation on CD71 expression on each T cell subset. Data are presented (A&B) as mean ±SEM, n=3; an unpaired student T-test was performed and significant differences are indicated with *P<0.05, **P<0.01, or ***P<0.001.
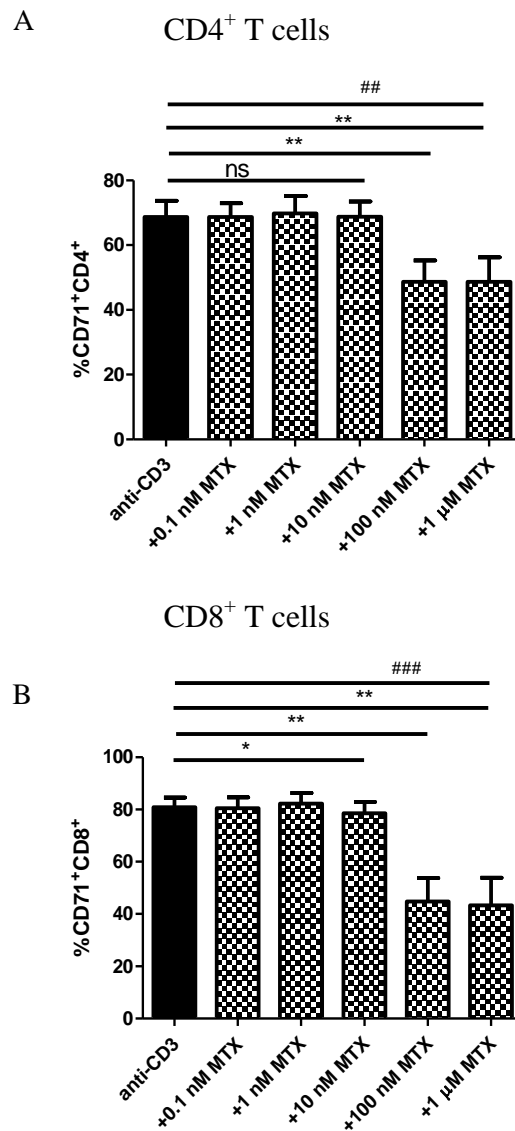
Figure 3.19. Methotrexate treatment resulted in significantly lower transferrin (CD71) expression on CD4$^+$ and CD8$^+$ T cells.

PBMCs were seeded (1 X 10$^{\wedge}$6 cells /ml and 3 ml/well) ± anti-CD3 (1 µg/ml) with a range of concentrations of MTX (0, 0.1, 10, 100 nM and 1 µM) for 72 h. PBMCs were then incubated in an antibody cocktail comprised of antibodies against the surface markers CD4, CD8 and CD71 for 30 min. Flow cytometric analysis then assessed the effect of MTX treatment on the anti-CD3-induced increase in CD71 expression on each T cell subset. Data are presented as mean ±SEM, n=4 or n=5, for (A) CD4$^+$ T cells and (B) CD8$^+$ T cells; a paired student T-test or a one-way ANOVA, followed by test for linear trend, was performed and significant differences are indicated with *P<0.05, **P<0.01, ***P<0.001 or ### P<0.001 representing a significant linear trend.
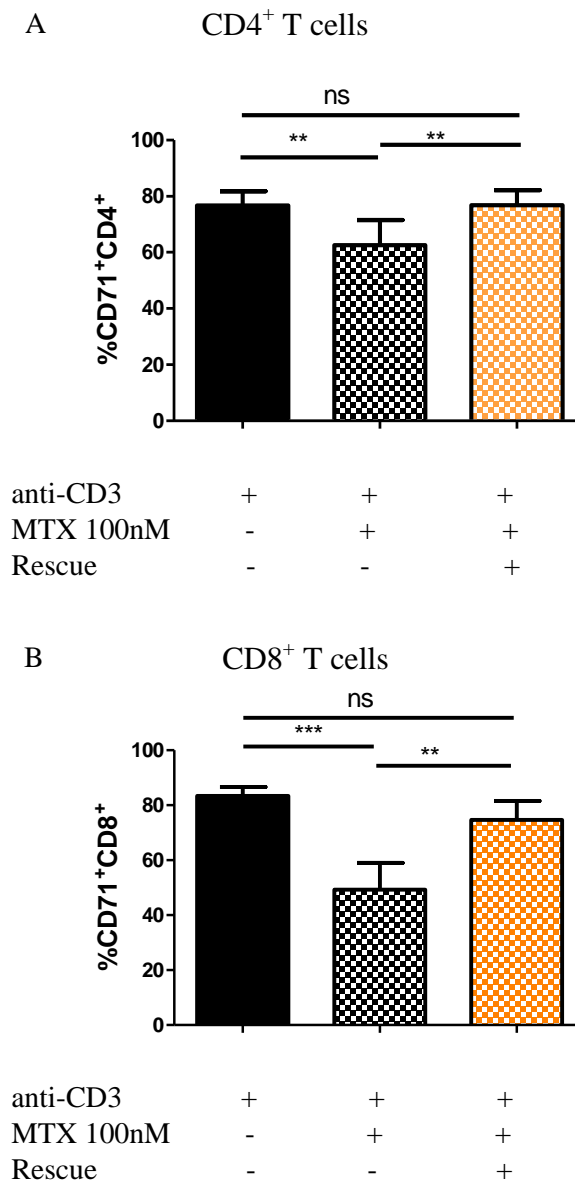
Figure 3.20. Hypoxanthine and thymidine can reverse the Methotrexate-induced lowering of transferrin (CD71) receptor expression in both CD4+ T cells and CD8+ T cells.

PBMCs (1 X 10^6 cells /ml and 3 ml/well) were cultured in the presence of anti-CD3 (1 µg/ml) ± MTX (100 nM), ± hypoxanthine (100 µM) and thymidine (100 µM) for 72 h. PBMCs were incubated in an antibody cocktail comprised of antibodies against the surface markers CD4, CD8 and CD71 for 30 min. Flow cytometric analysis then assessed the effect of MTX treatment on the anti-CD3-induced increase on CD71 expression on each T cell subset. Data are presented as (A) mean ± SEM, n=4 and (B) mean ± SEM, n=5; a one-way ANOVA, followed by Tukey's multiple comparison test was performed and significant differences are indicated with $*P<0.05$, $**P<0.01$, or $***P<0.001$.

A CD4$^+$ T cells

% blast CD4$^+$

***

anti-CD3   -   +

CD8$^+$ T cells

B

% blast CD8+

***
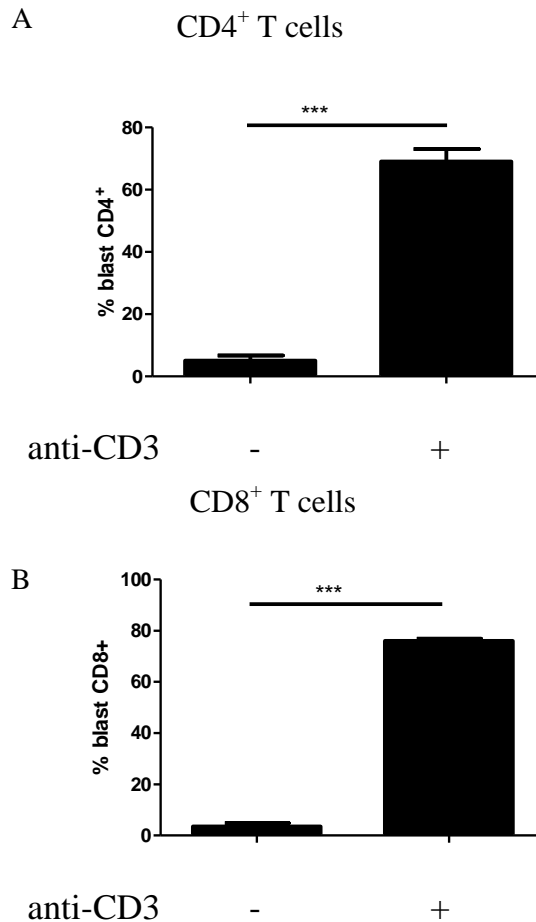
anti-CD3   -   +

Figure 3.21. Anti-CD3-activation results in the formation of blast CD4$^+$ and CD8$^+$ T cells.

PBMCs (1 X 10$^{\wedge}$6 cells /ml and 3 ml/well) were cultured in the presence of anti-CD3 for 72 h. Unactivated cells were taken from frozen stocks on the same day. PBMCs were incubated in an antibody cocktail comprised of antibodies against the surface markers CD4, CD8 for 30 min. Flow cytometric analysis then assessed the effect of anti-CD3-activation on the size of CD4$^+$ T cells based on their forward scatter measurements. (A) The percentage of CD4$^+$ T cells >35 k increases upon anti-CD3-activation. (B) The percentage of CD8$^+$ T cells >35 k increases upon anti-CD3-activation. Data are presented as mean ±SEM, n=3; an unpaired student T-test was performed and significant differences are indicated with *P<0.05, or **P<0.01.
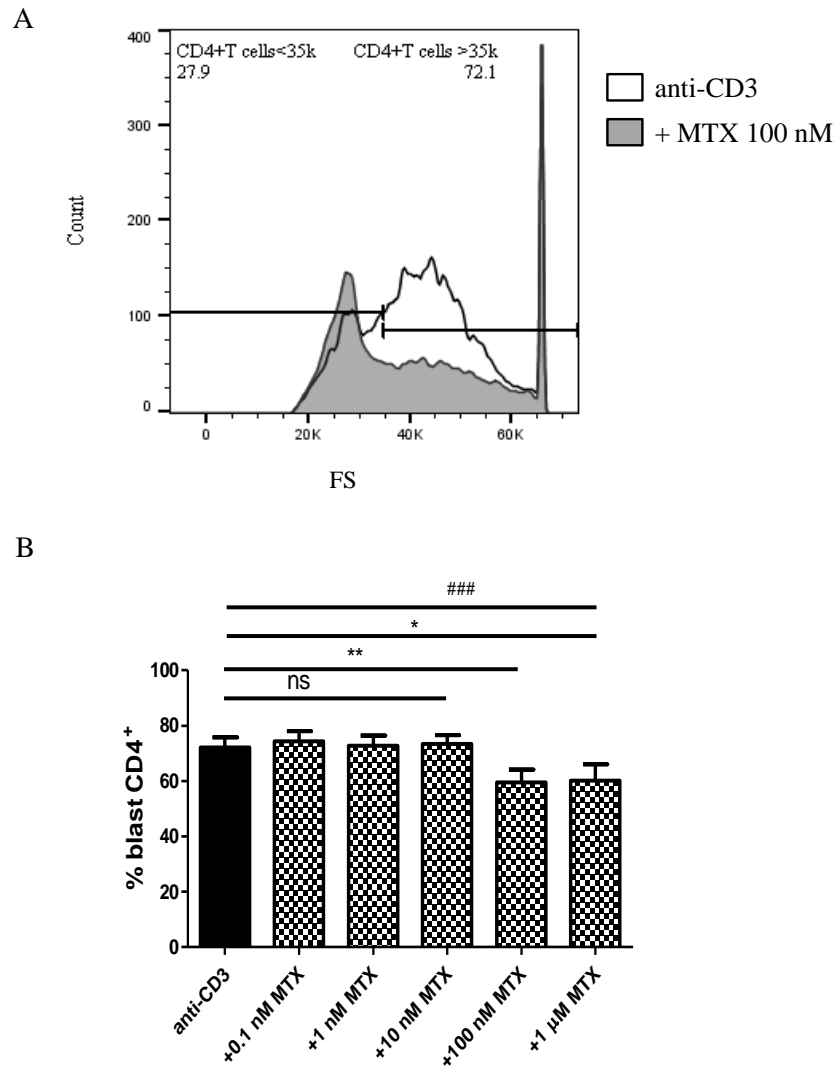
Figure 3.22. Methotrexate inhibited lymphoblast formation in anti-CD3-activated CD4⁺ T cells.

PBMCs were seeded (1 X $10^{\wedge}6$ cells /ml and 3 ml/well) ± anti-CD3 (1 µg/ml) with a range of concentrations of MTX (0, 0.1, 10, 100 nM and 1 µM) for 72 h. PBMCs were incubated in an antibody cocktail comprised of antibodies against the surface markers CD4, CD8 for 30 min. Flow cytometric analysis then assessed the effect of MTX treatment on the size of CD4⁺ T cells based on their forward scatter measurements. (A) Representative histogram of the reduction in PBMCs >35k with MTX 100 nM treatment. (B) MTX (100 nM and 1 µM) significantly inhibits the anti-CD3 induced growth of CD4⁺ T cells. Data are presented as mean ± SEM, n=5; a paired student T-test or a one-way ANOVA, followed by a test for a linear trend was performed and significant differences are indicated with *P<0.05, **P<0.01, ***P<0.001 or ### P<0.001 representing a significant linear trend.

A

B
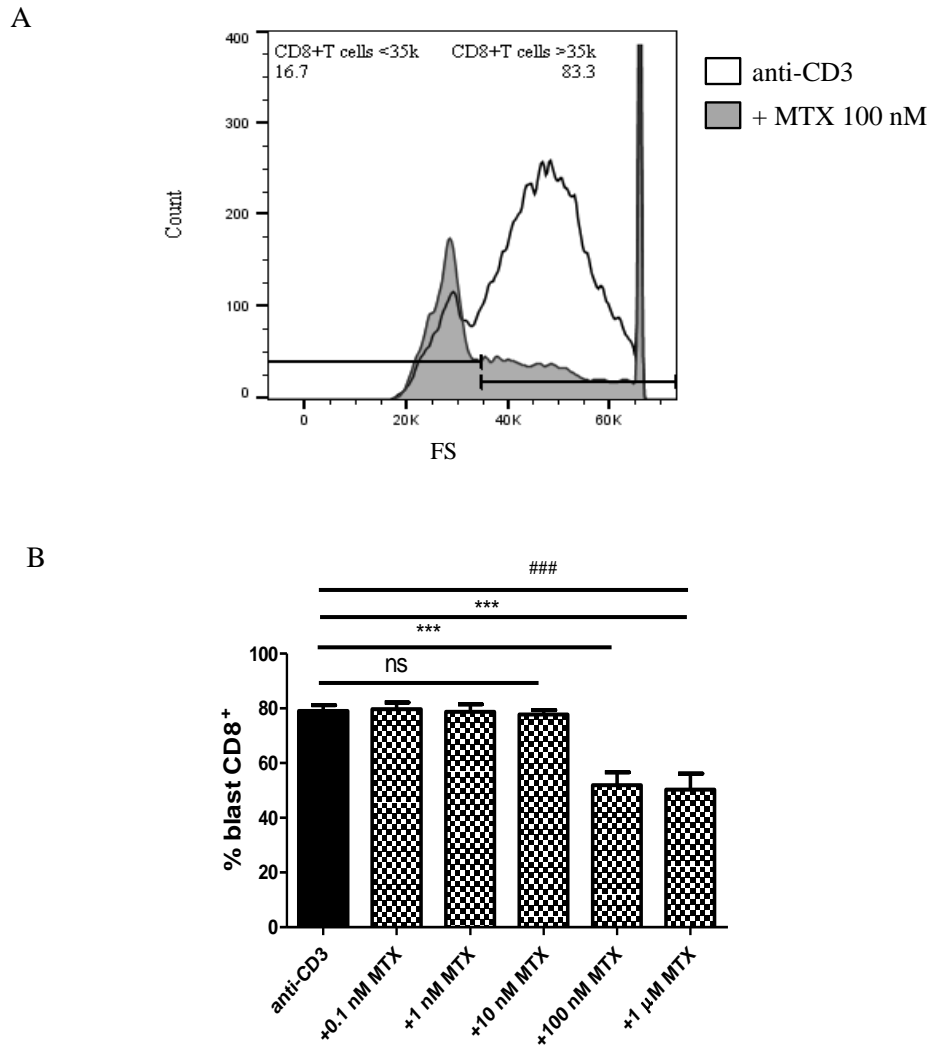
Figure 3.23. Methotrexate inhibited lymphoblast formation in anti-CD3-activated CD8^{+} T cells.

PBMCs were seeded (1 X $10^{\wedge}6$ cells /ml and 3 ml/well) ± anti-CD3 (1 µg/ml) with a range of concentrations of MTX (0, 0.1, 10, 100 nM and 1 µM) for 72 h. PBMCs were incubated in an antibody cocktail comprised of antibodies against the surface markers CD4, CD8 for 30 min. Flow cytometric analysis then assessed the effect of MTX treatment on the size of CD8^{+} T cells based on their forward scatter measurements. (A) Representative histogram of the reduction in PBMCs >35k with MTX 100 nM treatment. (B) MTX (100 nM and 1 µM) significantly inhibits the anti-CD3-induced growth of CD8^{+} T cells. Data are presented as mean ± SEM, n=7; a paired student T-test or a one-way ANOVA, followed by a test for linear trend was performed and significant differences are indicated with *$P<0.05$, **$P<0.01$, ***$P<0.001$ or ### $P<0.001$ representing a significant linear trend.

A CD4$^+$ T cells

B CD8$^+$ T cells

anti-CD3	+	+	+
MTX 100nM	-	+	+
Rescue	-	-	+
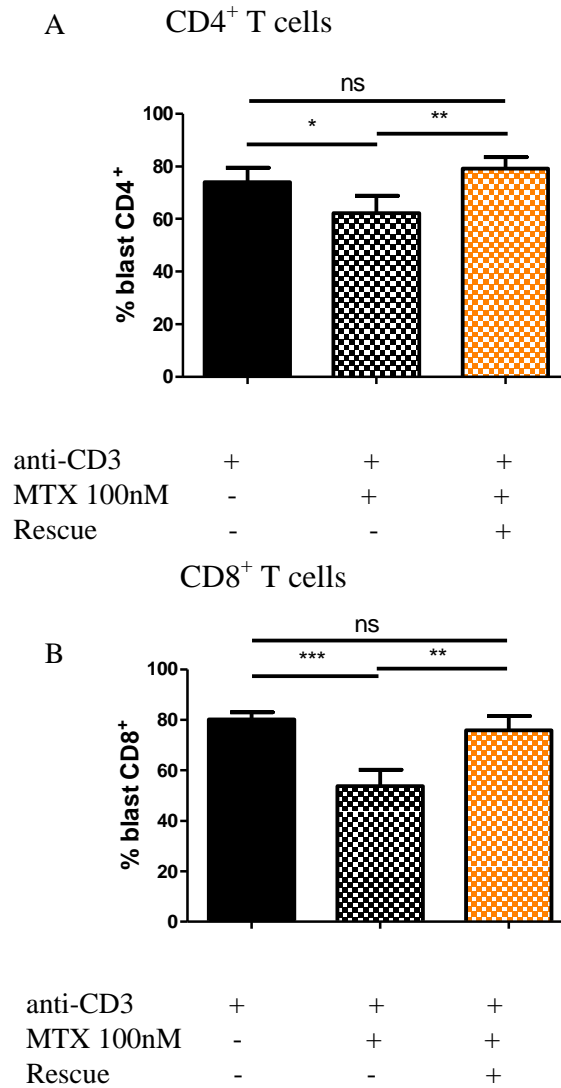
Figure 3.24. Hypoxanthine and thymidine reversed the Methotrexate-mediated-inhibition of CD4$^+$ T cells and CD8$^+$ T lymphoblast formation.

PBMCs were seeded (1 X 10$^{\wedge}$6 cells /ml and 3 ml/well) in the presence of anti-CD3 (1 μg/ml), ± MTX (100 nM) ± hypoxanthine (100 μM) and thymidine (100 μM) for 72 h. PBMCs were incubated in an antibody cocktail comprised of antibodies against the surface markers CD4, CD8 for 30 min. Flow cytometric analysis then assessed the effect of rescue the size of MTX treated, (A) CD8$^+$ T cells and (B), CD4$^+$ T cells based on their forward scatter measurements. Data are presented as (A&B) mean ± SEM, n=5 or a one-way ANOVA, followed by Tukey's multiple comparison test was performed and significant differences are indicated with *P<0.05, or **P<0.01.

3.4.5 MTX lowers the $\Delta\Psi_m$ in both unactivated and anti-CD3-activated PBMCs

The next point of investigation was to see whether MTX could limit the energetic and metabolic requirements for these morphological changes, by affecting mitochondrial function. In unactivated PBMCs, MTX (100 nM) treatment for 5 h significantly lowered the $\Delta\Psi_m$ compared to control cells (Fig 3.25A). Treatment with an ATP synthase inhibitor, oligomycin (1 µg/ml), had no effect but treatment with the positive control antimycin A (250 nM) for 15 min significantly lowered the $\Delta\Psi_m$ (Fig 3.25B). The addition of the uncoupler, FCCP (500 nM), which depolarised this $\Delta\Psi_m$, was used to identify the aggregate JC-1 population, as previously discussed (see **Section 3.3.4**).

Since MTX treatment seemed to have a significant effect on the $\Delta\Psi_m$ in unactivated PBMCs, the effect on anti-CD3-activated PBMCs was also assessed. Results showed that MTX (100 nM) also significantly reduced the $\Delta\Psi_m$ of PBMCs when added to anti-CD3 cultures during activation (Fig 3.26A). Neither antimycin A (250 nM) nor oligomycin (1 µg/ml) had any significant effect on the $\Delta\Psi_m$ (Fig 3.26B).

To see whether the reason for this reduction in the $\Delta\Psi_m$ was related to purine and thymidine inhibition, the experiment was repeated with thymidine and hypoxanthine (Fig 3.27). Purine and thymidine rescue partially reversed the $\Delta\Psi_m$ to that of the un-treated controls.

3.4.6 MTX increases ROS production in anti-CD3-activated but not in unactivated PBMCs

Since the $\Delta\Psi_m$ was lowered upon MTX treatment, it was imperative to investigate how else mitochondrial function was affected. The effect of MTX on ROS production in unactivated PBMCs following the same 5 h treatment was next examined (Fig 3.28A). MTX (100 nM) had no effect on ROS production in unactivated PBMCs after this time, compared to the significant linear increase in ROS production with antimycin A (Fig 3.28B). Parallel studies were also conducted on MTX treated anti-CD3-activated PBMCs. MTX (100 nM) significantly increased ROS production in these cells. (Fig 3.29A). Upon the addition of antimycin A (1 µM), ROS production also significantly increased (Fig 3.29B).

A

MTX 100nM   -   +

B

FCCP	-	+	-	-
Oligo	-	-	+	-
Aa	-	-	-	+
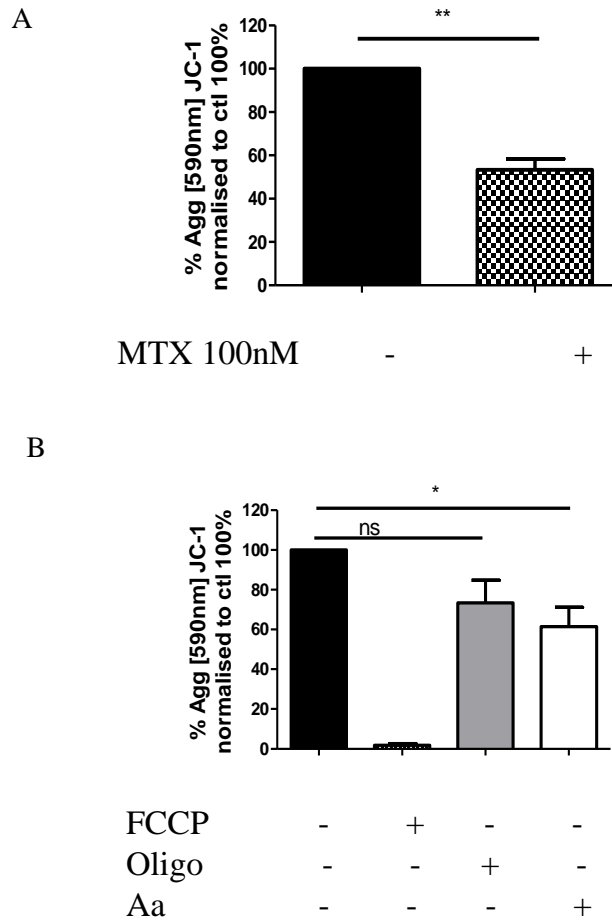
Figure 3.25: The $\Delta\Psi_m$ of unactivated PBMCs is reduced by Methotrexate and oxidative-phosphorylation inhibitors

PBMCs were seeded (1 X $10^{\wedge}6$ cells/ml and 3 ml/well) ± MTX (100 nM) for 5 h. PBMCs were then incubated in JC-1 (4 µM) for 15 min at 37°C. The PBMC population containing JC-1 was left untreated or treated with FCCP (500 nM), oligomycin (Oligo; 1 µg/ml) or antimycin A (Aa; 250 nM) for 15 min. Flow cytometry was used to assess the membrane potential. (A) MTX significantly reduced the $\Delta\Psi_m$ in unactivated PBMCs. (B) Antimycin A significantly reduced the $\Delta\Psi_m$ but oligomycin had no effect. Data are presented as (A&B) (% aggregate normalised to ctl set at 100%); mean ± SEM, n=4. A paired student T-test was performed with significance indicated by*P<0.05, or **P<0.01.
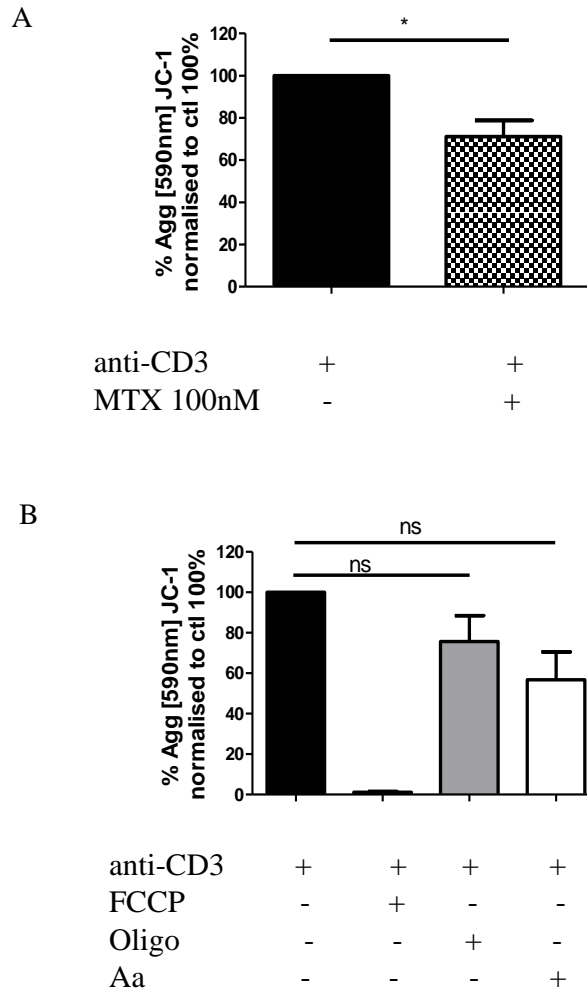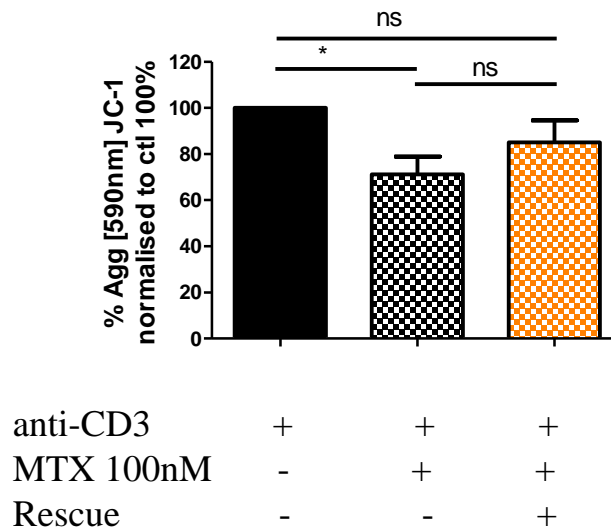
Figure 3.26. The $\Delta\Psi_m$ of anti-CD3-activated PBMCs is reduced by Methotrexate but not oxidative-phosphorylation inhibitors

PBMCs were seeded (1 X 10^6 cells /ml and 3 ml/well) in the presence of anti-CD3 (1 µg/ml) ± MTX (100 nM) for 72 h. PBMCs were then incubated in JC-1 (4 µM) for 15 min at 37°C. The PBMC population containing JC-1 was left untreated or treated with FCCP (500 nM), oligomycin (Oligo; 1 µg/ml) or antimycin A (Aa; 250 nM) for 15 min. Flow cytometry was used to assess the membrane potential. (A) MTX significantly reduced the $\Delta\Psi_m$ in anti-CD3-activated PBMCs. (B) Neither antimycin A nor oligomycin had any effect. Data are presented as (% aggregate normalised to ctl set at 100%) (A) mean± SEM, n=5; (B) mean± SEM, n=3; a paired student T-test was performed with significant differences indicated by *P<0.05, or **P<0.01.

Figure 3.27. Thymidine and hypoxanthine partially rescue the $\Delta\Psi_m$ from Methotrexate treatment in anti-CD3-activated PBMCs.

PBMCs (1 X 10^6 cells /ml and 3 ml/well) were cultured in the presence of anti-CD3 ± MTX (100 nM), ± thymidine (100 µM) and hypoxanthine (100 µM) for 72 h. Viable cells were counted using trypan blue exclusion dye. PBMCs were then incubated in JC-1 (4 µM) for 15 min at 37°C. The PBMC population containing JC-1 was either left untreated or treated with FCCP (500 nM). Flow cytometry was used to assess the membrane potential. Rescue did not reverse the MTX-induced lowering of the $\Delta\Psi_m$. Data are presented as mean ± SEM; n=5 (normalised to control set at 100%); a one-way ANOVA, followed by Tukey's multiple comparison test was performed and significant differences are indicated with *P<0.05, or **P<0.01.
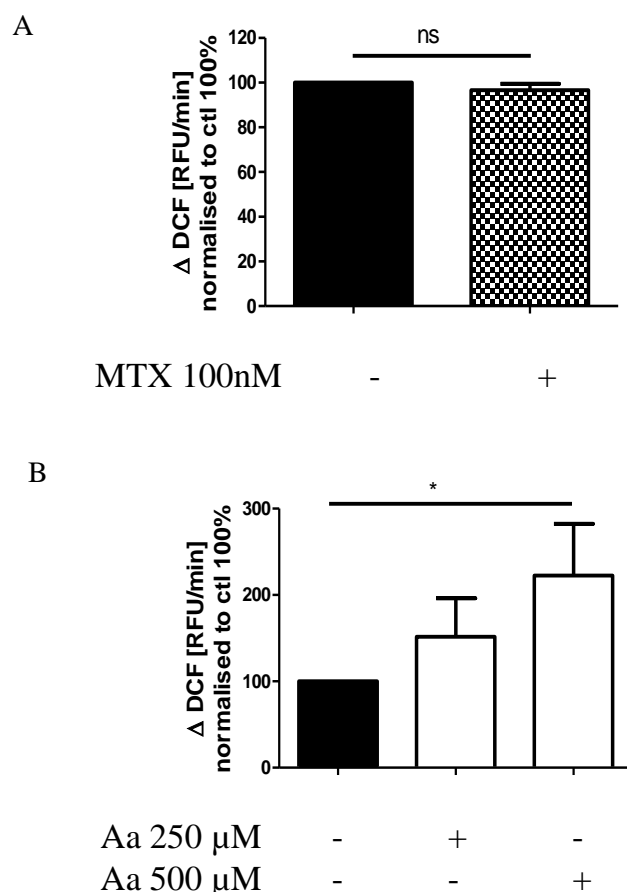
Figure 3.28. Methotrexate had no effect on ROS production in unactivated PBMCs compared to antimycin A.

PBMCs (1 X 10^6 cells /ml and 3 ml/well) were treated ± MTX (100 nM) for 5 h. They were then washed and seeded (6.6 X 10^5 cells/ml and 150 µl/well) in Krebs buffer in a black 96 well plate. Antimycin A (Aa; 0 nM, 250 nM or 500 nM) was added where appropriate, before the addition of 10 µM DCF-DA. Fluorescence measurements (excitation 485 nm/ emission 520 nm) were taken every 30 s over 1 h. The rates of ROS production were taken from the slopes of the linear part of the graph, after the initial lag phase. (A) MTX had no effect on the rate of DCF production, indicating that it had no effect on intracellular ROS production. (B) Antimycin A significantly increased the linear rate of ROS production in PBMCs. Data are presented as mean ± SEM; n=3; (normalised to control set at 100%) each in triplicate, (A) a paired student T-test (B) A one-way ANOVA, with linear trend test, was performed with significant differences indicated by *$P<0.05$, or **$P<0.01$.

A
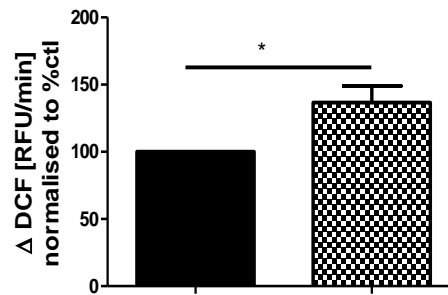
anti-CD3   +   +
MTX 100 nM   -   +

B
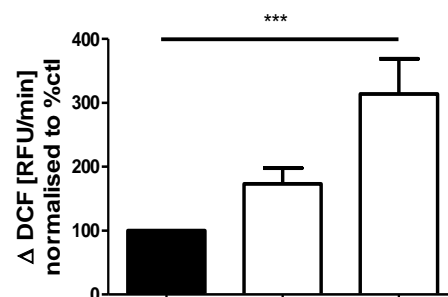
anti-CD3   +   +   +
Aa 250 nM   -   +   -
Aa 1 µM   -   -   +

Figure 3.29. **ROS production in anti-CD3-activated PBMCs is significantly increased by Methotrexate and antimycin A.**

PBMCs (1 X 10^6 cells /ml and 3 ml/well) were cultured in the presence of anti-CD3 ± MTX (100 nM) for 72 h. They were then washed and seeded (6.6 X 10^5 cells/ml and 150 µl/well) in Krebs buffer in a black 96 well plate. Antimycin A (Aa; 0 nM, 250 nM or 1 µM) was added where appropriate, before the addition of 10 µM DCF-DA. Fluorescence measurements (excitation 480 nm/ emission 520 nm) were taken every 30 s over 1 h. The rates of ROS production were taken from the slopes of the linear part of the graph, after the initial lag phase. (A) MTX significantly increased the rate of DCF production, a measure of ROS production. (B) Antimycin A significantly increased the linear rate of ROS production. Data are presented as (A) mean ± SEM, n=5, (B) mean± SEM, n=8;(normalised to ctl set at 100%) each in triplicate; (A) a paired student T-test, (B) A one-way ANOVA, with a test for linear trend was performed and significant differences are indicated by *P<0.05, or **P<0.01.

To evaluate whether the known effect of MTX on purine and thymidine inhibition contributed to this increase in ROS production, the above experiments were repeated upon the addition of hypoxanthine and thymidine. The MTX-induced increase in ROS production could be partially reversed upon the addition of hypoxanthine and thymidine (Fig 3.30).

anti-CD3	+	+	+
MTX 100nM	-	+	+
Rescue	-	-	+
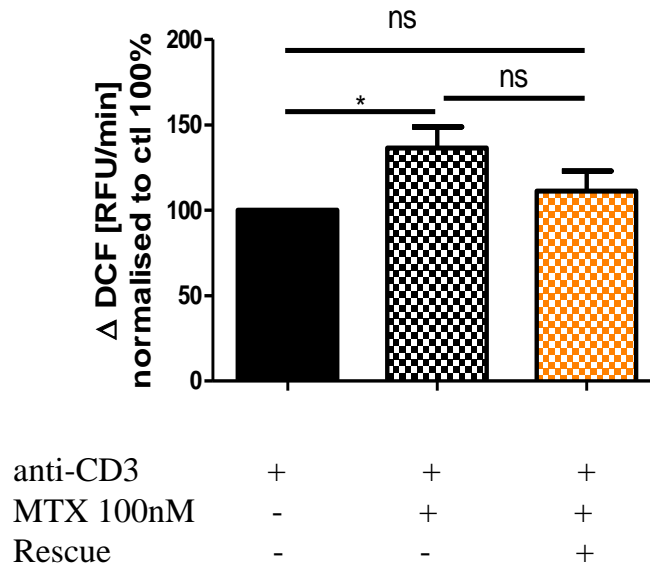
Figure 3.30 Thymidine and hypoxanthine partially reverse the Methotrexate-induced ROS production in anti-CD3-activated PBMCs.

PBMCs (1×10^6 cells /ml and 3 ml/well) were cultured in the presence of anti-CD3 ± MTX (100 nM), ± thymidine and hypoxanthine (100 µM) for 72 h. The viable cell count was measured using trypan blue exclusion dye to assess cell proliferation. PBMCs were seeded (6.6×10^5 cells/ml and 150 µl/well) in Krebs buffer in a black 96 well plate before the addition of 10 µM DCF-DA. Fluorescence measurements (excitation 485 nm/emission 520nm) was measured every 30 s over 1 h. The rates or ROS production were taken from the slopes of the linear part of the graph, after the initial lag phase. (A) Rescue reverses the MTX-induced ROS production. Data are presented as (A) mean ± SEM, n=5, each in triplicate, normalised to control (100%); a one-way ANOVA, followed by Tukey's multiple comparison test was performed with significant differences indicated by*$P<0.05$, or **$P<0.01$.

3.5 Discussion

Toxicity in immortalised cell lines and unactivated primary cells

Low-dose MTX is known to cause significant cell death in immortalised cell lines, even in those left unactivated. However, the concentration of MTX that is cytotoxic varies depending on the cell type and its state of activation. This was demonstrated in PMA-differentiated THP-1s and LPS-activated iBMDMs (Fig 3.4). Following a 4 h treatment with MTX (1 µM), few of the THP-1s were viable and at 17.44 µM, half of the LPS-activated iBMDMs remained. No literature can be found citing the inhibitory concentration of MTX on PMA-differentiated THP-1s, but it was shown that 9 nM caused more than 50% growth inhibition in unactivated THP-1s (Kimura et al., 2004). Other studies found that higher concentrations were needed, with one particular study demonstrating that MTX (1 µM) caused only a 25% drop in viability after 24 h (Herman et al., 2005). In other monocytic cell lines, similar concentrations of MTX (0.1 µM and 1 µM) have been shown to induce significant cell death. This was shown in both unactivated and LPS (25 µg/ml) activated U937 cells, after 16 h and after 72 h (Phillips et al., 2003, Olsen et al., 2014). It is known that differentiation of THP-1 cells with PMA stops proliferation, thus these alamar blue results are indeed cell death (Dreskin et al., 2001). However, iBMDMs are not known to cease dividing upon LPS-activation thus the alamar blue results could be either cell death or inhibition of proliferation. Affirmative assays such as propidium iodide or annexin V would confirm these results.

MTX has not been shown to be toxic to unactivated primary cells. In unactivated peripheral blood lymphocytes (PBL), MTX did not cause cell death with doses as high as 100 µM (Genestier et al., 1998). These findings were verified with a 96 h MTX (2.2 µM) treatment in CD4^{+} and CD8^{+} T cells, and up to 24 h MTX (10 µM) treatment in PBMCs (Strauss et al., 2002, Herman et al., 2003). The results shown here are in agreement with those cited above, showing that MTX (1 µM) had no effect on cell viability in both human PBMCs and murine DCs after 24 h (Fig 3.5). The absence of a cytotoxic effect of MTX on unactivated T cells was also demonstrated in vivo. The T cells of mice treated with MTX (7mg/kg/day) before T cell extraction were not determined to be apoptotic (Izeradjene et al., 2001).

Activation-dependent toxicity

However, MTX has been shown to have a cytotoxic effect in activated cells and is very much dependent on the type of antigen (Johnston et al., 2005). Toxicity is also dependent on the duration of activation and the stage of activation in which treatment is administered. Admittedly, this makes comparisons difficult and has yielded conflicting results. With regard to non-mitogenic activation, most reports demonstrate little toxicity with low-dose MTX treatment. Superantigen or streptococcal antigen-stimulated PBMCs displayed no reduction in cell viability following a 120 h incubation in the presence of MTX (1 µM) (Johnston et al., 2005). Flu antigen stimulated-PBMCs also showed no reduction in cell viability in the presence of MTX (20 nM) for up to 96 h (Collinge et al., 2010). Here it was shown that LPS-activated human PBMCs and murine DCs, incurred no loss in cell viability following a 24 h MTX (1 µM) treatment (Fig 3.6). However, there is evidence to suggest that MTX treatment with non-mitogenic stimuli can be toxic. There was a significant increase in apoptosis in tetanus toxin or *Candida Albicans* treated CD4^{+} T cells, following MTX (2.2 µM or 22 µM) treatment (Nielsen et al., 2007). A significant increase in apoptosis was also shown in super antigen (SEB)-activated T cells isolated from mice treated with MTX (7 mg/kg/day), equivalent to low-dose MTX treatment in humans (Izeradjene et al., 2001).

The most consistent results of MTX having a cytotoxic effect on activated primary cells have been shown with mitogenic stimuli, such as PHA, and the T cell mitogens concavalin A and anti-CD3. PBL incubated in the presence of PHA (5 µg/ml) with MTX (1 µM) for 72 h, incurred 15% more cell death compared to PHA alone (Quemeneur et al., 2003). The same dose was also found to cause significant apoptosis, as measured by annexin V staining, in 72 h PHA-activated PBMCs and in PHA-activated T cells; (Herman et al., 2003, Phillips et al., 2003, Sigmundsdottir et al., 2004, Johnston et al., 2005). Even MTX (100 nM) treatment during PHA-activation resulted in cell death of PBLs (Genestier et al., 1998). Interestingly, MTX treatment following mitogen activation was also shown to cause significant cell death, presumably because these cells were still cycling. This was demonstrated in 72 h-PHA (5 µg/ml)-activated PBMCs, whereby MTX (0.1-100 µM) treatment caused apoptosis (Genestier et al., 1998, Swierkot et al., 2004). Experiments involving other mitogens such as concavalin A, showed similar toxic effects with low-dose MTX. This was shown in PBMCs incubated with MTX (500 nM) with concavalin A for 4 days (Tohyama et al., 2013).

Mitogenic activation with anti-CD3 has also been shown to cause cell death upon MTX treatment, even if treatment was administered after activation. MTX (1 μM) induced the apoptosis of PBL, already activated with anti-CD3 (Genestier et al., 1998). Another study of PBMCs stimulated with anti-CD3, followed by PMA and ionomycin were treated with 2.2μM MTX for a further 72 h and found that treatment led to 30-60% apoptosis (Quemeneur et al., 2003). However, it was shown here that MTX treatment in the last 4 h, 6 h, 8 h and 24 h of a 72 h anti-CD3 activation had no effect on cell viability (Fig 3.7). Indeed the same concentration of MTX (1 μM) induced significant death of PBMCs previously activated for 72 h with PHA, but not in those activated for 24 h with PHA (Herman et al., 2003).This indicates that the duration of exposure and the activation state of the cell, influences the extent of cytotoxicity.

Treatment for the duration of the activation period was more consistent with what has been shown in the literature. MTX (100 nM and 1 μM) treatment for the duration of the 72 h anti-CD3-activation caused a significant reduction in the viable cell count (Fig 3.8A). However, because MTX is known to exert an anti-proliferative effect, it was important to determine whether the reduction in viable cells was due to failure of the cells to proliferate or the induction of cell death.

The interdependence of inhibition of cell proliferation and cell death

A growth curve conducted over the course of 120 h, verified that after 72 h of activation MTX (100 nM) had also inhibited cell proliferation (Fig 3.8B). After 48 h, MTX treated and the untreated PBMCs had equally low numbers of viable cells. However, if this normal fluctuation in activated PBMCs was not determined, the difference in viable cell counts at 72 h following MTX treatment may have been misinterpreted as cell death by MTX treatment only. After 48 h, activated cells started to divide at a faster rate than the MTX treated cells, resulting in a significant difference in numbers of viable cells after 72 h. This growth curve also shed light on why a 24 h incubation with MTX had no effect on the anti-CD3-activated PBMCs (see **Section 3.4.1**). Between 48 h and 72 h there was a difference in the proliferation rate compared to untreated cells, but there were low levels of proliferation occurring. The limited proliferative capacity shown in those MTX-treated cells probably reflected the workings of the salvage pathways or perhaps that MTX had not displaced all existing polyglutamated intracellular folate. After 72 h this rate seemed

to plateau, perhaps suggesting that the salvage pathway had been exhausted and that intracellular folate-depleted.

To investigate if cell death did contribute to the reduction in viable cell numbers, propidium iodide was added to cells after this 72 h activation in the presence of a range of MTX concentrations (0.1 nM-1 μM). MTX (100 nM and 1 μM) caused significant cell death of PBMCs, (~75%) compared to the control (~90%) (Fig 3.9). These findings are consistent with similar studies monitoring levels of apoptosis after 96 h MTX treatment, albeit at a higher dose (2.2 μM) (Strauss et al., 2002). This 72 h anti-CD3-activation in the presence of MTX inhibited cell proliferation, whilst still maintaining an acceptable level of viability and so was determined to be the optimum condition for this study. Indeed a 72 h activation using anti-CD3 is not uncommon for these studies (Wang et al., 2011a).

Despite the evidence demonstrating the apoptotic effect of MTX on mitogen-activated primary cells, there are studies which negate this effect. The first is a 30 min MTX (2 μM) pre-treatment of PBMCs, before PHA activation (50 μg/ml) for 72 h (Fairbanks et al., 1999). However, 30 mins may not be enough time for substantial MTX uptake and for polyglutamation to take place in order to retain MTX intracellularly. For this reason, these findings have not been considered. The second stems from experiments conducted in CD4$^+$ T cells, incubated with PHA (10 μg/ml) for 7 days with MTX (2.2 μM or 22 μM) added in the last day of activation (Nielsen et al., 2007). The authors found insignificant increases in apoptosis however, it must be questioned whether the cells were still dividing on the 6th day and whether they were thus susceptible to the effects of MTX. It also poses the same question of whether a 24 h treatment is enough to deplete the salvage compensatory pathways and to displace intracellular folate, which was discussed previously (see **Section 3.4.1**). Thus, the only real conflicting evidence, negating the cytotoxic effect of MTX on dividing cells comes from studies with anti-CD3/CD28-activated T cells with a 96 h MTX (2.2 μM) treatment (Haroon et al., 2008). Alas, these doses exceed the low-dose MTX (<1 μM) treatment given to patients, and are thus irrelevant to this study.

<u>The cytotoxic effect of MTX on T cells</u>

Since anti-CD3-activation induced proliferation of those cells carrying a CD3 receptor, namely CD3$^+$ T cells, it was important to determine the viability of these CD3$^+$ T cells

following MTX treatment. Backgating on both CD4$^+$ and CD8$^+$ T cells revealed that both subsets were significantly affected by the highest doses of MTX (Fig 3.11). This was an expected result as it was shown that apoptosis increased with the number of cell divisions in 96 h PHA-activated PBL in the presence of MTX (1 µM) (Quemeneur et al., 2003). Indeed these CD4$^+$ and CD8$^+$ T cells were shown to be the fastest cycling cells (Fig 3.14). The proportions of these CD3$^+$ T cells revealed that T cells were the predominant PBMC cell subset after this 72 h activation (Fig 3.10). This is unsurprising as it was shown that after 6 days of PHA-activation of mononuclear cells containing mixed populations of T and B lymphocytes, NK cells and monocytes, >95% were CD3$^+$ cells (Courtemanche et al., 2004).

Purine and thymidine rescue

To determine whether the inhibition of proliferation preceded cell death, proliferation was rescued upon the addition of hypoxanthine and thymidine and cell viability measured. Nucleotide salvage was shown to rescue the cellular proliferation of antibody-forming B cells and in the immortalised human T cell line, CEM following MTX treatment (Rosenthal et al., 1988, Budzik et al., 2000). Thymidine alone only partially reversed the anti-proliferative effect of MTX (1 µM) in PBLs, verifying that both purines and thymidine were required for cellular proliferation (Quemeneur et al., 2003). In this study, the addition of hypoxanthine and thymidine reversed the anti-proliferative effect of MTX and also recovered cell viability. (Fig 3.12). Combined with the fact that MTX has not been shown to cause cell death in either unactivated or non-mitogen activated PBMCs, these data support the anti-proliferative-dependent cytotoxic effect of MTX. It was also shown that blocking the transition from G1 to S phase prevented MTX-induced apoptosis, suggesting that apoptosis was initiated at the S phase of the cell cycle (Neradil et al., 2012). Finally, the toxicities of MTX treatment have been shown to occur in tissues that are known to have high levels of cell turnover such as the bone marrow and gastrointestinal tract (van Ede et al., 1998). However, MTX can also induce apoptosis in post mitotic cells, suggesting that MTX can induce distinct pathways of cell death (Neradil et al., 2012).

The anti-proliferative effect of MTX

To verify this anti-proliferative effect, CFSE was employed as a method used to quantify the proliferation induced by anti-CD3 and measure the changes in proliferation induced

by MTX. Histograms of the CFSE dye, with increasing peaks to the left, reflected loss of CFSE labelled lysine residues after each round of cell division. A greater loss in CFSE, measured by the % proliferation, reflected greater proliferation and high levels of CFSE reflected lower proliferation rates. Anti-CD3-activation induced cell proliferation but in the absence of anti-CD3, there was a basal rate of cell division. Following MTX (1 µM) treatment, the anti-CD3-induced proliferation was shown to revert back to unactivated levels (Fig 3.13A). A dose response of MTX (0.1 nM- 1 µM) was tested and MTX (100 nM and 1 µM) was found to significantly inhibit the anti-CD3-induced proliferation (Fig 3.13B). These findings were consistent with what was found in the literature. MTX (1 µM) significantly inhibited the cellular proliferation of PBL activated with PHA (5 µg/ml) for 6 days (Quemeneur et al., 2003). MTX (2.2 µM) although considered high-dose treatment, also significantly inhibited the IL-6-induced proliferation of fibroblast-like-synoviocytes after 72 h (Ji-Yeon Sung a et al., 2000). Cells cultured in folate-deplete media have also been shown to have a limited proliferative capacity, mimicking the folate antagonist, MTX. Lymphocytes activated with PHA (22.5 µg/ml) for 10 days in folate-deplete media or at concentrations found in individuals considered to be folate-deficient, proliferated ~50% less than those cultured in folate-replete conditions (Courtemanche et al., 2004). In vivo studies of mice also demonstrated this anti-proliferative effect at doses corresponding to low-dose treatment in humans. Mice treated with MTX (7 mg/kg/24 h) before selective expansion of a CD8^{+} T cell clone and during its 72 h proliferation, was also found to have its proliferation impeded (Quemeneur et al., 2004). Interestingly, lower doses of MTX have also been found to exert an anti-proliferative effect. MTX (50 nM) significantly inhibited the proliferation of PBMCs stimulated with Concavalin A (5 µg/ml) for 96 h (Tohyama et al., 2013). Even MTX (20 nM) inhibited the proliferation of 72 h flu antigen-stimulated PBMCs to ~50% of its control (Collinge et al., 2010). In this study MTX (10 nM) was found to have no significant anti-proliferative effect, however mid-range concentrations between 10-90 nM were not tested (Fig 3.13B). MTX (10 nM) was also shown to have no anti-proliferative effect in B cells stimulated with anti-Ig and B cell growth factor over the course of 72 h (Rosenthal et al., 1988).

The only conflicting data which disputes this anti-proliferative effect of MTX (<1 µM) comes from studies which add treatment in the last 24 h of activation. It was shown that 96 h PHA (5 µg/ml)-activated PBMCs, when incubated with MTX (0.1-10 µM) for an additional 24 h, had no significant anti-proliferative effect (Herman et al., 2003).

Furthermore, MTX (2.2 µM) had no significant anti-proliferative effect when added in the last 24 h of CD4$^+$ T cells previously incubated with PHA for 6 days (Nielsen et al., 2007). Although the anti-proliferative effect of MTX, when treated for 4, 6, 8 or 24 h on the last day of activation was not measured here, there was no loss in cell viability found (Fig 3.7).

Bystander activation

Interestingly, it was found that non-CD3 receptive cells, not carrying a CD3 receptor, had proliferated under these conditions (Fig 3.14). This concept of bystander activation, whereby cells in the vicinity of activated cells indirectly activate other cells by way of cytokine secretion or other environmental stimuli, is relatively new (Jasiulewicz et al., 2015). These authors found that B cells proliferated within a population of anti-CD3-stimulated PBMCs. The data shown here suggested that CD19$^+$CD11c$^-$ PBMC subsets also proliferated due to anti-CD3 (Fig 3.15). CD11c$^+$CD19$^-$ PBMC subsets also proliferated but this was not due to anti-CD3-activation, suggesting that the basal proliferation of these cells was high. Although the CD11c$^+$ surface marker demonstrates high plasticity amongst DCs, monocytes and macrophages, it is uncommon for DCs to proliferate. Primary macrophages have demonstrated a proliferative capacity in vitro. Primary macrophages can be grown for a few weeks in culture and murine macrophages were found to proliferate upon receptor Fc-γ crosslinking (Coelho et al., 2012). Although the identity was not confirmed using more definitive surface markers, such as MHC class II, it was not deemed important for this study (Jongbloed et al., 2010).

The PBMC subsets, CD4$^+$ and CD8$^+$ T cells were shown to proliferate and were thus susceptible to the effects of 100 nM and 1 µM MTX (Fig 3.16). This is in keeping with another study, albeit at a higher dose (2.2 µM) (Strauss et al., 2002). Interestingly, the proliferation of these CD11c$^+$CD19$^-$ PBMCs subsets succumbed to the same doses of MTX, verifying that these cells were in fact also proliferating, just not due to anti-CD3-activation (Fig 3.16). There was no anti-proliferative effect with MTX treatment in the CD19$^+$CD11c$^-$ PBMC subsets although these cells were proliferating in response to anti-CD3, possibly because these cells were not proliferating at a fast enough rate (Fig 3.17). Indeed folate-deficiency was shown to inhibit CD8$^+$ T cell proliferation more than CD4$^+$ T cells, because these cells were growing at faster rates (Courtemanche et al., 2004). It

has been shown that B cells stimulated with anti-Ig and B cell growth factor were susceptible to the anti-proliferative effect of MTX (100 nM) over the course of 72 h (Rosenthal et al., 1988).

Inhibition of transferrin receptor expression

Since MTX inhibited the activation-induced proliferation of these PBMCs, the effect of MTX on transferrin (CD71) receptor expression, an iron transporter and a parameter of T cell-activation was also investigated (Goronzy et al., 1987, Reddy et al., 2004). This increase in transferrin receptor expression upon anti-CD3-activation was shown here in both CD4$^+$ and CD8$^+$ T cells, reflecting the need for iron in a variety of cellular processes (Fig 3.18). Transferrin expression is regulated by mTOR, in keeping with its key role in managing cell cycle processes (Zheng et al., 2007). It is well documented that MTX inhibits mTOR (Fernandez-Ramos et al., 2016). Hence, it was important to investigate whether MTX could directly affect transferrin expression in these anti-CD3-activated PBMCs, a previously unexplored area. MTX significantly reduced transferrin receptor expression in both CD4$^+$ and CD8$^+$ T cells during anti-CD3-activation (Fig 3.19). There was no effect on transferrin receptor expression following MTX (<10 nM) treatment, reflecting the dose-dependent anti-proliferative effect shown previously. Importantly, it was not clear whether MTX reduced or prevented the increase in CD71 expression that accompanies cellular activation. Interestingly, thymidine and hypoxanthine rescue could reverse this inhibitory effect of MTX, suggesting that this reduction in transferrin expression was related to purine and thymidine inhibition (Fig 3.20).

Inhibition of T cell blastogenesis

The enlargement of CD3$^+$ T cells that accompanies cellular activation, termed lymphoblast formation was also measured (Darzynkiewicz et al., 1976) (Fig 3.21). This has been shown by a variety of T cell mitogens, including concavalin A and anti-CD3/CD28, respectively (Whitfield et al., 1974, Wang et al., 2011a). This early stage in activation, associated with an increase in the nucleus to cytoplasm ratio, allowing for the uptake of building blocks preceding mitosis, has been shown to be regulated by c-Myc (Wang and Green, 2012a). Since mTOR lies upstream of c-Myc, the effect of MTX on this characteristic of cellular activation was investigated. A direct effect of MTX on c-Myc expression was shown in the A549 Human lung adenocarcinoma cell line, which led to growth inhibition (Fernandez-Ramos et al., 2016). However, it was not determined

whether MTX was inhibiting c-Myc expression or some part of the mTOR pathway via purine and thymidine inhibition or whether the absence of these building blocks was responsible.

In keeping with the other parameters of cellular activation, the effective dose of MTX (100 nM and 1 μM) significantly reduced the proportion of $CD4^+$ T cells that were (>35k) in size compared to anti-CD3-activation alone (Fig 3.22). $CD8^+$ T cells also failed to undergo activation-induced growth in response to anti-CD3-activation with MTX treatment (Fig 3.23). Other reports have found that MTX reduces the anti-CD3/CD28 activation-induced growth of PBMCs (de Lathouder et al., 2002). However, there is one report where MTX was found to have no effect on blast formation in T cells isolated from mice activated with the SEB superantigen (Izeradjene et al., 2001). To investigate if this inhibition of blast formation following MTX treatment was related to purine and thymidine inhibition, MTX-treated cells were rescued with hypoxanthine and thymidine. Similar to what was observed in the proliferation experiments and transferrin expression, the addition of hypoxanthine and thymidine significantly reversed the MTX (100 nM)-mediated inhibition of lymphoblast formation (Fig 3.24). Since the effects at 1 μM were also observed at 100 nM, the lower dose was used in subsequent experiments. Although no reports have been found regarding the effect of thymidine and hypoxanthine rescue on the MTX-induced reduction in cell size in anti-CD3-activated PBMCs, it was demonstrated that rescue could reverse the enlargement of cells unable to undergo mitosis following MTX treatment in leukemic cell lines (Taylor and Tattersall, 1981). It was also shown that 5-methyl-THF and 5-formyl-THF protected blastogenesis in PHA-activated PBL from MTX 1 μM (Groff and Blakley, 1978). This suggests that either folate antagonism or indeed purine and thymidine antagonism is responsible for the inhibition of blastogenesis found here.

Dissipation of the $\Delta\Psi_m$

Since MTX exerted global effects on anti-CD3-induced cellular activation, it was important to investigate any metabolic changes accompanying these phenotypic ones. As cellular activation has high energetic demands, optimal mitochondrial function is required, which relies on an adequate $\Delta\Psi_m$. This $\Delta\Psi_m$ was measured using JC-1, a dimeric dye which exhibits potential dependent differences. As outlined in the methods section, the mitochondrial uncoupler, FCCP (500 nM), was first used to identify the aggregate JC-

142

1. As a protonophore, FCCP instantly depolarized the membrane and depleted the aggregate JC-1. The effect of FCCP in dissipating the $\Delta\Psi_m$ is well established. For instance, FCCP (10 μM) was shown to dissipate the $\Delta\Psi_m$ in MCF-7 breast cancer cells (Fodor et al., 2016). This depolarization was used as a gate on which changes in the aggregate JC-1 were measured. After a 5 h MTX (100 nM) treatment in unactivated PBMCs, the aggregate population was significantly reduced, indicating that the $\Delta\Psi_m$ was lowered (Fig 3.25A). Although there is no information regarding the effect of MTX on the $\Delta\Psi_m$ in PBMCs, this reduction of the $\Delta\Psi_m$ has been shown in other cell types. In platelets, it was shown that treatment with MTX (10 μM) for 1 h dissipated the $\Delta\Psi_m$ (Paul et al., 2015). In the Human Carcinoma, JAR cell line, MTX (0.22 μM) was found to significantly lower the $\Delta\Psi_m$ (Chen et al., 2009). The same effect was demonstrated in IE-6 cells treated with MTX (1 μM) for 24 h (Chang, 2013). However, there is also a report which found that MTX treatment increases the $\Delta\Psi_m$ in the breast cancer line, MCF-7, albeit at a high dose (10 μM) (Fodor et al., 2016). Thus, although no direct comparison can be made with our findings and those in the literature, this lowering of the $\Delta\Psi_m$ by MTX seems to be accepted in the majority of studies.

The effect of oligomycin, (an ATP synthase inhibitor) and antimycin A (a complex III inhibitor) on the $\Delta\Psi_m$ were next evaluated (Pfanner and Neupert, 1986, Zheng and Ramirez, 2000). The importance of ATP synthase in maintaining an adequate $\Delta\Psi_m$ is well documented (Schleyer et al., 1982). As such, inhibition of ATP synthase by the addition of oligomycin (0.1 μg/ml) has been shown to increase the $\Delta\Psi_m$ in mitochondria isolated from lymphocytes (Rottenberg and Wu, 1998). Antimycin A, which completely blocks respiration by complex III inhibition, has been shown to dissipate the chemical and electrical potential, reducing the $\Delta\Psi_m$ (Pfanner and Neupert, 1985). In keeping with those experiments, in this study, the addition of antimycin A (250 nM) significantly lowered the $\Delta\Psi_m$ however, oligomycin had no effect on the $\Delta\Psi_m$ in unactivated PBMCs (Fig 3.25B). This reason for the latter finding was not determined. This concentration of antimycin A was used because a lower dose (10 nM) was shown to have no effect on the $\Delta\Psi_m$ in lymphocytes (Rottenberg and Wu, 1998).

The effect of MTX on the $\Delta\Psi_m$ in anti-CD3-activated PBMCs was next investigated. MTX (100 nM) also significantly dissipated the $\Delta\Psi_m$ in these anti-CD3-activated PBMCs (Fig 3.26A). Although there were no data found regarding the effect of MTX on anti-CD3-activated PBMCs, a 15 h MTX (1 μM) treatment was shown to significantly lower

the $\Delta\Psi_m$ in 72 h PHA-activated PBLs (Genestier et al., 1998). The oxidative-phosphorylation inhibitor antimycin A (250 nM) had no effect on the $\Delta\Psi_m$, nor did oligomycin (Fig 3.26B).

These results showed that MTX dissipated the $\Delta\Psi_m$ in both unactivated and anti-CD3-activated PBMCs. To determine whether this dissipated $\Delta\Psi_m$ was a result of purine and thymidine inhibition by MTX, the effect of thymidine (100 μM) and hypoxanthine (100 μM) was investigated. The dissipation of the $\Delta\Psi_m$ by MTX could be partially reversed (Fig 3.27). Thus, it was concluded that MTX partially lowered the $\Delta\Psi_m$ by way of purine and thymidine inhibition. Indeed it was shown in platelets that rescue of the MTX (50 μM)-dissipated $\Delta\Psi_m$ could be reversed upon the addition of the antioxidant, NAC (1 mM) (Paul et al., 2015). The authors thus postulated that ROS production contributed to this reduction in the $\Delta\Psi_m$ which was related to the induction of apoptosis at those high MTX concentrations. However, in this study, MTX was not found to cause cell death in unactivated PBMC, yet the $\Delta\Psi_m$ was dissipated. Furthermore, previous experiments demonstrated that recovery of purine and thymidine synthesis also recovered cell viability (see **Section 3.4.1**). Thus, although cell viability was recovered in MTX-treated, anti-CD3-activated PBMCs following rescue, the addition of thymidine and hypoxanthine only partially recovered the $\Delta\Psi_m$.

Effects on ROS production

Since MTX (100 nM) dissipated the $\Delta\Psi_m$, a gradient on which efficient ATP production depends, it was important to determine how else mitochondrial function was affected. In light of the previous report that dissipation of the $\Delta\Psi_m$ preceded ROS production, the effect of MTX treatment on ROS production was investigated using H_2DCF-DA (Paul et al., 2015). Antimycin A was used as a positive control in these experiments since the inhibition of complex III has been shown to generate superoxide production (Brand et al., 2004). This was shown because complex III inhibition increases leakage of electrons, which are then converted to hydrogen peroxide and other radicals. Antimycin A exhibited a dose-dependent increase in ROS production in unactivated PBMCs (Fig 3.28B). However, a 5 h MTX (100 nM) treatment, had no effect on ROS production in these unactivated PBMCs, despite lowering the $\Delta\Psi_m$ under the same conditions (Fig 3.28A). These findings are consistent with studies using polymorphonuclear leukocytes (PMNL) whereby only high MTX concentrations (22 μM) were found to significantly increase

ROS production (Hara et al., 1990). This increase in ROS production with high dose MTX (10 µM) was also shown in PBMCs and platelets, respectively (Fernanda Barbisan2 et al., 2014, Paul et al., 2015). Interestingly, in immortalised cell lines, low-dose MTX has been shown to have an effect on ROS production. MTX (<1 µM) was shown to increase ROS production in immortalised HL-60 cells, IE-6, and Jurkat T cell lines (Huang et al., 2005, Spurlock et al., 2011, Chang, 2013).

Parallel experiments were conducted in anti-CD3-activated PBMCs. Similarly, antimycin A exhibited a dose-dependent increase in ROS production (Fig 3.29B). MTX (100 nM) significantly increased ROS production, just as it had dissipated the $\Delta\Psi_m$ in these cells (Fig 3.29A). These findings are consistent with parallel studies using low-dose MTX (<1 µM) treatment (Paillot et al., 1998). Even other mitogens, such as PHA, showed a significant increase in ROS production upon MTX (1 µM) treatment in activated T cells (Phillips et al., 2003). However, other studies have found inhibitory effects of MTX on ROS production. This was shown with MTX (2.2 µM) in synoviocytes isolated from synovial fluid from RA patients (Ji-Yeon Sung a et al., 2000). Despite this conflicting report, MTX, by way of reducing ROS, was shown to exert an anti-inflammatory effect as ROS was crucial to the proliferation of these synoviocytes, as the addition of NAC to IL-6-stimulated cultures abrogated this proliferation. The other report demonstrated that MTX (1 µM) inhibited ROS production when added to neutrophils already primed with TNFα (Okuda et al., 1997). Alas, direct comparisons cannot be made as the aforementioned examples use different stimuli. Interestingly, the fact that MTX reduced the $\Delta\Psi_m$ in both unactivated and activated PBMCs suggests that perhaps MTX does affect mitochondrial function, distinct from the effects on cellular activation. To assess whether this increase in ROS production by MTX was related to purine and thymidine inhibition, the experiment was repeated with thymidine and hypoxanthine rescue. The MTX-induced increase in ROS production in these anti-CD3-activated PBMCs was partially reversed following purine and thymidine rescue which suggested that the increase in ROS production was related to the MTX-inhibition of purine and thymidine synthesis (Fig 3.30). Similar results were also shown upon the addition of hypoxanthine or hypoxanthine with guanosine in LPS and TNFα stimulated neutrophils (Okuda et al., 1997). However, as of yet, no such study has related the effect of purine and thymidine inhibition to the increased ROS production of MTX.

Overall, MTX was shown to exert cytotoxic effects, which were related to the cytostatic effects following purine and thymidine inhibition. A variety of the other effects found with MTX treatment including inhibition of transferrin receptor expression, blastogenesis, dissipation of the $\Delta\Psi_{m,}$ and ROS production were also completely or partially reversed upon thymidine and hypoxanthine rescue. Further investigation into the secondary effects of purine and thymidine inhibition by MTX could yield interesting findings.

Dissipation of the $\Delta\Psi_{m}$ was the only effect found in unactivated PBMCs. Inhibition of proliferation, transferrin receptor expression, blastogenesis,, ROS production and the induction of cell death were only found following mitogenic-activation of PBMCs using anti-CD3. The aforementioned effects were not limited to CD3$^+$ T cells. CD11c$^+$ PBMC subsets were susceptible to the anti-proliferative effect of MTX, suggesting that they could contribute to the observed effects found in the PBMC population. Although there was no significant anti-proliferative effect in CD19$^+$ PBMC subsets, these PBMC subsets were shown to be indirectly activated by way of anti-CD3-activation, highlighting the need for future work to determine the effects of anti-CD3-activation on every PBMC subset. These findings suggest that other non-T cell PBMC subsets could also be affected by MTX and support studies measuring effects on the entire PBMC population, containing different cell subsets.

<u>Chapter 4:</u>

To develop a quantitative method for the evaluation of the effect of Methotrexate treatment on the cell-surface sialome

4.1 Introduction

Barry Sharpless coined the term "Click chemistry" which has proved to be a valuable technique in measuring intracellular glycoproteins, glycans on the surface of intact cells as well as in live mice, and enzyme function (Kolb et al., 2001, Speers and Cravatt, 2004, Baskin et al., 2007, Zaro et al., 2011). It is the reaction of two chemical groups, typically on separate compounds, which results in the ligation of two molecules. One molecule contains a reporter probe which selectively binds to and thus signals the presence of the other ligand. Click chemistry encompasses the ligation of azides and alkynes, achieved using a copper catalyst or strained cycloalkyne, which lowers the activation requirements of the reaction. It also includes the reaction of azides and phosphines, typically known as the Staudinger ligation (Laughlin and Bertozzi, 2007). For the analysis of cell-surface glycans, various sugars have been modified to contain an azide in their molecule which enters the normal biosynthesis pathway, is incorporated on surface glycans and is thus detected using an alkyne-containing fluorescent probe. For these experiments, PBMCs were treated with ManNAz, an azide-modified derivative of *N*-acetylmannosamine (ManNAc), shown to enter the sialic acid processing pathways for presentation on the cell-surface (Saxon et al., 2002). The presence of this sugar on the cell-surface was then detected following the copper-catalysed addition of a fluorescent alkyne. Since sialic acids are the most abundant terminal components on the glycoproteins and glycolipids of mammalian cells, this sugar was chosen in this study to determine the effect of drug treatment on the cell-surface sialome (Mahal et al., 1997).

Click chemistry is now widely used in drug discovery by virtue of the ease of drug synthesis, facilitated by this method (Nwe and Brechbiel, 2009). It has also been extensively applied for use in targeted drug therapy, whereby one study used it to evaluate drug infiltration of tumours (Samuelson et al., 2015). However, the importance of this method in determining the effect of drug treatment on cell-surface sialylation has not been shown. It has also not been shown whether drugs that act by inhibiting cellular activation or reducing metabolic precursors, can also indirectly impinge on cell-surface sialylation.

4.1.1 Labelling and quantifying the cell-surface sialome using click chemistry

Before the widespread use of these azido-modified sugars, cell-surface glycans were identified using fluorescently tagged lectins, which bind to specific sugars on the cell-surface (Laughlin and Bertozzi, 2009). However, the use of click chemistry allows for monitoring of specific glycan biosynthesis pathways by using specific modified sugars. Flow cytometry has been used to successfully quantify these sugars on the cell-surface in a variety of cell types, using the Staudinger ligation. This has been shown in Jurkat cells, CHO cells and Lewis lung cancer cells (Saxon and Bertozzi, 2000, Saxon et al., 2002, Hang et al., 2003, Chang et al., 2007, Neves et al., 2013, Wainman et al., 2013). Quantification of primary mammalian cells has also been achieved. Cell suspensions of zebrafish embryos and mouse splenocytes have been quantified using flow cytometry, using the Staudinger ligation however there are limitations to using this method (Dube et al., 2006, Dehnert et al., 2011) . The Staudinger ligation suffers from slow kinetics and competing oxidation of the phosphine reagents in air (Besanceney-Webler et al., 2011). The former means that it can't be used for studying faster time scales and the latter limits the specificity of the reaction, since the azide may not be the only reacting oxidant (Boyce and Bertozzi, 2011). The copper-catalysed click chemistry reaction, using azides and alkynes proceeds at a faster rate and is the preferred method for quantification of the cell-surface sialome.

4.1.2 The toxicity associated with copper-catalysed click chemistry

There are few publications describing the copper-catalysed addition of azides to alkynes as this method was thought to be too toxic for live cells (Agard et al., 2006). There is only one record where quantification was achieved using the copper-catalysed click chemistry reaction in Jurkat cells (Hsu et al., 2007). Copper toxicity was shown in various immortalised cell lines, including HeLa cells, after a 72 h incubation with a variety of copper complexes (Kennedy et al., 2011). Shorter incubations have also proved to be toxic as it was found that 90% of mammalian cells underwent apoptosis following a 1 mM Cu(I) incubation (Sletten and Bertozzi, 2009). The same authors also showed that zebrafish embryos exhibited similar copper sensitivities only after a 15 min incubation.

Importantly, toxicity was not shown to be correlated with uptake of these copper complexes into cells (Kennedy et al., 2011). Neither was this toxicity attributed to the copper itself, but to the dehydroascorbate by-product, an electrophilic-variant, formed upon addition of this ascorbic acid reductant. This dehydroascorbate by-product was shown to cleave plasmid DNA and after 90 min resulted in the oxidation of 16% of N-benzoyl histidine molecules (Liu et al., 2006, Hong et al., 2009). It also led to the oxidation of BSA after only a 10 min incubation with 0.1 mM copper sulphate ($CuSO_4$) and ascorbic acid (Kumar et al., 2011). Toxicity was attributed to ROS production in the form of hydroxide radicals which was shown after a 2 h copper complex incubation (Liu et al., 2006). Even after 10 mins, hydrogen peroxide (50 µM) was found to be produced upon the addition of copper (0.5 mM) and sodium ascorbate (3.5 mM) measured by amplex red (Hong et al., 2009). In addition to oxidative damage, this dehydroascorbate by-product was also shown to react with and result in the crosslinking of surface amine and arginine surface groups (Hong et al., 2009). As such, mechanisms have been employed to combat this toxicity. These include the addition of aminoguanidine to prevent the cross-linking of surface side chains and the inclusion of various chelating ligands (Hong et al., 2009). In addition to maintaining copper in the reduced state (1+), these chelating ligands prevented the reduced copper from undergoing further redox reactions, enabling it to continue working as a catalyst thereby reducing the copper incubation time and minimising possible toxicity (Kennedy et al., 2011, Presolski et al., 2011). These chelating ligands such as BTTPS, BTTES, TBTA and THPTA have all shown promise under various conditions (Chan et al., 2004, Hong et al., 2009, Besanceney-Webler et al., 2011, Wang et al., 2011b). For instance, THPTA was shown to prevent the oxidation of histidine residues that occurred after a 90 min incubation and accelerated the decomposition of peroxide (Hong et al., 2009). BTTES ligand catalysed the click reaction to such an extent that it enabled the visualisation of fucosylated glycans in live embryos following a 3 min click reaction with minimal toxicity (Zheng et al., 2012).

Toxicity was also shown to be time-dependent. Incubations of copper (50 µM) with various ligands and ascorbic acid induced minimal toxicity in a variety of cell lines, provided incubation times were less than 20 min (Kennedy et al., 2011). However, it was suggested that copper incubation times longer than 5 min induce toxicity in most systems (Hong et al., 2010). Copper toxicity was also related to the time for incubation with the

azide (Hong et al., 2010). In these experiments, short incubations for both the sugar azide (24 h) and the copper solution (5 min) were employed to minimise toxicity. In addition the reaction substituents and cell suspensions were kept on ice. Indeed, one group found that incubation of the copper-ligand reaction at 4 degrees improved the viability of Jurkat cells from 60% to 85%, for the 15 min duration (Wang et al., 2011b). In this way it was shown that this copper-catalysed click reaction could be used to quantify surface *N*-glycosylation following drug treatment, provided precautions were taken to minimise toxicity.

4.1.3 The effect of drug treatment on cell-surface sialyl glycans

In order to demonstrate that this method could be used to quantify the effect of drug treatment on cell-surface sialylation and on cellular activation, tunicamycin (a known *N*-glycosylation inhibitor) and MTX (an anti-inflammatory drug that acts by limiting cellular activation), were employed. Metabolic inhibitors have been shown to affect the sialyl-lewis glycans on the surface of the glycoprotein, P-selectin glycoprotein-1 (Kanabar et al., 2016). To date, no publications can be found regarding the effects of metabolic inhibitors on the cell-surface sialome, or whether MTX can affect cell-surface sialylation, either directly by affecting the glycosylation pathway or indirectly as a metabolic or cellular activation inhibitor. It is known that MTX can affect antibody glycosylation since it has been shown to reduce the agalactosylated IgG in RA patients during treatment, which correlates with an improvement in clinical score (Ercan et al., 2012). Although sialic acids have also been shown to be decreased on the cell-surface of plasmablasts of RA patients, measured using lectin binding, there are no reports describing the effects of MTX treatment on cell-surface sialyl-glycans (Pfeifle et al., 2016). Thus, this study sought to investigate whether MTX could affect cell-surface sialylation on PBMCs and whether this was related to the levels of intracellular nucleotides, in keeping with our hypothesis that MTX could have an effect on glycosylation by limiting the availability of sugar-nucleotide donors.

4.2 Aims of the chapter

1. To visualise changes in the cell-surface sialome in anti-CD3-activated and unactivated PBMCs.

2. To develop a quantitative method to measure incorporation of a sugar on the cell-surface of PBMCs.

3. To apply the aforementioned quantitative method to test the effect of tunicamycin and MTX on cell-surface sialylation.

4. To investigate whether the cell-surface sialome could be characterised as a measurable parameter of cellular activation.

5. To investigate the effect of MTX in PBMCs activated with anti-CD3 and their unactivated counterparts on the cell-surface sialome.

6. To investigate whether the effects of MTX can be reversed following purine and thymidine rescue.

4.3 Material and methods

4.3.1 Click IT reaction

Click IT chemistry is a cycloaddition reaction between an azide and alkyne, catalysed by copper, which joins two compounds together containing these functional groups. For the purposes of these experiments, the sugar N-acetylmannosamine, (ManNAc) was modified to contain an azide functional group. This modified sugar, N-azidomannosamine (ManNAz), infiltrated the CMP-N-acetylneuraminic acid processing pathway and was incorporated on to cell-surface sialic acid residues. The azide present on the sialic acid was then detected upon the addition of a fluorescent-labelled alkyne probe, in the presence of copper (Fig 4.1).

4.3.2 Preparation of PBMCs for confocal microscopy

PBMCs (1 X 10^{6} cells/ml and 1.2 ml per well) were seeded in a 12 well plate for 24 h or were activated with anti-CD3 (1 µg/ml) ± MTX 100nM for 72 h. Both unactivated and activated PBMCs were incubated with ManNAz (50 µM) for the last 24 h of treatment. The PBMCs were gently centrifuged (50 x g) on to poly-D-lysine-coated slips. The media was carefully pipetted off and the cells washed twice with PBS. Click-iT® Cell Reaction Buffer Kit by Life Technologies (catalogue number C10269), containing alexa fluor 488 (3 µM), CuSO$_4$ (1.96 mM), and a patented formulation of the reducing agent, (sodium ascorbate in Tris buffer) was pipetted (100 µl) onto the slips. After this 5 min incubation, the cells were washed once with PBS and recovered upon the addition of 100 µl complete RPMI for 30 min. The cells were then washed twice before the addition of 500 µl of 4% paraformaldehyde (PFA) for 10 mins.

4.3.3 Co-staining with CD3$^+$, CD4$^+$ and CD8$^+$ antibodies

For the identification of the CD3$^+$ or CD4$^+$ and CD8$^+$ T cell subsets, the cells were washed twice with PBS after fixing with PFA. Cells were treated with individual antibodies (2 µl antibody in 200 µl PBS) at 4 degrees overnight. The cells were then washed three times with PBS before incubation with a secondary antibody against mouse IgG conjugated to alexa 594 (1 h on ice) in order to amplify the signal.

154
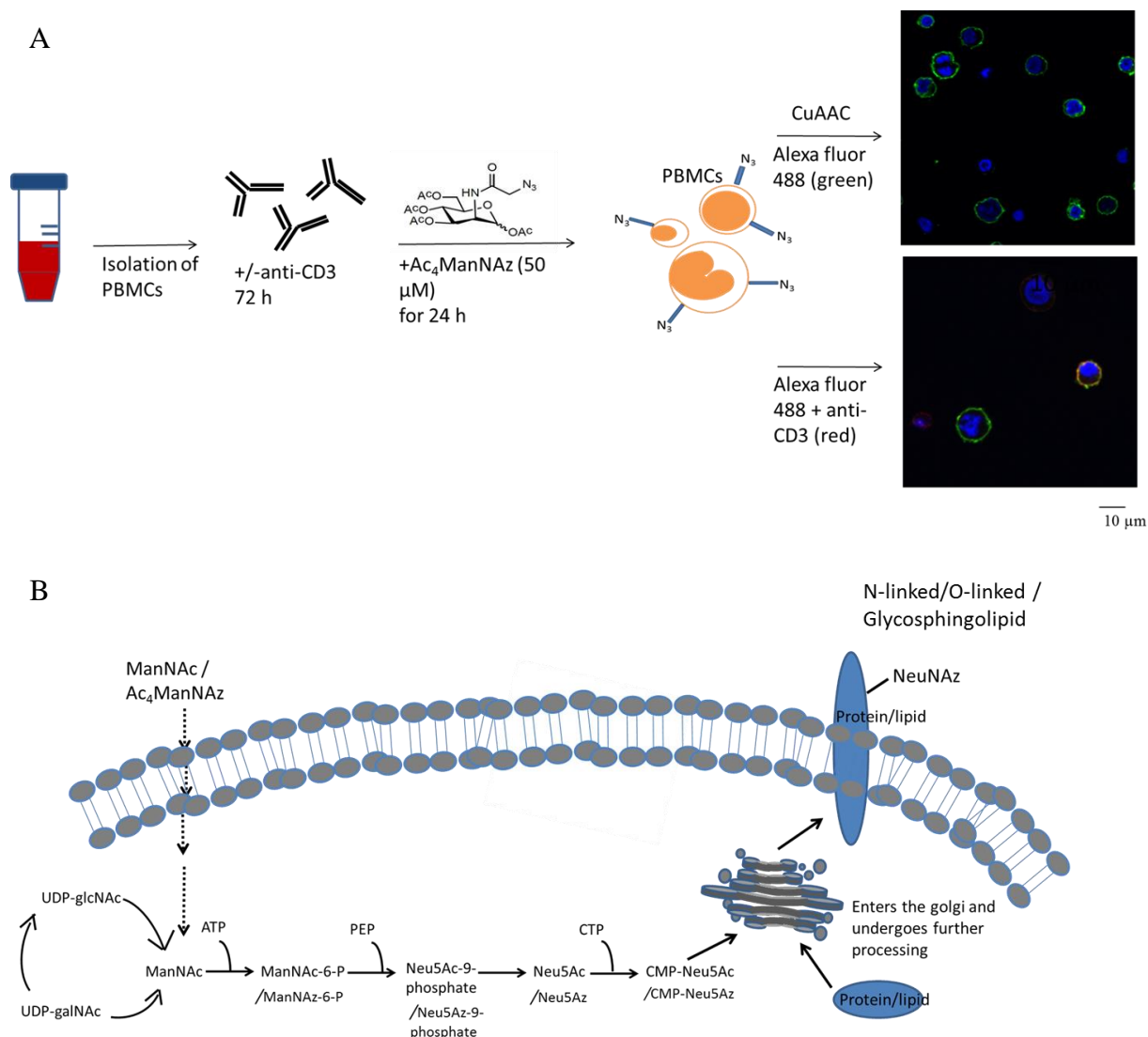
Figure 4.1. Incorporation of the Click IT-reactive, modified sugar, ManNAz, into the CMP-*N*-acetylneuraminic acid metabolic pathways for detection on the cell-surface.

(A) Schematic of the incorporation of ManNAz on the cell-surface of anti-CD3-activated PBMCs and its detection following ligation of a fluorescent probe, alexa 488 using the copper catalysed click reaction, in the absence or presence of alexa 594, for the identification of the CD3 surface marker. (B) Tetra-acetylated ManNAz is membrane permeable and diffuses through the membrane and enters the CMP-*N*-acetylneuraminic acid (CMP-Neu5Ac) processing pathway at the ManNAc entry point for the presentation of neuraminic acid-type sialic acids on the cell-surface. It is incorporated on to proteins or lipid acceptors in the golgi, undergoes further processing and is incorporated on the surface attached to either an *N*-linked or *O*-linked protein or lipid glycan.

These antibody-stained PBMCs, or PBMCs treated with the alexa fluor 488 solution only, were then washed (twice with PBS, and once with milliQ water). The coverslips were then gently removed using a forceps and blotted dry on tissue before placing cell-side down on to DAPI coated slides. These were then left to dry for 10 min before sealing with nail varnish and imaged using confocal microscopy. Importantly, the secondary pAb to mouse IgG would bind both CD3-PE as well as the functional purified anti-CD3 used to activate the PBMCs, as the origin of both antibodies is Mouse, isotype IgG2a K. This excludes the possibility that some CD3 surface receptors were not detected because of the occupation of the same CD3ε chain target sites by the anti-CD3 antibodies during activation, preventing the binding of CD3-PE.

4.3.4 Confocal microscopy

Fixed PBMCs were imaged using a Leica SP8 scanning confocal at a 60X oil immersion objective. Excitation of DAPI, alexa fluor 488 and 594 allowed imaging of the nucleus, surface sialyl-glycans and cell specific surface markers, respectively. Fixed samples were imaged at a resolution of 512 X 512.

4.3.5 Quantification using flow cytometry

Cell treatments

PBMCs (1 X 10^6 cells/ml and 1.2 ml/well) in a 12 well plate were incubated ± MTX (100 nM) ± ManNAz (50 µM) for 24 h or for anti-CD3-activation experiments, seeded (1 X 10^6 cells/ml and 1.2 ml/well) in an anti-CD3 (1 µg/ml) coated 12 well plate ±MTX (100 nM) or Tunicamycin (1 µM) for 72 h with ManNAz (50 µM) added to wells for the last 24 h of activation. In the absence of ManNAz, the same concentration of DMSO (0.1%) was added to wells as a vehicle control.

Following treatments, cells were centrifuged at 480 x g before being resuspended in 2% FACS buffer (complete media diluted 1:5 with PBS) and kept on ice. Cells were kept on ice for the duration of the preparation to minimise exchange of the modified sugar ManNAz with un-modified mannose in media. Viable cells were counted on a haemocytometer using trypan blue exclusion dye before the copper-catalysed click

chemistry reaction. From each treatment, including vehicle control, ~450,000 cells were then centrifuged at 480 x g and washed once with PBS. The cells were then pelleted again and resuspended in 95 µl of a solution containing alexa fluor 488 (3 µM), $CuSO_4$ (1.96 mM), and a patented formulation of the reducing agent, (sodium ascorbate in Tris buffer). After 5 min, cells were rescued with complete media and centrifuged to remove the copper solution. Cells were then washed twice in PBS before resuspending in 400 µl 2% FACS buffer for analysis on flow cytometry.

Flow cytometric gating strategies

Samples were acquired using a BD flow cytometer Cyan and a total of 50,000 events were measured for each condition. The vehicle control and copper-treated PBMCs were either left unstained or stained with PI for compensation controls. A sample of the ManNAz treated cells was added to these unstained cells for positive and negative compensation of alexa fluor 488 to be made. PBMCs were first gated on Forward Scatter (FS) against Side Scatter parameters to remove cell debris. Following this, doublet cells were excluded by gating of FS against pulse width. Importantly, in the absence of PI, alexa fluor 488 was detected in the PI channel. A gate was drawn from cells stained with alexa fluor 488 only and used to determine the PI negative population for each treatment. Following the addition of PI (1 µg/ml), the viable cells were then determined after gating of FS against PI. Background fluorescence was excluded from samples by determining any fluorescence from the copper-treated controls in the absence of alexa fluor 488 (Fig 4.2). ManNAz positive cells for the whole PBMC population was determined by gating of FS against alexa fluor 488. For the determination of ManNAz positive blast and non-blast PBMCs, the population was divided into PBMCs with a FS of >35k or <35k and against alexa fluor 488 for each population. The geometric mean fluorescence intensity of this population was then determined.
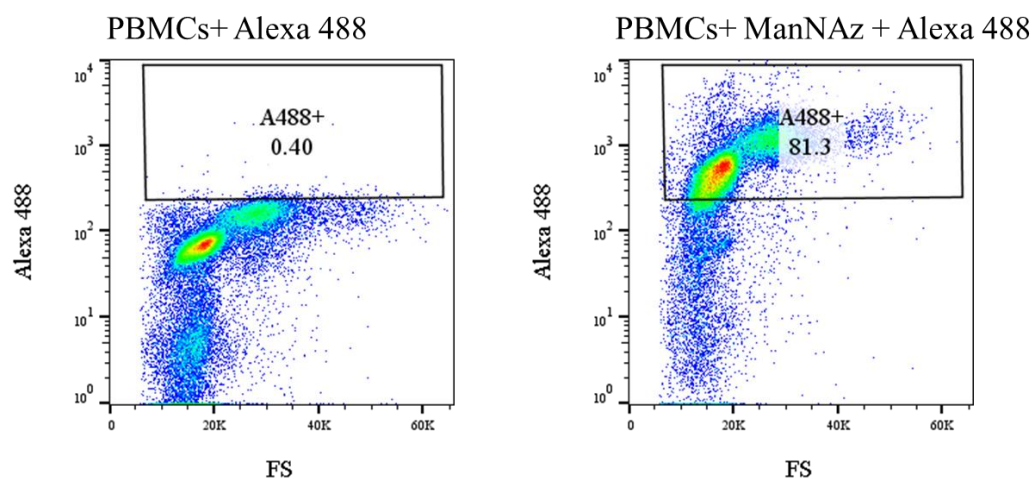
Figure 4.2. The specific binding of alexa 488 to the ManNAz ligand was measured following the exclusion of background fluorescence.

PBMCs were treated in the absence of ManNAz, with the alexa 488 probe in the presence of copper. A gate was drawn to exclude any unspecific binding, and was set to <1, which was applied to other treatments in the presence of the ManNAz ligand to determine the specific binding of alexa 488. The mean fluorescence intensity (MFI) of this population was then determined.

Transferrin receptor expression determination

For the analysis of transferrin (CD71) receptor expression on blast and non-blast CD4$^+$ and CD8$^+$ T cells, PBMCs (1 X 10$^{\wedge}$6 cells/ml and 3 ml/well) were seeded ± anti-CD3 ± the indicated MTX concentrations for 72 h, ± thymidine and hypoxanthine (100 µM). After this time PBMCs were counted on a haemocytometer and resuspended in 2% FACS buffer (1 X 10$^{\wedge}$7 cells/ml). Two cell samples were left unstained with antibodies to serve as an unstained and PI only control. Two microliters of each antibody against the surface marker CD4, CD8, CD71 was added to 100 µl of cells from each condition and incubated on ice for 40-60 min. After this time, cells were centrifuged and the pellet resuspended in 600 µl 2% FACS buffer. This was repeated 3 times. PBMCs were then resuspended in 400 µl 2% FACS buffer for flow cytometric analysis. Single stained cells and compensation beads were ran for compensation controls. PI (1 µg/ml) was added to each condition. Cell debris was first excluded following gating against FS and SS measurements. Doublets were excluded following gating against FS and pulse width. Viable cells were determined as those cells negative for PI stain in the total population (% PI negative). Blast and non-blast populations were determined following gating at 35k, after observing that PBMCs >35k significantly increased following anti-CD3 activation. The percentage of CD4$^+$ and CD8$^+$ T cells in each population was then identified following gating for the surface markers CD4 or CD8. CD4$^+$ T cells which were negative for CD8, were then analysed for CD71 expression. CD8$^+$ T cells which were negative for CD4, were then analysed for CD71 expression.

4.4 Results

4.4.1 The cell-surface sialome of CD4^{+} T cells and CD8^{+} T cell subsets can be visualised using confocal microscopy

Preliminary observations showed that the sialome was not uniform amongst the PBMC subsets. Some cells modelled a smooth outer membrane, whereas others were more rough and distorted. This was observed in both unactivated and anti-CD3-activated PBMCs respectively (Fig 4.3; Fig 4.4). Furthermore, using a nuclear dye DAPI, in conjunction with this click chemistry technique allowed for preliminary identification of these lymphocytes to be made. Lymphocytes are known to have a high nucleus to cytoplasm ratio in comparison to other PBMC subsets, to the point where the cytoplasm is barely visible (Marshall A. Lichtman). These cells were observed in both unactivated and anti-CD3-activated PBMCs, respectively (Fig 4.3; Fig 4.4). After this 72 h anti-CD3-activation, where T lymphocytes were the predominant population, other PBMC subsets, such as plasma cells and eosinophils, could be identified by their morphology. In this respect, the cell-specific surface sialome of plasma and eosinophils could also be visualised.

The identity of these T lymphocytes was confirmed following incubation with antibodies against the T cell-surface markers, CD3, CD4 and CD8, alongside alexa fluor 488 labelling of the sialome (Fig 4.3). This proved that this method was a useful technique to co-visualise cell-specific surface glycans in a mixed population of cells. It also allowed affirmative visualisation of the relative proportions of these cells. Indeed, there was a greater proportion of PBMCs positive for the CD3 receptor, compared to CD4^{+} and CD8^{+} T cells (Fig 4.3).

It was also important to identify whether morphological changes occurred on this cell-surface sialome upon activation, a previously unexplored area. By virtue of these sialic acid glycans decorating the cell-surface, the size of these PBMCs was measured upon anti-CD3 activation. Indeed, these PBMCs increased in size from between 0-5 μm to between 0-10 μm upon anti-CD3 activation, respectively (Fig 4.3; Fig 4.4). However, it was not clear whether changes occurred on the cell-surface sialome.

CD3$^+$ T cells   CD4$^+$ T cells   CD8$^+$ T cells

A   B   C

10 μm

10 μm
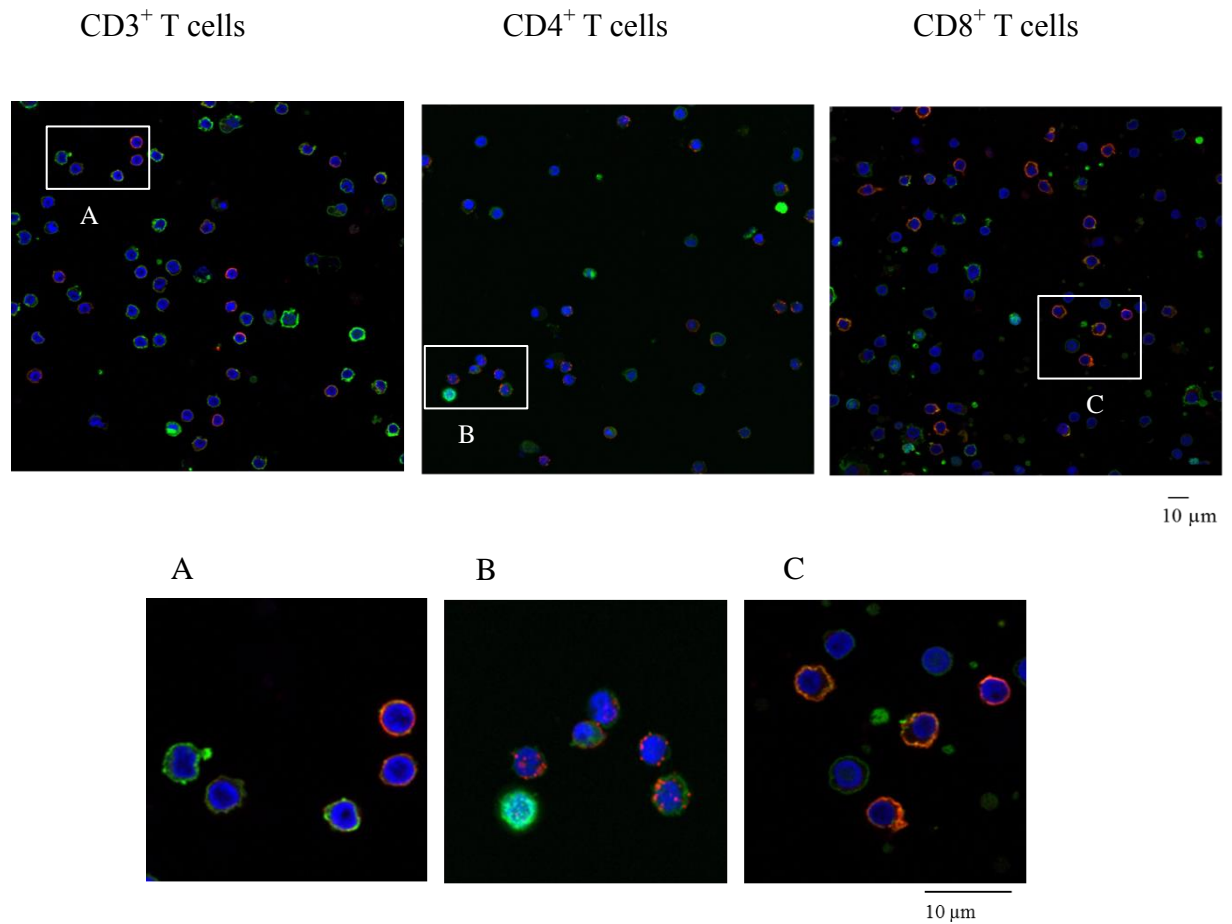
Figure 4.3. The cell-surface sialome of CD3$^+$ T cells, CD4$^+$ T cells and CD8$^+$ T cells can be visualised in a mixed population of PBMCs, but there were no detectable differences between subsets.

PBMCs were incubated with ManNAz (50 μM; green), a modified *N*-acetlymannosamine sugar, compatible with Click IT chemistry for 24 h. After 24 h, PBMCs were spun down on poly-D-lysine coated coverslips. alexa fluor 488 was then added along with the Click IT reaction mix for 5 min. PBMCs were washed with PBS, fixed with 4% PFA and incubated with antibodies against the surface markers CD3, CD4 or CD8 at 4 degrees, overnight. The cells were then washed, incubated with an anti-mouse (goat) secondary antibody for 1 h. The cells were then washed again and the cover slips transferred, face down on DAPI coated slides for imaging. The sialome (green) of CD3$^+$ T cells, CD4$^+$ T cells, or CD8$^+$ T cells was visualised following co-staining with an antibody against the surface marker CD3, CD4 or CD8 and a secondary antibody (red).

161
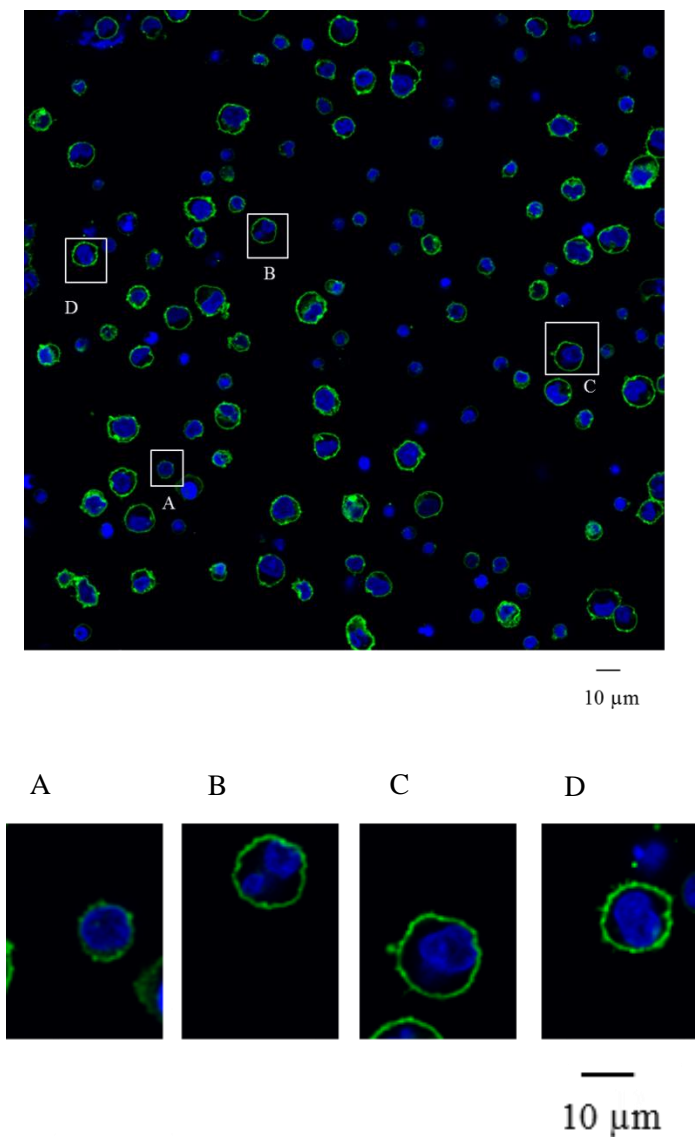
Figure 4.4. The cell-surface sialome of anti-CD3-activated PBMCs and of some individual cell subsets were visualised, but there were no detectable differences.

PBMCs were activated with anti-CD3 (1 µg/ml) for 72 h and incubated with ManNAz (50 µM; -green), in the last 24 h of activation. After 24 h, PBMCs were spun down on poly-D-lysine coated coverslips. alexa fluor 488 was then added along with the Click IT reaction mix for 5 min. PBMCs were washed with PBS, fixed with 4% PFA and the cover slips transferred, face down on DAPI coated slides for imaging. can be visualised in PBMC subsets. The sialome (green) of different PBMC cell subsets with different morphology can be visualised. (A) unactivated lymphocyte, (B) eosinophil, (C) plasma cell, and- (D) activated lymphocyte.

4.4.2 The incorporation of ManNAz on the cell-surface sialome of PBMCs can be quantified using flow cytometry

Since quantification of the sialic acid content proved difficult using confocal microscopy, flow cytometry was employed. However, before it could be used as a method to evaluate the effect of drug treatment on this pathway, working parameters had to be established. First it was important to determine the optimal working range of ManNAz in these PBMCs to maximise fluorescence detection without inducing significant cell death. A range of concentrations of ManNAz (50 µM, 75 µM and 100 µM) were tested using two parameters: the percentage of PBMCs that were positive for ManNAz incorporation on the cell-surface (percentage ManNAz) and the mean fluorescence intensity (MFI). Importantly, there was no dose-dependent difference in the percentage of PBMCs that were positive for these sialic acid residues with ManNAz (50 µM, 75 µM and 100 µM) (Fig 4.5A). In the absence of ManNAz, only minimal background fluorescence was detected upon incubation with alexa fluor 488. No significant changes were detected in the MFI values upon ManNAz treatment (Fig 4.5B). Since 50 µM ManNAz was found to have the highest MFI with no effect on cell viability, this was used for future experiments (Fig 4.5C).

In order for this method to be quantifiable, it was important to show that there were time-dependent differences in the incorporation of ManNAz on these sialic acid residues. It was shown that the process of ManNAz uptake from the media and subsequent incorporation on the surface occurred as early as 12 h (Fig 4.6A). After this time, there was no observable change in the percentage of PBMCs that were positive for the presence of these modified sialic acid residues on the cell-surface sialome. However, there was a significant upward linear trend in the total ManNAz incorporated on the cell-surface over the course of 12, 18 and 24 h (Fig 4.6B).

Following the experiments conducted in unactivated PBMCs, the same parameters were established in anti-CD3-activated PBMCs to allow comparisons to be made upon drug treatment. The same concentration of ManNAz, (50 µM), significantly reduced the viability of anti-CD3-activated PBMCs after a 24 h treatment (Fig 4.7). Since the cell viability was determined to be at an acceptable level, of ~70%, the same concentration of
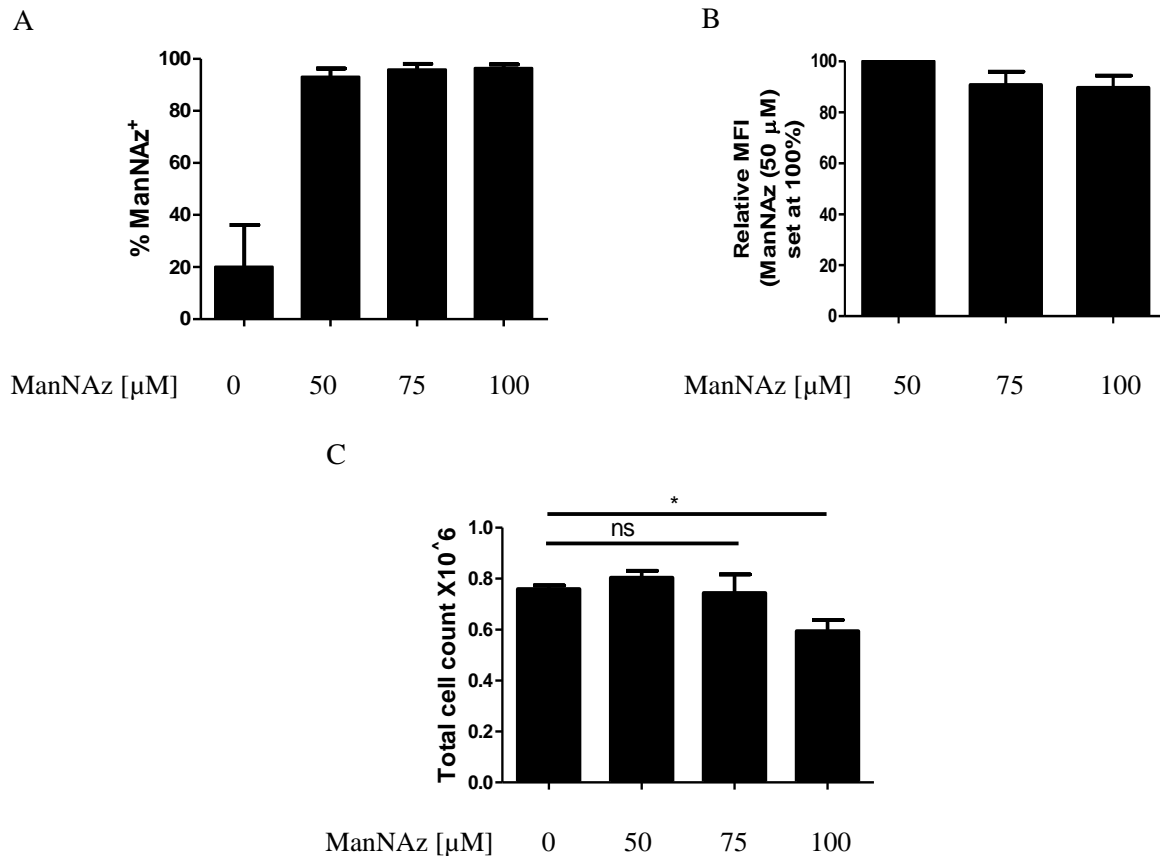
Figure 4.5. ManNAz (50 µM) reflects changes in fluorescence on the PBMC cell-surface sialome.

PBMCs were incubated with ManNAz (0, 50 µM, 75 µM or100 µM) for 24 h. PBMCs were then counted for viability assessment (C). They were then washed with PBS before resuspending ~450,000 cells in 95 µl alexa fluor 488 copper solution for 5 min. Cells were then washed 3 times with PBS before resuspending in 2% FACS buffer for flow cytometric analysis. Viable cells were determined following PI exclusion and ManNAz incorporation was determined following gating for those positive for alexa fluor 488. The percentage of cells positive for ManNAz (488 nm) incorporation is independent of the concentrations used (A). Maximal fluorescence was observed with ManNAz (50 µM), (B). without a loss in cell viability (C). Data are presented as (A) percent ManNAz, (B) mean fluorescence intensity (MFI) normalised to ManNAz (50 µM), (C) total cell count, with (A&B) representative of the mean ± SEM, n=3 or (C) mean ± SEM, n=4. A paired student T-was performed and significant differeneces are indicated with *P<0.05, or **P<0.01.

164
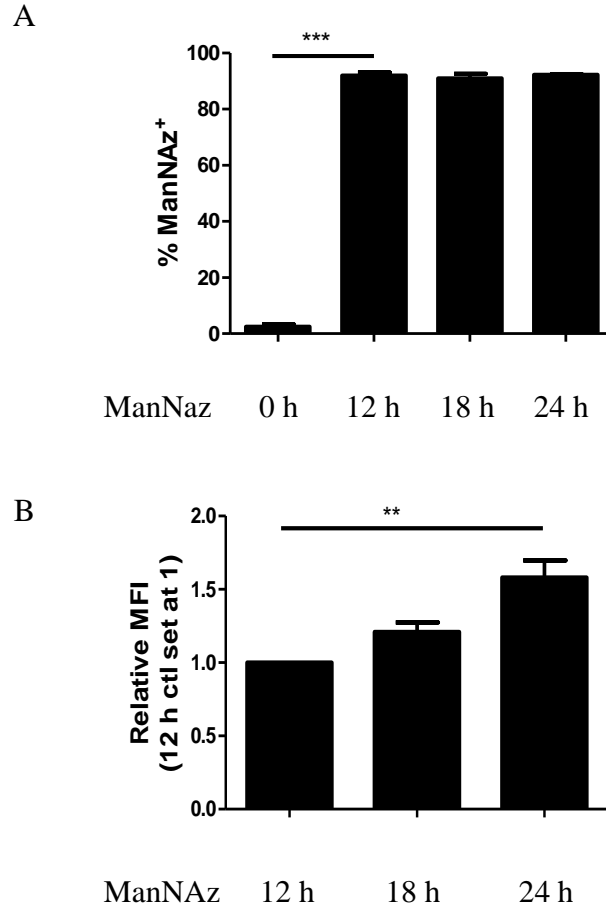
Figure 4.6. Incorporation of ManNAz is time-dependent in unactivated PBMCs.

PBMCs were incubated with ManNAz (50 µM) for 0 h, 12 h, 18 h, 24 h. Cells were then washed with PBS before resuspending ~450,000 cells in 95 µl alexa fluor 488 copper solution for 5 min. Cells were then washed 3 times with PBS before resuspending in 2% FACS buffer for flow cytometric analysis. Viable cells were determined following PI exclusion and ManNAz incorporation was determined following gating for those positive for alexa fluor 488. (A) ManNAz is detectable on the cell-surface at 12 h. (B) ManNAz incorporation on the cell-surface increases over 12 h, 18 h and 24 h. Data are presented as (A) percent ManNAz, (B) mean fluorescence intensity (MFI) normalised to 12 h ctl, mean ± SEM, n=3; a paired student T-test (A) or a one-way ANOVA followed by a test for linear trend (B) was performed and significant differences are indicated with *P<0.05 or **P<0.01.
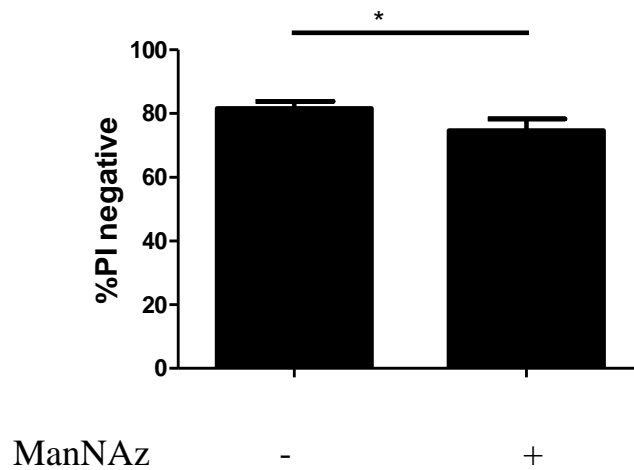
Figure 4.7. ManNAz (50 μM) and copper sulphate (1.96 mM) cause significant cell death in anti-CD3-activated PBMCs.

PBMCs were incubated ± ManNAz (50 μM) in the last 24 h of a 72 h anti-CD3 activation. Cells were then counted and washed with PBS before resuspending ~450,000 cells in 95 μl alexa fluor 488 copper solution for 5 min. Cells were then washed 3 times with PBS before resuspending in 2% FACS buffer for flow cytometric analysis. Cell death was assessed by measuring the percentage of PBMCs that were PI negative. Data are presented as mean ± SEM, n=7; a paired student T-test was performed and significant differences are indicated with *P<0.05 or **P<0.01.

ManNAz was used to allow for comparisons to be made with their unactivated counterparts. Similar time-point experiments were conducted to see if there were changes in ManNAz uptake in these activated cells. Additionally, a 6 h time-point was introduced to determine if the sugar was present on the cell-surface at an earlier time, reflecting heightened metabolic processes in these cells. The majority of activated PBMCs had processed the modified sugar and displayed it on their cell-surface by 6 h (Fig 4.8A). The MFI values were then evaluated and it was found that there was a significant increase in fluorescence between 6 h and 12 h (Fig 4.8B)-however, only a modest change was seen between the 12 h and 24 h incubation in these anti-CD3-activated PBMCs (Fig 4.8C). The MFI values for 12 h, 18 h, or 24 h ManNAz incubation were higher for the anti-CD3-activated PBMCs than the unactivated PBMCs.

After the working parameters of this method were established the effect of a known *N*-glycosylation inhibitor, tunicamycin (1 μM), was investigated to demonstrate that this method could be used to evaluate the effect of drug treatment on this *N*-glycosylation pathway. Tunicamycin was added to ManNAz-treated anti-CD3-activated PBMCs and was found to significantly reduce incorporation of the sugar on the cell-surface (Fig 4.9A). The reduction in incorporation of the sugar was not due to cell death as there was no significant decrease in the percentgage of PI negative cells (Fig 4.9B). However, it appeared that Tunicamycin did exert some affect on the proliferation of these cells since there was also a signifcant reduction in the total cell count (Fig 4.9 C).

4.4.3 MTX treatment reduces ManNAz incorporation on the cell-surface sialome

It was also shown that this click technique could be used to analyse the effect of anti-inflammatory drugs that act by limiting activation induced changes, to either cellular metabolism or the cell-surface sialome. However, because it is not known whether MTX treatment can directly affect cell-surface sialylation, it was important to determine the effect of MTX in unactivated PBMCs. MTX (100 nM) had no significant effect in reducing ManNAz incorporation on the surface of these unactivated PBMCs (Fig 4.10). However, MTX (100 nM) significantly reduced the incorporation of ManNAz on the surface sialic acid residues in anti-CD3-activated PBMCs (Fig 4.11A). At this dose, the proliferation of these cells was also significantly inhibited (Fig 4.11B). In accordance
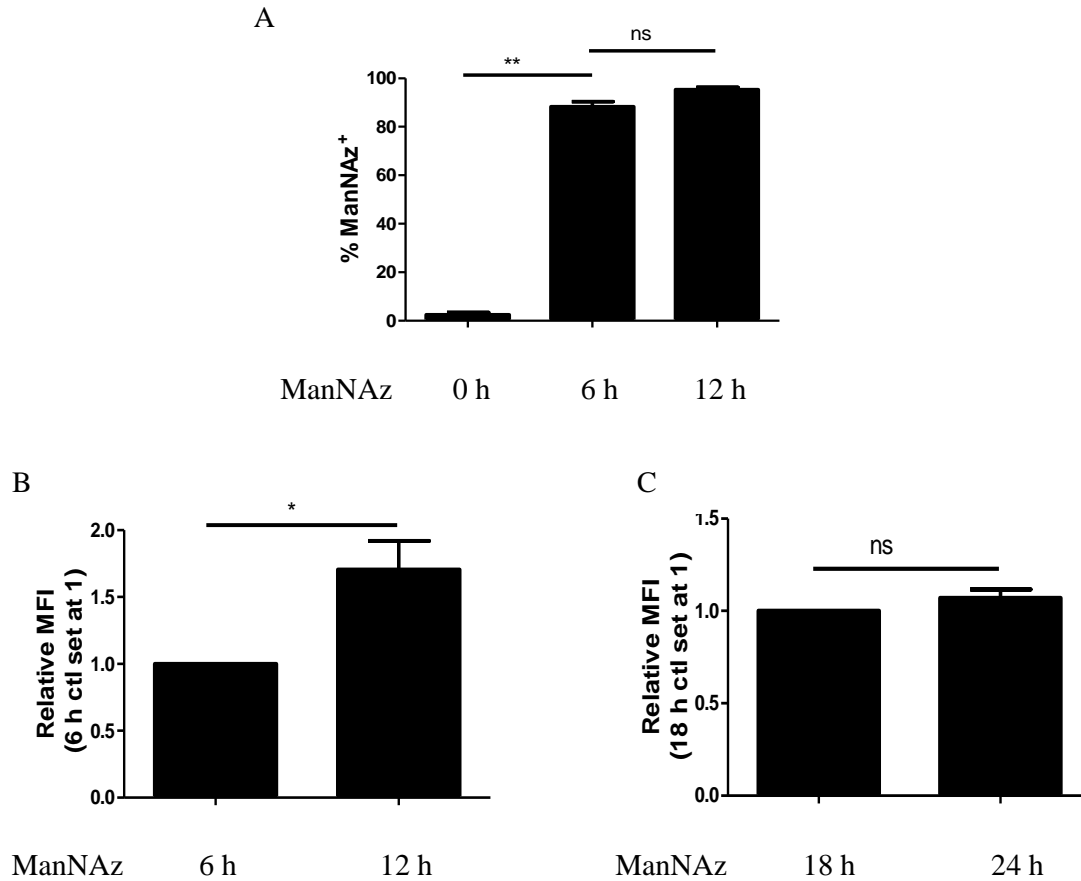
Figure 4.8. Incorporation of ManNAz is time-dependent in anti-CD3-activated PBMCs.

PBMCs were treated with ManNAz ± (50 µM) for the last 6, 12, 18, or 24 h of a 72 h anti-CD3 activation. PBMCs were counted and washed with PBS before resuspending ~450,000 cells in 95 µl alexa fluor 488 copper solution for 5 min. Cells were then washed 3 times with PBS before resuspending in 2% FACS buffer for flow cytometric analysis. Viable cells were determined following PI exclusion and ManNAz incorporation was determined following gating for those positive for alexa Fluor 488. (A) ManNAz incorporation occurs as early as 6 h after treatment. (B) Incorporation of ManNAz (50 µM) increases over 6 h and 12 h. (C) There is no significant increase in the incorporation of ManNAz between 18 h and 24 h in anti-CD3-activated PBMCs. Data are presented as (A) percent ManNAz, mean ± SEM, n=3; (B) mean fluorescence intensity (MFI) normalised to 6 h ctl, mean ± SEM, n=5; (C) MFI normalised to 18 h ctl, mean ± SEM, n=8. A paired student T-test was performed and significant differences are indicated with *P<0.05, **P<0.01 or ***P<0.001.
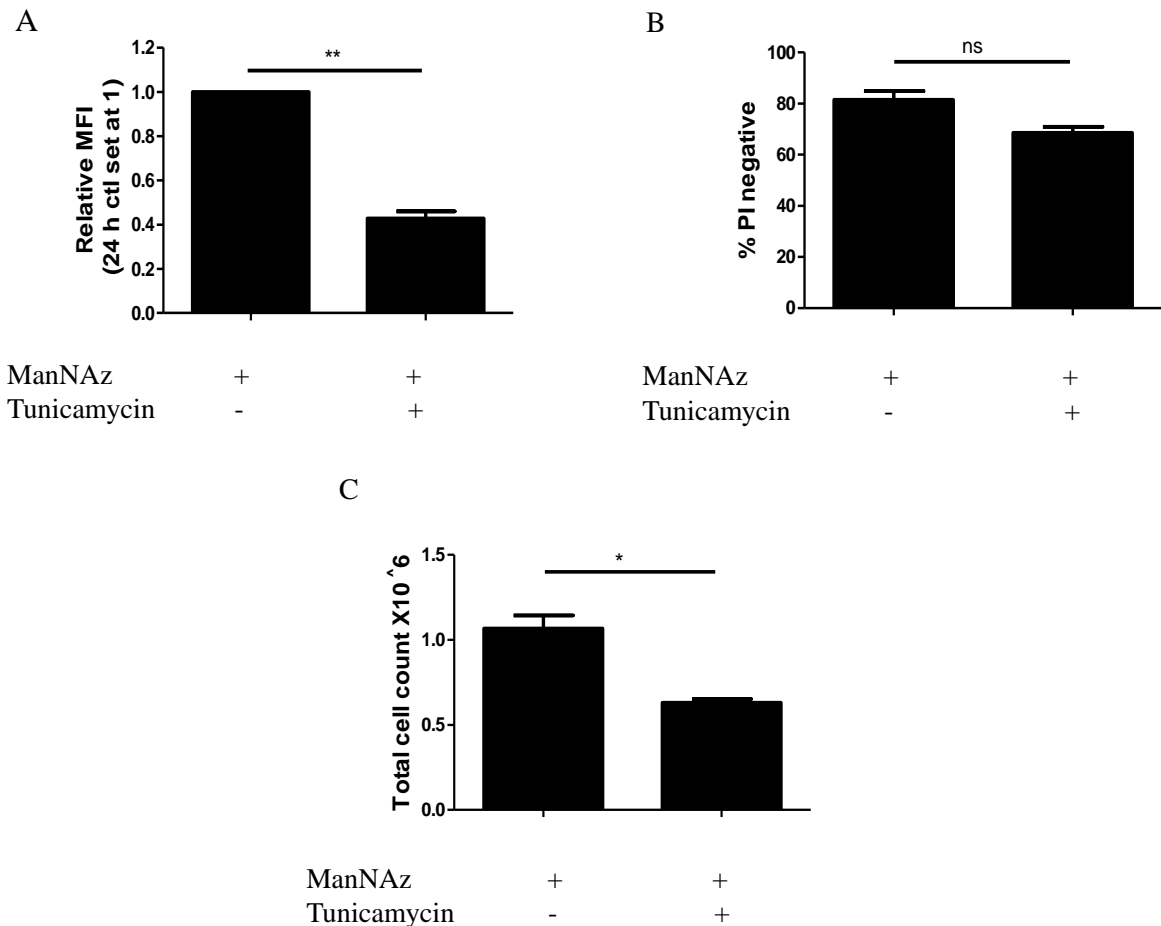
Figure 4.9. Tunicamycin affects ManNAz incorporation on the cell-surface of anti-CD3-activated PBMCs.

PBMCs were incubated with ManNAz (50 μM) ± Tunicamycin (1 μM). in the last 24 h of a 72 h anti-CD3 activation. PBMCs were then counted and washed with PBS before resuspending ~450,000 cells in 95 μl alexa fluor 488 copper solution for 5 min. Cells were then washed 3 times with PBS before resuspending in 2% FACS buffer for flow cytometric analysis. Viable cells were determined following PI exclusion and ManNAz incorporation was determined following gating for those positive for alexa fluor 488. (A) Tunicamycin results in lowered expression of ManNAz on the cell-surface. (B) Tunicamycin has no effect on cell viability following a 24 h treatment. (C) Tunicamycin has a significant inhibitory effect on the proliferation of these anti-CD3-activated PBMCs. Data are presented as as (A) mean fluorescence intensity (MFI) normalised to 24 h ctl, (B) percent PI negative, (C) total cell count, mean ± SEM, n=3 a paired student T-test was performed and significant differences are indicated with *P<0.05 or **P<0.01.
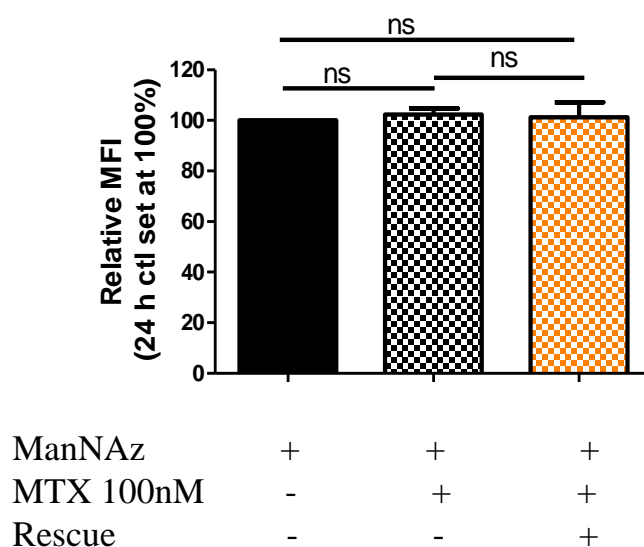
Figure 4.10. Methotrexate has no significant effect on ManNAz incorporation on the cell-surface of unactivated PBMCs.

PBMCs were incubated with ManNAz (50 μM) ± MTX (100 nM) ± thymidine and hypoxanthine (100 μM) for 24 h. PBMCs were then counted and washed with PBS before resuspending ~450,000 cells in 95 μl alexa fluor 488 copper solution for 5 min. Cells were then washed 3 times with PBS before resuspending in 2% FACS buffer for flow cytometric analysis. Viable cells were determined following PI exclusion and ManNAz incorporation was determined following gating for those positive for alexa fluor 488. Data are presented as mean fluorescence intensity (MFI), normalised to 24 h ctl, mean ± SEM, n=3; a one-way ANOVA, followed by Tukey's multiple comparison test was performed and significant differences are indicated with *P<0.05 or **P<0.01.

Figure 4.11. Methotrexate treatment results in significantly lower ManNAz incorporation on the cell-surface of anti-CD3-activated PBMCs.

PBMCs were activated with anti-CD3 (1 µg/ml) for 72 h ± MTX (100 nM). ManNAz (50 µM) was added in the last 24 h of the activation period. PBMCs were then counted and washed with PBS before resuspending ~450,000 cells in 95 µl alexa fluor 488 copper solution for 5 min. Cells were then washed 3 times with PBS before resuspending in 2% FACS buffer for flow cytometric analysis. Viable cells were determined following PI exclusion and ManNAz incorporation was determined following gating for those positive for alexa Fluor 488. (A) MTX treatment results in significantly reduced incorporation of ManNAz and (B) MTX significantly inhibited the proliferation of activated PBMCs. Data are presented as as (A) mean fluorescence intensity (MFI) normalised to 24 h ctl, (B) total cell count, mean ± SEM, n=7; a paired student T-test was performed and significant differences are indicated with *P<0.05 or **P<0.01.

with previous experiments, it was important to deduce if the MTX-mediated inhibition of the incorporation of ManNAz could be reversed. Intriguingly, the addition of exogenous thymidine and hypoxanthine could significantly reverse this MTX-mediated inhibition of ManNAz incorporation on cell-surface sialome (Fig 4.12A).In the same cells, these s nucleotides also reversed the anti-proliferative effect of MTX (Fig 4.12B).

4.4.4 MTX has differential effects on the incorporation of ManNAz on the cell-surface sialome of distinct populations of activated PBMCs

Upon anti-CD3-activation, the proportion of blast cells (>35 k) significantly increased and the proportion of non-blast cells (<35 k) signifcantly decreased (Fig 4.13), probably reflecting T cell blastogenesis discussed in the previous chapter since CD3$^+$ T cells comprise ~60% of the PBMC population (Fig 3.10). MTX significantly reduced the population of blast cells and increased the population of non-blast cells, possibling reflecting the limitation of T cell-activation in a population of PBMCs comprising about 60% CD3$^+$ T cells (Fig 4.14). Both non-blast and blast cells had significantly increased ManNAz on their cell-surface compared to their unactivated counterparts (Fig 4.15). Examination of the effect of MTX on ManNAz incorporation revealed that MTX exerted contrasting effects on both populations. MTX (100 nM) significantly reduced ManNAz incorporation on the proportion of non-blast cells yet increased ManNAz incorporation in blast cells (Fig 4.16). It was important to determine if these differential effects of MTX on ManNAz incorporation in non-blast and blast populations was linked to purine and thymidine inhibition. Rescue of these MTX-treated cells reversed the MTX-mediated reduction in ManNAz incorporation on the surface of non-blast cells and the MTX-mediated increase in ManNAz incorporation on the surface of blast cells (Fig 4.17).

To investgate if these differences in ManNAz incorporation following MTX treatment were activation-dependent, unactivated PBMCs were treated with MTX and ManNAz and gated as before. There was no significant difference in ManNAz incorporation in these non-blast compared to blast cells and rescue had no effect (Fig 4.18).

To determine if MTX exerted contrasting effects on blast and non-blast population because these populations were differentailly activated, transferrin (CD71) recetor expression was evaluated in the CD4$^+$ and CD8$^+$ T cells from both blast and non-blast
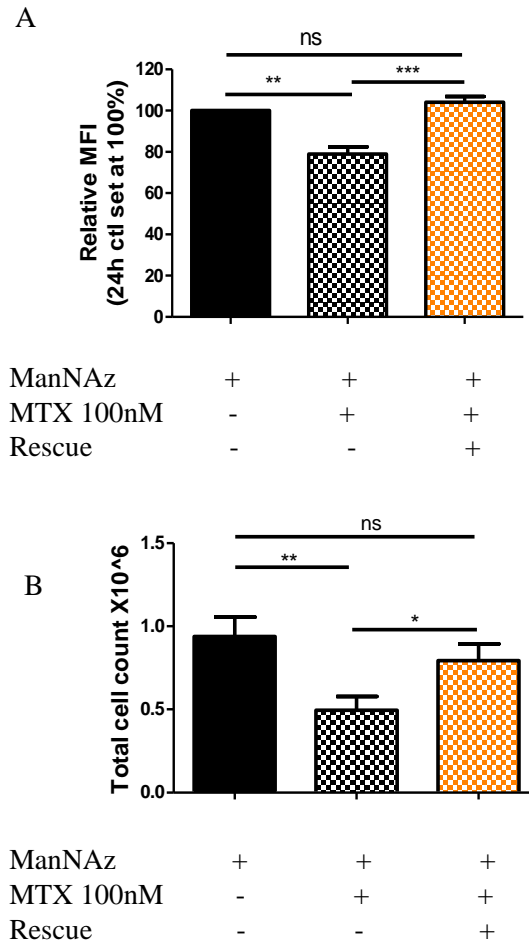
Figure 4.12. Thymidine and hypoxanthine can reverse the effect of Methotrexate on ManNAz incorporation on the cell-surface of anti-CD3-activated PBMCs.

PBMCs were activated with anti-CD3 (1 μg/ml) for 72 h ± MTX (100 nM) ± thymidine and hypoxanthine (100 μM). ManNAz (50 μM) was added in the last 24 h of the activation period. PBMCs were then counted and washed with PBS before resuspending ~450,000 cells in 95 μl alexa fluor 488 copper solution for 5 min. Cells were then washed 3 times with PBS before resuspending in 2% FACS buffer for flow cytometric analysis. Viable cells were determined following PI exclusion and ManNAz incorporation was determined following gating for those positive for alexa Fluor 488. (A) Thymidine and hypoxanthine can reverse the MTX-mediated reduction in ManNAz incorporation on the cell-surface. (B) Thymidine and hypoxanthine can reverse the anti-proliferative effect of MTX. Data are presented as (A) mean fluorescence intensity (MFI), normalised to 24 h ctl, mean ± SEM, n=7 (B) total cell count, mean ± SEM, n=6 or a one-way ANOVA followed by Tukey's multiple comparison test was performed and significant differences are indicated with *P<0.05, **P<0.01 or, ***P<0.001.
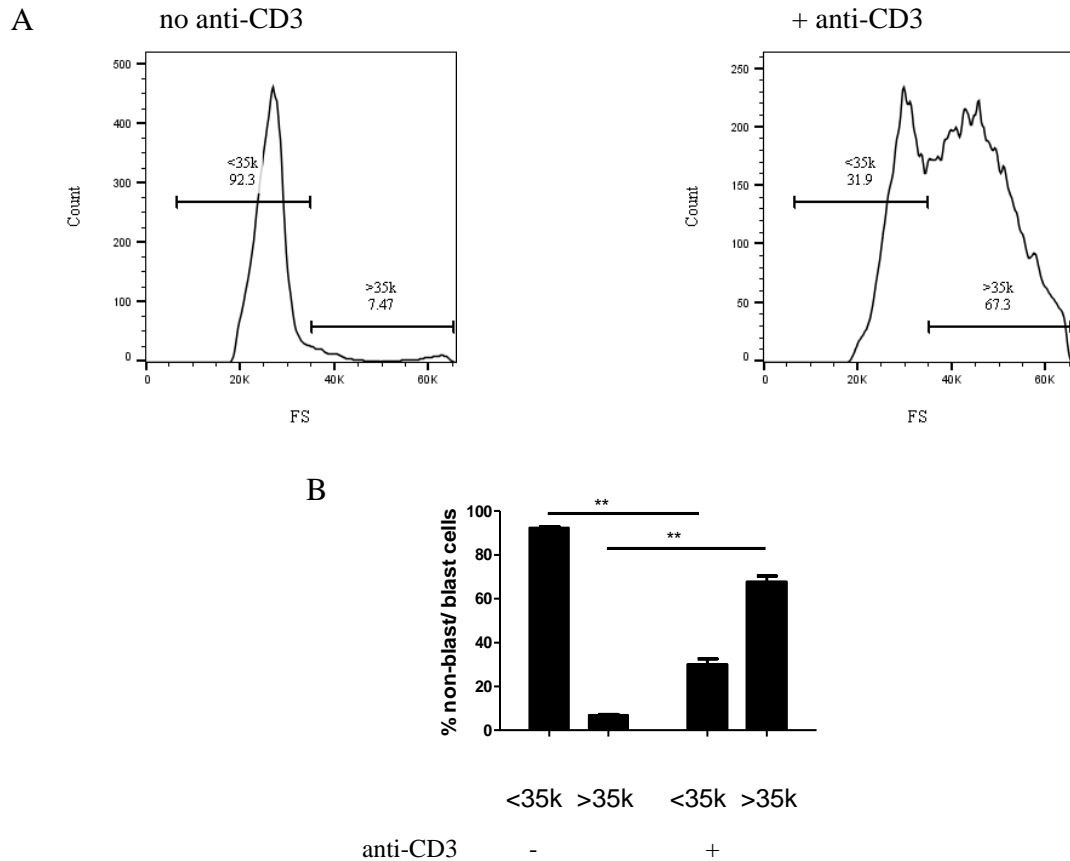
Figure 4.13. Changes occur in distinct populations of PBMCs following anti-CD3-activation.

PBMCs (1 X 10$^{\wedge}$6 cells /ml and 3 ml/well) were cultured in the presence of anti-CD3 for 72 h. Unactivated cells were taken from frozen stocks on the same day. The size of the unactivated and anti-CD3-activated PBMCs were determined following gating for PI negative cells by analysing their forward scatter measurements using flow cytometry. (A) Representative histograms of the percentage of non-blast (<35k) and blast (>35k) PBMCs before and after anti-CD3 activation. (B) Anti-CD3 activation significantly increases the proportion of PBMCs >35k. Data are presented as mean ±SEM, n=3; a paired student T- was performed and significant differences are indicated with *P<0.05, **P<0.01, or ***P<0.001
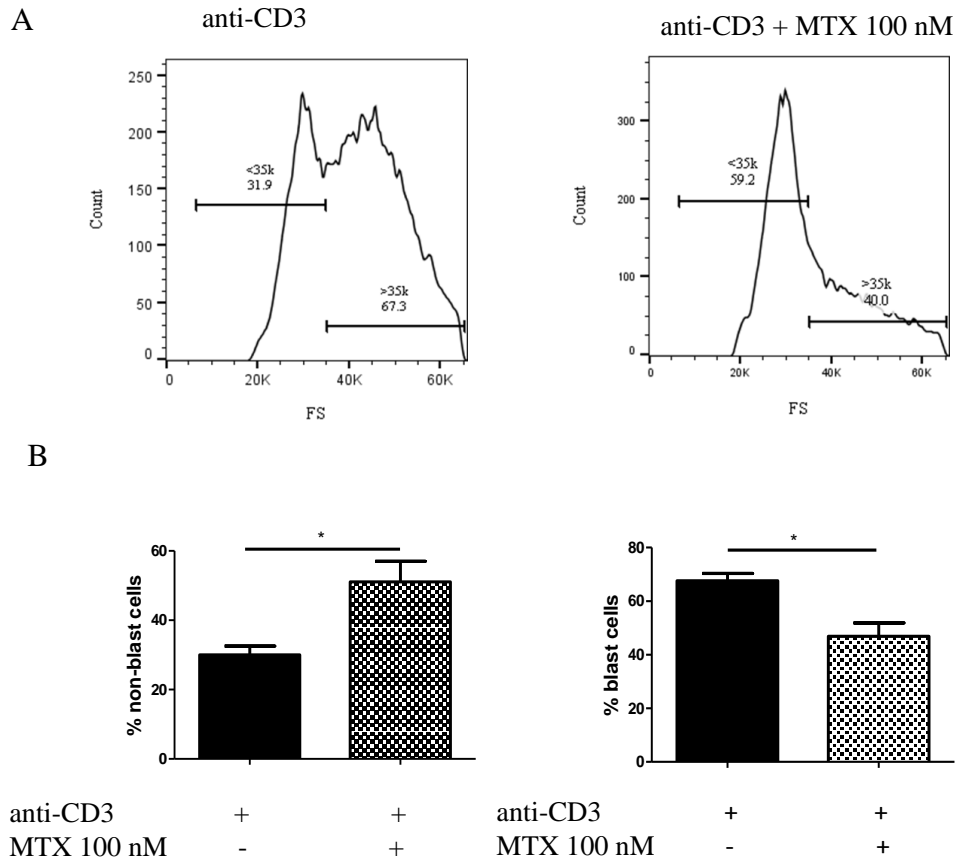
Figure 4.14. Methotrexate treatment increases the proportion of non-blast cells and decreases the proportion of blast cells during anti-CD3-activation.

PBMCs (1 X 10^6 cells /ml and 3 ml/well) were cultured in the presence of anti-CD3 ± MTX 100 nM for 72 h. The size of the anti-CD3-activated PBMCs were determined following gating for PI negative cells by analysing their forward scatter measurements using flow cytometry. (A) Representative histograms of the percentage of non-blast and blast PBMCs before and after MTX treatment (B) MTX significantly reduces the proportion of PBMCs >35k during anti-CD3 activation. Data are presented as mean ±SEM, n=3 a paired student T-test was performed and significant differences are indicated with *P<0.05, **P<0.01, or ***P<0.001.
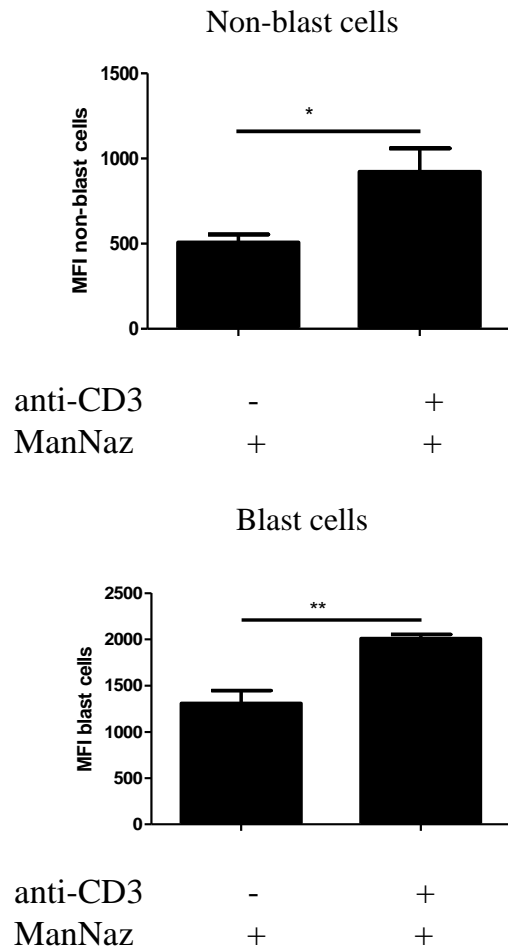
**Figure 4.15. Anti-CD3-activated non-blast and blast cells have increased ManNAz on their cell-surface.**

PBMCs (1 X 10^6 cells /ml and 3 ml/well) were cultured in the presence of anti-CD3 for 72 h. Unactivated cells were taken from frozen stocks in the last 24 h of the 72 h activation. ManNAz (50 μM) was added to both unactivated and activated PBMCs in the last 24 h. PBMCs were then counted and washed with PBS before resuspending ~450,000 cells in 95 μl alexa fluor 488 copper solution for 5 min. Cells were washed 3 times with PBS and reuspended in 2% FACS buffer for flow cytometric analysis. Viable cells were determined following PI exclusion and blast or non-blast cells were identified as cells having forward scatter measurements greater than 35k and less than 35k, respectively. ManNAz incorporation on both populations was determined following gating for those positive for alexa fluor 488. Data are presented as mean fluorescence intensity (MFI), mean ±SEM, n=3; an unpaired student T-test was performed (as 6 different donors were used on separate occasions (3 unactivated MFI and 3 activated MFI) and significant differences are indicated with *P<0.05, **P<0.01, or ***P<0.001.
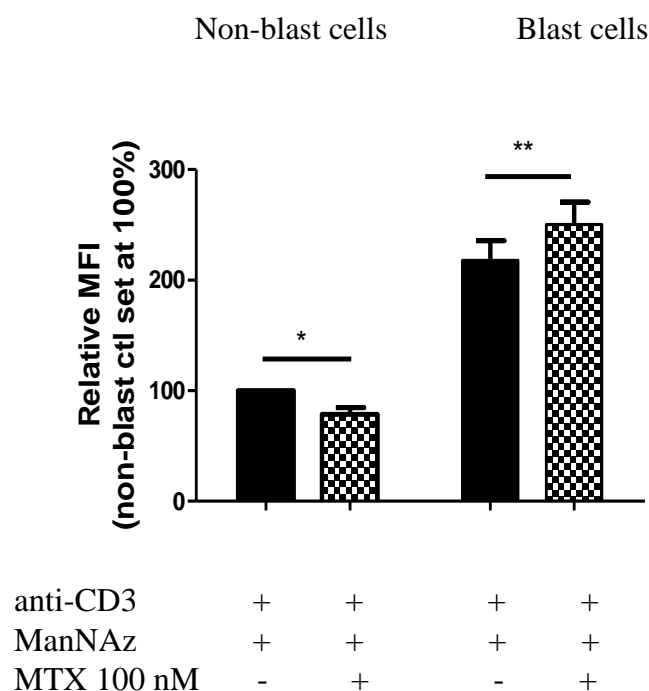
Figure 4.16 Methotrexate has differential effects on the incorporation of ManNAz on non-blast compared to blast cells.

PBMCs were activated with anti-CD3 (1 µg/ml) for 72 h ± MTX (100 nM). ManNAz (50 µM) was added in the last 24 h. PBMCs were then counted and washed with PBS before resuspending ~450,000 cells in 95 µl alexa fluor 488 copper solution for 5 min. Cells were washed 3 times with PBS and reuspended in 2% FACS buffer for flow cytometric analysis. Viable cells were determined following PI exclusion and blast or non-blast cells were identified as cells having forward scatter measurements greater than 35k and less than 35k, respectively. ManNAz incorporation on both populations was determined following gating for those positive for alexa fluor 488. MTX resulted in significantly reduced ManNAz incorporation on the cell-surface of non-blast cells but significantly increased ManNAz incorporation on the cell-surface of blast cells. Data are presented as mean fluorescence intensity (MFI) normalised to 24 h non-blast ctl, mean ± SEM, n=7; a paired student T-test was performed and significant differences are indicated with *P<0.05, **P<0.01 or,***P<0.001.

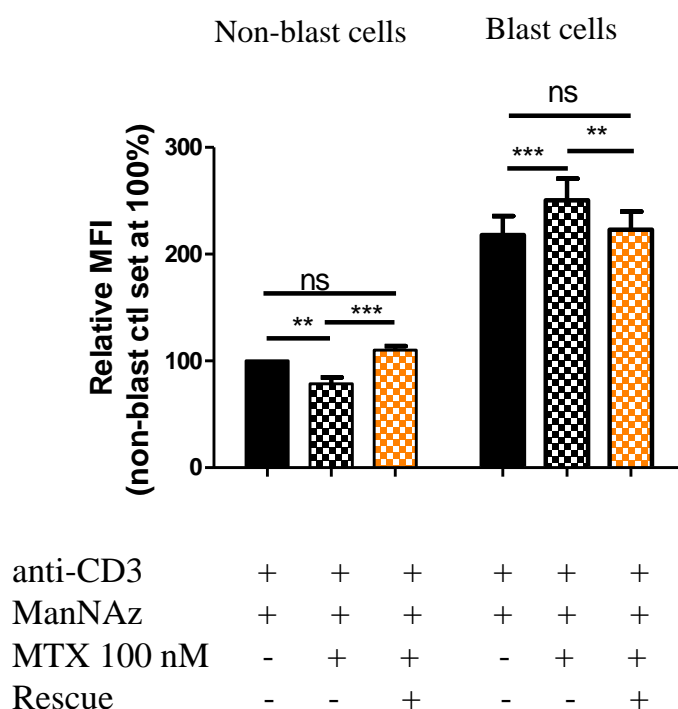**Figure 4.17 The differential effects of Methotrexate on ManNAz incorporation in both non-blast and blast cells is reversed upon thymidine and hypoxanthine rescue.**

PBMCs were activated with anti-CD3 (1 µg/ml) for 72 h ± MTX (100 nM)) ± thymidine and hypoxanthine (100 µM). ManNAz (50 µM) was added in the last 24 h. PBMCs were then counted and washed with PBS before resuspending ~450,000 cells in 95 µl alexa fluor 488 copper solution for 5 min. Cells were washed 3 times with PBS and reuspended in 2% FACS buffer for flow cytometric analysis. Viable cells were determined following PI exclusion and blast or non-blast cells were identified as cells having forward scatter measurements greater than 35k and less than 35k, respectively. ManNAz incorporation on both populations was determined following gating for those positive for alexa fluor 488. MTX significantly reduced ManNAz incorporation on non-blast cells but increased ManNAz incorporation on blast cells, both of which were reversed upon purine and thymidine rescue. Data are presented as mean fluorescence intensity (MFI) normalised to 24 h non-blast ctl, mean ± SEM, n=7; a one-way ANOVA followed by Tukey's multiple comparison test was performed and significant differences are indicated with *P<0.05, **P<0.01 or,***P<0.001.
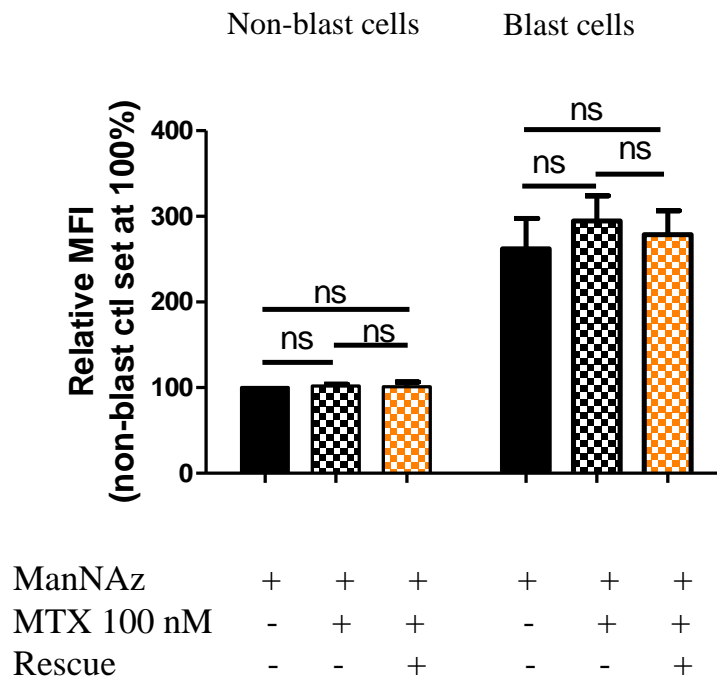
Figure 4.18. Methotrexate has no significant effect on ManNAz incorporation in un-activated non-blast or blast cells.

PBMCs were incubated with ManNAz (50 μM) ± MTX (100 nM)) ± thymidine and hypoxanthine (100 μM) for 24 h. PBMCs were then counted and washed with PBS before resuspending ~450,000 cells in 95 μl alexa fluor 488 copper solution for 5 min. Cells were washed 3 times with PBS before resuspending in 2% FACS buffer for flow cytometric analysis. Viable cells were determined following PI exclusion and blast or non-blast cells were identified as cells having forward scatter measurements greater than 35k and less than 35k, respectively was then determined. ManNAz incorporation on both populations was determined following gating for those positive for alexa fluor 488. Data are presented as mean fluorescence intensity (MFI) normalised to 24 h non-blast ctl, mean ± SEM, n=3; a one-way ANOVA followed by Tukey's multiple comparison test was performed and significant differences are indicated with *P<0.05, **P<0.01 or ***P<0.001.

populations. Non-blast cells had increased CD71 receptor expression, just like blast cells (Fig 4.19). To investigate if these differential effects were due to differential uptake of MTX, CD71 receptor expression was compared. MTX decreased CD71 receptor expression on both non- blast $CD4^+$ and $CD8^+$ T cells just like the blast populations (Fig 4.20). The proportions of $CD4^+$ and $CD8^+$ T cells as well the CD3 negative cells, ($CD4^-$ $CD8^-$) in both populations were next examined with MTX treatment. MTX significantly reduced the proportion of non-blast $CD4^+$ and $CD8^+$ T cells and signifcantly increased the proportion of non-blast $CD4^-CD8^-$ cells (Fig 4.21). Although MTX significantly reduced the proportion of blast $CD8^+$ T cells and increased the proportion of blast CD3 negative cells, it had no effect on the proportion of blast $CD4^+$ T cells (Fig 4.22). Thus, differential effects of MTX on different PBMC subsets were found in blast and non-blast populations, which exhibited differences in ManNAz incorporation on the cell-surface sialome.

To determine if rescue could reverse these changes in the blast and non-blast popoulations, as it had reversed the changes in ManNAz incorporation, the proportions of PBMC subsets were examined upon purine and thymidine rescue. Hypoxanthine and thymidine (100 µM) reversed the effects of MTX on $CD4^+$ and $CD8^+$T cells as well as on CD3 negative cells in both populations. (Fig 4.23 & Fig 4.24).

The proportion of non-blast and blast CD3 negative cells increased following MTX treatment so it was important to determine whether this was a relative increase or if MTX led to an increase in the size of some PBMC subsets by inhibiting mitosis or causing DNA fragmentation, thus forming megaloblast cells. To this aim, images were taken of these MTX treated cells to see if there was evidence of blast CD3 negative cells. DAPI used in conjunction with alexa fluor 488, allowed for morphological observations to be made about the plasma membrane and nuclear integrity (Fig 4.25). Mitotic DNA was observed in anti-CD3-activated PBMCs, and MTX was added to anti-CD3-activated PBMCs to visualise an apoptotic cell. Whilst many MTX-treated PBMCs had increased in size and contained fragmented DNA, in a distorted plasma membrane, megaloblastic cells contained fragmented DNA in an intact plasma membrane.

To determine whether these megaloblast cells containing fragmented DNA were $CD3^+$ T cells, an antibody against the surface marker, CD3 was added to cells during MTX treatment. A secondary antibody directed against this primary antibody, conjugated to alexa fluor 594 alongside the click IT reaction enabled the determination of the cell
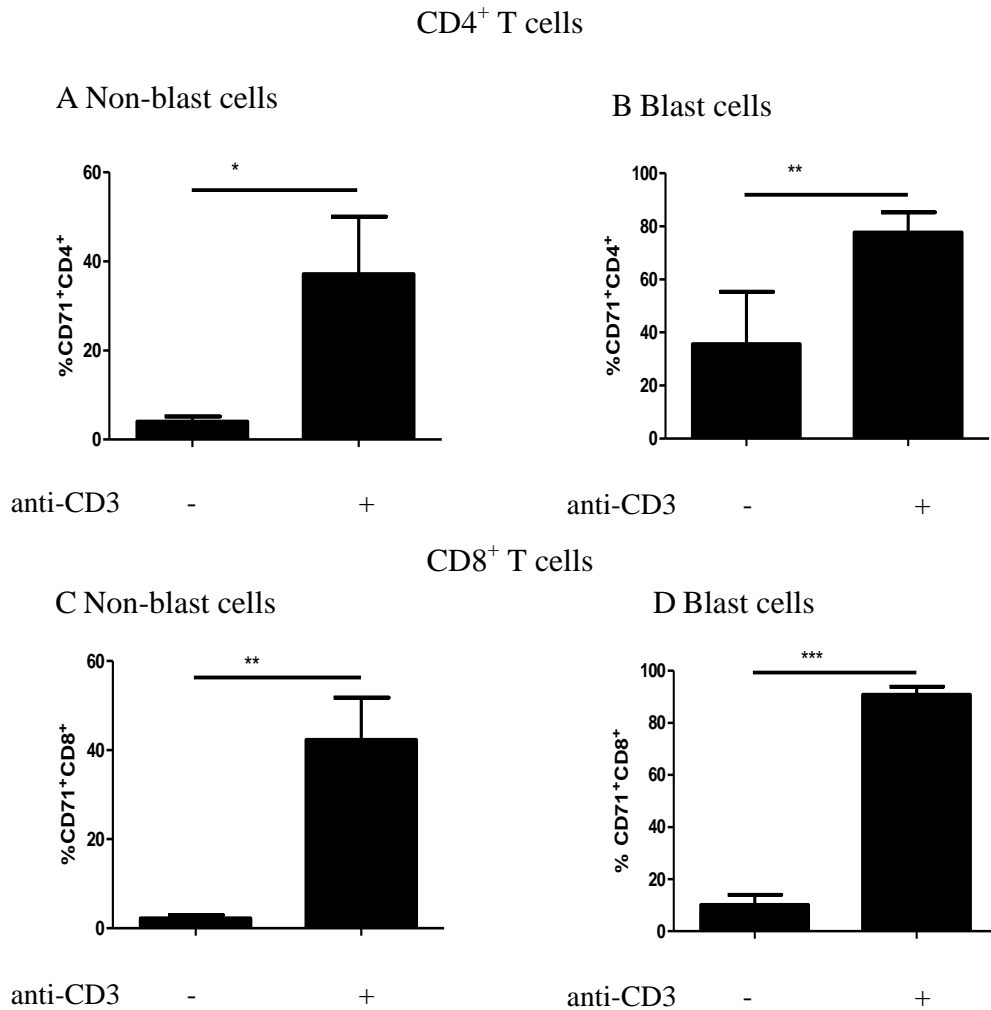
Figure 4.19. Anti-CD3-activated non-blast and blast cells have increased CD71 receptor expression on their cell-surface.

PBMCs (1 X $10^{\wedge}6$ cells /ml and 3 ml/well) were cultured in the presence of anti-CD3 for 72 h. Unactivated cells were taken from frozen stocks in the last 24 h of the 72 h activation. PBMCs were incubated in an antibody cocktail comprised of antibodies against the surface markers CD71, CD4 and CD8, for 30 min. Viable cells were determined following PI exclusion and blast or non-blast cells were identified as cells having forward scatter measurements greater than 35k and less than 35k, respectively using flow cytometry. The percentage $CD71^{+}CD4^{+}$ T cells or $CD71^{+} CD8^{+}$ T cells in both these populations was then determined. Data are presented as (A, C, D) mean ±SEM, n=4, (B) mean ±SEM, n=3; a unpaired student T-test was performed and significant differences are indicated with *P<0.05, **P<0.01, or ***P<0.001.

CD4+ T cells

A Non-blast cells   B Blast cells

CD8+ T cells

C Non-blast cells   D Non-blast cells
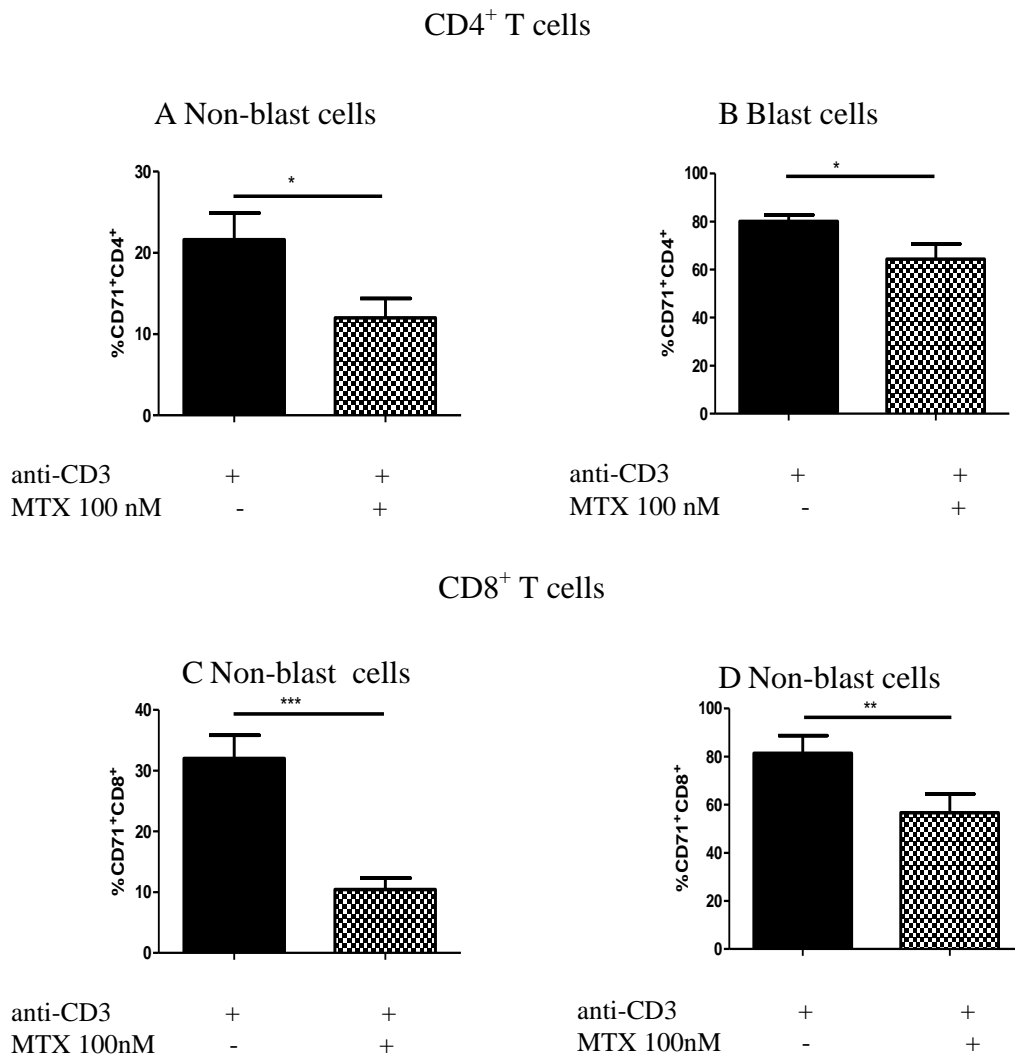
Figure 4.20. Non-blast and blast CD4+ T cells and CD8+ T cells have reduced levels of transferrin (CD71) receptor expression following Methotrexate treatment.

PBMCs were activated with anti-CD3 (1 µg/ml) for 72 h ± MTX (100 nM). PBMCs were incubated in an antibody cocktail comprised of antibodies against the surface markers CD71, CD4 and CD8, for 30 min. Viable cells were determined following PI exclusion and blast or non-blast cells were identified as cells having forward scatter measurements greater than 35k and less than 35k, respectively using flow cytometry. The percentage $CD71^+CD4^+$ T cells or $CD71^+$ $CD8^+$ T cells in both these populations was then determined. Data are presented as (A & C) mean ± SEM, n=7, (B) mean ± SEM, n=4 (D) mean ± SEM, n=5 a paired student T-test was performed and significant differences are indicated with. *P<0.05 or, **P<0.001.
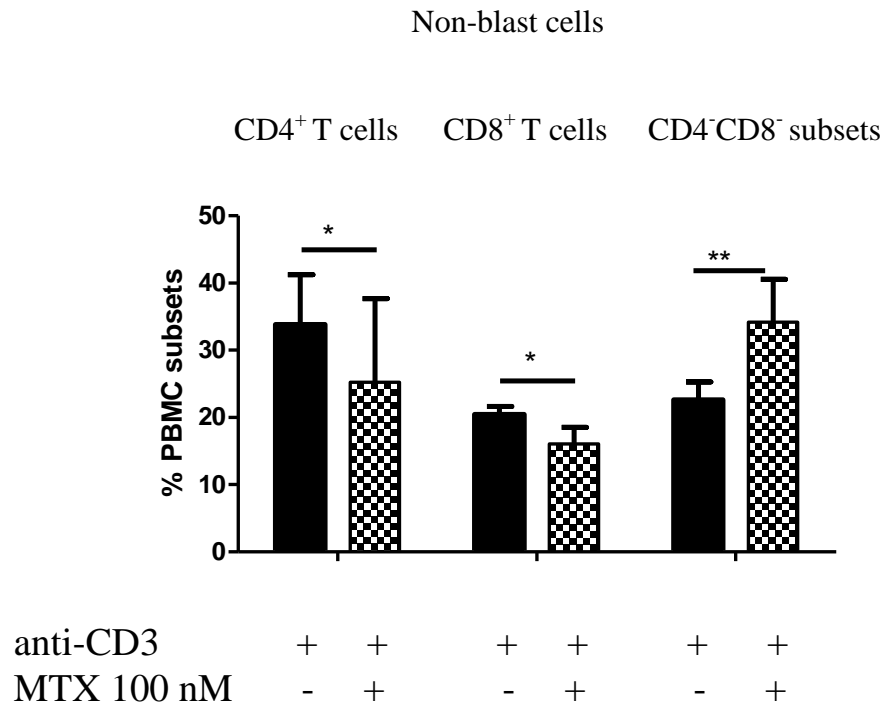
Figure 4.21 Methotrexate treatment has differential effects on non-blast PBMC cell subsets.

PBMCs were activated with anti-CD3 (1 µg/ml) for 72 h ± MTX (100 nM) and then incubated in an antibody cocktail comprised of antibodies against the surface markers CD4 and CD8 for 30min. Viable cells were determined following PI exclusion and non-blast cells were identified as cells having forward scatter measurements less than 35k using flow cytometry. The proportion of cell subsets was then determined. The proportion of non-blast CD8$^+$ T cells as well as non-blast CD4$^+$ T cells significantly decreased following MTX treatment. The proportion of non-blast CD4$^-$CD8$^-$ cells significantly increased. Data are presented as mean ± SEM, n=5; a paired student T-test was performed and significant differences are indicated with *P<0.05 or, **P<0.01.

Blast cells

CD4$^+$ T cells   CD8$^+$ T cells   CD4$^-$CD8$^-$ subsets
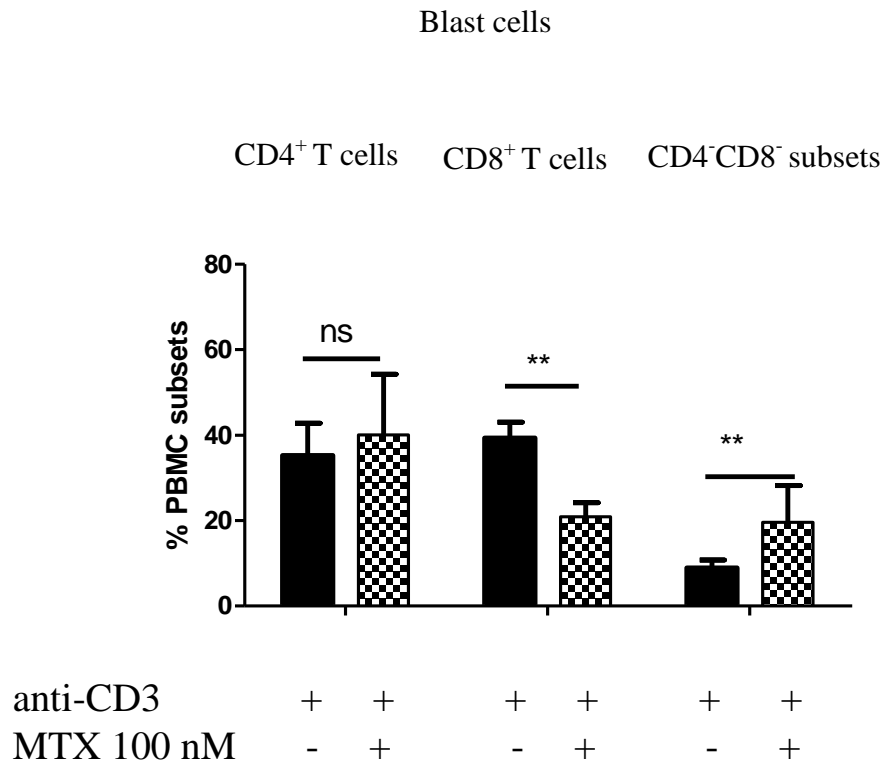
anti-CD3   +   +   +   +   +   +
MTX 100 nM   -   +   -   +   -   +

Figure 4.22. Methotrexate treatment has differential effects on blast PBMC cell subsets.

PBMCs were activated with anti-CD3 (1 μg/ml) for 72 h ± MTX (100 nM) and then incubated in an antibody cocktail comprised of antibodies against the surface markers CD4 and CD8 for 30min. Viable cells were determined following PI exclusion and blast cells were identified as cells having forward scatter measurements greater than 35k. The proportion of cell subsets was then determined using flow cytometry. Following MTX treatment the percentage of blast CD8$^+$ T cells significantly decreased, but there was no change in the blast CD4$^+$ T cells. The percentage of blast CD4$^-$CD8$^-$ cells significantly increased. Data are presented as mean ± SEM, n=5; a paired student T-test was performed and significant differences are indicated with *P<0.05 or, **P<0.01.

Non-blast cells

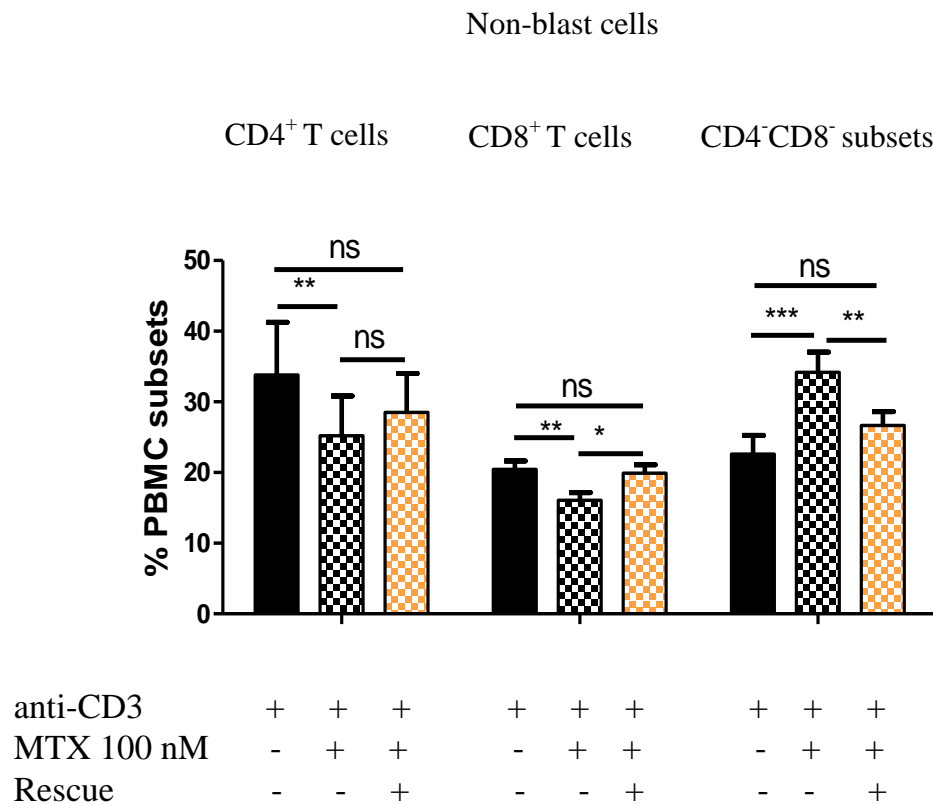**Figure 4.23 The effect of Methotrexate on the proportion of non-blast PBMC subsets is significantly reversed upon thymidine and hypoxanthine rescue.**

PBMCs were activated with anti-CD3 (1 µg/ml) for 72 h ± MTX (100 nM) ± thymidine and hypoxanthine (100 µM) and then incubated in an antibody cocktail comprised of antibodies against the surface markers CD4 and CD8 for 30min. Viable cells were determined following PI exclusion and blast or non-blast cells were identified as cells having forward scatter measurements greater than 35k and less than 35k, respectively. The proportion of cell subsets in each population was then determined using flow cytometry. Thymidine and hypoxanthine reversed the MTX-mediated reduction in non-blast CD8$^+$ and CD4$^+$ T cells as well as the MTX-mediated increase in CD4$^-$CD8$^-$ cells. Data are presented as mean ± SEM, n=5; a one-way ANOVA followed by Tukey's multiple comparison test was performed and significant differences are indicated with *P<0.05 or, **P<0.01.
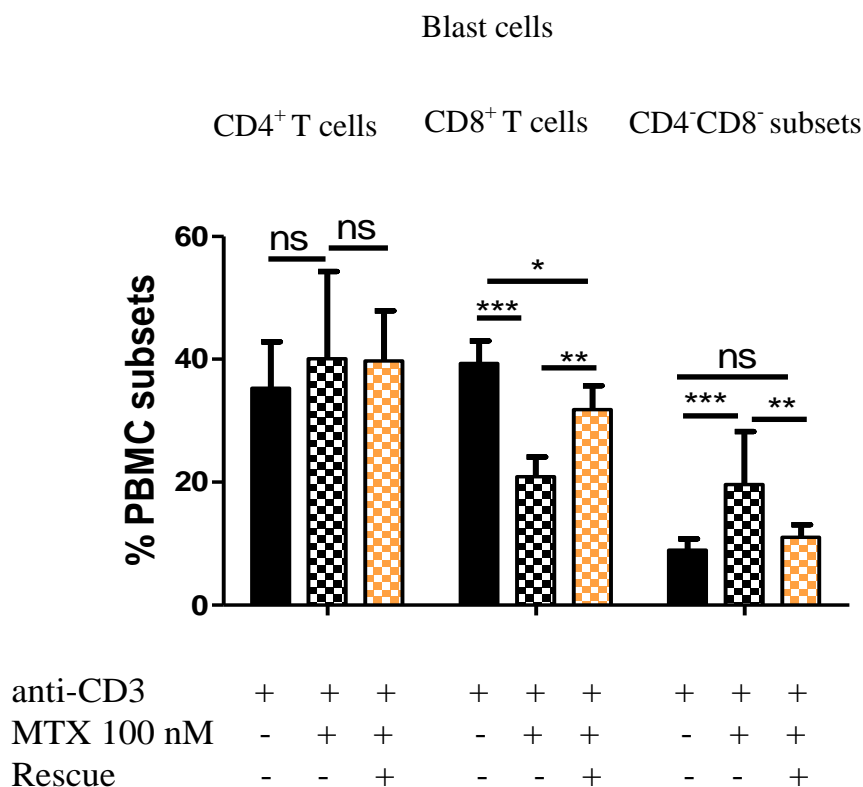
Figure 4.24 The effect of Methotrexate on the proportion of blast PBMC subsets is significantly reversed upon hypoxanthine and thymidine treatment.

PBMCs were activated with anti-CD3 (1 μg/ml) for 72 h ± MTX (100 nM) ± thymidine and hypoxanthine (100 μM) and then incubated in an antibody cocktail comprised of antibodies against the surface markers CD4 and CD8 for 30min. Viable cells were determined following PI exclusion and blast or non-blast cells were identified as cells having forward scatter measurements greater than 35k and less than 35k, respectively. The proportion of cell subsets in each population was then determined using flow cytometry. Thymidine and hypoxanthine reversed the MTX-mediated reduction in CD8^{+} T cells and the MTX-mediated increase in CD4^{-}CD8^{-} cells. Data are presented as mean ± SEM, n=5; a one-way ANOVA followed by Tukey's multiple comparison test was performed and significant differences are indicated with *P<0.05 or, **P<0.01.
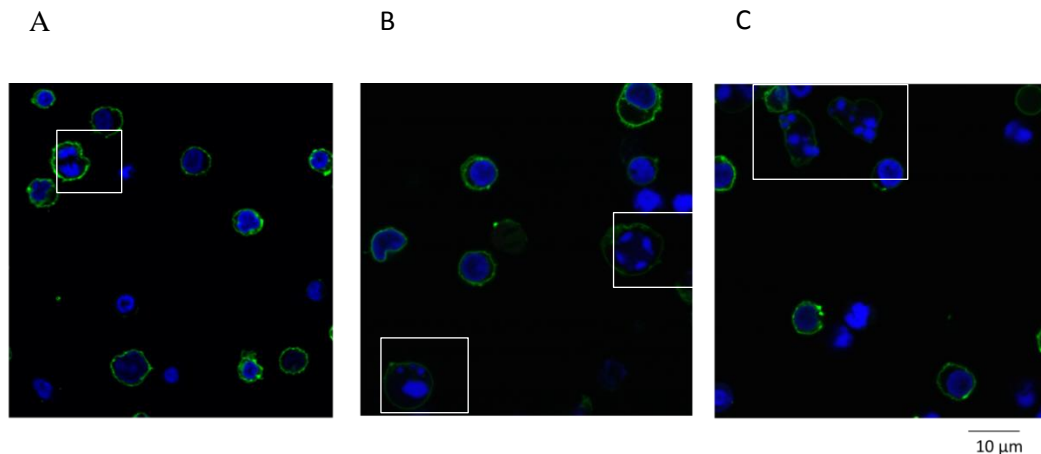
Figure 4.25. Insults to the nucleus can be visualised by DAPI stain.

PBMCs were activated with anti-CD3 (1 µg/ml) for 72 h ± MTX (100 nM). ManNAz (50 µM;green) was added in the last 24 h of the activation period. PBMCs were then counted and washed with PBS before resuspending ~450,000 cells in 95 µll alexa fluor 488 copper solution for 5 min. PBMCs were spun down on poly-D-lysine coated coverslips. PBMCs were washed with PBS, and fixed with 4% PFA. These were then washed and the slips transferred, face down on DAPI coated slides for imaging using confocal microscopy. (A) a mitotic cell, (B) a fragmented nucleus in a megaloblast cell after MTX treatment and (C) an apoptotic cell after MTX treatment. Representative of one experiment, conducted in triplicate.

surface sialome of CD3 positive PBMCs. Following MTX treatment, these blast cells containing fragmented DNA stained negative for the CD3 surface marker, indicating that MTX had increased the size of CD3 negative cells (Fig 4.26).

A

1.   2.   3.   4.

B

anti-CD3

10 µm
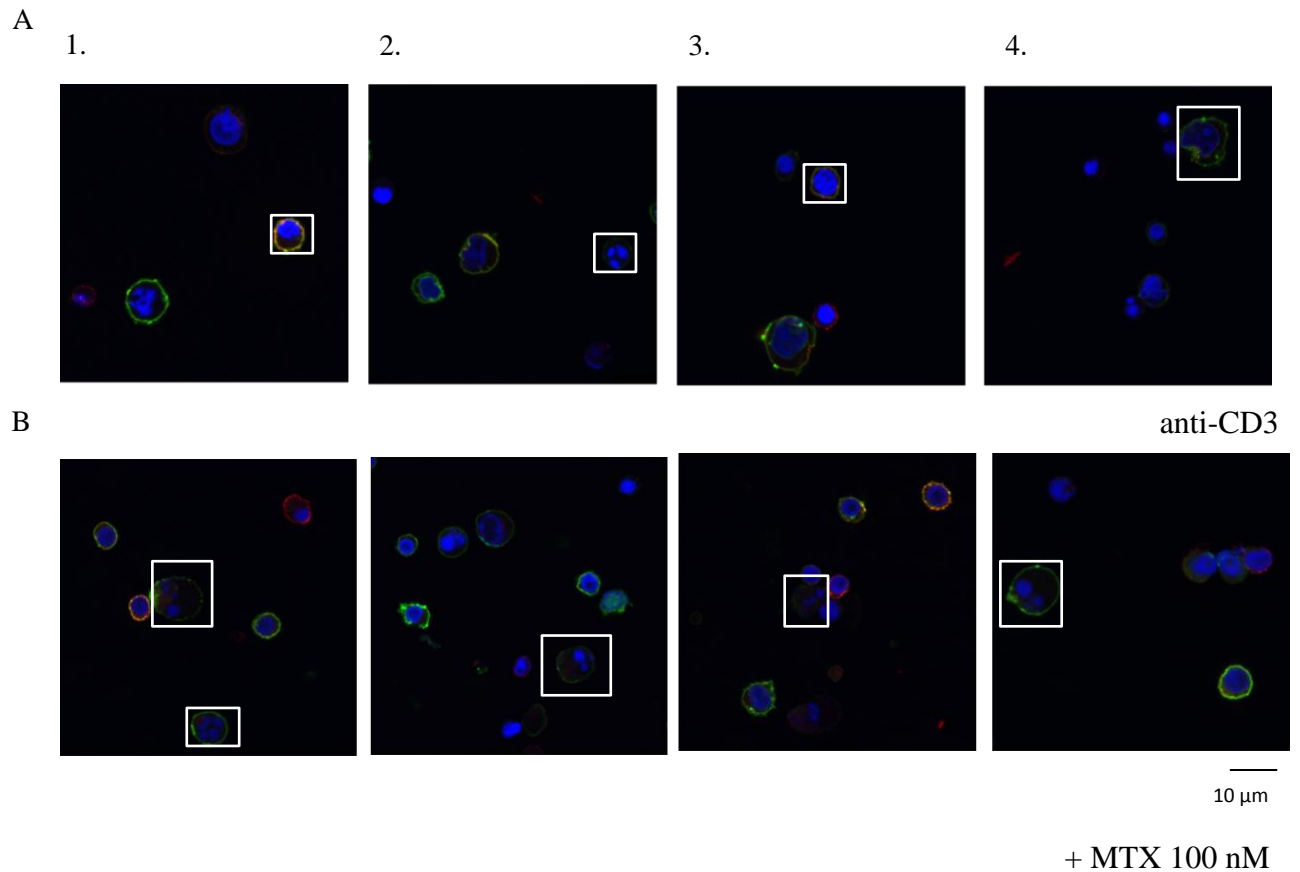
+ MTX 100 nM

Figure 4.26. Methotrexate treatment results in the formation of megaloblast CD3 negative cells.

PBMCs were activated with anti-CD3 (1 µg/ml) for 72 h ± MTX (100 nM). ManNAz (50 µM; green) was added in the last 24 h of the activation period. PBMCs were then counted and washed with PBS before resuspending ~450,000 cells in 95 µl alexa fluor 488 copper solution for 5 min. PBMCs were spun down on poly-D-lysine coated coverslips. PBMCs were washed with PBS, fixed with 4% PFA and incubated with antibodies against the surface markers CD3 at 4 degrees overnight. The cells were then washed, incubated with an anti-mouse secondary antibody (red) for 1 h. The cells were then washed again and the cover slips transferred, face down on DapI (blue) coated slides for imaging. (A1-4) activated $CD3^+$ T cell, neutrophil (unconfirmed), unactivated $CD3^+$ T cell, an apoptotic cell. (B1-4) megaloblast CD3 negative cell and (below) hypersegmented neutrophil (1); other images of megaloblast CD3 negative cells (2-4). Representative of one experiment, conducted in triplicate.

4.5 Discussion

<u>Visualising the cell-surface sialome of PBMCs</u>

The cell-surface sialome of PBMCs has not yet been visualised to determine whether there are cell-specific differences in the sialic acids on the cell-surface. Exploration of the sialome is pertinent to understanding the cellular interactions that take place on the cell-surface. Monitoring the sialome can also offer insights into the function of the sialic acid (sia) cellular processing pathway and how it is affected upon drug treatment or cellular activation. In this study, the incorporation of *N*-acetylmannosamine (ManNAc) on the cell-surface of a variety of PBMC subsets was visualised, following preliminary morphological identification or using T cell-surface markers (Fig 4.3&4.4). However, the linkage in which the sia moiety was attached to the underlying galactose residue was not determined. It was also possible that some sia moieties were cleaved by sialyltransferases released from dead cells, so the detected fluorescence was a measure of the final glycan product at a certain time. Monitoring this specific route in the sialic acid processing pathway from entry of *N*-acetylmannosamine (see **Section 1.17.2**) was achieved by feeding cells an azide-modified *N*-acetylmannosamine sugar (ManNAz) and detecting the sugar following the copper-catalysed addition of a fluorescent alkyne specific for that modified sugar. Although this was the first time the sialome of specific subsets in a mixed population was visualised (Fig 4.3), co-labelling of the sialome of different cell subsets of mouse splenocytes has been shown. This was depicted in flow cytometric plots of fluorochrome labelled sugars against the mouse B and T lymphocyte surface markers, CD20 and CD3 respectively (Dube et al., 2006). Imaging of the cell-surface glycome has been shown in a variety of immortalised cells using various azide-modified sugars. These include Jurkats and CHO cells, as well as other cancer cell lines (Chang et al., 2007, Hsu et al., 2007, Wainman et al., 2013). It has also been demonstrated in various tissues from mice fed these modified sugars (Neves et al., 2013). Interestingly, even *in vivo* imaging has been achieved in zebrafish embryos and in mice, demonstrating that this technique is at the forefront in expanding knowledge about the cell-surface glycome (Dehnert et al., 2011).

The cell-surface sialome has not yet been imaged upon cellular activation and it was not known how this changed upon activation. Using a combination of click chemistry and a

nuclear stain, DAPI, activation-dependant changes in cell size were observed and preliminary identification of specific cell subsets was made (Fig 4.4). The presence of blast lymphocytes indicated that these cells had undergone activation-induced growth. Eosinophils were identified by their bilobe nucleus, plasma cells, by their off-centre nucleus, and lymphocytes by their high nuclear:cytoplasmic ratio (Adewoyin and Nwogoh, 2014, Khvastunova et al., 2015). The addition of an antibody against the cell-surface marker CD3, verified the identity of the CD3$^+$ T cell subsets in this mixed population. In this way, ManNAz-derived sialic acids on the cell-surface of specific cell subsets was visualised using either cell specific surface markers or morphological characteristics.

Quantification of the cell-surface sialome of PBMCs

Since quantification of the ManNAz-derived sialic acids proved difficult using this method, Flow cytometry was utilised to determine whether activation-induced changes to the sialome had occurred. In order to establish this as a quantifiable method, a working range of ManNAz was first determined. The time-dependent nature of ManNAz incorporation was also assessed. Furthermore, since this copper-catalysed click reaction had also been shown to be toxic, viability assays were conducted to exclude the possibility of ManNAz toxicity contributing to any drug-induced changes in the sialic acid on the cell-surface.

There was no dose-dependent increase in the mean fluorescence intensity (MFI) at various concentrations of ManNAz as the higher concentrations proved toxic to these cells (Fig 4.5B). Importantly, toxicity has been shown previously to be due to the incubation time of both ManNAz and the copper click reaction and copper incubation times longer than 5 min have been shown to induce toxicity (Hong et al., 2010). For these experiments, toxicity was minimised by incubating PBMCs with ManNAz (50 µM) for 24 h followed by a 5 min copper click incubation (Fig 4.5C). These conditions achieved maximal fluorescence in the absence of toxicity and were used for future experiments. The conditions used for labelling these sugars have been shown to vary between groups with some investigators using the same concentration of ManNAz for 72 h labelling experiments of HeLa and Jurkat T cells, or for 2 days in HeLa and CHO cells (Hong et al., 2010, Soriano Del Amo et al., 2010, Wang et al., 2011b). Lower concentrations of ManNAz (25 µM) have also successfully been used to label Jurkat cells following a 48-

72 h incubation (Agard et al., 2006). Importantly, in the absence of ManNAz, only low background fluorescence was detected, which highlighted the specificity of the azido-alkyne reaction, crucial for the quantification of any drug-induced changes (Fig 4.5A). Incorporation of ManNAz proved to be time dependent as there was a significant increasing linear trend in the incorporation of ManNAz at 12 h, 18 h and 24 h and the incorporation of ManNAz occurred as early as 12 h (Fig 4.6B).

The anti-CD3-activated PBMCs were more sensitive to ManNAz (50 µM) and copper-induced toxicity than unactivated cells. However, viability levels of these anti-CD3-activated PBMCs were still an acceptable ~75%, so this concentration was used for the remaining experiments (Fig 4.7).

Activation-dependent changes to the cell-surface sialome

To determine whether ManNAz incorporation was a characteristic of cellular activation in anti-CD3-activated PBMCs, the time taken for all the PBMCs to be positive for the alexa fluor 488 probe on the cell-surface (% ManNAz$^+$) was measured in both unactivated and activated PBMCs. ~95% of PBMCs were positive for ManNAz incorporation on the cell-surface of activated PBMCs after only 6 h, compared to 12 h in the unactivated cohorts (Fig 4.6&4.8). The total surface ManNAz also increased in unactivated PBMCs, at 12 h, 18 h or 24 h. In contrast to the increasing incorporation of ManNAz over 12 h, 18 h and 24 h in unactivated PBMCs, ManNAz incorporation almost doubled from 6 h to 12 h, but there was no significant increase in ManNAz from 18 h to 24 h in anti-CD3-activated PBMCs (Fig 4.8). It is possible that these time points coincided with cellular mitosis, which could half the biosynthetic precursors for incorporation into the new daughter cell. Although very little is known about nutrient allocation in the daughter cell, it is known that intracellular folate is halved following the first mitotic division. This was discovered because cells cultured in folate deficient media were able to undergo a few cycles of cell division because they were previously cultured in folate replete media (Borman and Branda, 1989). If this was indeed the case, cells undergoing mitotic division would have less intracellular levels of ManNAz following mitosis therefore measuring the mean sugar incorporation on the cell-surface for a population of cells may be substantially less at this time.

Differences were not due to differential uptake, as these per-O-acetylated azido sugars, as was used here (Ac$_4$ManNAz), have been shown to passively diffuse across the membrane,

192

by virtue of the acetyl groups (Saxon et al., 2002, Laughlin and Bertozzi, 2007). These quantifiable differences did not reflect conversion from *N*-acetylglucosamine (GlcNAc) precursors, as only ManNAc was modified and thus only entry from this point in the pathway could be measured (Saxon et al., 2002). Thus, the differences observed were due to higher flux of ManNAz through the sialic acid processing pathway in activated PBMCs. This suggested that the sialic acid glycan pathway, from ManNAc entry is an activation dependent metabolic pathway and is upregulated upon anti-CD3 activation. There is only one report found which assessed the effects of anti-CD3 activation on T cell-surface sialyation (Villanueva-Cabello et al., 2015). Using click chemistry, the authors showed that ManNAz incorporation was significantly increased on the cell-surface of anti-CD3-activated human T helper cells over 24 h, 48 h, and 72 h, compared to unactivated cells. However, the authors failed to stipulate the membrane permeability of the per-O-acetylated sugar, which meant they did not delineate increased flux through the sialyl-glycan pathway as a mechanism behind the increase in ManNAz incorporation. Furthermore, the authors did not identify increased incorporation of ManNAz-derived sialic acids as a measurable parameter of T cell-activation, as was shown here; they explored this increase in sialylation in contrast to the reported decrease in surface epitope expression of specific sialic acid linkages, α2, 3 and α2, 6 following T cell-activation. Specifically, this report found an activation-dependent decrease of CD8^{+} T cell-surface α2, 6 sialyl linkages, following binding of a fluorochrome-conjugated SN ligand (Comelli et al., 2006). Elsewhere, a decrease in sialylation of these *N*-glycans was found along with decreased expression of sialyltransferase ST*6*Gal 1(Comelli et al., 2006). The increase in sialic acids can on the cell-surface shown here identified an increase in sialic acids as a parameter of cellular activation. Changes in intracellular levels of specific sialic acids, *N*-acetylneuraminic acid and *N*-glycosylneuraminic acid, have been found upon anti-CD3 activation in murine splenic T cells (Naito-Matsui et al., 2014). These intracellular changes, upon activation reflect changes to the most abundant T cell-surface glycoproteins, CD45 and CD43, involved in cell recognition (Clark and Baum, 2012).

<u>*N*-linked glycosylation</u>

To show that intracellular changes reflected changes in ManNAz incorporation on the cell-surface, and that the sialic acids being visualised were *N*-linked, it was important to demonstrate a reduction in the mean fluorescence intensity following the addition of an

N-glycosylation inhibitor, tunicamycin, which acts as a competing substrate for GlcNAc-1-phosphotransferase (Schneider et al., 1978). Indeed, the amount of ManNAz incorporated on these surface sialic acids was significantly reduced with tunicamycin (1 µM), a reduction not attributable to toxicity induced by the inhibitor (Fig 4.9). Annexin V staining would confirm whether this concentration of tunicamycin is toxic to anti-CD3-activated PBMCs after 72 h. However, there was a significant reduction in viable cell counts following treatment, suggesting that tunicamycin did exert an anti-proliferative effect on these cells. This inhibitor has been used to prove that click chemistry is a quantifiable method to evaluate the sialic acid content on the cell-surface of Jurkat cells (Saxon et al., 2002). However, for these experiments, it was used to demonstrate that intracellular changes can reflect changes to the cell-surface sialome.

The effect of MTX on cell-surface sialylation in unactivated and anti-CD3-activated PBMCs

It is not known how MTX can affect the changing glycosylation patterns on antibodies (see **Section 1.18.3**). The effect of MTX treatment on a specific glycosylation pathway, specifically the CMP-*N*-acetylmannosamine sialic acid processing pathway, by measuring ManNAz incorporation, was investigated in unactivated PBMCs. No significant changes in ManNAz incorporation was found on the cell-surface of these cells (Fig 4.10). This result excludes the possibility that MTX could exert a direct effect on the ManNAz-derived sialic acid processing pathway, a finding that has not been shown.

MTX is known to limit the various physiological events that accompany cellular activation via the potentiation of activation of AMPK (O'Neill and Hardie, 2013). In light of the activation-dependence of ManNAz incorporation, another aim of this study was to investigate whether MTX could directly impact surface sialylation during activation. Intriguingly, MTX (100 nM) treatment was found to significantly reduce ManNAz incorporation on the cell-surface, sialyl-glycans of anti-CD3-activated PBMCs (Fig 4.11). A direct effect of MTX on cell-surface sialylation has not been shown, and the fact that these changes occurred in activated cells only has interesting implications. Since, many anti-inflammatory drugs limit cellular activation this method could establish a new way of monitoring the effectiveness of anti-inflammatory drugs by measuring the incorporation of ManNAz on surface sialyl-glycans in activated cells. It also has interesting applications for individualised drug monitoring by comparison of the ManNAz-derived sialyl-glycans

from untreated cells to those following treatment. Importantly, this reduction of surface sialic acids on anti-CD3-activated PBMCs could infact be a reduction in galactose residues, on which sialic acids bind. As an anti-inflammatory agent a reduction in surface sialic acids on anti-CD3-activated PBMCs by MTX could result in a reduction in siglec binding or an increased affinity for immune cells for galectin binding due to the exposed galactose residues which could give rise to an anti-inflammatory response.

Although the mechanism of action in which MTX affected ManNAz incorporation was not related to reduced uptake due to the membrane permeability of the per-O-acetylated sugar discussed earlier, other explanations were not further investigated.

Differential effects of metabolic inhibitors on cell-surface sialylation in activated compared to unactivated PBMCs have been shown before, but specific surface glycoproteins have been investigated following IL-1β activation. The group observed changes in the sialic acids on the surface glycoprotein, P-selectin glycoprotein ligand 1 (PSGl-1) as well as sialyl lewis expression with the metabolic inhibitor, β,1-4 galactosyltransferase on the surface of IL-1β stimulated PBMCs, but had no effect in unactivated cells (Kanabar et al., 2016). To our knowledge, the effects of metabolic inhibitors or inhibitors of cellular activation, like MTX, on the ManNAz-derived sialyl-glycans had not yet been investigated.

Rescue from the effects of MTX on surface sialylation

At this concentration of MTX, the proliferation of these cells was also inhibited. In accordance with previous experiments it was pertinent to determine whether these changes were related to purine and thymidine inhibition. Interestingly, reversal of this anti-proliferative effect also prevented the MTX-induced inhibition of ManNAz incorporation (Fig 4.12A). This suggested that the mechanism behind this MTX-induced reduction of ManNAz on the surface sialyl-glycans was related to purine and thymidine inhibition. However, it was unclear if this was directly related to the reduction in nucleotide precursors, as the sugar donors for glycan synthesis, or if purines and thymidine exerted some regulatory effect on the transcriptional control exerted by MTX. Interestingly, it was shown that follinic acid or thymidine could partially reverse the MTX inhibition of NF-kB following TNF stimulation of Jurkat cells (Majumdar and Aggarwal, 2001). Future work will examine whether purine and thymidine rescue can limit the potentiation of AMPK activation by MTX, as a mechanism of action.

<u>Population-dependent effects of MTX</u>

Upon further examination, there appeared to be two distinctive populations of anti-CD3-activated PBMCs. Non-blast cells comprised the largest proportion of the unactivated PBMCs, but following activation-induced cell growth blast cells became the most prevalent (Fig 4.13). MTX significantly reduced the proportion of blast cells and increased the proportion of non-blast cells (Fig 4.13). Similar inhibition of CD4$^+$ T cell and CD8$^+$ T cell growth was shown in the previous chapter (see **Section 3.4.4**). An increase in ManNAz incorporation following activation confirmed that both populations were indeed activated compared to their un-activated counterparts (Fig 4.15). However, examining the effect of MTX on ManNAz incorporation in both blast and non-blast cells revealed contrasting results. MTX increased ManNAz incorporation on the cell-surface of blast cells, yet decreased ManNAz on the surface of non-blast cells (Fig 4.16). To investigate if these changes in ManNAz incorporation were related to different toxicities associated with purine and thymidine inhibition, the effects following rescue of these nucleotides was also measured. Interestingly, purine and thymidine rescue reversed the MTX mediated reduction in ManNAz on the cell-surface of non-blast cells and the MTX-mediated increase in ManNAz on blast cells, back to control levels in both populations (Fig 4.17). These results suggest that MTX exerts specific effects on the incorporation of ManNAz on cell-surface anti-CD3-activated PBMCs by way of purine and thymidine inhibition.

To investigate whether these changes in the cell ManNAz-derived sialic acids upon MTX treatment were activation dependent, ManNAz incorporation on the surface of unactivated PBMCs following MTX treatment was measured. There was no significant change in these non-blast or blast cells which had not undergone anti-CD3 activation nor was there any change upon rescue (Fig 4.18).

Possible reasons for these contrasting effects on ManNAz incorporation in both blast and non-blast cells were evaluated. First, the activation status was examined to see if both populations had upregulated transferrin (CD71) receptor expression upon activation, like the increase in transferrin receptor expression found in CD4$^+$ and CD8$^+$ T cells in the previous chapter (see **Section 3.4.3**). Transferrin receptor expression had increased on these non-blast CD4$^+$ and CD8$^+$ T cells just like the blast CD4$^+$ and CD8$^+$ T cells. This indicated that these cells had been activated (Fig 4.19).

Differential intracellular concentrations of MTX were next investigated to see if this could account for the contrasting effects on ManNAz incorporation. Differential MTX uptake due to cell specific expression of folate receptors has been shown (Wu et al., 1999). Natural T regulatory cells (nTreg) express higher amounts of folate receptor 4 than other naïve or active T cells. The same authors showed that even differential activation of CD4$^+$ T cells resulted in varied expression of folate receptors (Yamaguchi et al., 2007). Since folate receptors have different affinities for folate, these cells containing different types and combinations of folate receptors have different propensities to take up folate and therefore, MTX. Indeed, cellular uptake of MTX has been shown to occur via the Reduced Folate Carrier (RFC) in immune cells, but macrophages have been shown to predominantly express the folate receptor β (Blits et al., 2013). The intracellular concentration of MTX is also determined by MTX efflux. Both folate and MTX can be extruded from cells as the non-polyglutamated form via ATP binding cassette (ABC) transporters including ABCC1 and ABCG2 (Blits et al., 2013). Alterations in the production of these transporters or affinity for their substrates have also been shown to lead to reduced intracellular concentrations of MTX. However, MTX significantly reduced transferrin receptor expression in both non-blast and blast CD4$^+$ and CD8$^+$ T cells (Fig 4.20), which paralleled what was shown in the previous chapter (see **Section 3.4.3**). These results suggest that both populations had taken up MTX. Moreover significant effects on transferrin receptor expression were observed at the same doses, excluding the possibility that either population contained lower concentrations of MTX.

To determine if cell specific changes could account for these differences, the effect of MTX on the cell subsets in blast and non-blast populations were analysed. MTX significantly reduced the proportion of CD8$^+$ T cells and increased the proportion of CD3 negative (CD4$^-$CD8$^-$) cells in both blast and non-blast populations (Fig 4.21 and 4.22). However, MTX failed to reduce the proportion of blast CD4$^+$ T cells like it did the non-blast CD4$^+$T cells. Thus differential effects by MTX on CD4$^+$ T cells compared to CD8+ T cells were found. MTX has not been shown to exhibit preferential cytotoxic effects on CD4$^+$ T cell or CD8$^+$ T cell subsets, in pokeweed activated PBMCs which was suggested by the authors to indicate that MTX has no preferential effect on cells dividing at the same rate (Nesher and Moore, 1990). However, elsewhere, CD8$^+$ T cells proved more sensitive to the anti-proliferative effect of folate-deficiency (Courtemanche et al., 2004).

Thus, it is possible that differential effects on $CD4^+$ T cell subsets by MTX contributed to the increase in ManNAz on blast cells.

Since rescue reversed both the MTX-mediated increase in ManNAz in blast cells and decrease in non-blast cells, the effects of rescue on the cell subsets was examined to determine if differential sensitivities in different cell subsets were related to different sensitivities to purine and thymidine inhibition. Rescue reversed the MTX-mediated effects on blast and non-blast $CD8^+$ T cells and CD3 negative cells ($CD4^-CD8^-$) (Fig 4.23&4.24). Rescue had no effect on blast $CD4^+$ T cells yet reversed the MTX-mediated increase in ManNAz which suggested that the means by which ManNAz incorporation was affected, was not through $CD4^+$ T cells.

<u>Megaloblastic phenotype</u>

A further look into the effects of MTX on the different PBMC subsets revealed that MTX had increased the proportion of both blast and non-blast CD3 negative cells, (Fig 4.21&4.22) so it was important to determine if this was a relative increase or if treatment was increasing the size of these PBMCs (Fig 4.27). DAPI was employed as a nuclear dye to measure the integrity of the DNA. DAPI staining revealed cells undergoing mitosis and detected fragmented DNA in MTX treated cells (Fig 4.25). Following incubation with ManNAz and the Click IT reaction, the plasma membrane was imaged. Apoptotic cells were present following MTX treatment and were identified as having fragmented DNA and a disintegrated plasma membrane. Large cells containing fragmented DNA inside an intact plasma membrane following MTX treatment were also observed, suggesting the formation of a megaloblast cell.

To identify whether megaloblast cells were CD3 positive, PBMCs were incubated with an antibody directed against the surface marker, CD3. Probing with a fluorescent-conjugated secondary antibody against this primary antibody revealed that megaloblast CD3 negative cells formed under these MTX-treated conditions (Fig 4.26B). In contrast to the inhibition of activation induced growth discussed previously (see **Section 3.1.3**), folate-deficiency has also been shown to cause macrocytosis which is an increase in the mean corpuscular volume, leading to an increase in cell size (Weinblatt and Fraser, 1989). These megaloblast CD3 negative cells contained fragmented DNA due to defects in the replication of DNA (Taheri et al., 1981). Although defects usually occur in the bone marrow, chromosome breaks have been observed in both bone marrow cells and
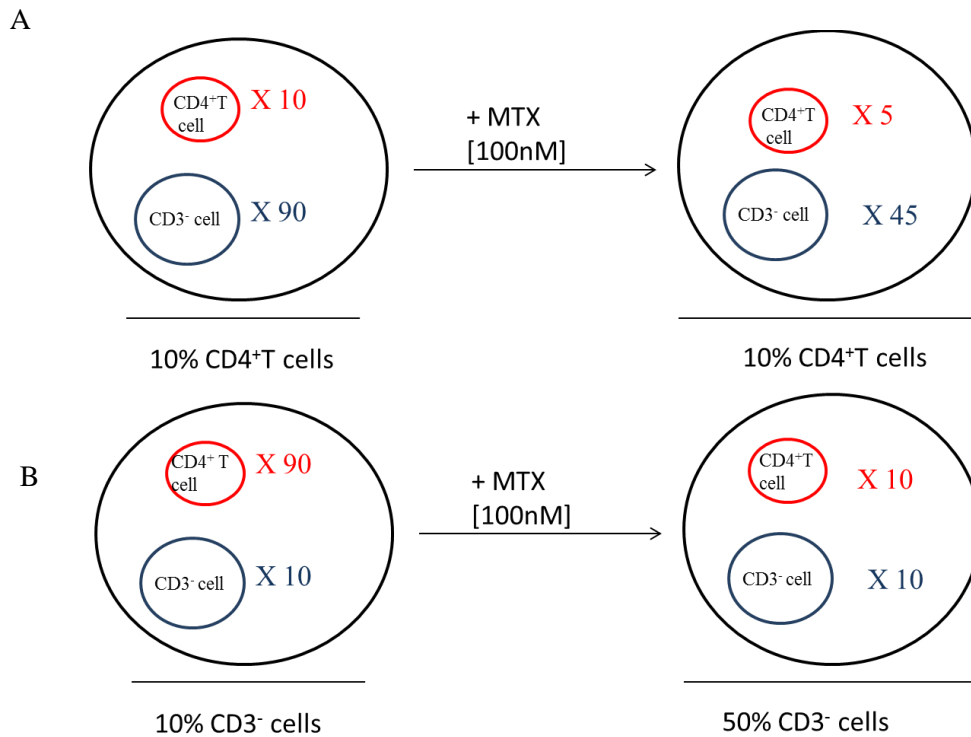
Figure 4.27. Schematic of the relative changes in PBMC subsets with Methotrexate treatment.

(A) The proportion of CD4$^+$ T cells could have been reduced with MTX treatment but it may not be clear if the proportion of CD3 negative cells is also reduced. (B) The proportion of CD3 negative cells may increase if the relative numbers of CD4$^+$ T cells drop.

leukocytes from patients with megaloblastic anaemia (Keller and Norden, 1967). This has even been shown to result in the enlargement of neutrophils (Sallah et al., 1999). Indeed, a multi-lobed neutrophil was observed under these conditions although the identity was not confirmed.

In support of these findings, megaloblastic anaemia has been reported during low-dose MTX treatment in RA patients (Weinblatt and Fraser, 1989). These were referred to as multinucleated giant cells following MTX treatment in another report (Chan and Cronstein, 2010). Megaloblast formation was observed for short term (one week) treatment with high dose MTX (Anderson et al., 1966). Although there were no papers found regarding the development of megaloblast cells following a 72 h culture with low-dose MTX, the extent of folate-deficiency would depend on the requirement for folate by those activated PBMCs.

Even for those CD3 negative cells not undergoing activation-induced cell growth, regular folate homeostasis is still required; a process perturbed by the anti-folate, MTX. In this study megaloblastic anaemia was not confirmed, as neither red blood cell (RBC) folate nor a reduction in red blood cell counts was measured (John Lindenbaum, 1994). Megaloblast cells containing fragmented DNA were observed in a known folate-deficient state, suggesting a megaloblastic process, a finding that under these culture conditions has not yet been shown. Since MTX increased the proportion of CD3 negative megaloblast cells in both blast and non-blast populations in which contrasting effects on ManNAz incorporation were found, it is unlikely that these megaloblast cells contributed to the observed effects on the cell-surface sialome.

Overall, the findings shown here indicate that ManNAz incorporation is an activation-dependent process and can be affected by drugs that inhibit part of the glycosylation pathway or drugs that inhibit cellular activation. This method can also be used to quantify the effects of anti-inflammatory drugs that limit cellular activation. Since MTX had no effect on ManNAz incorporation in unactivated PBMCs, it suggests that MTX has no direct effect on the cell-surface sialome. The finding that purine and thymidine rescue reverses the effects of MTX on ManNAz incorporation indicates that the means in which MTX affected the cell-surface sialome was purine and thymidine inhibition. It suggests that purine and thymidine nucleotides can impact on the cell-surface sialome which requires these sugar donors, a finding which rivals another report which found no link

between purine and thymidine inhibition and glycosylation (De Graaf et al., 1993). However, it doesn't elucidate whether it is the absence of these nucleotide precursors which are responsible, or whether purine and thymidine nucleotides exert some regulatory effect. This study also revealed that MTX could have differential effects on the cell-surface sialome in different populations of anti-CD3-activated PBMCs. This effect was not due to differential activation as the T cells in both populations had increased CD71 receptor expression. Neither was this effect due to differential MTX uptake or intracellular concentration of MTX as CD71 receptor expression was reduced in the T cells of both populations. Future work will analyse the cell cycle of each population to determine whether these differences are attributed to differentially-cycling PBMCs. Although blast CD4$^+$ T cells seemed to demonstrate a reduced sensitivity to MTX, rescue had no effect on the proportions of this subset but rescue reversed the effect of MTX on ManNAz incorporation. Thus, the mechanism in which purine and thymidine inhibition affected ManNAz incorporation in these differential populations was not determined. It was also not clear how MTX treatment affected processing of ManNAz through the metabolic pathways as a means of altering ManNAz incorporation.

Chapter 5:

To elucidate the effects of Methotrexate on intracellular sugar-nucleotides and nucleotides in unactivated and anti-CD3-activated PBMCs

5.1 Introduction

Sugar-nucleotides are donors in glycosylation reactions and their availability, together with the availability of the compartment specific glycosyltransferases, largely dictates the type and extent of glycosylation that can take place (Drickamer, 2003). The sugar-nucleotides themselves are formed from specific nucleotides, as it was found that [^{14}C] uridine significantly increased in UDP-glucose over the course of 72 h in PHA-activated CD4$^+$ T lymphocytes (Fairbanks et al., 1995).

As such, chemicals that inhibit the use of these nucleotides, as either analogs or inhibitors of these biosynthetic pathways, have been shown to affect sugar-nucleotides. By virtue of their similar structure to nucleotides, nucleotide analogs have been shown to act as a competitive substrate in the formation of sugar-nucleotides. Treatment of human lymphoblast cells with 5-Flurodeoxyuridine (5-FdUrd), a uridine analog, resulted in the formation of 5-FdUDP-*N*-acetylglucosamine (Peterson et al., 1983). Inhibitors of nucleotide synthesis, such as Mycophenolate mofetil (MPA) were also shown to affect the nucleotide substrate, required for the backbone of the sugar nucleotide and in particular, the purine nucleotide ATP, required to create the activated sugar during the reaction (Fig 5.1). MPA inhibits the rate limiting enzyme in de novo synthesis of guanosine nucleotides, inosine monophosphate dehydrogenase (IMPDH), and results in the depletion of guanosine nucleotides, which was shown to decrease mannose on the cell-surface and inhibit the transfer of fucose and mannose to glycoproteins (Allison and Eugui, 2000). This suggests that nucleotide inhibition can drastically affect the type and extent of glycosylation that occurs. However, it is not known whether this inhibition is specific for the purine-based sugar and its purine nucleotide precursor. One report examined the pyrimidine analog, 5-Fluorouridine (5FU) and the purine analog, Mercaptopurine (6-MP) and found that both affected the incorporation of [^{3}H]Gal and [^{3}H]Man into their respective pyrimidine and purine-based sugars (UDP-galactose and GDP-mannose) (De Graaf et al., 1993). Since the pyrimidine analog also affected the purine-based sugar, it was concluded by the authors that these nucleotide analogs did not affect sugar-nucleotides through their nucleotide precursors. However, nothing has been shown for the folate analog, MTX and any possible effects on sugar-nucleotides. As an anti-folate, MTX is known to exert drastic effects on nucleotide synthesis, (see **Section 1.7.2**&**1.7.4**) as well as affecting glycosylation patterns, which validates the investigation
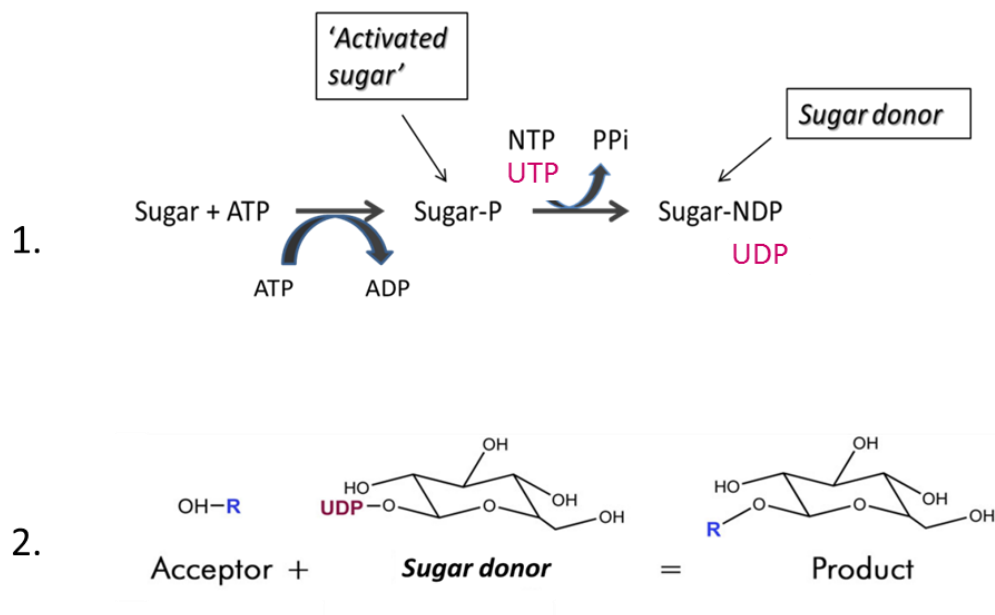
Figure 5.1. The nucleotide requirement for sugar-nucleotide synthesis and the glycan end-product.

(1). ATP hydrolysis is used to create an activated sugar which reacts with a nucleotide triphosphate, forming a sugar-nucleotide diphosphate. (2) The addition of a sugar to a protein or lipid acceptor begins with the formation of a sugar-nucleotide donor. This sugar is then transferred by specific glycosyltransferases from the sugar donor to an acceptor protein or lipid to form the glycan. Adapted from (p450.kvl.dk).

of whether the MTX-mediated inhibition of purine and thymidine synthesis can affect their respective purine and pyrimidine-based intracellular sugar-nucleotides, a possible link to how it may effect glycosylation, (see Section **1.18.2**) a study never conducted before. It was shown that MTX (10 µM) treatment resulted in the formation of a tritiated sugar, dUDP-*N*-acetylglucosamine following the addition of [^{3}H]dUrd, in a human lymphoblast cell line which was not detected in control cells (Peterson et al., 1983). This suggested that MTX affected cellular nucleotide levels, necessitating the use of the exogenous nucleotide in glycosylation reactions but does not explain the mechanism in which this occurred, or whether purine and thymidine inhibition was the cause.

5.1.1 The effect of MTX on intracellular nucleotides

There are conflicting findings regarding the effect of MTX on both purine and pyrimidine ribonucleotides as well as deoxyribonucleotides, formed from their ribonucleotide precursors. Most reports have found that MTX treatment reduced purine levels. ATP levels were reduced with a lesser reduction in ADP levels in both P3 cells and a MCF-7 breast cancer cell line after a 4 h and 8 h MTX (100 nM) treatment (Tedeschi et al., 2013, 2015). This reduction in the purine nucleotides AMP, ATP, ADP, GTP, GDP, and cGMP by MTX (2.5 nM) was also shown after a 72 h treatment in Jurkat cells (Miura et al., 2010). ATP and GTP were reduced after a 4 h MTX (2 µM) treatment in Ehrlich tumour cells and a 48 h MTX (66 nM) treatment in CCRF-CM cells (Kaminskas, 1982, Chen et al., 1998). dATP and dGTP were also reduced upon a 48 h MTX (66 nM) treatment in CCRF-CM cells and an 18 h MTX (66 µM) treatment in a human T MOLT-4 cell line (Kazmers et al., 1983, Chen et al., 1998). A decrease in de novo synthesis of IMP, ATP and GTP after a 2 h MTX (0.1 µM) treatment in growing mouse L1210 leukemic cells was also found (Sant et al., 1992). However there is one report which found that MTX (50 nM) increased dATP levels after a 4 h treatment in HCT116 cells (Uehara et al., 2009).

One study found that MTX (100 nM) had little effect on pyrimidine levels after a 8 h treatment in in the MCF-7 breast cancer cell line (Tedeschi et al., 2015). Numerous other studies found pyrimidines decreased with treatment. dTTP and dCTP were reduced upon a 48 h MTX (66 nM) treatment in CCRF-CM cells (Chen et al., 1998). dTDP levels also decreased after a 4 h MTX (50 nM) treatment in HCT116 cells (Uehara et al., 2009). A 72

h MTX (2.5 nM) treatment also reduced UDP in Jurkat cells (Miura et al., 2010). However, there are some reports which found that MTX increased the concentrations of uridine-based nucleotides. UTP was shown to be increased after a 48 h MTX (66 nM) treatment in CCRF-CM cells (Chen et al., 1998). UTP as well as CTP also increased following a 4 h MTX (2 µM) treatment in Ehrlich tumour cells (Kaminskas, 1982). dUMP increased after a 4 h MTX (50 nM) treatment in HCT116 cells and a 4 h MTX (100 nM) in HeLa cells (Myint et al., 2009, Uehara et al., 2009). dUTP also increased following MTX (10 µM) treatment in a cultured human lymphoblast cell line (Peterson et al., 1983).

MTX (100 nM) has been shown to increase the ATP/AMP ratio in the MCF-7 breast cancer cell line (Tedeschi et al., 2015). MTX (5 µM) was also found to decrease ATP levels in PC-3M-luc-C6, and A-431 cells after a 16 h treatment (Beckers et al., 2006). This has been suggested to be one of the mechanisms in which MTX potentiates the activation of AMPK, the other via increasing AICAR, the AMP mimetic (Kuznetsov et al., 2011). Indeed MTX (0.1 µM) increased both SAICAR and AICAR in growing mouse L1210 leukemic cells (Sant et al., 1992). However, it was recently shown that MTX (100 nM- 30 µM) alone cannot activate AMPK, in purified rat liver and that MTX (5 µM) was not sufficient to increase the AICAR:ATP ratio in L6 myotubes for 16 h (Chibalin, 2015). Although this has not been proven in PBMCs, activated or unactivated, measurement of the ATP/AMP ratio is still an important indicator of energy homeostasis, on which the effect of MTX can be measured.

5.1.2 The effect of MTX on intracellular sugar-nucleotides

There are no significant findings regarding the effect of MTX on intracellular sugar-nucleotides, which act as sugar donors in glycosylation reactions. There have only been two reports found which examined the effect of MTX on UDP-*N*-acetylglucosamine and neither showed whether the MTX-induced changes were significant. One report found that MTX (10 µM) treatment for 6 h showed an upward trend in the levels of dUDP-*N*-acetylglucosamine compared to untreated cells in a cultured human lymphoblast cell line (Peterson et al., 1983). Another found that MTX (2.5 nM) treatment for 72 h, reduced the levels of UDP-*N*-acetylglucosamine in Jurkat cells (Miura et al., 2010). The effect of MTX on the concentration of any other sugar nucleotide has not been investigated.

5.1.3 Activation-dependent effects on nucleotides and sugar-nucleotides

Activated T cells undergo metabolic reprogramming, with a shift to a more glycolytic phenotype, for greater ATP production and to allow for increased flux through the pentose phosphate and other building block-plenty pathways (Fernandez-Ramos et al., 2016). Indeed, a sustained increase in PRPP was found during mitogenic-stimulation of human lymphocytes to allow for the increased requirement for de novo purine synthesis (Allison and Eugui, 2000). The rate of de novo purine synthesis was also shown to increase during polyclonal activation of T cells, measured by an increase in [^{14}C]glycine incorporation into purine nucleotides (Allison and Eugui, 2000). However, detailed analysis on changes to nucleotides and sugar-nucleotides during activation is limited, with the most extensive studies conducted on PHA-stimulated CD4^{+} T cells and anti-CD3/CD28-activated T cells (Fairbanks et al., 1995, Wang et al., 2011a).

Anti-CD3/CD28 activated CD4^{+} and CD8^{+} T cells were shown to have elevated levels of UDP-*N*-acetylglucosamine 24 h after activation (Swamy et al., 2016). Ribulose-5-phosphate has been shown to be increased in T cells activated for up to 30 h (Wang et al., 2011a). There are also two reports of changes to UDP-glucose following activation (Fairbanks et al., 1995, Wang et al., 2011a). However, it is not known whether activation-dependent changes occur for all the sugar-nucleotides.

It is not known whether changes to the ATP/AMP ratio that occur early in activation are sustained for the duration of the activation period. The switch to a more glycolytic phenotype upon T cell-activation following TCR ligation is widely accepted, with a resultant increase in intracellular ATP 24 h post activation prior to the first cell division (Wang and Green, 2012b). However, the ATP/AMP ratio has not been measured after a 72 h anti-CD3 activation. Understanding the global changes that accompany any alteration in the ATP/AMP ratio is crucial in investigating how MTX can limit cellular function.

Knowledge of the specific intracellular nucleotides and sugar-nucleotides which show activation-dependent changes is crucial for understanding any MTX-mediated effects seen in the absence and following activation.

5.2 Aims of the chapter

Detailed flux analysis, measuring a variety of purine and pyrimidine nucleotides, as well as a variety of sugar-nucleotides upon activation has not been shown. Analysis of these intracellular sugar-nucleotides during activation could highlight how global glycosylation changes occur during cellular activation, as discussed in (see Section 1.22.5). It is also not known how low-dose MTX can affect this pathway and whether there are differential effects of MTX treatment in activated compared to unactivated PBMCs. Exploration of both these may shed light as to whether MTX may affect glycosylation patterns by perturbing the level of sugar nucleotide donors via purine and thymidine nucleotide inhibition.

Specifically, the aims of this project are:

1. To quantify the activation-induced changes in the levels of nucleotides and sugar-nucleotides in anti-CD3-activated PBMCs using HPLC.

2. To measure the effect of MTX on the ATP/AMP ratio in unactivated and anti-CD3-activated PBMCs.

3. To compare the effect of MTX on the nucleotide and sugar nucleotide pathway in unactivated and anti-CD3-activated PBMCs and in particular CMP-*N*-acetylneuraminic acid to see if correlations can be made with the intracellular levels of this sugar nucleotide with MTX treatment to the changes on the cell-surface ManNAz-derived sialic acids.

4. To investigate whether purine and thymidine nucleotide levels can affect the resultant sugar nucleotide, in both anti-CD3-activated and unactivated PBMCs.

5.3 Materials and methods

5.3.1 Extraction of intracellular nucleotides and nucleotide sugars

The extraction of intracellular nucleotides and sugar-nucleotides was developed by Dr Paul Voorheis and adapted by Dr Yongjing Xie, as shown in (Fig 5.2). PBMCs were counted on a haemocytometer after treatments. PBMCs (1.2 X 10^7 cells) were then pelleted and suspended in 20 ml PBS. After centrifugation, the supernatant was completely removed and the pellet resuspended in 3 ml ice-cold 50% (v/v) acetonitrile (ACN). The cells were vortexed vigorously for a total of 5 min per sample, alternating between samples for 1 min intervals. The cells were then flash-frozen before thawing on ice for 15 min. The cells were vortexed again for 5 min. The 3 ml extraction volume was divided into two 1.5 ml eppendorfs and centrifuged at 16,000 g for 10 min at 4°C. 1.4 ml of supernatant was taken off the pellet and then dried in a Speed Vac set at room temperature. This extraction procedure was repeated twice more on the remaining pellet, with each supernatant being added to the existing eppendorf in the Speed Vac. The accumulated extractions were then dried at 35°C for ~3-4 h until the pellet was visibly dry and frozen at -80°C immediately after drying. Before running on HPLC, the sample was resuspended in 100 µl potassium phosphate buffer 100 mM, ph. 5.5 and the samples centrifuged for 16,000 g for 1 h at 4°C. 25 µl of the sample was applied to the column.

5.3.2 Ion-pair RP-HPLC analysis

Gradient separation was carried out on a Gemini C18 reverse-phase column (3 µm, 150 X 4.6 mm), on a Waters 2695 Separations module fitted with a Waters 2487 Dual λ absorbance detector. Components were separated using a Potassium phosphate 100 mM mobile phase containing the ion-pair reagent, tetrabutylammonium bisulphate hydrogen sulphate 8 mM, and the pH adjusted to 5.5 with potassium hydroxide (KOH) (buffer A) and a second identical buffer, containing 25% methanol (buffer B). The buffers were degassed and passed through a 0.22 µm filter. Detection of nucleotides and sugar-nucleotides was measured at 254 nm. Before each run, the solvent lines, seal and injection needle were primed with their respective buffers (7.5 mL/min, 10 min). The column was preheated to 30°C and equilibrated with buffer A (0.8 mL/min) for 30 min.
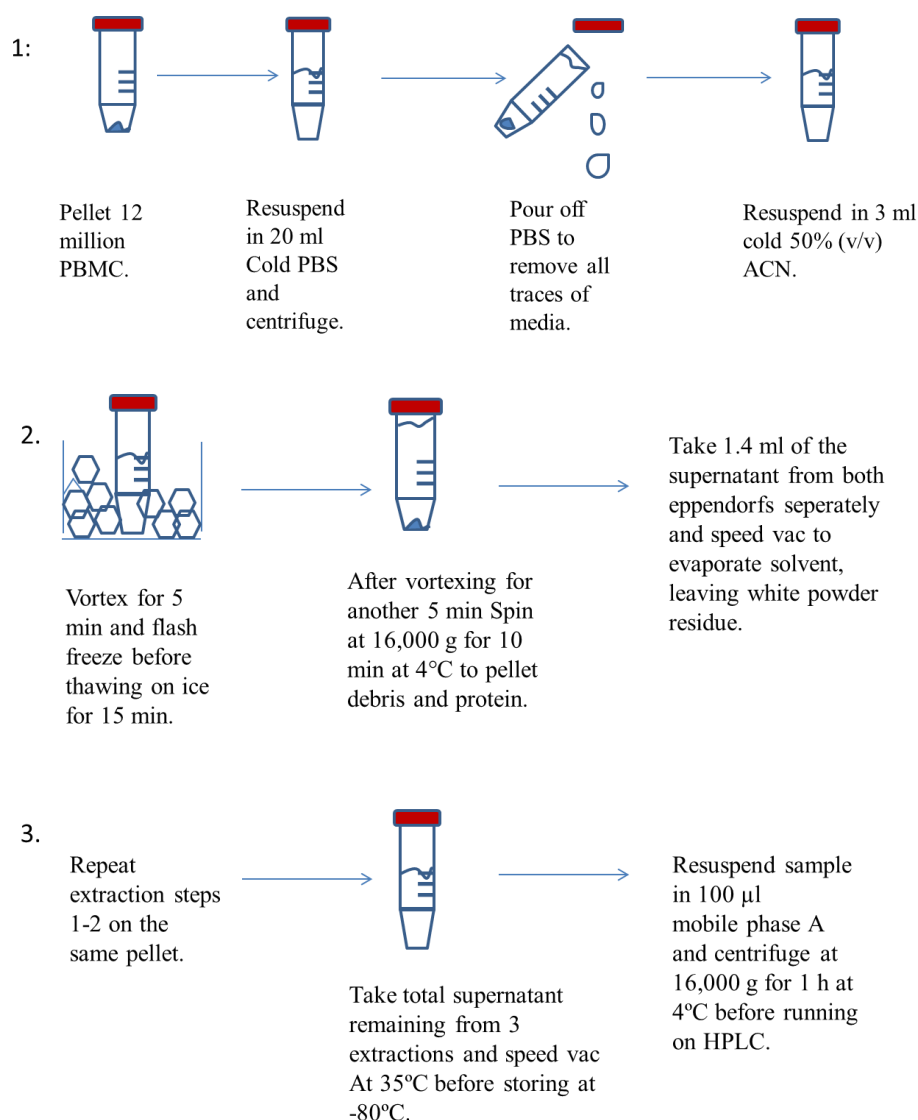
Figure 5.2. PBMC extraction method for HPLC analysis.

Cells were washed with PBS to remove any media contaminants. The supernatant was poured off and the pellet resuspended in 3 ml cold 50% ACN. The solution was then vortexed for 5 min before being flash frozen and thawed on ice for 15 min. The sample was vortexed for another 5 min before being centrifuged at 16,000 *g* for 10 min at 4°C to pellet the cellular debris and large soluble proteins. 1.4 ml of the supernatant was taken off and dried using a speed vac (at r.t). The extraction was repeated twice more on the pellet before combining the supernatants and drying at 35°C on the same day for ~3-4 h until the pellet was completely dry and immediately storing at -80°C. Before HPLC analysis the samples were suspended in 100 µl and centrifuged at 16,000 *g* for 1 h at 4°C. Based on the extraction developed by Dietmair et al. (2010).

The separation was carried out according to the flow gradient below.

The elution gradient was carried out at a constant flow rate of 0.8 ml/min as follows: At 0 min, the gradient was 100% buffer A flowing for 8 min. At 8 min 35% buffer B was introduced over the next 24 min and at 32 min, was increased to 38% buffer B over the next 2 min. At 34 min the gradient adjusted to 100% buffer B over the course of 5 min and was maintained at 100% buffer B for 10 min. At 49 min, buffer A was brought up to 100% over the course of 2 min and was maintained at 100% buffer A for 8 min to re-equilibrate the column for the next run. The column was cleaned following each set of runs using buffer C (30% MeOH in H20) and buffer D (50% MeOH in H20) for 30 min.

## 5.3.3 Determination of metabolite concentrations from standards

Standards were diluted to the required concentration using 100 mM phosphate buffer and filtered with a VWR acetate cellulose syringe filter (0.22 μm). A 25 μL volume of each standard was injected onto the column. Standards of the nucleotides and sugar-nucleotides were run individually and then after as a mixture, containing the 27 purine and pyrimidine nucleotides as well as the 7 sugar-nucleotides at 10 μM. These were used to identify compounds in the cell extracts based on the retention time on the column (Fig 5.3). Resolution of each compound was achieved except for the co-elution of the following standard pairs: GMP/IMP, ADP/UTP, GDP/GDP-fucose, UDP/UDP-*N*-acetylglucosamine and adenosine/TMP/GDP-mannose/UDP-*N*-acetylgalactosamine.

Qualitative analysis of the metabolites was achieved by either using a standard concentration curve ranging from 0.9375 μM-120 μM as a reference, which was generated as part of the HPLC programme or for metabolites that were measured later in this study, using a published integrative-method (Giannattasio et al., 2003). This details the integration of a known concentration of a standard to determine an unknown concentration of the same standard by solving for 'x'. Qualitative analysis for ATP, TTP, uracil, TDP, inosine and guanosine, CDP, hypoxanthine, CMP was carried out using this method. The integration was carried out by calculating the area under the peak using Empower 3 Chromatography Data software, for the μmoles present in 25 μl of each standard at a known concentration. Concentrations of the unknown peaks were calculated using Graph Pad Prism.
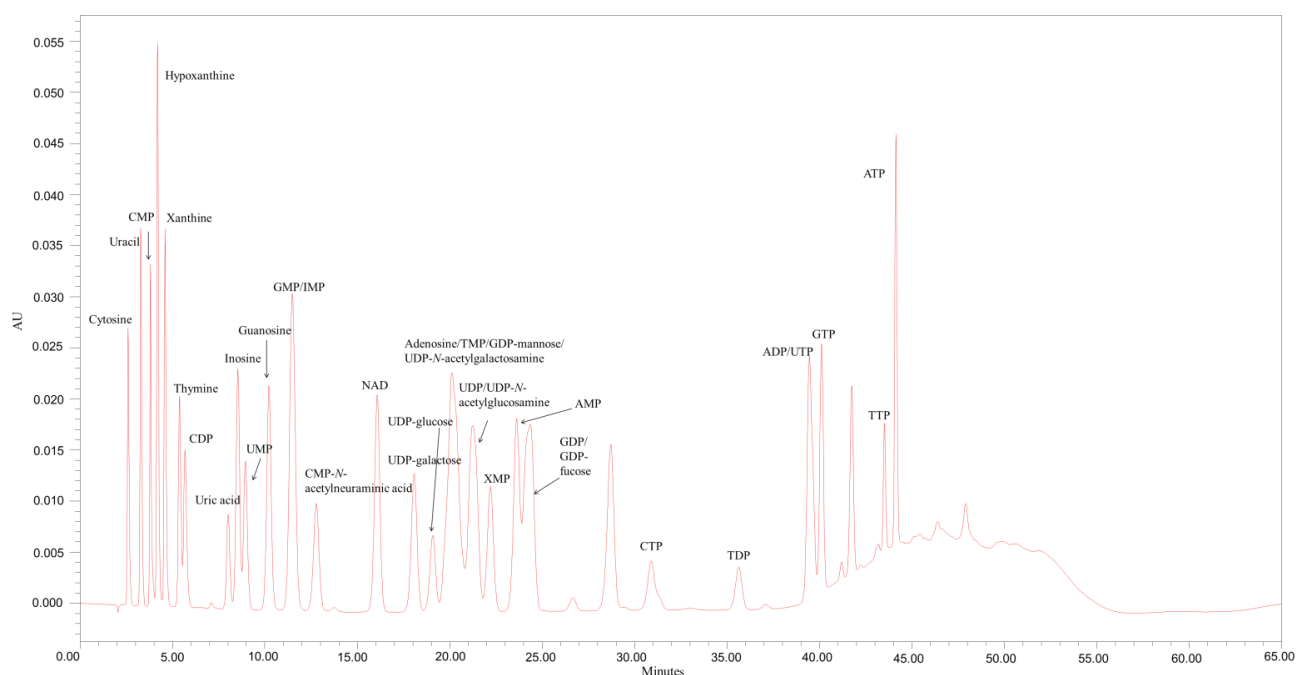
Figure 5.3. **HPLC profile of the standard mix of pyrimidines, purines and sugar-nucleotides**.

Separation was achieved using potassium phosphate buffer 100 mM, containing the ion-pair reagent, tetrabutylammonium bisulphate hydrogen sulphate 8 mM with a gradual introduction of organic solvent, methanol. Pyrimidines (10 μM); cytosine, uracil, CDP, CMP, CTP, thymine, UMP, TMP, UDP, UTP, TDP, TTP, purines (10 μM); uric acid, IMP, ADP, adenosine, XMP, ATP, GDP, guanosine, xanthine, inosine, GMP, AMP, GTP ,hypoxanthine and the sugar-nucleotides (10 μM); CMP-*N*-acetylneuraminic acid, UDP-galactose, UDP-glucose, UDP-*N*-acetylgalactosamine, UDP-*N*-acetylglucosamine, GDP-fucose, GDP-mannose, along with NAD, were run individually and then as a mixture. The standard peak at 29 min was unidentified. Peaks were identified from individual runs of each standard and used to identify unknown compounds from cellular extracts.

212
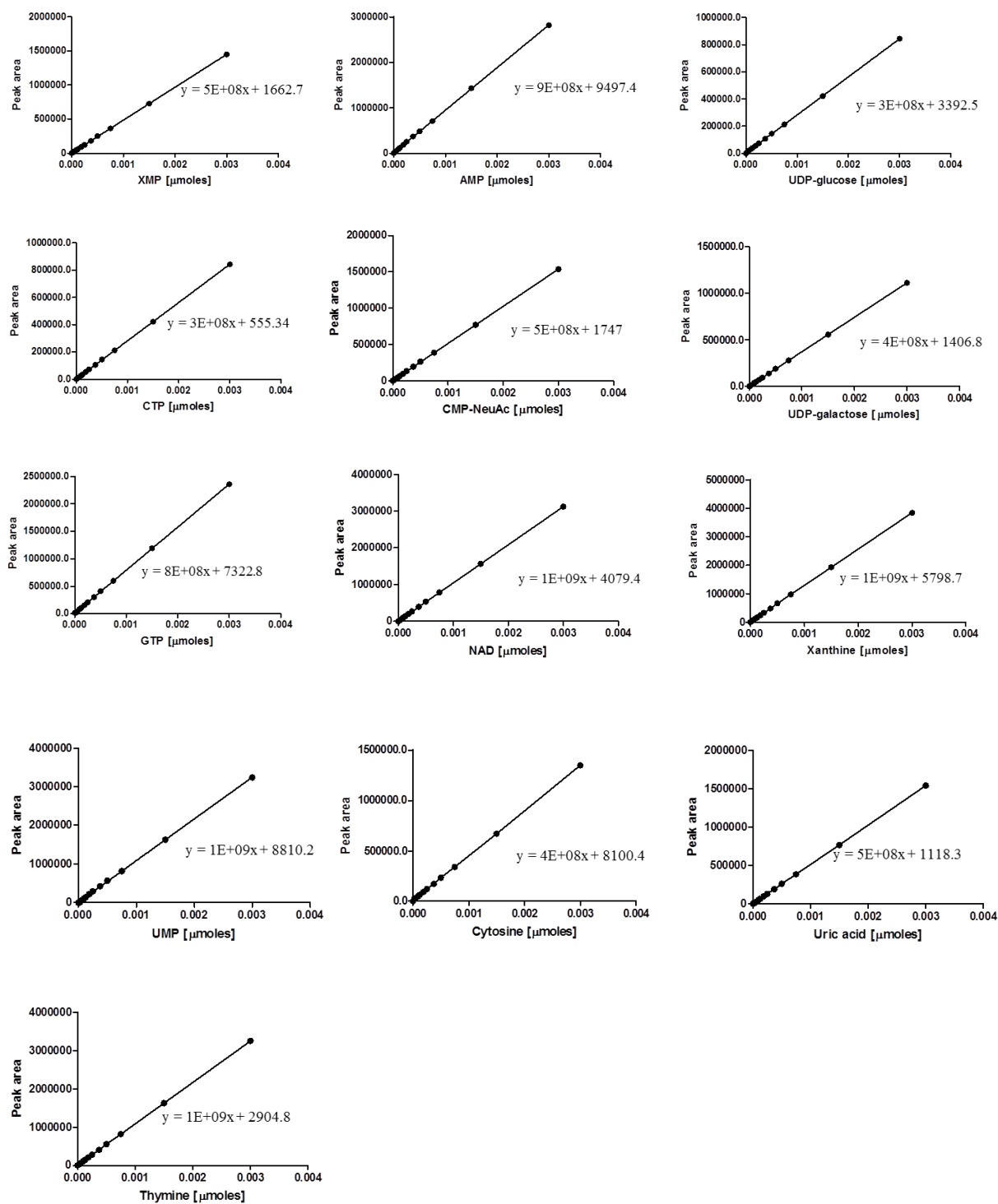
Figure 5.4 Standard curves used to determine the concentration of the peaks from the PBMC extracts.

A range of concentrations of each standard was run from 0.9375 μM-120 μM. The peak area corresponding to the μmoles in 25 μl for each concentration was plotted and a linear regression curve used to determine the μmoles in each extracted metabolite.

The contribution of dead cells to the metabolite profile was unknown and dead cell numbers varied between conditions and donors. However, it was not possible to account for any contribution made by dead cells. As such, the number of μmoles per million PBMCs was determined by accounting for the total μmoles present in 100 μl from 12 million PBMCs, when only 25 μl of this sample was injected on to the HPLC column, and dividing by 12.

5.3.4 Standard recovery

To ensure that any possible differences detected in the metabolites were not due to differential recoveries from the acetonitrile extraction, standard mixes were put through the extraction in triplicate and compared to the same standard mixture which was not brought through the extraction (Fig 5.5) The % standard recovery [extracted standard] *100/ [non-extracted standard] was carried out for each standard showing that there was no loss of metabolites following the extraction (Fig 5.5).

A
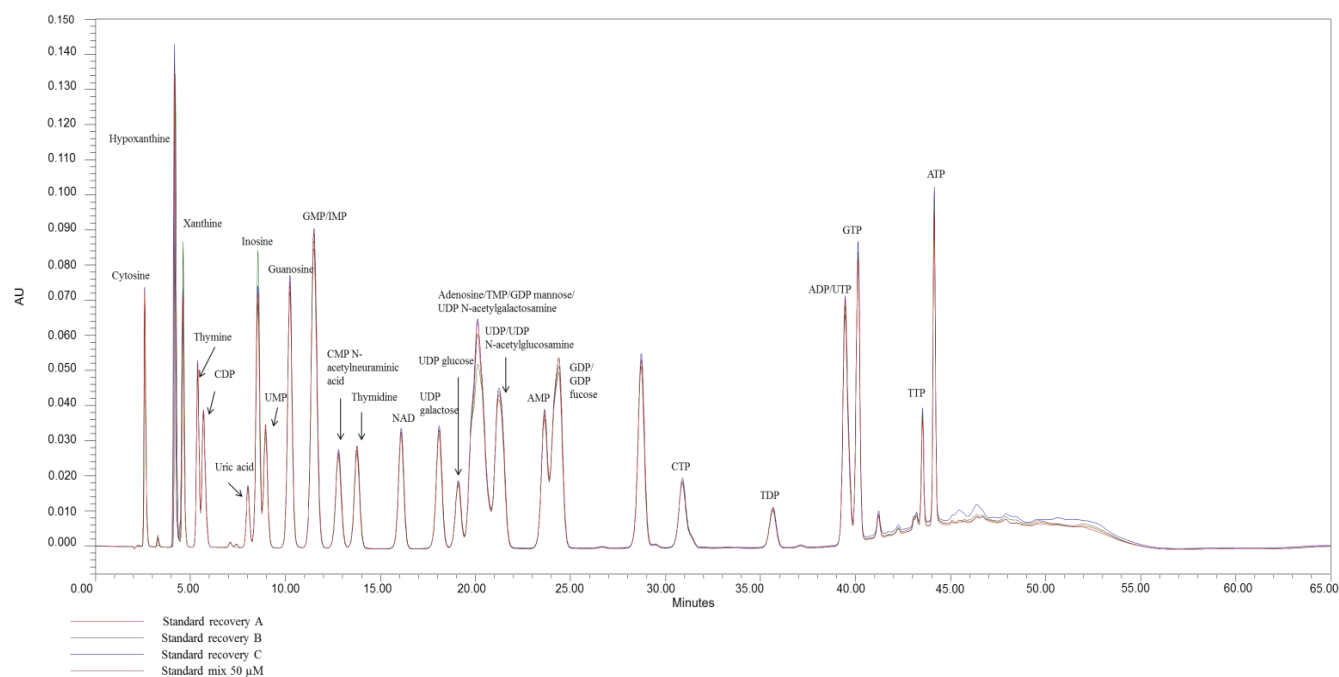
B
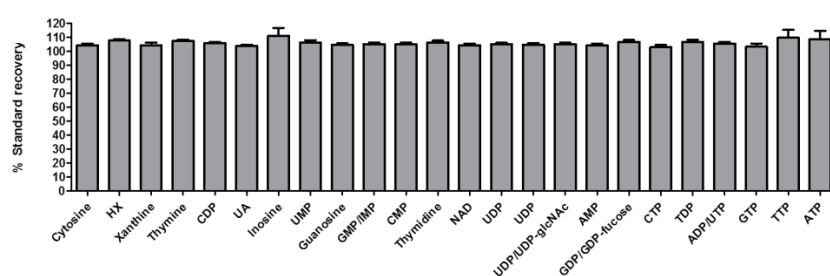
Figure 5.5. The 50% acetonitrile extraction procedure results in minimal loss of metabolites.

The complete set of standards (50 μM), (uracil, XMP and CMP were omitted), as well as thymidine were brought through the entire extraction procedure in triplicate (standard recovery A, B and C) and compared to the identical mixture not brought through the extraction (standard mix 50 μM). 100 μl of each standard mix was extracted with 3 freeze thaw cycles of 3 ml 50% ACN before combining the extracted solution and drying. The remaining standard mix was frozen at -80°C. Each extracted standard mix was dissolved in 100 μl potassium phosphate buffer. The peaks were compared to the same volume of frozen standards. Data are presented as (A) representative HPLC traces and (B) the mean ± SEM of the % standard recovery [extracted standard] *100/ [non-extracted standard].

5.4 Results

The extraction procedure conducted in triplicate, from 12 million PBMCs from the same donor showed little variability (Fig 5.6). Metabolites were identified based on the retention times of known standards. CMP, XMP, uric acid, TDP, guanosine and CMP-*N*-acetylneuraminic acid were not detected in the samples and the identification of hypoxanthine, thymine, and thymidine was unclear due to variability in peak shape between runs. In addition, the metabolites which co-eluted as standards (adenosine, TMP, GDP-mannose, UDP-GalNAc) as well as (GDP/GDP-fucose), (UDP/UDP-GlcNAc), (GMP/IMP), were omitted from further quantitative analysis. Peaks which did not correspond with the retention times of the standard mixes were unidentified.

The activation of PBMCs with anti-CD3 resulted in an increase in specific metabolites to varying degrees (Fig 5.7). Any significant differences between the unactivated PBMCs after 24 h were compared to their activated counterparts after 72 h using an unpaired student T-test because although the donors were matched the data sets were not. XMP increased to detectable levels in the anti-CD3-activated samples and although there was an upward trend, there was no significant increase in the concentration of inosine, GTP or xanthine (Fig 5.8). NADH was later found to co-elute with NAD (not shown) which means it is only possible to measure the nicotinamide moieties, NAD/NADH which showed no change upon activation.

The concentrations of the pyrimidine nucleotides CDP, CTP and TTP significantly increased upon activation but there was no significant increase in cytosine or uracil (Fig 5.9). UMP was not detectable in unactivated PBMCs extracted from two donors. The concentration of AMP significantly increased but there was no significant increase in ATP or the ATP/AMP ratio (Fig 5.10). Significant activation-dependent differences were also detected for UDP-glucose and UDP-galactose, as well as CMP-*N*-acetylneuraminic acid which was undetectable in the unactivated PBMCs but was present at low concentrations following activation (Fig 5.11). The fold increase was not the same for each metabolite upon activation (Table 5.1).
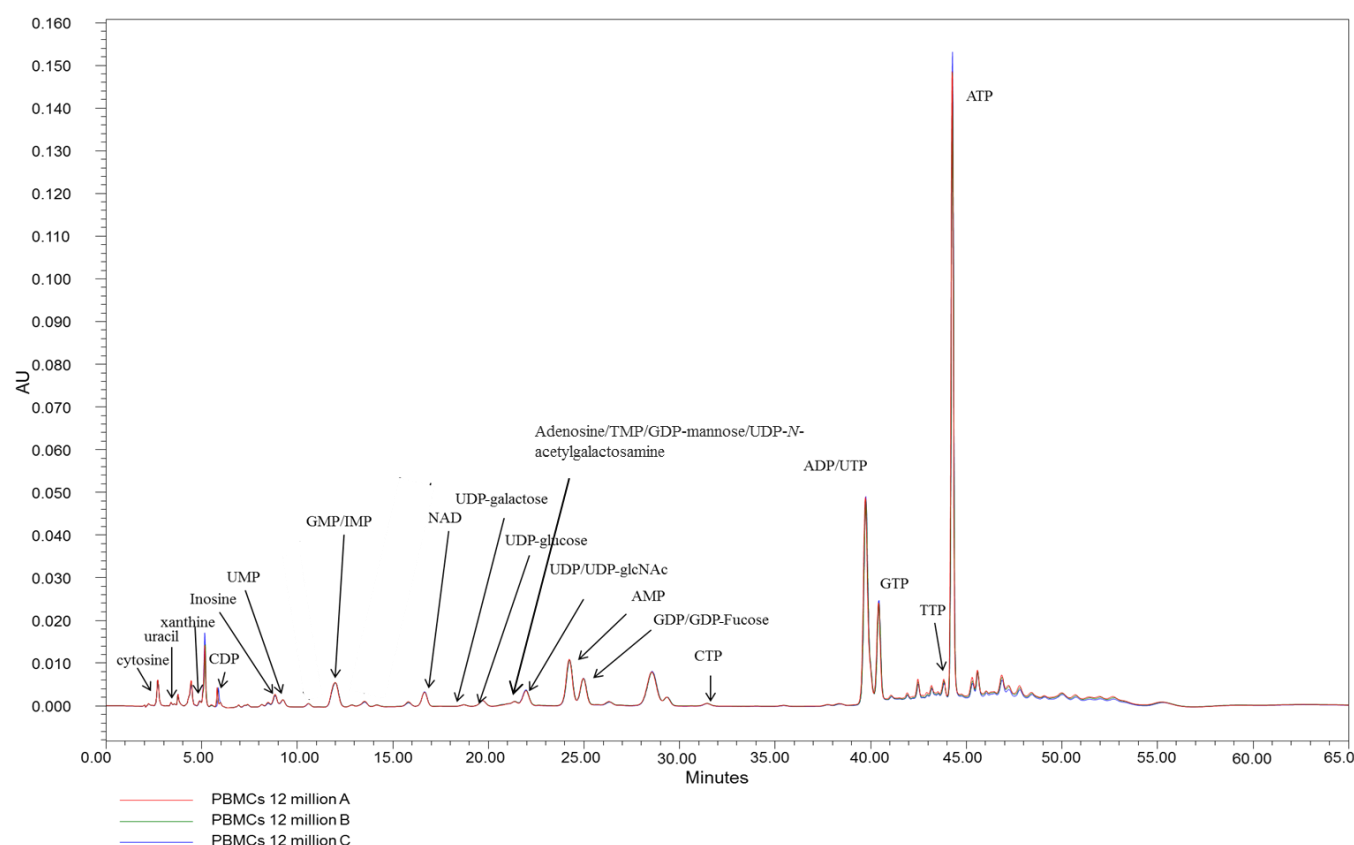
Figure 5.6. Reproducibility of the extraction method from PBMCs.

12 million viable PBMCs were washed in PBS and centrifuged. The samples were subjected to 3 freeze thaw cycles using 3 ml 50% ACN, overtaxing for 5 min before and after each freeze thaw cycle. 1.4 ml of the supernatant was collected after centrifugation at 16,000 g for 10 min at 4°C leaving 100 µl to avoid disturbing the pellet. The accumulated supernatant was then dried at 35°C before being stored at -80°C. The sample was then resuspended in 100 µl phosphate buffer, further diluted 1:2 and 20 µl of the sample was then loaded on the HPLC C18 column. Data are representative of three separate extractions conducted at the same time from the same donor.
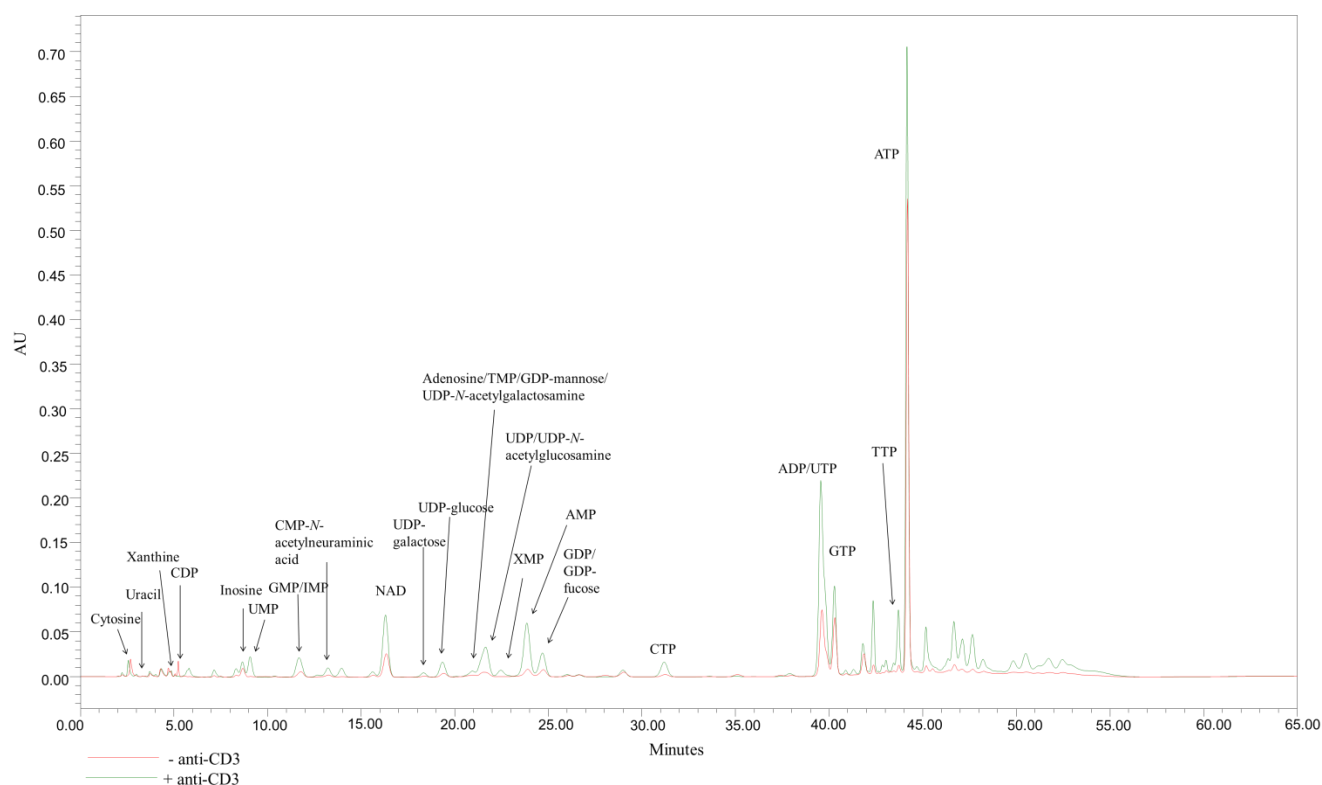
Figure 5.7. Analysis of nucleotides and sugar-nucleotides in unactivated and anti-CD3-activated PBMCs.

PBMCs (1 X $10^{\wedge}6$ cells/ml and 55 ml/T175 flask) were seeded in anti-CD3-coated plates for 72 h or left unactivated for 24 h. 12 million viable PBMCs were subjected to 3 freeze thaw cycles using 3 ml 50% ACN. The accumulated supernatant was then dried at 35°C before being stored at -80°C. The sample was then resuspended in 100 μl phosphate buffer. 25 μl of the sample was then loaded on the HPLC C18 column. Data are representative of one donor.
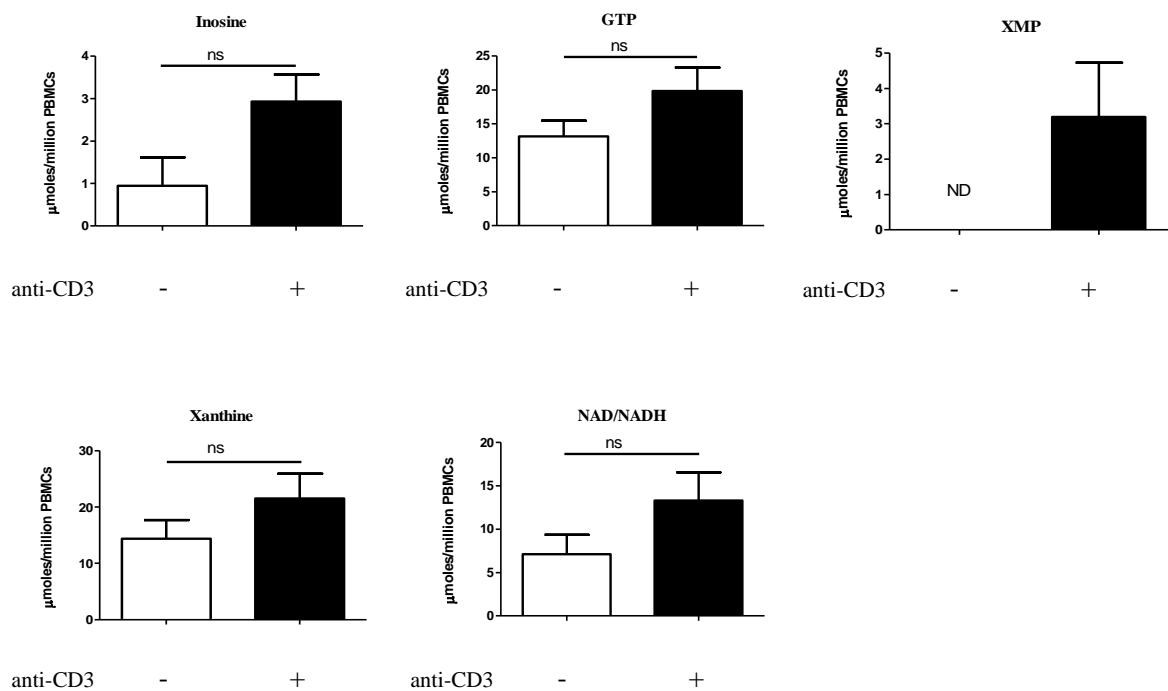
Figure 5.8. Qualitative analysis of purine and NAD/NADH nucleotides following anti-CD3-activation.

PBMCs (1 X 10^6 cells/ml and 55 ml/T175 flask) were seeded in anti-CD3-coated plates for 72 h or left unactivated for 24 h. 12 million viable PBMCs were subjected to 3 freeze thaw cycles using 3 ml 50% ACN. The accumulated supernatant was then dried at 35°C before being stored at -80°C. The sample was then resuspended in 100 μl phosphate buffer. 25 μl of the sample was then loaded on the HPLC C18 column. No significant increase was found for inosine, GTP, xanthine or NAD/NADH upon activation, except for XMP which was detected in activated samples. Data are represented as mean ± SEM, n=3, an unpaired student T-test was performed except for XMP which was not detectable (ND) in unactivated PBMCs and significant differences are indicated with *P<0.05 or, **P<0.01.

.

Figure 5.9. The pyrimidine nucleotides CDP, CTP and TTP increase in PBMCs following anti-CD3-activation.

PBMCs (1 X $10^{\wedge}6$ cells/ml and 55 ml/T175 flask) were seeded in anti-CD3-coated plates for 72 h or left unactivated for 24 h. 12 million viable PBMCs were subjected to 3 freeze thaw cycles using 3 ml 50% ACN. The accumulated supernatant was then dried at 35°C before being stored at -80°C. The sample was then resuspended in 100 µl phosphate buffer. 25 µl of the sample was then loaded on the HPLC C18 column. There was no significant change found in cytosine or uracil. Data are represented as mean ± SEM, n=3, (except for UMP which is an n=1), an unpaired student T-test was performed and significant differences are indicated with *P<0.05 or, **P<0.01.

.

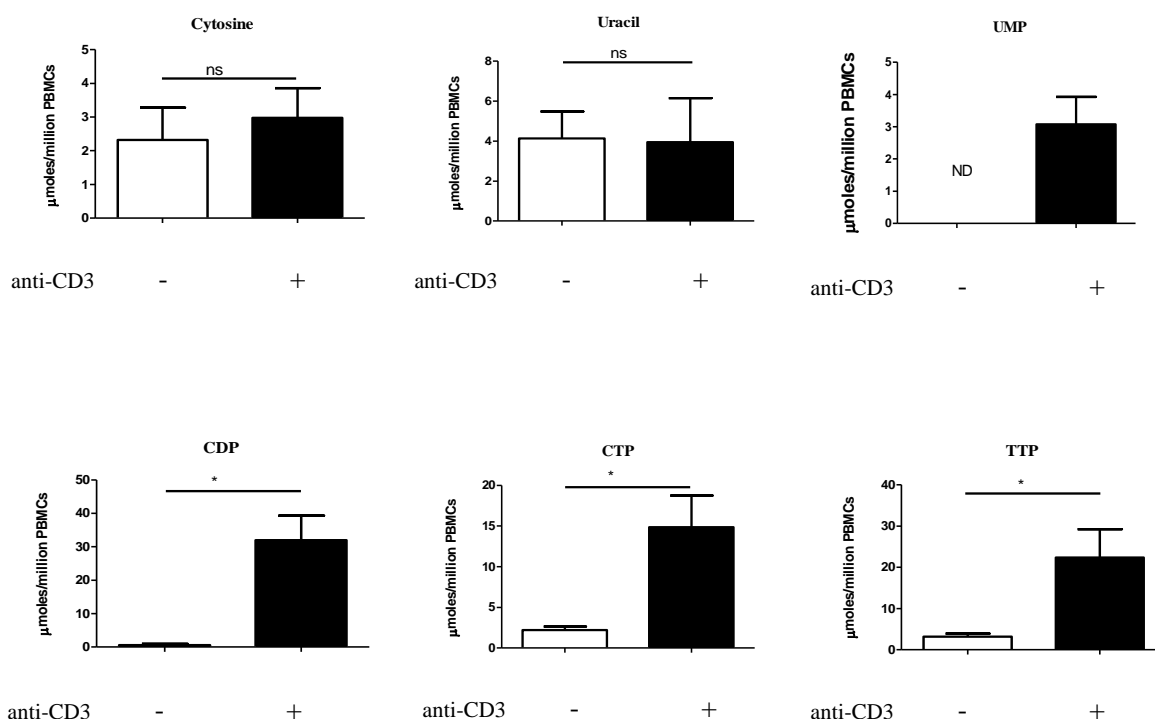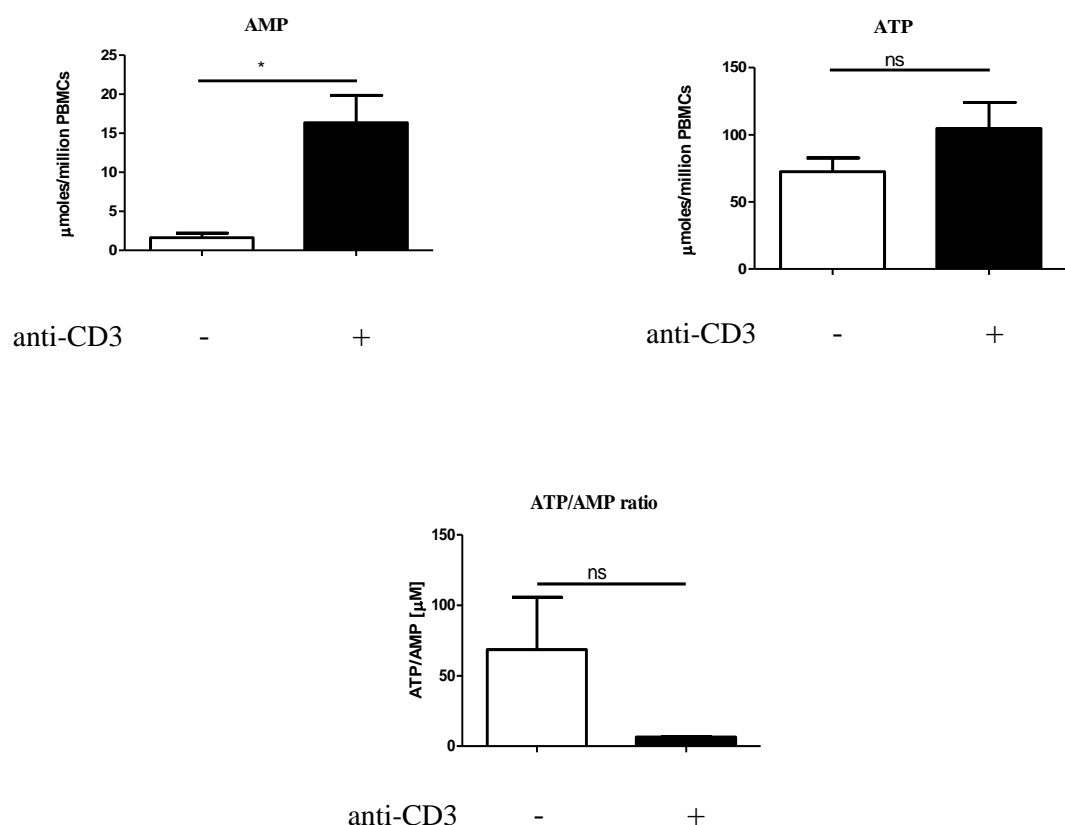**Figure 5.10. Qualitative analysis of AMP and ATP following anti-CD3-activation.**

PBMCs (1 X 10^6 cells/ml and 55 ml/T175 flask) were seeded in anti-CD3-coated plates for 72 h or left unactivated for 24 h. 12 million viable PBMCs were subjected to 3 freeze thaw cycles using 3 ml 50% ACN. The accumulated supernatant was then dried at 35°C before being stored at -80°C. The sample was then resuspended in 100 µl phosphate buffer. 25 µl of the sample was then loaded on the HPLC C18 column. There was a significant increase in AMP, but no significant change was found in ATP or the ATP/AMP ratio after activation. Data are represented as mean ± SEM, n=3, an unpaired student T-test was performed and significant differences are indicated with *P<0.05 or, **P<0.01.
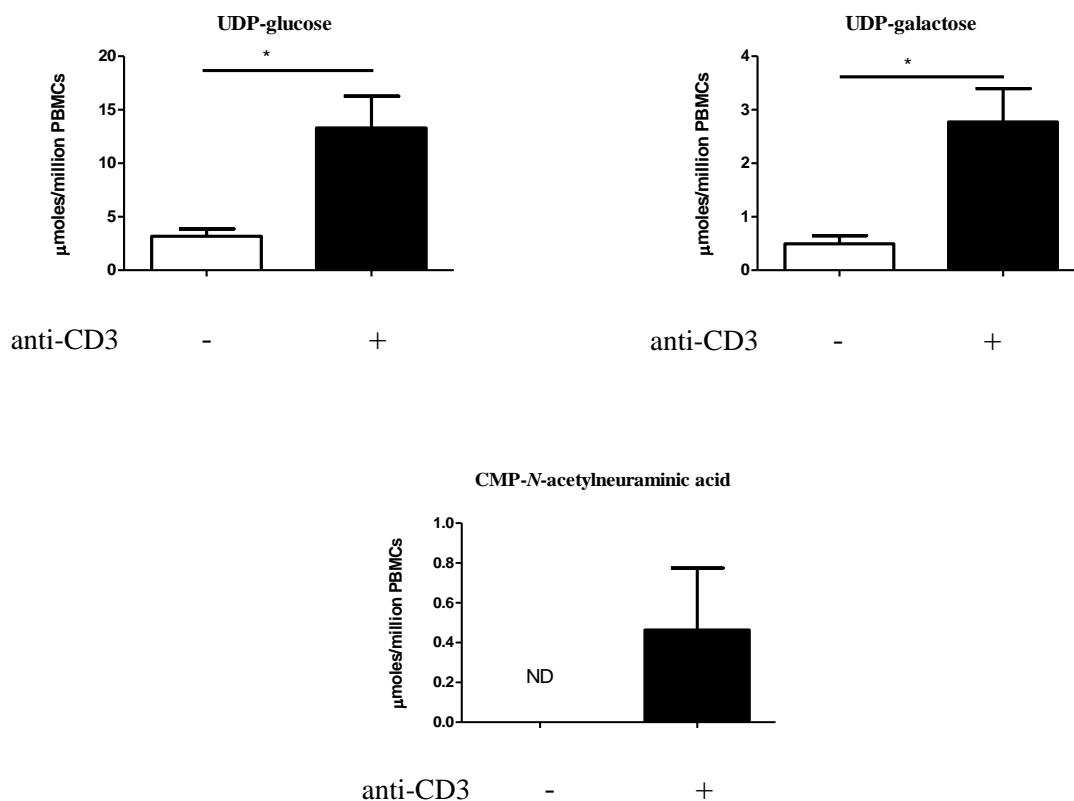
Figure 5.11. UDP-galactose, UDP-glucose and CMP-*N*-acetylneuraminic acid increase during anti-CD3-activation.

PBMCs (1 X 10^6 cells/ml and 55 ml/T175 flask) were seeded in anti-CD3-coated plates for 72 h or left unactivated for 24 h. 12 million viable PBMCs were subjected to 3 freeze thaw cycles using 3 ml 50% ACN. The accumulated supernatant was then dried at 35°C before being stored at -80°C. The sample was then resuspended in 100 µl phosphate buffer. 25 µl of the sample was then loaded on the HPLC C18 column. Data are represented as mean ± SEM, n=3, an unpaired student T-test was performed (except for CMP-*N*-acetylneuraminic acid which was not detectable (ND) in unactivated PBMCs and is an n=2 in activated donors) and significant differences are indicated with *P<0.05 or, **P<0.01.

| Average fold change upon anti-CD3 activation			
	mean		SEM
Cytosine	1.9 ±		1.1
Uracil	1.4 ±		0.9
Xanthine	1.8 ±		0.7
CDP	24.5 * ±		15.9
Inosine	4 ±		2.3
GMP/IMP	8.1 ±		2.2
NAD/NADH	2.5 ±		1
UDP-galactose	7.1* ±		3.2
UDP-glucose	4.7* ±		1.6
UDP/UDP-glcNAc	8.1 ±		3.1
AMP	12.0* ±		2.9
GDP/GDP-fucose	3.7 ±		0.7
CTP	7.5* ±		2.7
ADP/UTP	3.4 ±		0.6
GTP	1.7 ±		0.5
TTP	6.9* ±		0.6
ATP	1.5 ±		0.4
ATP/AMP	0.2 ±		0.1

Table 5.1. The fold change following anti-CD3-activation varies for each metabolite.

The fold change was not possible to detect for metabolites not present in unactivated PBMCs, including XMP and CMP-*N*-acetylneuraminic acid. Data are presented as the mean ± SEM, of the fold change ([anti-CD3-activated]/[unactivated]), n=3, with significant differences indicated by *P<0.05 or, **P<0.01.

The effect of MTX (100 nM) on these metabolites was investigated in both unactivated and anti-CD3-activated PBMCs (Fig 5.12). Treatment with MTX for 24 h had no significant effect on the concentration of purine salvage nucleotides xanthine and inosine, or GTP and NAD/NADH nucleotides (Fig 5.13). There was also no significant effect on the pyrimidine nucleotides and their precursors, CDP, CTP, TTP, cytosine and uracil (Fig 5.14). No significant difference was found in the levels of AMP, ATP nucleotides or in the ATP/AMP ratio following MTX treatment (Fig 5.15). Purine and thymidine rescue had no effect on reversing MTX treatment in any metabolite tested, but rescue potentiated the effect of MTX on reducing normalised CDP levels. No significant difference was found in UDP-glucose or UDP-galactose levels following MTX treatment or with purine and thymidine rescue in unactivated PBMCs (Fig 5.16).

The effect of MTX treatment was also investigated in anti-CD3-activated PBMCs (Fig 5.17). Analysis of the raw data revealed that MTX reduced the concentration of NAD/NADH nucleotides but had no significant effect on inosine, GTP, xanthine or XMP levels (Fig 5.18). Purine and thymidine rescue reversed the MTX-mediated reduction of NAD/NADH.

MTX also significantly reduced the concentration of CDP which was normalised to control levels, and although there was a downward trend in the levels of normalised CTP and raw data values for cytosine, these were not found to be significant. No significant effect was found on the pyrimidines TTP, uracil or UMP (Fig 5.19). Purine and thymidine rescue had no effect on the MTX-mediated reduction of CDP. No effect was found on ATP or AMP nucleotides following MTX treatment (Fig 5.20). Although there was a downward trend, there was no significant effect of MTX on the ATP/AMP ratio in these anti-CD3-activated PBMCs. The effects of MTX on the concentration of sugar-nucleotides was next evaluated. It revealed that there was no significant effect of MTX on either UDP-glucose, UDP-galactose (Fig 5.21). Purine and thymidine rescue had no effect in reversing or potentiating the effects of MTX.
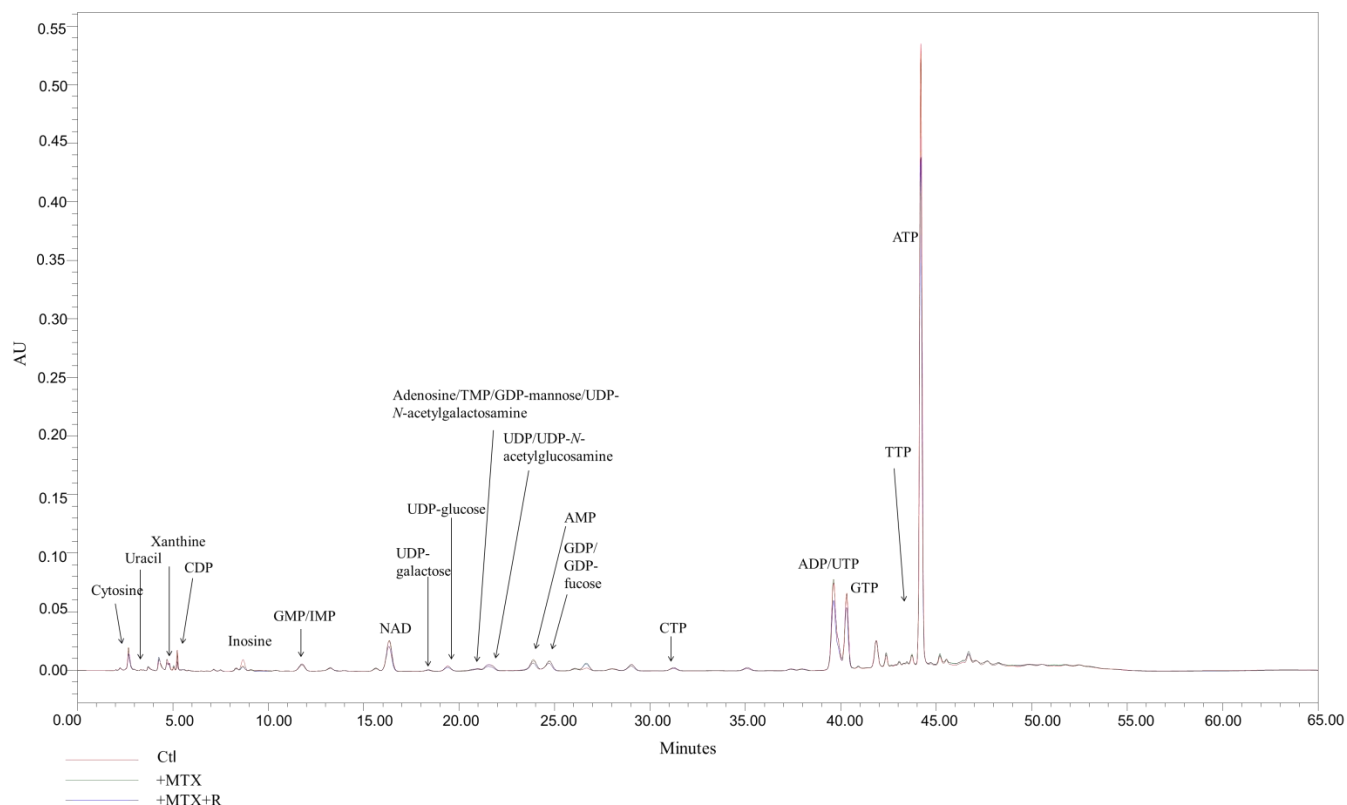
Figure 5.12. Analysis of nucleotides and sugar-nucleotides in unactivated PBMCs ± Methotrexate.

PBMCs (1 X 10$^{\wedge}$6 cells/ml and 55 ml/T175 flask) were seeded in the presence or absence of MTX 100 nM ± thymidine and hypoxanthine 100 μM. for 24 h. 12 million viable PBMCs were subjected to 3 freeze thaw cycles using 3 ml 50% ACN. The accumulated supernatant was then dried at 35°C before being stored at -80°C. The sample was then resuspended in 100 μl phosphate buffer. 25 μl of the sample was then loaded on the HPLC C18 column. Data are representative of one donor.
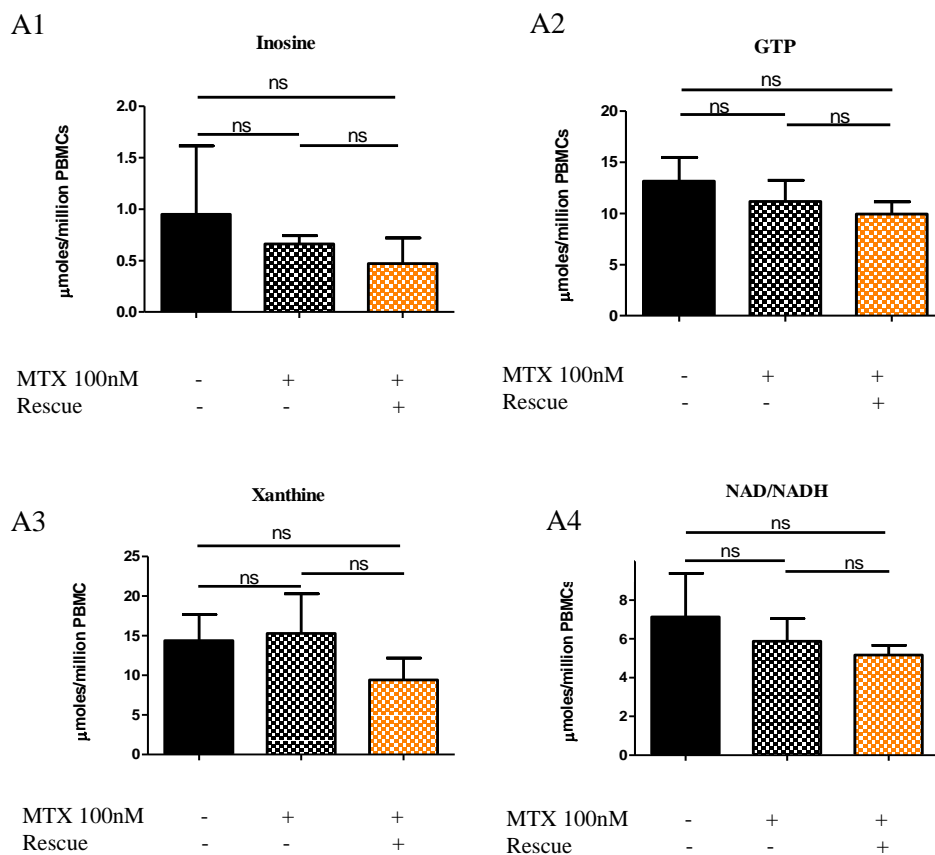
Figure 5.13. Qualitative analysis of purines and NAD/NADH nucleotides in unactivated PBMCs ± Methotrexate.

PBMCs (1 X 10^6 cells/ml and 55 ml/T175 flask) were seeded in the presence or absence of MTX 100 nM ± thymidine and hypoxanthine 100 μM. for 24 h. 12 million viable PBMCs were subjected to 3 freeze thaw cycles using 3 ml 50% ACN. The accumulated supernatant was then dried at 35°C before being stored at -80°C. The sample was then resuspended in 100 μl mobile phase A. 25 μl of the sample was then loaded on the HPLC C18 column. There was no significant change in inosine, xanthine, GTP or NAD/NADH nucleotides with MTX treatment. Data are represented as (A1-A4) mean ± SEM, n=3, (B1-B4) mean ± SEM, n=3, normalised to ctl (set at 100%). A one-way ANOVA followed by Tukey's multiple comparison test was performed with significant differences indicated by *$P<0.05$ or, **$P<0.01$.

B1

Inosine

| MTX 100nM | - | + | + |
| Rescue | - | - | + |

B2

GTP

| MTX 100nM | - | + | + |
| Rescue | - | - | + |

B3

Xanthine

| MTX 100nM | - | + | + |
| Rescue | - | - | + |

B4

NAD/NADH
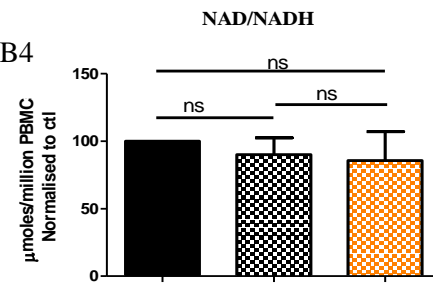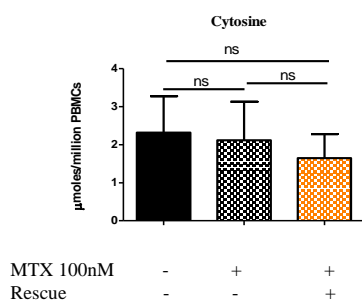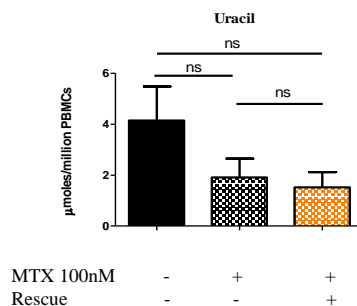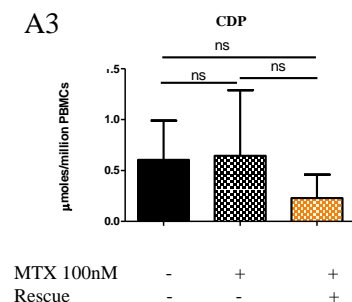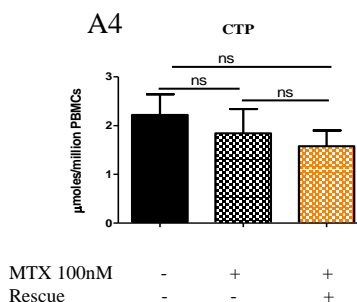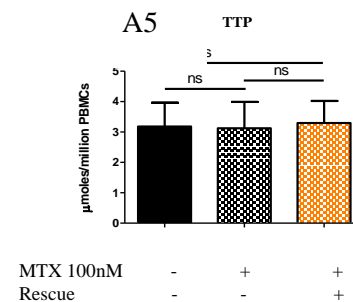
| MTX 100nM | - | + | + |
| Rescue | - | - | + |

Figure 5.14. Qualitative analysis of pyrimidine metabolites in unactivated PBMCs ± Methotrexate.

PBMCs (1 X 10^6 cells/ml and 55 ml/T175 flask) were seeded in the presence or absence of MTX 100 nM ± thymidine and hypoxanthine 100 μM. for 24 h. 12 million viable PBMCs were subjected to 3 freeze thaw cycles using 3 ml 50% ACN. The accumulated supernatant was then dried at 35°C before being stored at -80°C. The sample was then resuspended in 100 μl phosphate buffer. 25 μl of the sample was then loaded on the HPLC C18 column. No significant change was found in the concentration of cytosine, uracil, CTP, TTP or CDP with MTX treatment. MTX with rescue significantly reduced the concentration of normalised CDP. Data are represented as (A1-A6) mean ± SEM, n=3, (B1-B6) mean ± SEM, n=3, normalised to ctl (set at 100%). A one-way ANOVA followed by Tukey's multiple comparison test was performed with significant differences indicated by *P<0.05 or, **P<0.01.
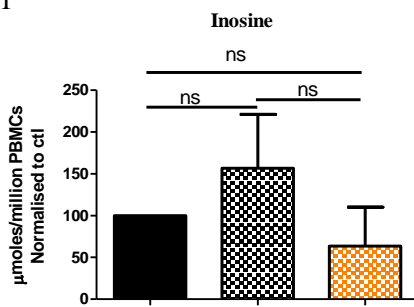
B1

Cytosine

B2

Uracil

B3

CDP

B4

CTP

B5

TTP

229
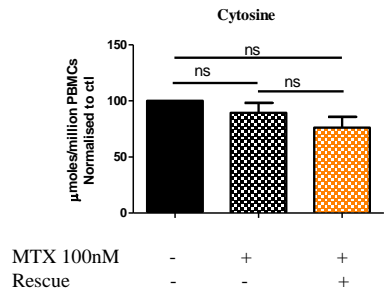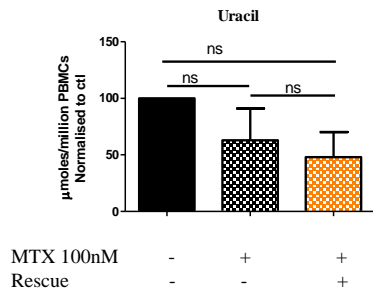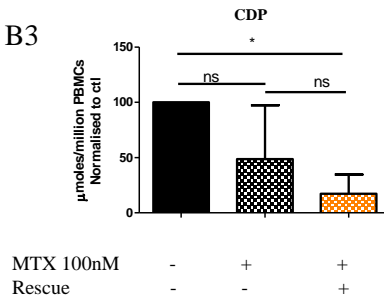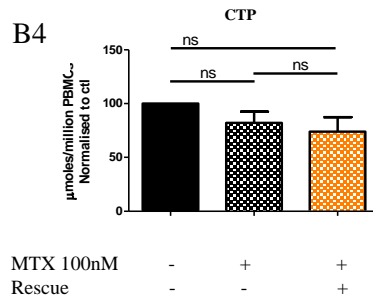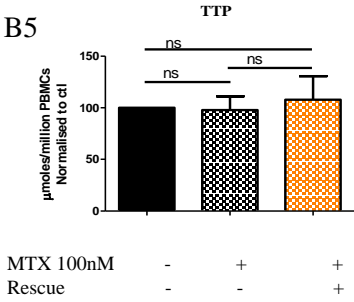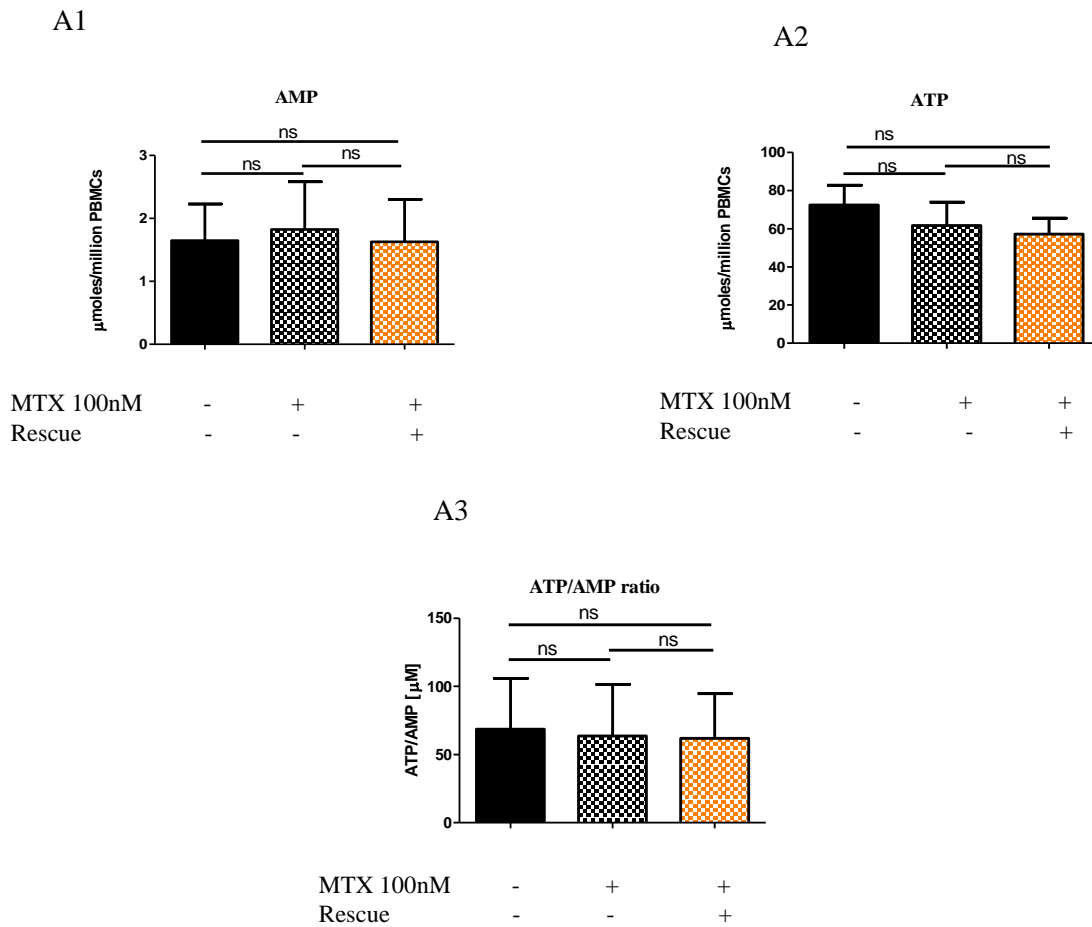
Figure 5.15. Qualitative analysis of AMP and ATP nucleotides in unactivated PBMCs ± Methotrexate.

PBMCs (1 X 10$^{^6}$ cells/ml and 55 ml/T175 flask) were seeded in the presence or absence of MTX 100 nM ± thymidine and hypoxanthine 100 µM. for 24 h. 12 million viable PBMCs were subjected to 3 freeze thaw cycles using 3 ml 50% ACN. The accumulated supernatant was then dried at 35°C before being stored at -80°C. The sample was then resuspended in 100 µl phosphate buffer. 25 µl of the sample was then loaded on the HPLC C18 column. There is no significant change in the concentration of AMP, ATP or the ATP/AMP ratio with MTX treatment. Data are represented as (A1-A3) mean ± SEM, n=3, (B1-B3) mean ± SEM, n=3, normalised to ctl (set at 100%). A one-way ANOVA followed by Tukey's multiple comparison test was performed with significant differences indicated by *P<0.05 or, **P<0.01.

B1
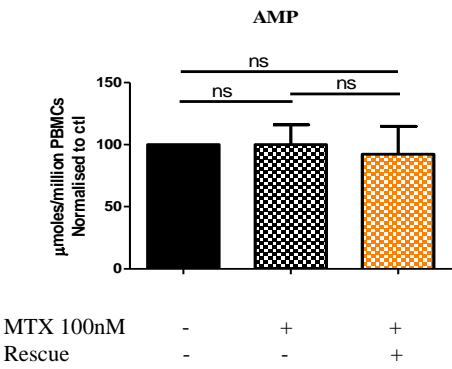
B2
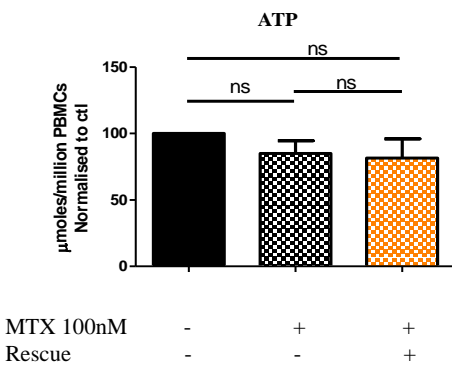
B3
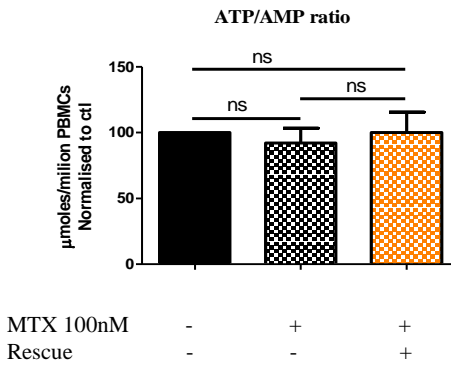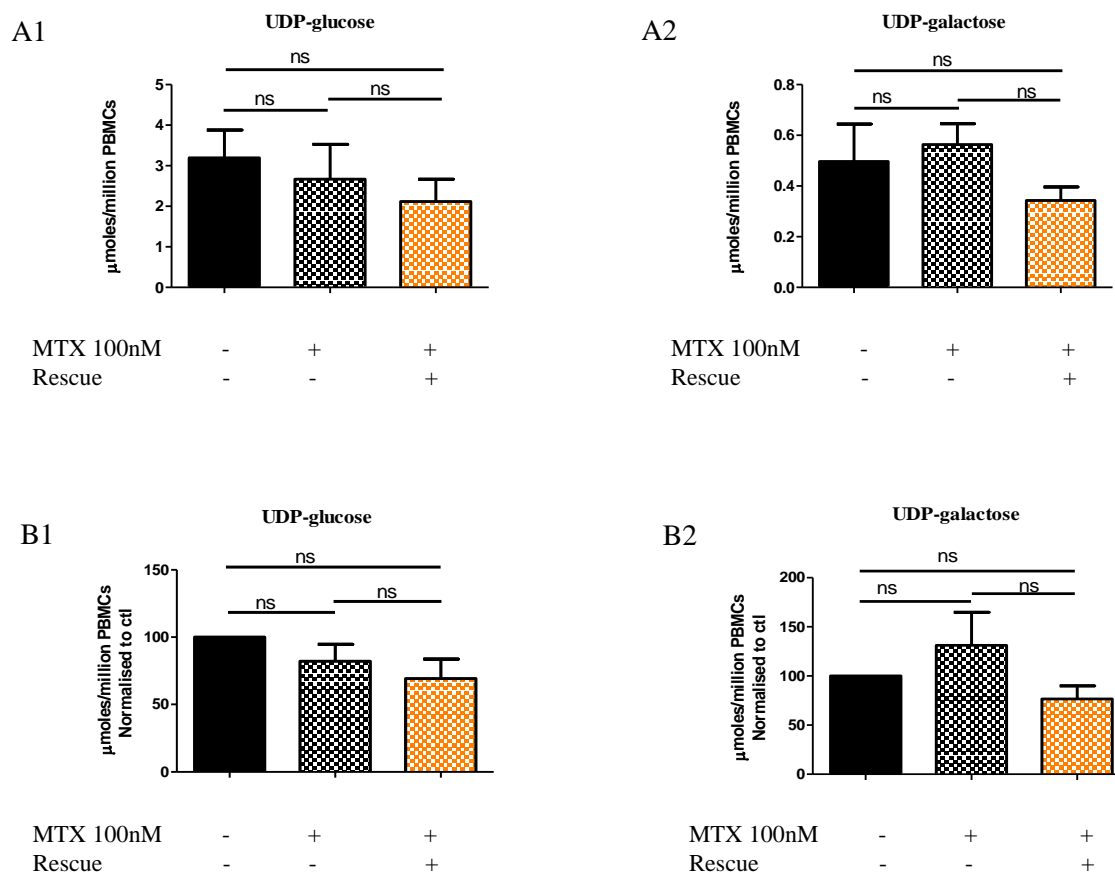
Figure 5.16. Qualitative analysis of the sugar-nucleotides in unactivated PBMCs ± Methotrexate.

PBMCs (1 X 10^{6} cells/ml and 55 ml/T175 flask) were seeded in the presence or absence of MTX 100 nM ± thymidine and hypoxanthine 100 μM. for 24 h. 12 million viable PBMCs were subjected to 3 freeze thaw cycles using 3 ml 50% ACN. The accumulated supernatant was then dried at 35°C before being stored at -80°C. The sample was then resuspended in 100 μl phosphate buffer. 25 μl of the sample was then loaded on the HPLC C18 column. There is no significant difference in UDP-glucose or UDP-galactose following MTX treatment. Data are represented as (A1-A2) mean ± SEM, n=3, (B1-B2) mean ± SEM, n=3, normalised to ctl (set at 100%). A one-way ANOVA followed by Tukey's multiple comparison test was performed and significant differences indicated by *P<0.05 or, **P<0.01.
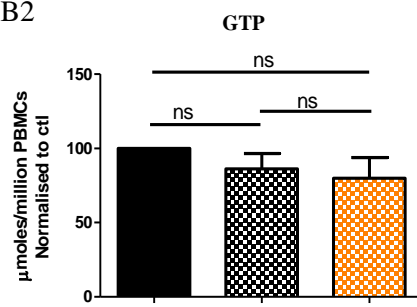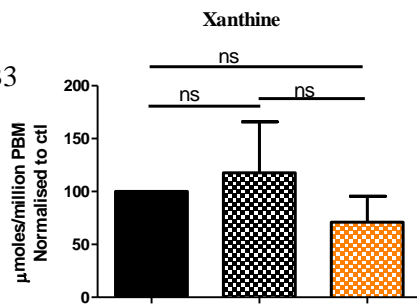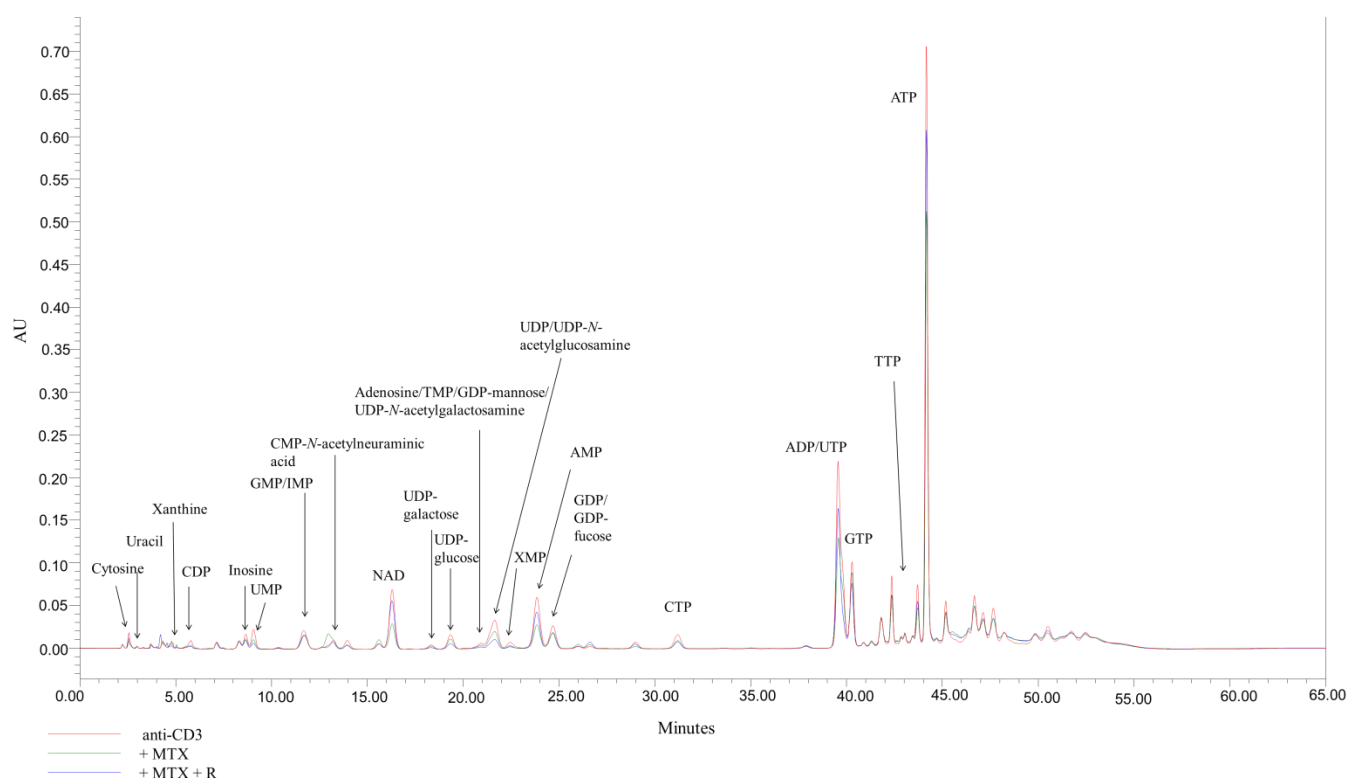
Figure 5.17. Analysis of nucleotides and sugar-nucleotides in anti-CD3-activated PBMCs ± Methotrexate.

PBMCs (1 X 10^6 cells/ml and 55 ml/T175 flask) were seeded in anti-CD3 coated plates in the presence or absence of MTX 100 nM ± thymidine and hypoxanthine 100 μM. for 72 h. 12 million viable PBMCs were subjected to 3 freeze thaw cycles using 3 ml 50% ACN. The accumulated supernatant was then dried at 35°C before being stored at -80°C. The sample was then resuspended in 100 μl phosphate buffer. 25 μl of the sample was then loaded on the HPLC C18 column. Data are representative of one donor.
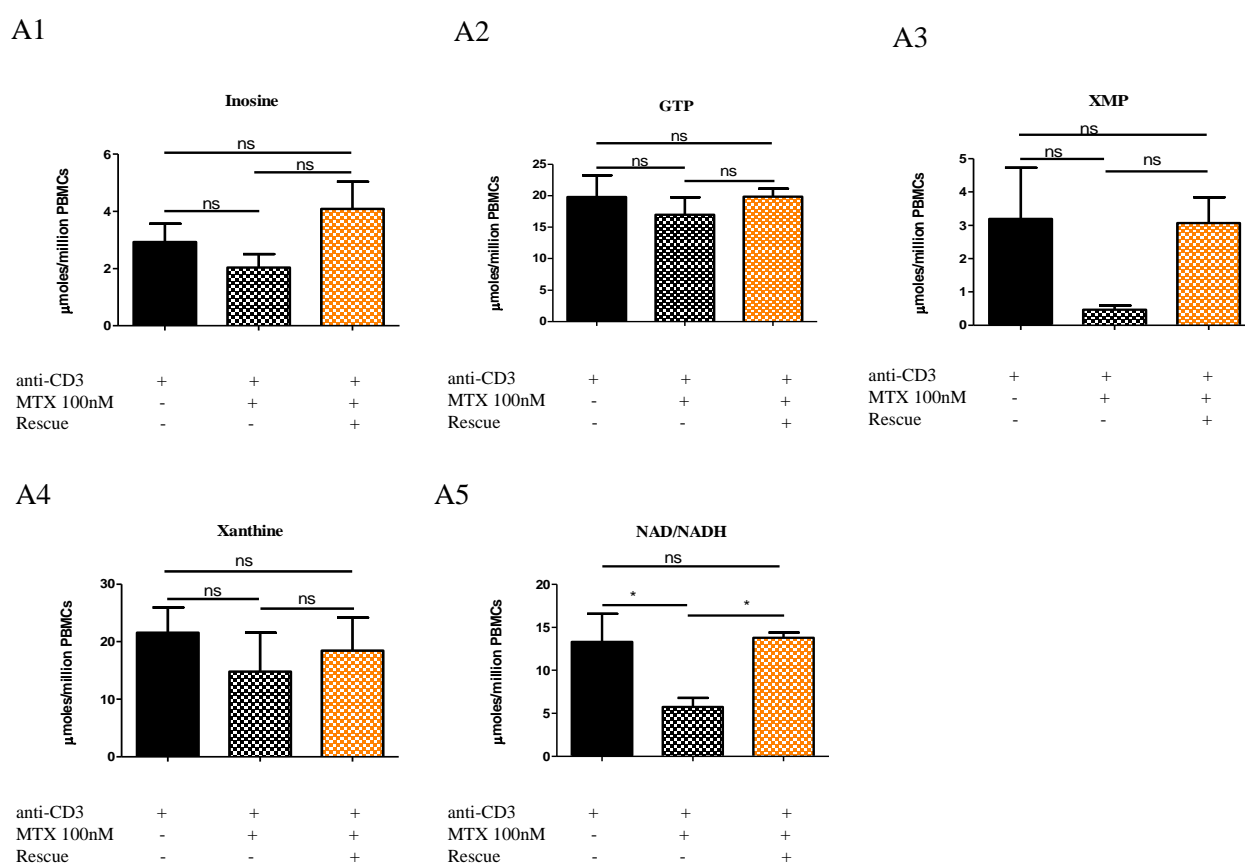
Figure 5.18. Methotrexate significantly decreases the concentration of NAD/NADH in anti-CD3-activated PBMCs, which is reversed by purine and thymidine rescue.

PBMCs (1 X $10^{\wedge}6$ cells/ml and 55 ml/T175 flask) were seeded in anti-CD3-coated plates in the presence or absence of MTX 100 nM ± thymidine and hypoxanthine 100 μM for 72 h. 12 million viable PBMCs were subjected to 3 freeze thaw cycles using 3 ml 50% ACN. The accumulated supernatant was then dried at 35°C before being stored at -80°C. The sample was then resuspended in 100 μl phosphate buffer. 25 μl of the sample was then loaded on the HPLC C18 column. There was no significant difference in xanthine, inosine, GTP or XMP following MTX treatment. Data are represented as (A1-A5) mean ± SEM, n=3, (B1-B5) mean ± SEM, n=3, normalised to ctl (set at 100%). A one-way ANOVA followed by Tukey's multiple comparison test was performed with significant differences indicated by *P<0.05 or **P<0.01.

B1

Inosine

anti-CD3	+	+	+
MTX 100nM	-	+	+
Rescue	-	-	+

B2

GTP

anti-CD3	+	+	+
MTX 100nM	-	+	+
Rescue	-	-	+

B3

XMP

anti-CD3	+	+	+
MTX 100nM	-	+	+
Rescue	-	-	+

B4

Xanthine

anti-CD3	+	+	+
MTX 100nM	-	+	+
Rescue	-	-	+

B5

NAD/NADH
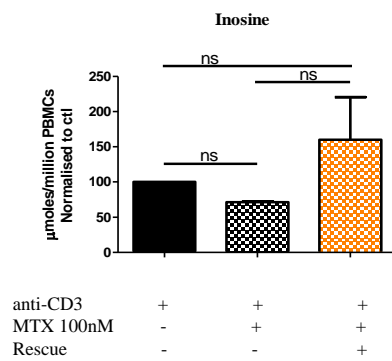
anti-CD3	+	+	+
MTX 100nM	-	+	+
Rescue	-	-	+
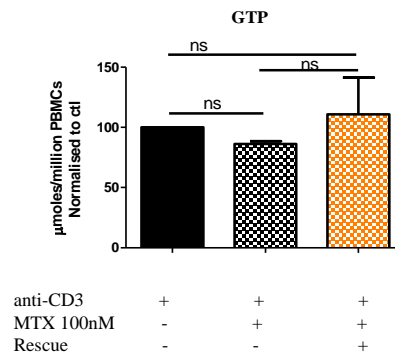
235

Figure 5.19. Methotrexate decreases the concentration of CDP nucleotides in anti-CD3-activated PBMCs.

PBMCs (1 X 10^6 cells/ml and 55 ml/T175 flask) were seeded in anti-CD3 coated plates in the presence or absence of MTX 100 nM ± thymidine and hypoxanthine 100 μM. for 72 h. 12 million viable PBMCs were subjected to 3 freeze thaw cycles using 3 ml 50% ACN. The accumulated supernatant was then dried at 35°C before being stored at -80°C. The sample was then resuspended in 100 μl mobile phase A. 25 μl of the sample was then loaded on the HPLC C18 column. MTX significantly reduced normalised CDP levels which was not reversed following purine and thymidine rescue. MTX had no effect on the other pyrimidine nucleotides. Data are represented as (A1-A6) mean ± SEM, n=3, (B1-B6) mean ± SEM, n=3, normalised to ctl (set at 100%). A one-way ANOVA followed by Tukey's multiple comparison test was performed with significant differences indicated by *P<0.05 or **P<0.01

B1

Cytosine

anti-CD3	+	+	+
MTX 100nM	-	+	+
Rescue	-	-	+

B2

Uracil

anti-CD3	+	+	+
MTX 100nM	-	+	+
Rescue	-	-	+

B3

UMP

anti-CD3	+	+	+
MTX 100nM	-	+	+
Rescue	-	-	+

B4

CDP

anti-CD3	+	+	+
MTX 100nM	-	+	+
Rescue	-	-	+

B5

CTP
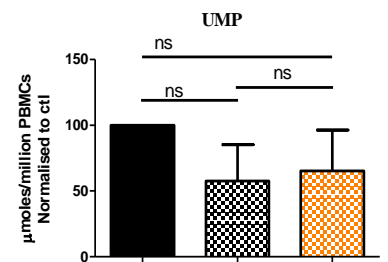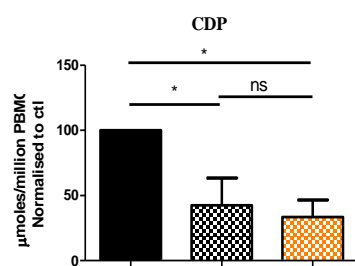
anti-CD3	+	+	+
MTX 100nM	-	+	+
Rescue	-	-	+

B6

TTP

| anti-CD3 | + | + | + |
| MTX 100nM | - | + | + |
| Rescue | - | - | + |

A1

A2

A3

Figure 5.20. Qualitative analysis of AMP and ATP nucleotides in anti-CD3-activated PBMCs ± Methotrexate.

PBMCs (1 X 10^{6} cells/ml and 55 ml/T175 flask) were seeded in anti-CD3-coated plates in the presence or absence of MTX 100 nM ± thymidine and hypoxanthine 100 μM for 72 h. 12 million viable PBMCs were subjected to 3 freeze thaw cycles using 3 ml 50% ACN. The accumulated supernatant was then dried at 35°C before being stored at -80°C. The sample was then resuspended in 100 μl phosphate buffer. 25 μl of the sample was then loaded on the HPLC C18 column. MTX had no significant effect on the concentration of ATP, AMP or the ATP/AMP ratio. Data are represented as (A1-A3) mean ± SEM, n=3, (B1-B3) mean ± SEM, n=3, normalised to ctl (set at 100%). A one-way ANOVA followed by Tukey's multiple comparison test was performed with significant differences indicated by *P<0.05 or **P<0.01.

B1

AMP

anti-CD3	+	+	+
MTX 100nM	-	+	+
Rescue	-	-	+

B2

ATP

anti-CD3	+	+	+
MTX 100nM	-	+	+
Rescue	-	-	+

B3

ATP/AMP ratio
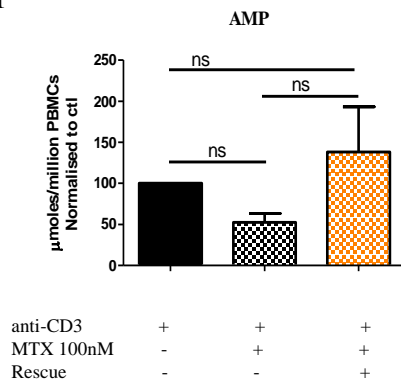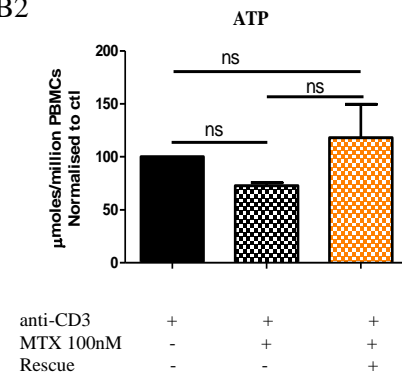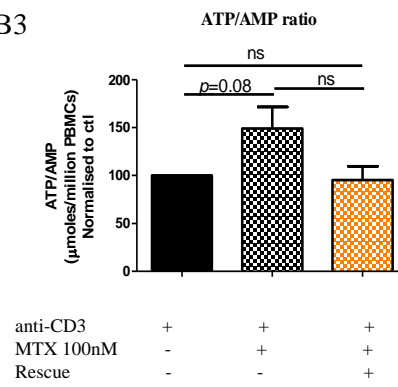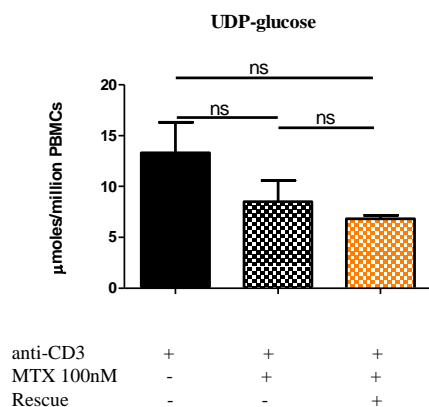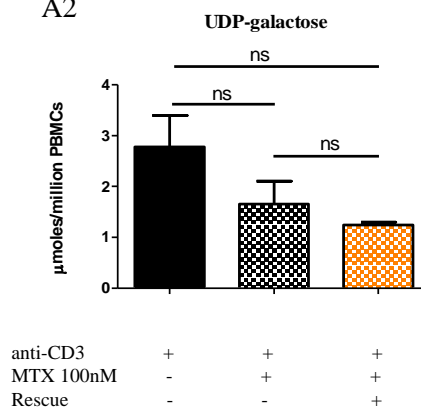
anti-CD3	+	+	+
MTX 100nM	-	+	+
Rescue	-	-	+
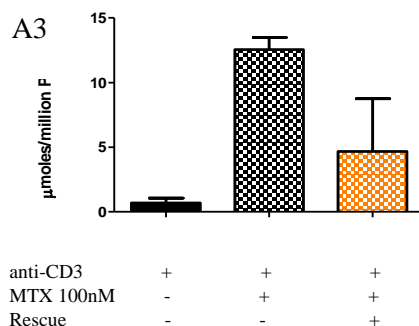
Figure 5.21. Qualitative analysis of sugar-nucleotides in anti-CD3-activated PBMCs ± MTX

PBMCs (1 X 10^6 cells/ml and 55 ml/T175 flask) were seeded in anti-CD3-coated plates in the presence or absence of MTX 100 nM ± thymidine and hypoxanthine 100 µM. for 72 h. 12 million viable PBMCs were subjected to 3 freeze thaw cycles using 3 ml 50% ACN. The accumulated supernatant was then dried at 35°C before being stored at -80°C. The sample was then resuspended in 100 µl mobile phase A. 25 µl of the sample was then loaded on the HPLC C18 column. There was no significant effect on the concentration of UDP-galactose or UDP-glucose and it was not determined whether CMP-*N*-acetylneuraminic acid changed with MTX treatment. Data are represented as (A1-A2) mean ± SEM, n=3, (A3) mean ± range, n=2, (B1-B2) mean ± SEM, n=3, (B3) mean ± range, normalised to ctl (set at 100%). A one-way ANOVA followed by Tukey's multiple comparison test was performed with significant differences indicated by *$P<0.05$ or, **$P<0.01$.

B1 UDP-glucose

B2 UDP-galactose

B3 CMP *N*-acetylneuraminic acid
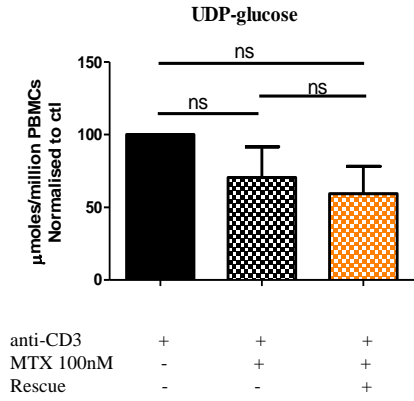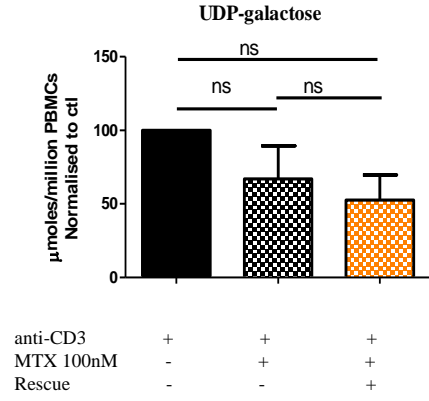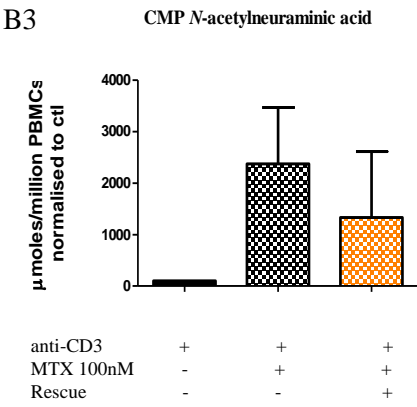
5.5 Discussion

Metabolic profiling offers a detailed insight into the global workings of a cell. The quantification of each metabolite is the summation of all the processes that synthesise and utilise that metabolite, so measuring metabolites from an entire biochemical pathway can provide information into how drug treatment can affect this process. This study successfully quantified nucleotides and sugar-nucleotides; the nature of the attached sugar, ribose, or deoxyribose was unknown, from unactivated and anti-CD3-activated PBMCs following MTX treatment. It was shown here that 50% ACN results in full recovery 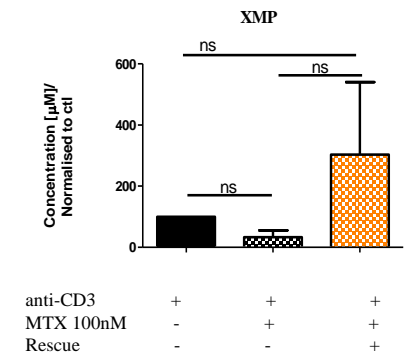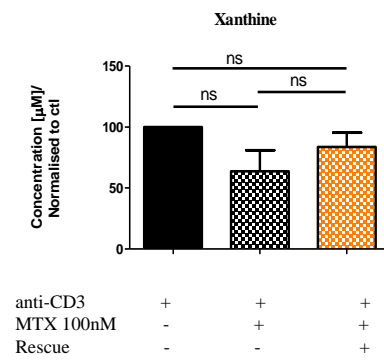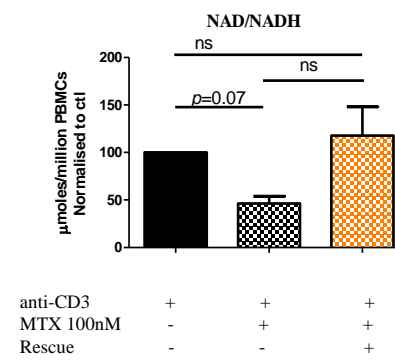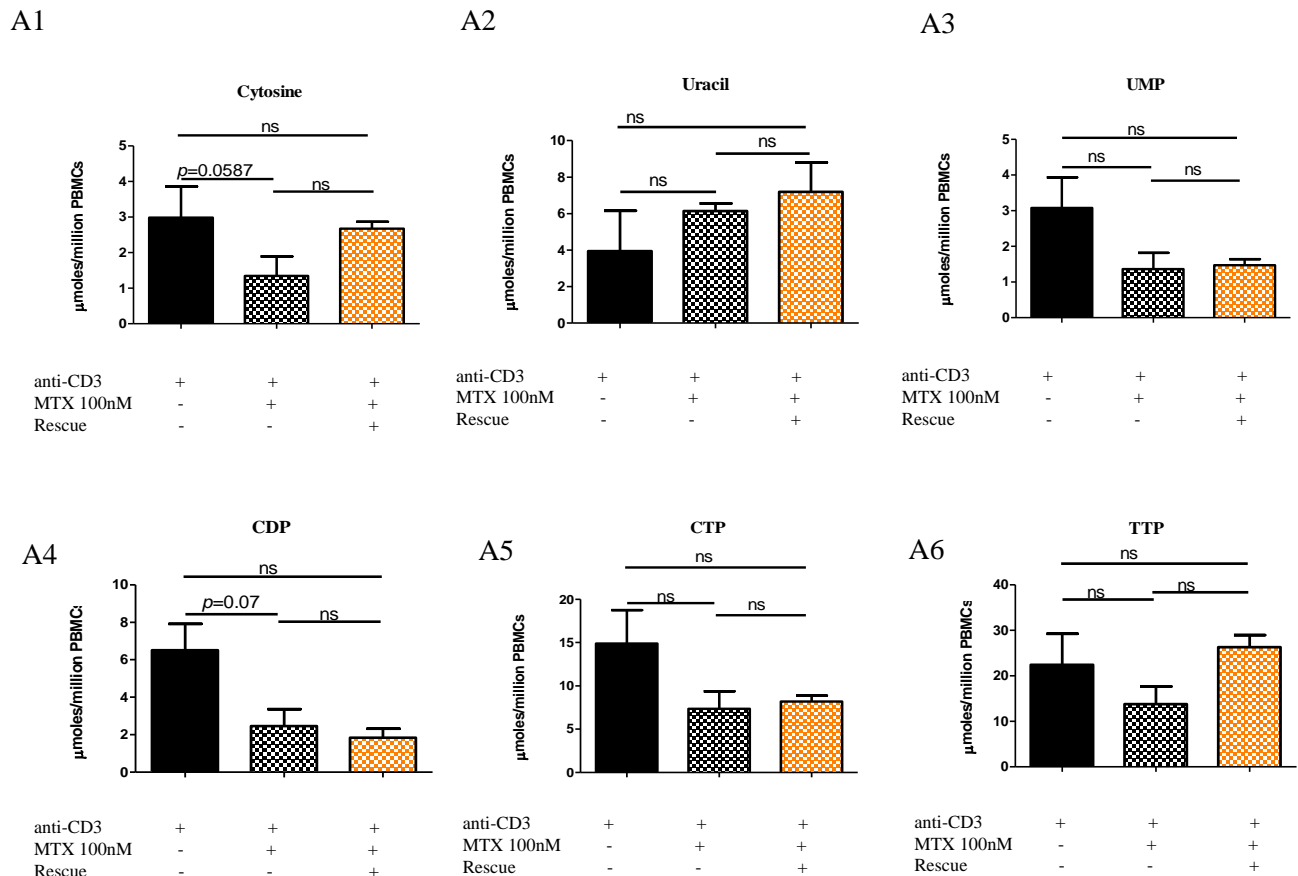of the nucleotides and sugar-nucleotides tested (Fig 5.5). CMP, XMP and uracil were originally not detected in unactivated PBMCs so were omitted from the standard recovery experiment however after loading a higher concentration uracil was detected in these samples. In another study, 50% ACN did not result in complete recovery of all nucleotides tested (Dietmair et al., 2010). Although the use of 50% ACN as the best extraction procedure was confirmed by another group, they found that the recovery of 5 metabolites, including GTP, UTP and UDP-galactose was statistically low (del Val et al., 2013). Here it was shown that it was possible to achieve full recovery, following 3 freeze-thaw-cycles provided that samples were subjected to minimal drying time. The extraction also proved to be highly reproducible with little variation in metabolites extracted from triplicate samples (Fig 5.6).

Activation-dependent effects

Activation-dependent differences varied between metabolites. The fold difference upon activation was calculated even for those metabolites which co-eluted, to demonstrate that the differences found were not simply a result of activation-induced growth (Table 5.1). XMP was undetectable in unactivated PBMCs and UMP was only detected in one unactivated donor, but both were found in the activated cells (Fig 5.8&5.9). To account for those metabolites not present in unactivated samples, an unpaired student T-test was used to calculate significant, activation-dependent differences across all the metabolites, because metabolites were extracted after 24 h in unactivated PBMCs compared to 72 h in anti-CD3-activated PBMCs. Analysis showed that there was no significant increase in nicotinamide moieties or the purine metabolites, inosine, xanthine or GTP following activation (Fig 5.8). However, XMP which was not detected in unactivated PBMCs was

present following activation. Elsewhere, a significant increase in xanthine, XMP, inosine and GMP was found but GTP was not measured after a 30 h anti-CD3-activation of T cells (Wang et al., 2011a). An increase in GTP was found over the course of 72 h in PHA-stimulated CD4$^+$ T lymphocytes (Fairbanks et al., 1995). The same authors found that guanosine increased following T cell-activation, but it could not be detected in our samples (Wang et al., 2011a). Another study also found that GMP increased between 24 and 96 h upon TCR ligation (Li et al., 2015).

The pyrimidine nucleotides, CDP, CTP and TTP significantly increased following anti-CD3-activation, and UMP was detected in activated PBMCs from all three donors (Fig 5.9). UMP was also found to be increased in T cells after a 30 h activation and although CTP, CDP and TTP levels were not measured, an increase in CMP and TMP was found (Wang et al., 2011a). An increase in CTP was also found in 72 h PHA-stimulated CD4$^+$ T lymphocytes (Fairbanks et al., 1995). UMP was found to increase between 24 and 96 h after TCR activation (Li et al., 2015). Fairbanks et al. (1995) showed that PHA-activated human CD4$^+$ and CD8$^+$ T cells contained 8-fold more pyrimidines and only 2-fold more purine nucleotides, so a larger increase in pyrimidine nucleotides would be expected for the anti-CD3-activated PBMCs population here composed of (~60%) T cells. Although no significant increase in uracil or cytosine was found in this study after a 72 h activation (Fig 5.9), an increase was found in those pyrimidine based metabolites after a 30 h activation (Wang et al., 2011a).

Most reports have demonstrated that the increase in ATP following TCR ligation is an immediate increase. An increase in ATP has been shown 1 h after TCR ligation in T cells (Kaminski et al., 2012). This increase was also shown over 72 h PHA-activated CD4$^+$ T lymphocytes (Fairbanks et al., 1995). However, ATP significantly decreased in CD4$^+$ T cells from 1-4 h after activation with anti-CD3 (Cammann et al., 2016). It is not known whether this elevation is sustained for the duration of the 72 h anti-CD3-activation but there was no significant increase in ATP in anti-CD3-activated PBMCs in this study (Fig 5.10). AMP significantly increased which is in agreement with experiments conducted in 30 h activated T cells (Fig 5.10) (Wang et al., 2011a). However, one report found no change in AMP levels over a 72 h activation with PHA in CD4$^+$ T lymphocytes (Fairbanks et al., 1995).

Although the ATP/ADP ratio was previously considered to be a better indicator of the energetic balance, by virtue of both nucleotides being present at higher concentrations, AMP has recently been shown to be more 10-fold more potent than ADP in inhibiting Thr172 dephosphorylation, which serves to activate AMPK and initiate signalling pathways that restore energy homeostasis (Gowans et al., 2013). Given the MTX-mediated inhibition of AMP deaminase and adenosine deaminase, MTX is thought to increase AMP thereby lowering the ATP/AMP ratio (Kuznetsov et al., 2011). Thus, the ratio of ATP/AMP is more apt in this study. It was also not possible to measure ADP as it co-eluted with UTP here. It is not known how this ratio changes after a 72 h anti-CD3-activation but there was no significant decrease in the ATP/AMP ratio in this study (Fig 5.10).

Changes in a variety of sugar-nucleotides upon anti-CD3-activation have never been measured. The significant increase in UDP-glucose found here in anti-CD3-activated PBMCs (Fig 5.11) has also been shown after a 30 h anti-CD3-activation of T cells and over 72 h PHA-activated CD4$^+$ T cells (Fairbanks et al., 1995, Wang et al., 2011a). However, the finding that UDP-galactose also significantly increased during activation and that CMP-*N*-acetylneuraminic acid, which is undetectable in unactivated PBMCs, is present after a 72 h activation has never been shown (Fig 5.11). These findings are in keeping with the fact that glutaminolysis is elevated after T cell-activation, a prerequisite for the synthesis of sugar-nucleotides (Fig 1.16) (Wang and Green, 2012b). These changes in sugar-nucleotides represent one way in which T cells regulate glycosylation during activation, alongside the expression of glycosidases and glycosyltransferases (Clark and Baum, 2012). These changes are important because this modification can have functional consequences such as altering the binding affinities for receptors (Collins et al., 2013).

The effects of MTX in unactivated PBMCs

In this study, low-dose MTX was found to have no effect on the nicotinamide moieties or the purine nucleotides xanthine, inosine, or GTP in unactivated PBMCs after a 24 h treatment (Fig 5.13). An upward trend in GMP and IMP was found following a 24 h treatment with MTX (100 nM) in CD4$^+$ T cells (Chimenti et al., 2013). There was also no change in the pyrimidines CTP, CDP or TTP as well as their precursors, uracil and cytosine (Fig 5.14). There have been no reports found which detail the effects of low-dose

MTX on pyrimidines in unactivated PBMCs. Many reports have been conducted on immortalised cell lines, as outlined in the introduction to this chapter but since these cells are dividing, no comparisons can be made with these unactivated PBMCs. No significant effect was found on the concentration of ATP or AMP, and it follows that there was no significant change in the ATP/AMP ratio in these cells, a finding that has not been shown (Fig 5.15). In the literature, an upward trend was found in the levels of AMP following a 24 h MTX (100nM) treatment in unactivated CD4$^+$T cells, however the group did not measure ATP levels (Chimenti et al., 2013).

The effect of low-dose MTX on the concentration of UDP-glucose or UDP-galactose has never been investigated in unactivated PBMCs. This finding demonstrates that MTX has no direct effect on glycosylation in unactivated PBMCs by affecting those sugar-nucleotides levels (Fig 5.16). Since neither UDP-*N*-acetylglucosamine, UDP-*N*-acetylgalactosamine, GDP-mannose nor GDP-fucose could be measured in these samples, other direct effects of MTX on these sugar-nucleotides cannot be ruled out.

The effects of MTX in anti-CD3-activated PBMCs

Comparison of the effect of MTX on a range of nucleotides and sugar-nucleotides in anti-CD3-activated PBMCs compared to unactivated PBMCs has never been conducted. This study presents the first evidence of the significant reduction of low-dose MTX on nicotinamide moieties levels, which was not found for unactivated PBMCs (Fig 5.18A). Interestingly, these nicotinamide moieties were reduced even though there was no significant increase in the levels of these metabolites during activation. This result implies an effect by MTX on a mechanism distinct from activation, but which only occurs in activated cells. It is possible that the reduction in nicotinamide moieties reflect effects of MTX on adenine nucleotides, however there was no significant reduction found in either ATP or AMP nucleotides (Fig 5.20). The lack of an effect of MTX on inosine, XMP, xanthine and GTP do not mean that MTX has no effect on these activated nucleotides, and increasing the population size may clarify whether there is an effect.

Analysis of the normalised data for pyrimidine nucleotides revealed that MTX also significantly depleted the pyrimidine nucleotide, CDP, in anti-CD3-activated PBMCs which showed activation-dependent changes (Fig 5.9&5.19B). It is understood that the principle pyrimidine-salvage pathways in mammalian cells, involves salvaging nucleotides from their nucleosides (Mathews, 2015). The decrease in CDP, may be a

result of cytidine being used in salvage processes to replete pyrimidine nucleotides (see Fig 1.11) (Garavito et al., 2015). This increased requirement for salvage processes could also explain why a downward trend in cytosine was found due to a reduction in the cytidine degradation pathway. To be sure this was the case, 3, 4 and 5 day time-points would have to be conducted to measure a greater loss in cytosine and CDP levels, and the subsequent decline of pyrimidine nucleotides after cytosine had been depleted. Indeed, this process may have already begun as there was a clear downward trend in the normalised values for CTP, but this observed effect was not found to be significant (Fig 5.19B). Indeed the pyrimidine salvage pathway using uridine nucleosides was found to be reduced from PBMCs isolated from RA patients on a course of MTX treatment (Smolenska et al., 1999). In this study, it was not clear whether MTX could affect UMP levels, which can be formed by a salvage process involving uridine and ATP, via uridine cytidine kinase (Levine et al., 1974). It is possible that uridine was depleted to rescue UMP levels in this study, but uridine was not measured here.

Purine and thymidine rescue was shown to partially reverse the MTX-mediated reduction in nicotinamide moieties, but rescue had no effect on recovering CDP levels in anti-CD3-activated PBMCs (Fig 5.18A and 5.19B). Hypoxanthine has been shown to be converted to IMP, via HGPRT and then by the 5'nucleotidase to inosine (see Fig 1.12). This could have replenished adenine nucleotides required for nicotinamide synthesis, suggesting that although ATP and AMP weren't reduced upon MTX treatment, adenine nucleotides required for other processes were sacrificed. The inability of thymidine to rescue CDP levels is supported by the fact that thymidine enters the salvage pathway at thymidine kinase for the synthesis of dTTP (see Fig 1.11), and it is not currently thought that thymidine could rescue cytidine-based nucleotides.

MTX had no effect on the concentration of ATP in anti-CD3-activated PBMCs in this study, but this does not rule out a possible effect following repeat experiments (Fig 5.20B). MTX was found to reduce ATP in other immortalised cell lines (Tedeschi et al., 2013, 2015). There was also no significant decrease in AMP and as such, there was no significant difference found in the ATP/AMP ratio, following low-dose MTX treatment in anti-CD3-activated PBMCs. Since there was a downward trend in the ATP/AMP ratio, this suggests that there may be an effect with MTX if the experiment is repeated with more donors. There is at least one report which found a significant reduction in both AMP and ATP nucleotides in Jurkat cells (Miura et al., 2010).

This pioneering study also demonstrated that MTX had no effect on the concentration of UDP-glucose or UDP-galactose in anti-CD3-activated PBMCs (Fig 5.21B). Further investigation into the effects of MTX on the sugar-nucleotides which could not be separated using this technique is warranted particularly if they also prove to be activation-dependent. Additional experiments may show whether MTX could impact on CMP-*N*-acetylneuraminic acid levels.

Analysis of the effect of MTX on the sugar nucleotide precursor, CTP, was also important in the investigation into whether the MTX-mediated inhibition of purine and thymidine nucleotides could affect the formation of the sugar nucleotide. There was no significant effect on CTP levels, but it was not determined whether MTX affected CMP-*N*-acetylneuraminic acid. If there was a significant reduction in CTP levels with MTX treatment, but no significant reduction in the sugar nucleotide then it could be deduced that MTX does not affect sugar nucleotide levels by limiting the nucleotide precursor. With regard to UDP-glucose and UDP-galactose in which no significant change was found with MTX treatment, UTP levels weren't measured because it co-eluted with ADP. Thus, it is not known if MTX can affect sugar-nucleotide levels by affecting their nucleotide precursors.

Overall, no effects were found following MTX treatment in unactivated PBMCs, however differences were found following activation. Nicotinamide moieties as well as CDP nucleotides were reduced upon MTX treatment, demonstrating that MTX had impacted part of the pyrimidine and purine biosynthesis pathway. Both raw and normalised data sets were compiled to minimise the error from individual variation. Trends observed with MTX, not considered to be significant, could yield interesting results if experiments are repeated with more donors, but a summary of the significant findings in this study are presented in Table 5.2. Rescue reversed the MTX-mediated reduction in nicotinamide moieties just as it reversed the anti-proliferative effect of MTX shown previously, via the inosine salvage pathways, confirming that hypoxanthine had infiltrated these pathways.

			Effects with MTX		
			unactivated PBMCs	activated PBMCs	
Purines		Inosine	no	no	
		GTP	no	no	
		XMP	nd	no	
		Xanthine	no	no	
		AMP	no	no	
		ATP	no	no	
		ATP/AMP ratio	no	ns	
Pyrimidines		Cytosine	no	ns	
		Uracil	no	no	
		UMP	nd	no	
		CDP	no	↓	
		CTP	no	ns	
		TTP	no	no	
Nicotinamide moieties		NAD/NADH	no	↓	
Sugar nucleotides		UDP-glucose	no	no	
		UDP-galactose	no	no	
		CMP-*N*-acetylneuraminic acid	no	no	

Table 5.2. Summary of the effects on Methotrexate on purines, pyrimidines, nicotinamide moieties and sugar-nucleotides in unactivated and anti-CD3-activated PBMCs.

Interpreted from data normalised to ctl (set at 100%), represented as mean ± SEM, n=3. A one-sample T test along with a paired student T-test was performed with significant differences indicated by *P<0.05 or, **P<0.01. NS- non significant, ND, not detected.

Chapter 6:

General Discussion:

This study aimed to examine a broad range of effects of MTX from mitochondrial function, to inhibition of T cell-activation, to effects on cell-surface sialylation and intracellular nucleotides as well as sugar-nucleotides, using a model of anti-CD3-activated PBMCs, the most applicable to studying an inflammatory disease potentiated by over-active T cells.

Understanding the effect of MTX has been limited by experiments conducted for different durations using different stimuli and doses of MTX. Few papers were found that examined more than one effect of MTX, which is why this study is so valuable to current research. In addition, the experiments on both unactivated and activated PBMCs were conducted with the aim to show how MTX could preferentially effect activated PBMCs, like the over-active T cells in the case of RA, whilst having little effect on other unactivated cells.

No significant change occurred in the presence of MTX in unactivated PBMCs throughout this study, except for the dissipation of the $\Delta\Psi_m$. It is not known whether these differential effects found in the unactivated PBMCs represents differential drug uptake in activated verses unactivated cells or if it is because these cells are not cycling. The unactivated PBMCs still required nutrient turnover and unsurprisingly, were found to be actively metabolising, demonstrated in the increased incorporation of ManNAz over time. Given the integrated role of 1C metabolism, it is likely that some level of MTX would be taken up using the same transporters as folate. Indeed one study hypothesised that resting lymphocytes could take up MTX at the concentrations found in serum (0.1 nM-1 μM) (Paillot et al., 1998). This has important applications for the therapeutic use of MTX. To maximise efficacy the most important parameter appears to be that these cells are dividing. MTX does not distinguish between different populations of PBMCs, it only distinguishes between PBMCs that are undergoing mitosis and in particular, those that are dividing at a sufficient rate. In these experiments, CD19$^+$ B cells were dividing however, the effects of MTX were not significant after 72 h. Perhaps in PBMCs dividing at a slow rate, longer time points are required for MTX to infiltrate the biochemical pathways and to observe any effect with MTX. Since these experiments found affects with MTX at the onset of activation, any therapeutic intervention should be made as soon as possible as it is not known whether the same effects would be observed if treatment was administered after activation.

Changes occurred in the presence of MTX in both activated cells which did proliferate and those activated PBMCs that did not proliferate in response to anti-CD3. Megaloblastic non-CD3 cells were found containing fragmented DNA, indicating that different cells were susceptible to nucleotide-inhibition by MTX, but in different ways. It also indicated that folate-deficiency had occurred under these conditions, suggesting that effects occurring with low-dose MTX could be related to folate-deficiency. As such, controls would have be included containing cells cultured under folate insufficient, not deplete conditions to mimic the reduced level of proliferation in the presence of MTX.

Paradoxically, the effects of MTX in activated PBMCs were not always activation-dependent. The nicotinamide moieties, NAD/NADH did not significantly increase during activation, but were significantly inhibited by MTX treatment. Other significant increases in nucleotides and sugar-nucleotides upon activation showed no effect with MTX treatment. These results would suggest that MTX does not solely affect activated cells in all cases and that MTX does not necessarily affect all activation-dependent processes. Of further note, the lack of effects mediated by MTX on these intracellular nucleotides could demonstrate the salvage pathways which work to minimise these effects, just as these pathways worked to maintain a low level of proliferation in 2 day activated PBMCs, the levels of which were exhausted by day 3.

MTX has been shown to inhibit c-Myc, which is responsible for events that occur early in T cell-activation (Fernandez-Ramos et al., 2016). Nothing has been found showing a direct effect of MTX on transferrin receptor expression. Reversal of the inhibitory effects of MTX during activation such as proliferation, transferrin receptor expression and blastogenesis, by purine and thymidine rescue, together, has never been shown. Whether purine and thymidine exert some regulatory control on the activation induced process was not determined. ManNAz incorporation was also found to be an activation-dependent parameter and was also susceptible to the effects of MTX.

The MTX mediated dissipation of the $\Delta\Psi_m$ and increase in ROS production in anti-CD3-activated PBMCs, could indicate that mitochondrial function has been affected during activation. The extent in which this insult to mitochondrial function could limit cell function was not measured here. What was shown was that it occurred alongside the inhibition of T cell proliferation, transferrin receptor expression and blastogenesis. Since rescue partially reversed the MTX-induced increase in ROS, and partially reversed the

dissipation of the $\Delta\Psi_m$ it suggests similar mechanisms for the effect of MTX on the $\Delta\Psi_m$ and for increased ROS production in anti-CD3-activated PBMCs.

MTX may also affect mitochondrial function by a mechanism unrelated to the inhibition of cellular activation since MTX dissipated the $\Delta\Psi_m$ in unactivated PBMCs. It is not known whether this mechanism could be related to changes in ADP which could not be measured. ADP in the presence of orthophosphate can induce State 3 respiration, and accompanies a different mitochondrial inner-membrane potential compared to the potential of cells in the absence of ADP, whereby state 4 respiration is induced. There was no significant effect of MTX in unactivated PBMCs on the concentration of ATP or AMP. However, to fully contextualise these results with the other experiments in this study, the effects of a 24 h MTX treatment on both the $\Delta\Psi_m$ and on ROS production in unactivated PBMCs would have to be measured, as these cells were only treated for 5 h.

The partial reversal of this increase in ROS production, upon purine and thymidine rescue, which has been shown to recover reduced folate levels, could be explained by the fact that tetrahydrofolate and 5-methyl-THF are potent anti-oxidants (Rezk et al., 2003). It suggests that the mechanism of increased ROS production by MTX could partially be attributed to folate antagonism. Importantly, these changes in ROS production may have no link with mitochondrial function as the source of this increase in ROS was not determined. It was also not possible to determine if any ROS production by dead cells was contributing to these effects. Rescue could simply have partially reversed ROS production because it also rescued cell viability.

Since the effects of MTX on glycosylation are still not understood, this project aimed to see if MTX could directly affect cell-surface sialylation. In light of the absence of a full metabolic profile in the presence of MTX, the detailed study of the effect of MTX on intracellular nucleotides and sugar-nucleotides in anti-CD3-activated and unactivated PBMCs was also investigated.

Using click chemistry, flux through the CMP-*N*-acetylneuraminic acid processing pathways from ManNAc entry was measured but the contribution from endogenous routes from UDP-GlcNAc and UDP-GalNAc, which contribute to endogenous ManNAc levels and ultimately to CMP-*N*-acetylneuraminic acid were not measured. Labelling, UDP-GlcNAc, UDP GalNAc as well as ManNAc with different flurochromes would enable the measurement of the flux through the entire CMP-*N*-acetylneuraminic acid

levels. ManNAz incorporation on the cell-surface sialome was found to be an activation-dependent parameter, in keeping with the finding that CMP-*N*-acetylneuraminic acid, synthesised downstream of ManNAc significantly increased upon anti-CD3 activation. By virtue of the diffusion of acetylated ManNAz across the membrane, flux through the pathway, not increased uptake was determined to be the mechanism in which this took place.

It is not known whether inhibition of ManNAz incorporation on the cell-surface sialome by MTX corresponded to significant changes in the levels of CMP-*N*-acetylneuraminic acid, as the results presented are representative of two donors since CMP-*N*-acetylneuraminic acid was undetectable in the third donor. The experiments conducted here show that MTX significantly affected ManNAz incorporation from a specific route in the CMP-*N*-acetylneuraminic acid processing pathway, following ManNAz uptake and endogenous ManNAc derived from other upstream precursors such as UDP-GlcNAc and UDP-GalNAc were not measured. An altered glycosylation prolife is not only indicative of a pathological process but can also have functional consequences (Boligan et al., 2015). As such, an effect of MTX on cell-surface sialylation may be a consequence of treatment, or it may function to instigate the drug-induced effects.

MTX was found to have differential effects on distinct populations of anti-CD3-activated PBMCs; both populations had increased transferrin receptor expression which indicated that they had both been activated, but one population was not undergoing activation-induced blastogenesis at that time. Although it was not determined whether these blast and non-blast cells were differentially cycling, MTX significantly reduced ManNAz incorporation in non-blast cells, but increased ManNAz incorporation in blast cells. Perturbations in the cell cycle can affect cellular glycosylation (De Graaf et al., 1993). This work suggests that the MTX-induced effect on cell-surface sialome could be cell cycle-dependent. Future work will investigate whether these populations are at different stages of the cell cycle.

Reversal of this effect of MTX on surface sialylation as well as on transferrin receptor expression, CD71, a glycoprotein, the sialylation of which was also demonstrated by Orberger et al. (1992), was found following purine and thymidine rescue. This is the first time a link has been shown of how MTX can affect glycosylation. Although, purine and thymidine inhibition has been shown to have effects on the resultant sugar-nucleotide, the

MTX-mediated inhibition of purine and thymidine synthesis was never shown to affect glycosylation in a similar manner. A further link between the MTX-mediated inhibition of purine and thymidine synthesis and intracellular sugar-nucleotides was not shown here. The levels of CTP showed no significant decrease upon MTX treatment and UTP could not be measured, so the effect of these particular nucleotides on their respective sugar-nucleotides, CMP-*N*-acetylneuraminic acid and UDP-glucose was unknown.

Although in recent years purine and thymidine inhibition has become more appreciated as one of the mechanisms of action of MTX in anti-inflammatory disease, no papers have been found which delineated a variety of the effects of low-dose MTX to purine and thymidine inhibition, by observing a partial or complete reversal as was shown here. Since folic acid or leucovorin rescue may compete with uptake for MTX, experiments which demonstrate a reversal of the effects of MTX do not explain the mechanism in which these occurred. Purine and thymidine rescue offer more selective rescue of the pathways utilising these nucleotides and offer greater insight into the mechanism of action of MTX in increasing ROS, altering ManNAz incorporation on the cell-surface, inhibiting activation-dependent parameters like transferrin receptor expression, the increase in cell size, and proliferation and significantly reducing the intracellular concentrations of nicotinamide moieties. The MTX-mediated purine and thymidine inhibition, was attributed to other distinct effects on glucose uptake, which was rescued by hypoxanthine following MTX (2 µM) treatment in Ehrlich ascite tumour cells and GM-CSF production which was rescued by both thymidine and hypoxanthine in anti-CD3-activated whole blood cultures (Kaminskas, 1979, Gerards et al., 2003). Together with the findings shown here, it is clear that the MTX-mediated inhibition of purine and thymidine synthesis has global effects aside from inhibition of proliferation, which means its contribution to any therapeutic effects by MTX cannot be disregarded.

Conclusion

This study investigated the effects of MTX on mitochondrial function, inhibition of cellular activation, as well as cell-surface sialylation and combined these with detailed metabolic profiling to provide insight into the mechanisms of action of MTX. The results found in unactivated compared to anti-CD3-activated PBMCs suggest that MTX can preferentially affect activated immune cells, whilst leaving the unactivated PBMCs unscathed (Fig 3.8,3.39,4.10,4.11,5.13-5.15,5.18-5.20). Its effects however, are not limited to activated PBMCs, as MTX dissipated the mitochondrial membrane potential in unactivated PBMCs as well as their activated counterparts (Fig 3.25&3.26). It was also found that MTX significantly reduced the concentration of nicotinamide moieties which had shown no activation-dependent effects (Fig 5.8&5.18A). Paradoxically, cellular activation did not ensure an effect of MTX possibly because the intricate salvage pathways limited the effects of MTX.

The MTX-mediated inhibition of purine and thymidine synthesis was shown to have global cellular effects, demonstrated upon the reversal of these effects by purine and thymidine rescue. These effects included inhibition of cellular activation, flux through the CMP-*N*-acetylneuraminic acid sialic acid processing pathway from ManNAc entry, as well as changes to specific intracellular nucleotides (Fig 3.12, 3.20, 3.24, 4.12, 5.18A). For the first time, this demonstrates a link between the inhibition of purine and thymidine synthesis and the cell-surface sialome, as well as between a particular cell-surface glycoprotein, CD71, a link which was activation-dependent (Fig 3.20&4.12).

Although no link was shown between the MTX-mediated purine and thymidine inhibition and their respective purine and pyrimidine-based sugars (Fig 5.19&5.21) effects with MTX treatment were demonstrated on specific nucleotides in Primary Human PBMCs (Fig 5.18A&5.19B). A range of nucleotides, nucleotide-precursors, and sugar-nucleotides were analysed upon anti-CD3 activation and many were shown to be activation-dependent (Fig 5.8-5.11).

Overall, the findings shown here suggest that the inhibition of purine and thymidine synthesis by MTX has effects more complex than simply limiting cellular proliferation. Since, it is not possible to delineate which effect of purine or thymidine inhibition, if any,

has any therapeutic value; these findings support the anti-proliferative effect of MTX as a crucial mechanism of action as an anti-arthritic drug.

Future Perspectives

This study investigated a variety of biochemical effects of MTX in both unactivated and anti-CD3-activated PBMCs, and undertook pioneering experiments to link all of these effects to the one-carbon metabolism pathway, by observing either partial or complete reversal of the effects upon purine and thymidine rescue. Further in depth analysis should be conducted, including the elucidation of the effects of MTX on other aspects of mitochondrial function, as well as assays to confirm the effects of MTX on surface glycosylation and intracellular metabolites. In addition, examination of the effects of MTX on AMPK, an area which was not explored should be carried out.

Since MTX was shown to dissipate the $\Delta\Psi_m$ and affect cellular redox status, investigation into the effects of MTX on cellular respiration and the measurement of complex activity from mitochondria isolated from unactivated and anti-CD3-activated PBMCs would clarify how MTX is exerting its effects. A citrate synthase assay would rule out any effects of MTX due to changes to mitochondrial number and should also be carried out alongside the measurement of complex activity, which should be normalised to citrate synthase. Determining whether purine and thymidine rescue could reverse these effects is also imperative to see if all of these effects are linked to purine and thymidine inhibition.

Many trends from the metabolic profiling experiments were not found to be significant. Increasing the number of donors and running the extracted samples during the same run, from PBMCs acquired on consecutive days, would minimise variation and combined with the data obtained here, would clarify whether MTX has effects on these nucleotides and sugar-nucleotides as well as determining whether these effects can be reversed upon purine and thymidine rescue.

Measurement of the effects of MTX on surface sialylation using a novel technique, click chemistry enabled the visualisation and quantification of the sialic acids on the PBMC surface derived from *N*-acetylmannosamine. Confirmative assays would need to be conducted to ensure the sialic acids were *N*-linked, such as separating the extracted proteins from PBMCs using gel electrophoresis and probing for an antibody against *N*-linked sugars. This would resolve both intracellular and membrane bound (surface) glycosylated sugars but the effects of MTX on these would complement the effects found on surface sialylation using click chemistry. Surface sialic acid analysis could also be conducted by separating these glycans on HPLC following cleavage with specific neuramidases to determine if MTX can reduce the expression of surface sialic acids and

confirm that this was activation-dependent. Cell cycle analysis should also be conducted on the blast and non-blast populations to test the hypothesis that MTX exerts cell cycle-dependent effects on the cell-surface sialome.

The effects of MTX on reducing transferrin receptor expression, inhibiting blastogenesis and cellular proliferation in anti-CD3-activated PBMCs would suggest that the mechanism in which MTX inhibits T cell-activation need to be investigated. Although ATP and AMP were not found to be effected by MTX, there was a upwardward trend in the ATP/AMP ratio which suggests that MTX could be affecting these nucleotides. Since nicotinamide moieties were significantly reduced during treatment, whose formation requires both ATP and AMP, it may suggest that adenine nucleotides, overall, are reduced. This hypothesis is supported upon rescue of nicotinamide moieties upon the addition of hypoxanthine and thymidine. This could even contribute to the effects of MTX on surface sialic acids as ATP is required in the generation of the activated sugar. Furthermore, although glutathione was not measured, the levels of this anti-oxidant could also be investigated in future as the MTX-mediated increase in ROS could be partly due to a reduction in glutathione, the synthesis of which requires ATP. Although experiments conducted elsewhere found that low-dose MTX alone did not activate AMPK, for the reasons just mentioned, the effects on AMPK need to be investigated under these conditions. Reversal of any of these effects upon purine and thymidine rescue also need to be investigated to determine if MTX is exerting these effects through either purine and thymidine inhibition or activation of AMPK.

Other lines of investigation include the measurement of NAD and NADH using their respective absorbance, to confirm that MTX can affect these nicotinamide moieties. An inhibitor of FPGS could confirm whether polyglutamated MTX is responsible for the observed effects by observing a waning of these effects in the presence of the inhibitor. Trypan blue and propidium iodide exclusion were used to assess cell viability however, other affirmative assays such as annexin V staining could determine the mechanism of cell death in this model.

Appendix

Supplementary material

Metabolite extraction for NMR analysis:

Metabolic analysis was originally undertaken using 1D NMR. ~100 million PBMCs were centrifuged and washed with PBS before centrifuging at 480 *g* for 5 minutes. The supernatant was poured off and the excess residue removed with tissue. PBMCs were lysed with 4 ml ice cold 60% ACN and vigorously vortexed for about 5 minutes, before being frozen in liquid nitrogen. Cells were thawed on ice, vortexed and centrifuged at 4000rpm for 10 minutes. The supernatant was then removed to an eppendorf before speed vac drying (37 degree).This extraction and freeze-thaw cycle was repeated 3 times. The supernatant was then pooled in the same tubes and speed vac dried once more.

The dried extracted metabolites were re-solubilized in 645 µl water mixture (580 µl H2O and 65 µl D2O). It was then centrifuged at 13200 rpm for 60 minutes, and 590 µl of the supernatant transferred to a new tube. 10 µl of a DSS stock (15mM stock) was then added to the supernatant bringing the final volume to 600 µl and the concentration of DSS to (0.25mM). The sample was then transferred to a NMR tube.

The extractions were analysed using 1D NMR (Sup fig 1.1). The identification of these peaks was achieved by comparison of the chemical shifts with databases of individual standards from the HMDB (Human metabolome database). Quantification was achieved by the inclusion of an internal standard, DSS at a known concentration.

The concentration of these identified metabolites were tabulated (Sup. Fig**,** providing the first extensive metabolic profile of PBMCs, encompassing nucleotides, sugar-nucleotides, amino acids as well as other metabolites. Although much initial work was conducted, this technique proved difficult to reproduce because of problems with salt causing high background signals in the cell samples. HPLC analysis of the extracted metabolites proved a much more successful strategy.
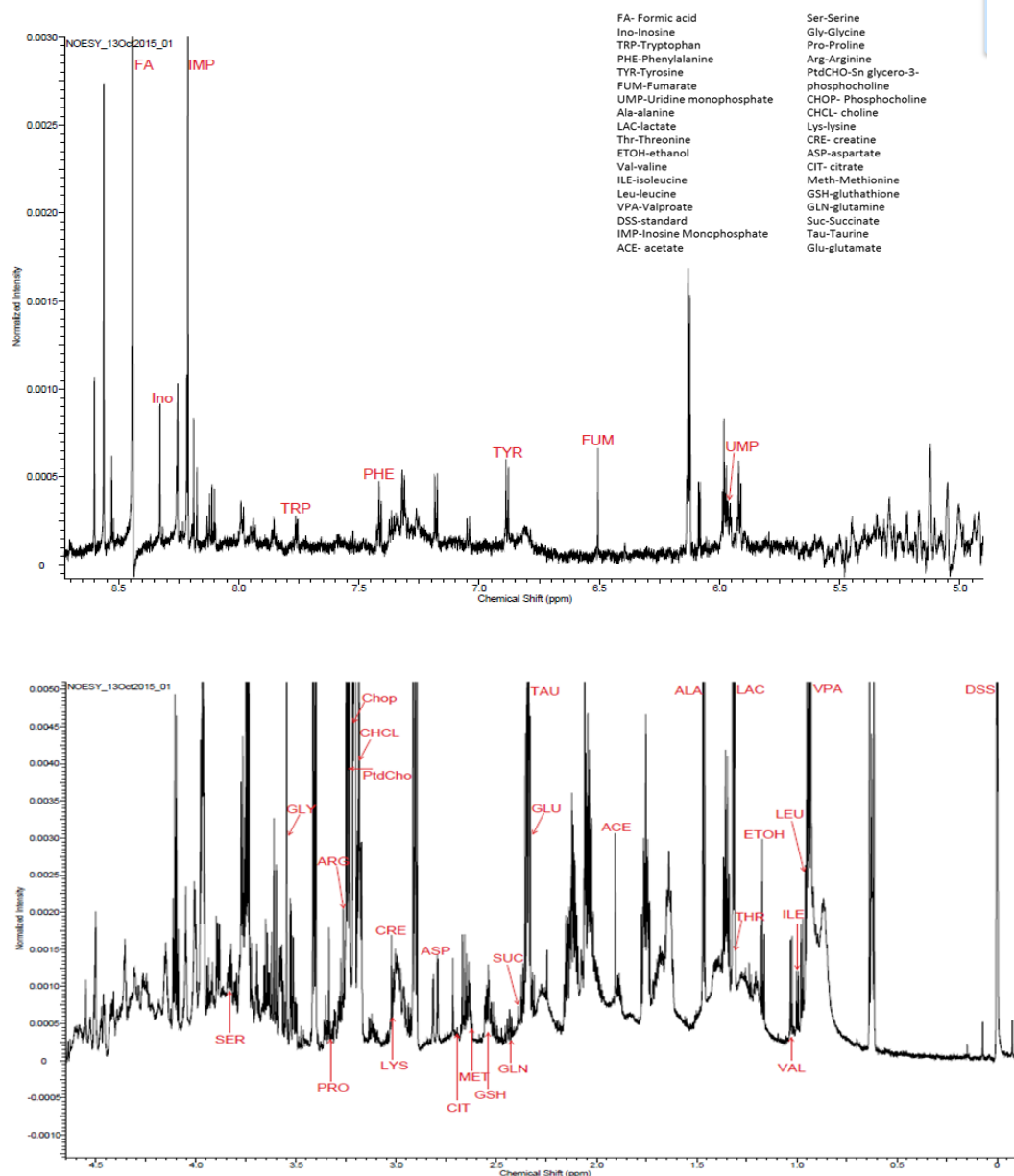
Supplementary figure 1.1. 60% cold Acetonitrile is suitable for the extraction and identification of metabolites from PBMCs on 1D NMR. ~

100 million PBMCs were washed in PBS, pelleted and lysed with 4 ml ice cold 60% ACN and vigorously vortexed for about 5 minutes, before being frozen in liquid nitrogen. Cells were thawed on ice, vortexed and centrifuged at 4000rpm for 10 minutes. The supernatant was then removed to an eppendorf before speed vac drying (37 C).This extraction and freeze-thaw cycle was repeated 3 times. The supernatant was then pooled in the same tubes and speed vac dried once more. The dried extracted metabolites were re-solubilized in 645 µl water mixture (580 µl H2O and 65 µl D2O) before NMR analysis.

Amino acids		
	μmoles /10^6 cells	
Valine	0.000131	
Tyrosine	8.07E-05	
Tryptophan	2.89E-05	
Threonine	0.000205	
Serine	0.000279	
Proline	0.000152	
Phenylalanine	7.61E-05	
Methionine	8E-05	
Lysine(3.015)	0.000183	
Leucine	0.000266	
Isoleucine	0.000102	
Glycine	0.000397	
Glutamate	0.002314	
Glutamine	0.000166	
Aspartate	0.000494	
Arginine(3.235ppm)	0.000752	
Alanine	0.000579	
Choline	0.000213	

Metabolites		
	μmoles /10^6 cells	
Acetate	0.000119	
Succinate	1.44E-05	
Formate	0.003833	
Fumarate	3.8E-05	
Pyruvate (2.36)	2.82E-05	
O-Phosphocholine	0.000458	
sn-Glycero-3-phosphocholine	0.00014	
Lactate	0.001827	

Nucleotides		
	μmoles /10^6 cells	
IMP (Inosine) (8.217,6.085)	0.00011	
GTP (5.925)	0.000145	
UMP(8.09,5.97)	7.41E-05	
AMP (8.586, 8.2534,6.125 ppm)	0.000113	
ADP(8.553,8.2575,6.133)	5.77E-05	
ATP(8.522,8.2554, 6.135)	8.2E-05	
CTP (7.86, 6.106)	3.61E-05	

Sugar Nucleotides		
	μmoles /10^6 cells	
UDP-N-Acetylglucosamine (5.50)	9.64E-05	
UDP-glucose(5.59)	0.000115	
UDP-galactose (5.63)	7.74E-05	

Supplementary figure 1.2. The concentration of metabolites identified per million PBMCs.

Amino acids (**A**), metabolites (**B**), nucleotides (**C**), Sugar-nucleotides (**D**) were identified by comparing the chemical shift (ppm) of each peak with that of known metabolic shifts from the NMR database (HMDB). The splitting pattern of each peak further identified the metabolite from other metabolites with similar chemical shifts. An external standard DSS, was used at a known concentration to quantify each metabolite.

References:

ADEWOYIN, A. S. & NWOGOH, B. 2014. Peripheral blood film - a review. *Ann Ib Postgrad Med,* 12**,** 71-9.

AGARD, N. J., BASKIN, J. M., PRESCHER, J. A., LO, A. & BERTOZZI, C. R. 2006. A comparative study of bioorthogonal reactions with azides. *ACS Chem Biol,* 1**,** 644-8.

ALLEGRA, C. J., CHABNER, B. A., DRAKE, J. C., LUTZ, R., RODBARD, D. & JOLIVET, J. 1985a. Enhanced inhibition of thymidylate synthase by methotrexate polyglutamates. *J Biol Chem,* 260**,** 9720-6.

ALLEGRA, C. J., DRAKE, J. C., JOLIVET, J. & CHABNER, B. A. 1985b. Inhibition of phosphoribosylaminoimidazolecarboxamide transformylase by methotrexate and dihydrofolic acid polyglutamates. *Proc Natl Acad Sci U S A,* 82**,** 4881-5.

ALLISON, A. C. & EUGUI, E. M. 2000. Mycophenolate mofetil and its mechanisms of action. *Immunopharmacology,* 47**,** 85-118.

ANDERSEN, S., HEINE, T., SNEVE, R., KONIG, I., KROKAN, H. E., EPE, B. & NILSEN, H. 2005. Incorporation of dUMP into DNA is a major source of spontaneous DNA damage, while excision of uracil is not required for cytotoxicity of fluoropyrimidines in mouse embryonic fibroblasts. *Carcinogenesis,* 26**,** 547-55.

ANDERSON, D. D., QUINTERO, C. M. & STOVER, P. J. 2011. Identification of a de novo thymidylate biosynthesis pathway in mammalian mitochondria. *Proc Natl Acad Sci U S A,* 108**,** 15163-8.

ANDERSON, D. D. & STOVER, P. J. 2009. SHMT1 and SHMT2 are functionally redundant in nuclear de novo thymidylate biosynthesis. *PLoS One,* 4**,** e5839.

ANDERSON, J. M., SMITH, M. D. & HUTCHISON, J. 1966. Megaloblastic anemia and methotrexate therapy. *Br Med J,* 2**,** 641-2.

ANDERSSON, S. E., JOHANSSON, L. H., LEXMULLER, K. & EKSTROM, G. M. 2000. Anti-arthritic effect of methotrexate: is it really mediated by adenosine? *Eur J Pharm Sci,* 9**,** 333-43.

ANGATA, T., MARGULIES, E. H., GREEN, E. D. & VARKI, A. 2004. Large-scale sequencing of the CD33-related Siglec gene cluster in five mammalian species reveals rapid evolution by multiple mechanisms. *Proc Natl Acad Sci U S A,* 101**,** 13251-6.

ANGATA, T. & VARKI, A. 2000a. Cloning, characterization, and phylogenetic analysis of siglec-9, a new member of the CD33-related group of siglecs. Evidence for co-evolution with sialic acid synthesis pathways. *J Biol Chem,* 275**,** 22127-35.

ANGATA, T. & VARKI, A. 2000b. Siglec-7: a sialic acid-binding lectin of the immunoglobulin superfamily. *Glycobiology,* 10**,** 431-8.

ANNUSSEK, T., SZUWART, T., KLEINHEINZ, J., KOIKY, C. & WERMKER, K. 2014. In vitro inhibition of HUVECs by low dose methotrexate - insights into oral adverse events. *Head Face Med,* 10**,** 19.

ANTHONY, K.-T. C. S. A. R. M. 2013. Antibody Glycosylation and Inflammation. *Antibodies,* 2**,** 392-414.

ARAVIND, L. & KOONIN, E. V. 2000. The alpha/beta fold uracil DNA glycosylases: a common origin with diverse fates. *Genome Biol,* 1**,** RESEARCH0007.

ARNOLD, J. N., WORMALD, M. R., SIM, R. B., RUDD, P. M. & DWEK, R. A. 2007. The impact of glycosylation on the biological function and structure of human immunoglobulins. *Annu Rev Immunol,* 25**,** 21-50.

ASSARAF, Y. G. 2007. Molecular basis of antifolate resistance. *Cancer Metastasis Rev,* 26**,** 153-81.

BAGGOTT, J. E. & MORGAN, S. L. 2009. Methotrexate catabolism to 7-hydroxymethotrexate in rheumatoid arthritis alters drug efficacy and retention and is reduced by folic acid supplementation. *Arthritis Rheum,* 60**,** 2257-61.

BAGGOTT, J. E., VAUGHN, W. H. & HUDSON, B. B. 1986. Inhibition of 5-aminoimidazole-4-carboxamide ribotide transformylase, adenosine deaminase and 5'-adenylate deaminase by

polyglutamates of methotrexate and oxidized folates and by 5-aminoimidazole-4-carboxamide riboside and ribotide. *Biochem J,* 236**,** 193-200.

BARLOWE, C. K. & APPLING, D. R. 1988. In vitro evidence for the involvement of mitochondrial folate metabolism in the supply of cytoplasmic one-carbon units. *Biofactors,* 1**,** 171-6.

BARNES, Y. C., SKELTON, T. P., STAMENKOVIC, I. & SGROI, D. C. 1999. Sialylation of the sialic acid binding lectin sialoadhesin regulates its ability to mediate cell adhesion. *Blood,* 93**,** 1245-52.

BASKIN, J. M., PRESCHER, J. A., LAUGHLIN, S. T., AGARD, N. J., CHANG, P. V., MILLER, I. A., LO, A., CODELLI, J. A. & BERTOZZI, C. R. 2007. Copper-free click chemistry for dynamic in vivo imaging. *Proc Natl Acad Sci U S A,* 104**,** 16793-7.

BAX, M., HUIZINGA, T. W. & TOES, R. E. 2014. The pathogenic potential of autoreactive antibodies in rheumatoid arthritis. *Semin Immunopathol,* 36**,** 313-25.

BECKERS, A., ORGANE, S., TIMMERMANS, L., VANDERHOYDONC, F., DEBOEL, L., DERUA, R., WAELKENS, E., BRUSSELMANS, K., VERHOEVEN, G. & SWINNEN, J. V. 2006. Methotrexate enhances the antianabolic and antiproliferative effects of 5-aminoimidazole-4-carboxamide riboside. *Mol Cancer Ther,* 5**,** 2211-7.

BESANCENEY-WEBLER, C., JIANG, H., ZHENG, T., FENG, L., SORIANO DEL AMO, D., WANG, W., KLIVANSKY, L. M., MARLOW, F. L., LIU, Y. & WU, P. 2011. Increasing the efficacy of bioorthogonal click reactions for bioconjugation: a comparative study. *Angew Chem Int Ed Engl,* 50**,** 8051-6.

BIRD, P. G. H. A. L. G. 2014. Methotrexate in Rheumatoid Arthritis: Efficacy and Safety. *J Pharmacovigilance,* 2.

BLITS, M., JANSEN, G., ASSARAF, Y. G., VAN DE WIEL, M. A., LEMS, W. F., NURMOHAMED, M. T., VAN SCHAARDENBURG, D., VOSKUYL, A. E., WOLBINK, G. J., VOSSLAMBER, S. & VERWEIJ, C. L. 2013. Methotrexate normalizes up-regulated folate pathway genes in rheumatoid arthritis. *Arthritis Rheum,* 65**,** 2791-802.

BLOUNT, B. C., MACK, M. M., WEHR, C. M., MACGREGOR, J. T., HIATT, R. A., WANG, G., WICKRAMASINGHE, S. N., EVERSON, R. B. & AMES, B. N. 1997. Folate deficiency causes uracil misincorporation into human DNA and chromosome breakage: implications for cancer and neuronal damage. *Proc Natl Acad Sci U S A,* 94**,** 3290-5.

BOGENHAGEN, D. & CLAYTON, D. A. 1976. Thymidylate nucleotide supply for mitochondrial DNA synthesis in mouse L-cells. Effect of 5-fluorodeoxyuridine and methotrexate in thymidine kinase plus and thymidine kinase minus cells. *J Biol Chem,* 251**,** 2938-44.

BOLIGAN, K. F., MESA, C., FERNANDEZ, L. E. & VON GUNTEN, S. 2015. Cancer intelligence acquired (CIA): tumor glycosylation and sialylation codes dismantling antitumor defense. *Cell Mol Life Sci,* 72**,** 1231-48.

BONDT, A., NICOLARDI, S., JANSEN, B. C., KUIJPER, T. M., HAZES, J. M. W., VAN DER BURGT, Y. E. M., WUHRER, M. & DOLHAIN, R. 2017. IgA N- and O-glycosylation profiling reveals no association with the pregnancy-related improvement in rheumatoid arthritis. *Arthritis Res Ther,* 19**,** 160.

BORMAN, L. S. & BRANDA, R. F. 1989. Nutritional folate deficiency in Chinese hamster ovary cells. I. Characterization of the pleiotropic response and its modulation by nucleic acid precursors. *J Cell Physiol,* 140**,** 335-43.

BOYCE, M. & BERTOZZI, C. R. 2011. Bringing chemistry to life. *Nat Methods,* 8**,** 638-42.

BRAMBELL, F. W. 1966. The transmission of immunity from mother to young and the catabolism of immunoglobulins. *Lancet,* 2**,** 1087-93.

BRAND, M. D., AFFOURTIT, C., ESTEVES, T. C., GREEN, K., LAMBERT, A. J., MIWA, S., PAKAY, J. L. & PARKER, N. 2004. Mitochondrial superoxide: production, biological effects, and activation of uncoupling proteins. *Free Radic Biol Med,* 37**,** 755-67.

BRAND, M. D. & ESTEVES, T. C. 2005. Physiological functions of the mitochondrial uncoupling proteins UCP2 and UCP3. *Cell Metab,* 2**,** 85-93.

BRENNAN, F. M. & MCINNES, I. B. 2008. Evidence that cytokines play a role in rheumatoid arthritis. *J Clin Invest,* 118**,** 3537-45.

BRINKMAN-VAN DER LINDEN, E. C. & VARKI, A. 2000. New aspects of siglec binding specificities, including the significance of fucosylation and of the sialyl-Tn epitope. Sialic acid-binding immunoglobulin superfamily lectins. *J Biol Chem,* 275**,** 8625-32.

BROSNAN, M. E., MACMILLAN, L., STEVENS, J. R. & BROSNAN, J. T. 2015. Division of labour: how does folate metabolism partition between one-carbon metabolism and amino acid oxidation? *Biochem J,* 472**,** 135-46.

BUDZIK, G. P., COLLETTI, L. M. & FALTYNEK, C. R. 2000. Effects of methotrexate on nucleotide pools in normal human T cells and the CEM T cell line. *Life Sci,* 66**,** 2297-307.

BURNS, C. M., TSAI, V. & ZVAIFLER, N. J. 1992. High percentage of CD8+, Leu-7+ cells in rheumatoid arthritis synovial fluid. *Arthritis Rheum,* 35**,** 865-73.

CAMMANN, C., RATH, A., REICHL, U., LINGEL, H., BRUNNER-WEINZIERL, M., SIMEONI, L., SCHRAVEN, B. & LINDQUIST, J. A. 2016. Early changes in the metabolic profile of activated CD8(+) T cells. *BMC Cell Biol,* 17**,** 28.

CHAN, E. S. & CRONSTEIN, B. N. 2002. Molecular action of methotrexate in inflammatory diseases. *Arthritis Res,* 4**,** 266-73.

CHAN, E. S. & CRONSTEIN, B. N. 2010. Methotrexate--how does it really work? *Nat Rev Rheumatol,* 6**,** 175-8.

CHAN, E. S. & CRONSTEIN, B. N. 2013. Mechanisms of action of methotrexate. *Bull Hosp Jt Dis (2013),* 71 Suppl 1**,** S5-8.

CHAN, T. R., HILGRAF, R., SHARPLESS, K. B. & FOKIN, V. V. 2004. Polytriazoles as copper(I)-stabilizing ligands in catalysis. *Org Lett,* 6**,** 2853-5.

CHANG, C.-J. 2013. Lutein Protects against Methotrexate-Induced and Reactive Oxygen Species-Mediated Apoptotic Cell Injury of IEC-6 Cells. *plosone*.

CHANG, P. V., PRESCHER, J. A., HANGAUER, M. J. & BERTOZZI, C. R. 2007. Imaging cell surface glycans with bioorthogonal chemical reporters. *J Am Chem Soc,* 129**,** 8400-1.

CHEN, L., QI, H., KORENBERG, J., GARROW, T. A., CHOI, Y. J. & SHANE, B. 1996. Purification and properties of human cytosolic folylpoly-gamma-glutamate synthetase and organization, localization, and differential splicing of its gene. *J Biol Chem,* 271**,** 13077-87.

CHEN, V. J., BEWLEY, J. R., ANDIS, S. L., SCHULTZ, R. M., IVERSEN, P. W., SHIH, C., MENDELSOHN, L. G., SEITZ, D. E. & TONKINSON, J. L. 1998. Preclinical cellular pharmacology of LY231514 (MTA): a comparison with methotrexate, LY309887 and raltitrexed for their effects on intracellular folate and nucleoside triphosphate pools in CCRF-CEM cells. *Br J Cancer,* 78 Suppl 3**,** 27-34.

CHEN, Y. X., LV, W. G., CHEN, H. Z., YE, F. & XIE, X. 2009. Methotrexate induces apoptosis of human choriocarcinoma cell line JAR via a mitochondrial pathway. *Eur J Obstet Gynecol Reprod Biol,* 143**,** 107-11.

CHERN, C. L., HUANG, R. F., CHEN, Y. H., CHENG, J. T. & LIU, T. Z. 2001. Folate deficiency-induced oxidative stress and apoptosis are mediated via homocysteine-dependent overproduction of hydrogen peroxide and enhanced activation of NF-kappaB in human Hep G2 cells. *Biomed Pharmacother,* 55**,** 434-42.

CHIBALIN, A. V. 2015. Methotrexate Promotes Glucose Uptake and Lipid Oxidation in Skeletal Muscle via AMPK Activation. *Diabetes,* 64**,** 360-369.

CHIMENTI, M. S., TUCCI, P., CANDI, E., PERRICONE, R., MELINO, G. & WILLIS, A. E. 2013. Metabolic profiling of human CD4+ cells following treatment with methotrexate and anti-TNF-alpha infliximab. *Cell Cycle,* 12**,** 3025-36.

CHLADEK, J., SIMKOVA, M., VANECKOVA, J., HROCH, M., CHLADKOVA, J., MARTINKOVA, J., VAVROVA, J. & BERANEK, M. 2008. The effect of folic acid supplementation on the pharmacokinetics and pharmacodynamics of oral methotrexate during the remission-induction period of treatment for moderate-to-severe plaque psoriasis. *Eur J Clin Pharmacol,* 64**,** 347-55.

CHONG, L., MA, G., BARTIER, W. A. & TATTERSALL, M. H. 2010. Effects of extracellular purines on cytotoxicity of methotrexate. *Cancer Chemother Pharmacol,* 66**,** 121-7.

CIAIOLO, C., FERRERO, D., PUGLIESE, A., BIGLINO, A., MARLETTO, G., TONELLO, M., COLZANI, G. & MARIETTI, G. 1988. Enhancement of methotrexate cytotoxicity by modulation of proliferative activity in normal and neoplastic T lymphocytes and in a myeloid leukemia cell line. *Tumori,* 74**,** 537-42.

CLARK, M. C. & BAUM, L. G. 2012. T cells modulate glycans on CD43 and CD45 during development and activation, signal regulation, and survival. *Ann N Y Acad Sci,* 1253**,** 58-67.

COELHO, C., TESFA, L., ZHANG, J., RIVERA, J., GONCALVES, T. & CASADEVALL, A. 2012. Analysis of cell cycle and replication of mouse macrophages after in vivo and in vitro Cryptococcus neoformans infection using laser scanning cytometry. *Infect Immun,* 80**,** 1467-78.

COHEN, I. J. 2013. Challenging the clinical relevance of folinic acid over rescue after high dose methotrexate (HDMTX). *Med Hypotheses*.

COHEN, I. J. & WOLFF, J. E. 2013. How long can folinic acid rescue be delayed after high-dose methotrexate without toxicity? *Pediatr Blood Cancer*.

COHEN, M. & VARKI, A. 2010. The sialome--far more than the sum of its parts. *OMICS,* 14**,** 455-64.

COLLINGE, M., COLE, S. H., SCHNEIDER, P. A., DONOVAN, C. B., KAMPERSCHROER, C. & KAWABATA, T. T. 2010. Human lymphocyte activation assay: an in vitro method for predictive immunotoxicity testing. *J Immunotoxicol,* 7**,** 357-66.

COLLINS, B. E., KISO, M., HASEGAWA, A., TROPAK, M. B., RODER, J. C., CROCKER, P. R. & SCHNAAR, R. L. 1997a. Binding specificities of the sialoadhesin family of I-type lectins. Sialic acid linkage and substructure requirements for binding of myelin-associated glycoprotein, Schwann cell myelin protein, and sialoadhesin. *J Biol Chem,* 272**,** 16889-95.

COLLINS, B. E., YANG, L. J., MUKHOPADHYAY, G., FILBIN, M. T., KISO, M., HASEGAWA, A. & SCHNAAR, R. L. 1997b. Sialic acid specificity of myelin-associated glycoprotein binding. *J Biol Chem,* 272**,** 1248-55.

COLLINS, D. P. 2000. Cytokine and cytokine receptor expression as a biological indicator of immune activation: important considerations in the development of in vitro model systems. *J Immunol Methods,* 243**,** 125-45.

COLLINS, E. S., GALLIGAN, M. C., SALDOVA, R., ADAMCZYK, B., ABRAHAMS, J. L., CAMPBELL, M. P., NG, C. T., VEALE, D. J., MURPHY, T. B., RUDD, P. M. & FITZGERALD, O. 2013. Glycosylation status of serum in inflammatory arthritis in response to anti-TNF treatment. *Rheumatology (Oxford),* 52**,** 1572-82.

COMELLI, E. M., SUTTON-SMITH, M., YAN, Q., AMADO, M., PANICO, M., GILMARTIN, T., WHISENANT, T., LANIGAN, C. M., HEAD, S. R., GOLDBERG, D., MORRIS, H. R., DELL, A. & PAULSON, J. C. 2006. Activation of murine CD4+ and CD8+ T lymphocytes leads to dramatic remodeling of N-linked glycans. *J Immunol,* 177**,** 2431-40.

COSGRAVE, E. F., STRUWE, W. B., HAYES, J. M., HARVEY, D. J., WORMALD, M. R. & RUDD, P. M. 2013. N-linked glycan structures of the human Fcgamma receptors produced in NS0 cells. *J Proteome Res,* 12**,** 3721-37.

COURTEMANCHE, C., ELSON-SCHWAB, I., MASHIYAMA, S. T., KERRY, N. & AMES, B. N. 2004. Folate deficiency inhibits the proliferation of primary human CD8+ T lymphocytes in vitro. *J Immunol,* 173**,** 3186-92.

CRISÓSTOMO, L. 2013. *Pilot-Model for oxidative post-competition recovery in swimmers.* UNIVERSIDADE DA BEIRA INTERIOR.

CROCE, A., FIRUZI, O., ALTIERI, F., EUFEMI, M., AGOSTINO, R., PRIORI, R., BOMBARDIERI, M., ALESSANDRI, C., VALESINI, G. & SASO, L. 2007. Effect of infliximab on the glycosylation of IgG of patients with rheumatoid arthritis. *J Clin Lab Anal,* 21**,** 303-14.

CROCKER, P. R., PAULSON, J. C. & VARKI, A. 2007. Siglecs and their roles in the immune system. *Nat Rev Immunol,* 7**,** 255-66.

CROCKER, P. R. & VARKI, A. 2001. Siglecs, sialic acids and innate immunity. *Trends Immunol,* 22**,** 337-42.

CRONSTEIN, B. N. 1996. Molecular therapeutics. Methotrexate and its mechanism of action. *Arthritis Rheum,* 39**,** 1951-60.

CRONSTEIN, B. N. 2005. Low-dose methotrexate: a mainstay in the treatment of rheumatoid arthritis. *Pharmacol Rev,* 57**,** 163-72.

CRONSTEIN, B. N. 2006. Going with the flow: methotrexate, adenosine, and blood flow. *Ann Rheum Dis,* 65**,** 421-2.

CRONSTEIN, B. N., NAIME, D. & OSTAD, E. 1993. The antiinflammatory mechanism of methotrexate. Increased adenosine release at inflamed sites diminishes leukocyte accumulation in an in vivo model of inflammation. *J Clin Invest,* 92**,** 2675-82.

CROSS, J. V. & TEMPLETON, D. J. 2006. Regulation of signal transduction through protein cysteine oxidation. *Antioxid Redox Signal,* 8**,** 1819-27.

CUTOLO, M., SULLI, A., PIZZORNI, C., SERIOLO, B. & STRAUB, R. H. 2001. Anti-inflammatory mechanisms of methotrexate in rheumatoid arthritis. *Ann Rheum Dis,* 60**,** 729-35.

CYBULSKI, R. L. & FISHER, R. R. 1977. Mitochondrial neutral amino acid transport: evidence for a carrier mediated mechanism. *Biochemistry,* 16**,** 5116-20.

CYBULSKI, R. L. & FISHER, R. R. 1981. Uptake of oxidized folates by rat liver mitochondria. *Biochim Biophys Acta,* 646**,** 329-33.

DA SILVA, C. P., DE OLIVEIRA, C. R., DA CONCEICAO, M. & DE LIMA, P. 1996. Apoptosis as a mechanism of cell death induced by different chemotherapeutic drugs in human leukemic T-lymphocytes. *Biochem Pharmacol,* 51**,** 1331-40.

DALZIEL, M., LEMAIRE, S., EWING, J., KOBAYASHI, L. & LAU, J. T. 1999. Hepatic acute phase induction of murine beta-galactoside alpha 2,6 sialyltransferase (ST6Gal I) is IL-6 dependent and mediated by elevation of exon H-containing class of transcripts. *Glycobiology,* 9**,** 1003-8.

DANENBERG, P. V., GUSTAVSSON, B., JOHNSTON, P., LINDBERG, P., MOSER, R., ODIN, E., PETERS, G. J. & PETRELLI, N. 2016. Folates as adjuvants to anticancer agents: Chemical rationale and mechanism of action. *Crit Rev Oncol Hematol,* 106**,** 118-31.

DARZYNKIEWICZ, Z., TRAGANOS, F., SHARPLESS, T. & MELAMED, M. R. 1976. Lymphocyte stimulation: a rapid multiparameter analysis. *Proc Natl Acad Sci U S A,* 73**,** 2881-4.

DE GRAAF, T. W., SLOT, S. S., PETERS, G. J. & VAN DIJK, W. 1993. Changes in glycosylation of L1210 cells after exposure to various antimetabolites. *Eur J Cancer,* 29A**,** 1760-5.

DE LATHOUDER, S., GERARDS, A. H., DE GROOT, E. R., VALKHOF, M. & AARDEN, L. A. 2002. Mycophenolic acid and methotrexate inhibit lymphocyte cytokine production via different mechanisms. *Eur Cytokine Netw,* 13**,** 317-23.

DEHNERT, K. W., BEAHM, B. J., HUYNH, T. T., BASKIN, J. M., LAUGHLIN, S. T., WANG, W., WU, P., AMACHER, S. L. & BERTOZZI, C. R. 2011. Metabolic labeling of fucosylated glycans in developing zebrafish. *ACS Chem Biol,* 6**,** 547-52.

DEL VAL, I. J., KYRIAKOPOULOS, S., POLIZZI, K. M. & KONTORAVDI, C. 2013. An optimized method for extraction and quantification of nucleotides and nucleotide sugars from mammalian cells. *Anal Biochem,* 443**,** 172-80.

DIETMAIR, S., TIMMINS, N. E., GRAY, P. P., NIELSEN, L. K. & KROMER, J. O. 2010. Towards quantitative metabolomics of mammalian cells: development of a metabolite extraction protocol. *Anal Biochem,* 404**,** 155-64.

DRESKIN, S. C., THOMAS, G. W., DALE, S. N. & HEASLEY, L. E. 2001. Isoforms of Jun kinase are differentially expressed and activated in human monocyte/macrophage (THP-1) cells. *J Immunol,* 166**,** 5646-53.

DRICKAMER, M. E. T. A. K. 2003. *Introduction to Glycobiology,* United States, Oxford University Press.

DROGE, W. 2002. Free Radicals in the Physiological Control of Cell Function. *Physiology Reviews,* 82**,** 47-95.

DUBE, D. H., PRESCHER, J. A., QUANG, C. N. & BERTOZZI, C. R. 2006. Probing mucin-type O-linked glycosylation in living animals. *Proc Natl Acad Sci U S A,* 103**,** 4819-24.

DUKE, O., PANAYI, G. S., JANOSSY, G., POULTER, L. W. & TIDMAN, N. 1983. Analysis of T cell subsets in the peripheral blood and synovial fluid of patients with rheumatoid arthritis by means of monoclonal antibodies. *Ann Rheum Dis,* 42**,** 357-61.

DUTHIE, S. J. & MCMILLAN, P. 1997. Uracil misincorporation in human DNA detected using single cell gel electrophoresis. *Carcinogenesis,* 18**,** 1709-14.

EBIOSCIENCE T cell activation in vitro. *Bioassays -best protocols*.

EDBERG, J. C., BARINSKY, M., REDECHA, P. B., SALMON, J. E. & KIMBERLY, R. P. 1990. Fc gamma RIII expressed on cultured monocytes is a N-glycosylated transmembrane protein distinct from Fc gamma RIII expressed on natural killer cells. *J Immunol,* 144**,** 4729-34.

EDBERG, J. C. & KIMBERLY, R. P. 1997. Cell type-specific glycoforms of Fc gamma RIIIa (CD16): differential ligand binding. *J Immunol,* 159**,** 3849-57.

ELANGO, T., DAYALAN, H., GNANARAJ, P., MALLIGARJUNAN, H. & SUBRAMANIAN, S. 2014. Impact of methotrexate on oxidative stress and apoptosis markers in psoriatic patients. *Clin Exp Med,* 14**,** 431-7.

ERCAN, A., CUI, J., CHATTERTON, D. E., DEANE, K. D., HAZEN, M. M., BRINTNELL, W., O'DONNELL, C. I., DERBER, L. A., WEINBLATT, M. E., SHADICK, N. A., BELL, D. A., CAIRNS, E., SOLOMON, D. H., HOLERS, V. M., RUDD, P. M. & LEE, D. M. 2010. Aberrant IgG galactosylation precedes disease onset, correlates with disease activity, and is prevalent in autoantibodies in rheumatoid arthritis. *Arthritis Rheum,* 62**,** 2239-48.

ERCAN, A., CUI, J., HAZEN, M. M., BATLIWALLA, F., ROYLE, L., RUDD, P. M., COBLYN, J. S., SHADICK, N., WEINBLATT, M. E., GREGERSEN, P., LEE, D. M. & NIGROVIC, P. A. 2012. Hypogalactosylation of serum N-glycans fails to predict clinical response to methotrexate and TNF inhibition in rheumatoid arthritis. *Arthritis Res Ther,* 14**,** R43.

EVANS, D. R. & GUY, H. I. 2004. Mammalian pyrimidine biosynthesis: fresh insights into an ancient pathway. *J Biol Chem,* 279**,** 33035-8.

FAIRBANKS, L. D., BOFILL, M., RUCKEMANN, K. & SIMMONDS, H. A. 1995. Importance of ribonucleotide availability to proliferating T-lymphocytes from healthy humans. Disproportionate expansion of pyrimidine pools and contrasting effects of de novo synthesis inhibitors. *J Biol Chem,* 270**,** 29682-9.

FAIRBANKS, L. D., RUCKEMANN, K., QIU, Y., HAWRYLOWICZ, C. M., RICHARDS, D. F., SWAMINATHAN, R., KIRSCHBAUM, B. & SIMMONDS, H. A. 1999. Methotrexate inhibits the first committed step of purine biosynthesis in mitogen-stimulated human T-lymphocytes: a metabolic basis for efficacy in rheumatoid arthritis? *Biochem J,* 342 (Pt 1)**,** 143-52.

FERNANDA BARBISAN2, J. S. D. R. M., ALEXIS TROTT4, VEROˆ NICA AZZOLIN2,, EDUARDO BORTOLUZZI DORNELLES3, M. M., THAıˊS DOELER ALGARVE3,, MARTA MARIA MEDEIROS FRESCURA DUARTE1, C. P. M., TAıˊS CRISTINA UNFER1, & KAREN LILIAN SCHOTT3, I. B. M. N. D. C., 2,3* 2014. Methotrexate-Related Response on Human Peripheral Blood Mononuclear Cells May Be Modulated by the Ala16Val-SOD2 Gene Polymorphism. *PLOS ONE,* 9.

FERNANDEZ-RAMOS, A. A., POINDESSOUS, V., MARCHETTI-LAURENT, C., PALLET, N. & LORIOT, M. A. 2016. The effect of immunosuppressive molecules on T-cell metabolic reprogramming. *Biochimie,* 127**,** 23-36.

FERRARA, C., GRAU, S., JAGER, C., SONDERMANN, P., BRUNKER, P., WALDHAUER, I., HENNIG, M., RUF, A., RUFER, A. C., STIHLE, M., UMANA, P. & BENZ, J. 2011. Unique carbohydrate-carbohydrate interactions are required for high affinity binding between FcgammaRIII and antibodies lacking core fucose. *Proc Natl Acad Sci U S A,* 108**,** 12669-74.

FERRARA, C., STUART, F., SONDERMANN, P., BRUNKER, P. & UMANA, P. 2006. The carbohydrate at FcgammaRIIIa Asn-162. An element required for high affinity binding to non-fucosylated IgG glycoforms. *J Biol Chem,* 281**,** 5032-6.

FITZGERALD, G. B. & WICK, M. M. 1987. Comparison of the inhibitory effects of hydroxyurea, 5-fluorodeoxyuridine, 3,4-dihydroxybenzylamine, and methotrexate on human squamous cell carcinoma. *J Invest Dermatol,* 88**,** 66-70.

FLESCHER, E., LEDBETTER, J. A., SCHIEVEN, G. L., VELA-ROCH, N., FOSSUM, D., DANG, H., OGAWA, N. & TALAL, N. 1994. Longitudinal exposure of human T lymphocytes to weak oxidative stress suppresses transmembrane and nuclear signal transduction. *J Immunol,* 153**,** 4880-9.

FODOR, T., SZANTO, M., ABDUL-RAHMAN, O., NAGY, L., DER, A., KISS, B. & BAI, P. 2016. Combined Treatment of MCF-7 Cells with AICAR and Methotrexate, Arrests Cell Cycle and Reverses Warburg Metabolism through AMP-Activated Protein Kinase (AMPK) and FOXO1. *PLoS One,* 11**,** e0150232.

FOX, R. M., TRIPP, E. H. & TATTERSALL, M. H. 1980. Mechanism of deoxycytidine rescue of thymidine toxicity in human T-leukemic lymphocytes. *Cancer Res,* 40**,** 1718-21.

FROUIN, I., PROSPERI, E., DENEGRI, M., NEGRI, C., DONZELLI, M., ROSSI, L., RIVA, F., STEFANINI, M. & SCOVASSI, A. I. 2001. Different effects of methotrexate on DNA mismatch repair proficient and deficient cells. *Eur J Cancer,* 37**,** 1173-80.

FURST, D. E. & KREMER, J. M. 1988. Methotrexate in rheumatoid arthritis. *Arthritis Rheum,* 31**,** 305-14.

FUSTER, M. M. & ESKO, J. D. 2005. The sweet and sour of cancer: glycans as novel therapeutic targets. *Nat Rev Cancer,* 5**,** 526-42.

GARAVITO, M. F., NARVAEZ-ORTIZ, H. Y. & ZIMMERMANN, B. H. 2015. Pyrimidine Metabolism: Dynamic and Versatile Pathways in Pathogens and Cellular Development. *J Genet Genomics,* 42**,** 195-205.

GARCIA-MARTINEZ, L. F. & APPLING, D. R. 1993. Characterization of the folate-dependent mitochondrial oxidation of carbon 3 of serine. *Biochemistry,* 32**,** 4671-6.

GENESTIER, L., PAILLOT, R., FOURNEL, S., FERRARO, C., MIOSSEC, P. & REVILLARD, J. P. 1998. Immunosuppressive properties of methotrexate: apoptosis and clonal deletion of activated peripheral T cells. *J Clin Invest,* 102**,** 322-8.

GENESTIER, L., PAILLOT, R., QUEMENEUR, L., IZERADJENE, K. & REVILLARD, J. P. 2000. Mechanisms of action of methotrexate. *Immunopharmacology,* 47**,** 247-57.

GERARDS, A. H., DE LATHOUDER, S., DE GROOT, E. R., DIJKMANS, B. A. & AARDEN, L. A. 2003. Inhibition of cytokine production by methotrexate. Studies in healthy volunteers and patients with rheumatoid arthritis. *Rheumatology (Oxford),* 42**,** 1189-96.

GIANNATTASIO, S., GAGLIARDI, S., SAMAJA, M. & MARRA, E. 2003. Simultaneous determination of purine nucleotides, their metabolites and beta-nicotinamide adenine dinucleotide in cerebellar granule cells by ion-pair high performance liquid chromatography. *Brain Res Brain Res Protoc,* 10**,** 168-74.

GINDZIENSKA-SIESKIEWICZ, E., KLIMIUK, P. A., KISIEL, D. G., GINDZIENSKI, A. & SIERAKOWSKI, S. 2007. The changes in monosaccharide composition of immunoglobulin G in the course of rheumatoid arthritis. *Clin Rheumatol,* 26**,** 685-90.

GORNIK, O. & LAUC, G. 2008. Glycosylation of serum proteins in inflammatory diseases. *Dis Markers,* 25**,** 267-78.

GORONZY, J., WEYAND, C., IMBODEN, J., MANGER, B. & FATHMAN, C. G. 1987. Heterogeneity of signal requirements in T cell activation within a panel of human proliferative T cell clones. *J Immunol,* 138**,** 3087-93.

GOTTLIEB, E., ARMOUR, S. M., HARRIS, M. H. & THOMPSON, C. B. 2003. Mitochondrial membrane potential regulates matrix configuration and cytochrome c release during apoptosis. *Cell Death Differ,* 10**,** 709-17.

GOULIAN, M., BLEILE, B. & TSENG, B. Y. 1980a. The effect of methotrexate on levels of dUTP in animal cells. *J Biol Chem,* 255**,** 10630-7.

GOULIAN, M., BLEILE, B. & TSENG, B. Y. 1980b. Methotrexate-induced misincorporation of uracil into DNA. *Proc Natl Acad Sci U S A,* 77**,** 1956-60.

GOWANS, G. J., HAWLEY, S. A., ROSS, F. A. & HARDIE, D. G. 2013. AMP is a true physiological regulator of AMP-activated protein kinase by both allosteric activation and enhancing net phosphorylation. *Cell Metab,* 18**,** 556-66.

GREEN, P. G., BASBAUM, A. I., HELMS, C. & LEVINE, J. D. 1991. Purinergic regulation of bradykinin-induced plasma extravasation and adjuvant-induced arthritis in the rat. *Proc Natl Acad Sci U S A,* 88**,** 4162-5.

GRINGHUIS, S. I., LEOW, A., PAPENDRECHT-VAN DER VOORT, E. A., REMANS, P. H., BREEDVELD, F. C. & VERWEIJ, C. L. 2000. Displacement of linker for activation of T cells from the plasma membrane due to redox balance alterations results in hyporesponsiveness of synovial fluid T lymphocytes in rheumatoid arthritis. *J Immunol,* 164**,** 2170-9.

GROFF, J. P. & BLAKLEY, R. L. 1978. Rescue of human lymphoid cells from the effects of methotrexate in vitro. *Cancer Res,* 38**,** 3847-53.

GU, X. & WANG, D. I. 1998. Improvement of interferon-gamma sialylation in Chinese hamster ovary cell culture by feeding of N-acetylmannosamine. *Biotechnol Bioeng,* 58**,** 642-8.

HA, H. C., SIRISOMA, N. S., KUPPUSAMY, P., ZWEIER, J. L., WOSTER, P. M. & CASERO, R. A., JR. 1998. The natural polyamine spermine functions directly as a free radical scavenger. *Proc Natl Acad Sci U S A,* 95**,** 11140-5.

HAMPSON, R. K., BARRON, L. L. & OLSON, M. S. 1983. Regulation of the glycine cleavage system in isolated rat liver mitochondria. *J Biol Chem,* 258**,** 2993-9.

HANG, H. C., YU, C., KATO, D. L. & BERTOZZI, C. R. 2003. A metabolic labeling approach toward proteomic analysis of mucin-type O-linked glycosylation. *Proc Natl Acad Sci U S A,* 100**,** 14846-51.

HARA, N., ICHINOSE, Y., MOTOHIRO, A., KUDA, T., ASO, H. & OHTA, M. 1990. Influence of chemotherapeutic agents on superoxide anion production by human polymorphonuclear leukocytes. *Cancer,* 66**,** 684-8.

HAROON, N., SRIVASTAVA, R., MISRA, R. & AGGARWAL, A. 2008. A novel predictor of clinical response to methotrexate in patients with rheumatoid arthritis: a pilot study of in vitro T cell cytokine suppression. *J Rheumatol,* 35**,** 975-8.

HAYES, J. M., COSGRAVE, E. F., STRUWE, W. B., WORMALD, M., DAVEY, G. P., JEFFERIS, R. & RUDD, P. M. 2014. Glycosylation and Fc receptors. *Curr Top Microbiol Immunol,* 382**,** 165-99.

HAYES, J. M., WORMALD, M. R., RUDD, P. M. & DAVEY, G. P. 2016. Fc gamma receptors: glycobiology and therapeutic prospects. *J Inflamm Res,* 9**,** 209-219.

HAZRA, A., SELHUB, J., CHAO, W. H., UELAND, P. M., HUNTER, D. J. & BARON, J. A. 2010. Uracil misincorporation into DNA and folic acid supplementation. *Am J Clin Nutr,* 91**,** 160-5.

HERMAN, S., ZURGIL, N. & DEUTSCH, M. 2005. Low dose methotrexate induces apoptosis with reactive oxygen species involvement in T lymphocytic cell lines to a greater extent than in monocytic lines. *Inflamm Res,* 54**,** 273-80.

HERMAN, S., ZURGIL, N., LANGEVITZ, P., EHRENFELD, M. & DEUTSCH, M. 2003. The induction of apoptosis by methotrexate in activated lymphocytes as indicated by fluorescence hyperpolarization: a possible model for predicting methotrexate therapy for rheumatoid arthritis patients. *Cell Struct Funct,* 28**,** 113-22.

HIRST, J., KING, M. S. & PRYDE, K. R. 2008. The production of reactive oxygen species by complex I. *Biochem Soc Trans,* 36**,** 976-80.

HO, P. I., ASHLINE, D., DHITAVAT, S., ORTIZ, D., COLLINS, S. C., SHEA, T. B. & ROGERS, E. 2003. Folate deprivation induces neurodegeneration: roles of oxidative stress and increased homocysteine. *Neurobiol Dis,* 14**,** 32-42.

HOFFBRAND, A. V. G., K; LAVOIE, A; TATTERSALL, M.H.N 1973. Thymidylate concentration in megalobastic anaemia. *Nature*.

HOGAN, P. G. 2017. Calcium-NFAT transcriptional signalling in T cell activation and T cell exhaustion. *Cell Calcium*.

HONG, V., PRESOLSKI, S. I., MA, C. & FINN, M. G. 2009. Analysis and optimization of copper-catalyzed azide-alkyne cycloaddition for bioconjugation. *Angew Chem Int Ed Engl,* 48**,** 9879-83.

HONG, V., STEINMETZ, N. F., MANCHESTER, M. & FINN, M. G. 2010. Labeling live cells by copper-catalyzed alkyne--azide click chemistry. *Bioconjug Chem,* 21**,** 1912-6.

HORNE, D. W., HOLLOWAY, R. S. & SAID, H. M. 1992. Uptake of 5-formyltetrahydrofolate in isolated rat liver mitochondria is carrier-mediated. *J Nutr,* 122**,** 2204-9.

HOUNSELL, E. F. & DAVIES, M. J. 1993. Role of protein glycosylation in immune regulation. *Ann Rheum Dis,* 52 Suppl 1**,** S22-9.

HSU, T. L., HANSON, S. R., KISHIKAWA, K., WANG, S. K., SAWA, M. & WONG, C. H. 2007. Alkynyl sugar analogs for the labeling and visualization of glycoconjugates in cells. *Proc Natl Acad Sci U S A,* 104**,** 2614-9.

HTTP://SYNENTEC.COM. *Mitochondrial membrane potential- Apoptosis studies with JC-1* [Online].

HUANG, C., HSU, P., HUNG, Y., LIAO, Y., LIU, C., HOUR, C., KAO, M., TSAY, G. J., HUNG, H. & LIU, G. Y. 2005. Ornithine decarboxylase prevents methotrexate-induced apoptosis by reducing intracellular reactive oxygen species production. *Apoptosis,* 10**,** 895-907.

HUANG, R. F., HO, Y. H., LIN, H. L., WEI, J. S. & LIU, T. Z. 1999. Folate deficiency induces a cell cycle-specific apoptosis in HepG2 cells. *J Nutr,* 129**,** 25-31.

HUANG, W. Y., YANG, P. M., CHANG, Y. F., MARQUEZ, V. E. & CHEN, C. C. 2011. Methotrexate induces apoptosis through p53/p21-dependent pathway and increases E-cadherin expression through downregulation of HDAC/EZH2. *Biochem Pharmacol,* 81**,** 510-7.

HUNT, S. A. & HADDAD, F. 2008. The changing face of heart transplantation. *J Am Coll Cardiol,* 52**,** 587-98.

IIDA, S., MISAKA, H., INOUE, M., SHIBATA, M., NAKANO, R., YAMANE-OHNUKI, N., WAKITANI, M., YANO, K., SHITARA, K. & SATOH, M. 2006. Nonfucosylated therapeutic IgG1 antibody can evade the inhibitory effect of serum immunoglobulin G on antibody-dependent cellular cytotoxicity through its high binding to FcgammaRIIIa. *Clin Cancer Res,* 12**,** 2879-87.

IKEHARA, Y., IKEHARA, S. K. & PAULSON, J. C. 2004. Negative regulation of T cell receptor signaling by Siglec-7 (p70/AIRM) and Siglec-9. *J Biol Chem,* 279**,** 43117-25.

INGRAHAM, H. A., DICKEY, L. & GOULIAN, M. 1986. DNA fragmentation and cytotoxicity from increased cellular deoxyuridylate. *Biochemistry,* 25**,** 3225-30.

INOUE, K. & YUASA, H. 2014. Molecular basis for pharmacokinetics and pharmacodynamics of methotrexate in rheumatoid arthritis therapy. *Drug Metab Pharmacokinet,* 29**,** 12-9.

IZERADJENE, K., REVILLARD, J. P. & GENESTIER, L. 2001. Inhibition of thymidine synthesis by folate analogues induces a Fas-Fas ligand-independent deletion of superantigen-reactive peripheral T cells. *Int Immunol,* 13**,** 85-93.

JACKSON, R. C. 1978. The regulation of thymidylate biosynthesis in Novikoff hepatoma cells and the effects of amethopterin, 5-fluorodeoxyuridine, and 3-deazauridine. *J Biol Chem,* 253**,** 7440-6.

JASIULEWICZ, A., LISOWSKA, K. A., PIETRUCZUK, K., FRACKOWIAK, J., FULOP, T. & WITKOWSKI, J. M. 2015. Homeostatic 'bystander' proliferation of human peripheral blood B cells in response to polyclonal T-cell stimulation in vitro. *Int Immunol*.

JEREMY M.BERG, J. L. T., LUBERT STRYER 2007. *Biochemistry*, W.H. Freeman and Company.

JI-YEON SUNG A, J.-H. H. A., HYUNG-SIK KANG B, INPYO CHOI B,, SANG-DEOK LIM C, J.-K. L. C., JEONG-HO SEOK A, JAE-HEUN LEE A, & GANG-MIN HUR A 2000. Methotrexate suppresses the interleukin-6 induced generation of reactive oxygen species in the synoviocytes of rheumatoid arthritis. *Immunopharmacology* 47**,** 35-44.

JOHN LINDENBAUM, R. H. A. 1994. Folate in Health and Disease; Chapter 3. Clinical spectrum and diagnosis of folate deficiency.

JOHNSTON, A., GUDJONSSON, J. E., SIGMUNDSDOTTIR, H., LUDVIKSSON, B. R. & VALDIMARSSON, H. 2005. The anti-inflammatory action of methotrexate is not mediated by lymphocyte apoptosis, but by the suppression of activation and adhesion molecules. *Clin Immunol,* 114**,** 154-63.

JONGBLOED, S. L., KASSIANOS, A. J., MCDONALD, K. J., CLARK, G. J., JU, X., ANGEL, C. E., CHEN, C. J., DUNBAR, P. R., WADLEY, R. B., JEET, V., VULINK, A. J., HART, D. N. & RADFORD, K. J. 2010. Human CD141+ (BDCA-3)+ dendritic cells (DCs) represent a unique myeloid DC subset that cross-presents necrotic cell antigens. *J Exp Med,* 207**,** 1247-60.

KAMINSKAS, E. 1979. Inhibition of sugar uptake by methotrexate in cultured Ehrlich ascites carcinoma cells. *Cancer Res,* 39**,** 90-5.

KAMINSKAS, E. 1982. Effects of methotrexate on ribonucleotide pools in growing and in growth-arrested tumor cells and antagonism by RNA synthesis inhibitors. *J Biol Chem,* 257**,** 4279-84.

KAMINSKI, M. M., SAUER, S. W., KAMINSKI, M., OPP, S., RUPPERT, T., GRIGARAVICIUS, P., GRUDNIK, P., GRONE, H. J., KRAMMER, P. H. & GULOW, K. 2012. T cell activation is driven by an ADP-dependent glucokinase linking enhanced glycolysis with mitochondrial reactive oxygen species generation. *Cell Rep,* 2**,** 1300-15.

KANABAR, V., TEDALDI, L., JIANG, J., NIE, X., PANINA, I., DESCROIX, K., MAN, F., PITCHFORD, S. C., PAGE, C. P. & WAGNER, G. K. 2016. Base-modified UDP-sugars reduce cell surface levels of P-selectin glycoprotein 1 (PSGL-1) on IL-1beta-stimulated human monocytes. *Glycobiology*.

KARSTEN, C. M. & KOHL, J. 2012. The immunoglobulin, IgG Fc receptor and complement triangle in autoimmune diseases. *Immunobiology,* 217**,** 1067-79.

KAZMERS, I. S., DADDONA, P. E., DALKE, A. P. & KELLEY, W. N. 1983. Effect of immunosuppressive agents on human T and B lymphoblasts. *Biochem Pharmacol,* 32**,** 805-10.

KELLER, R. & NORDEN, A. 1967. Chromosome observations in bone marrow cells and lymphocytes of peripheral blood of patients with megaloblastic anemia. *Hereditas,* 58**,** 265-83.

KENNEDY, D. C., MCKAY, C. S., LEGAULT, M. C., DANIELSON, D. C., BLAKE, J. A., PEGORARO, A. F., STOLOW, A., MESTER, Z. & PEZACKI, J. P. 2011. Cellular consequences of copper complexes used to catalyze bioorthogonal click reactions. *J Am Chem Soc,* 133**,** 17993-8001.

KHVASTUNOVA, A. N., KUZNETSOVA, S. A., AL-RADI, L. S., VYLEGZHANINA, A. V., ZAKIROVA, A. O., FEDYANINA, O. S., FILATOV, A. V., VOROBJEV, I. A. & ATAULLAKHANOV, F. 2015. Anti-CD antibody microarray for human leukocyte morphology examination allows analyzing rare cell populations and suggesting preliminary diagnosis in leukemia. *Sci Rep,* 5**,** 12573.

KIKUCHI, G. 1973. The glycine cleavage system: composition, reaction mechanism, and physiological significance. *Mol Cell Biochem,* 1**,** 169-87.

KIMBERLY, R. P., TAPPE, N. J., MERRIAM, L. T., REDECHA, P. B., EDBERG, J. C., SCHWARTZMAN, S. & VALINSKY, J. E. 1989. Carbohydrates on human Fc gamma receptors. Interdependence of the classical IgG and nonclassical lectin-binding sites on human Fc gamma RIII expressed on neutrophils. *J Immunol,* 142**,** 3923-30.

KIMURA, E., NISHIMURA, K., SAKATA, K., OGA, S., KASHIWAGI, K. & IGARASHI, K. 2004. Methotrexate differentially affects growth of suspension and adherent cells. *Int J Biochem Cell Biol,* 36**,** 814-25.

KLEIVELAND, C. 2015. The Impact of Food Bioactives on Health; in vitro and ex vivo models.

KLIONSKY, D. J., ABDELMOHSEN, K., ABE, A., ABEDIN, M. J., ABELIOVICH, H., ACEVEDO AROZENA, A., ADACHI, H., ADAMS, C. M., ADAMS, P. D., ADELI, K., ADHIHETTY, P. J., ADLER, S. G., AGAM, G., AGARWAL, R., AGHI, M. K., AGNELLO, M., AGOSTINIS, P., AGUILAR, P. V., AGUIRRE-GHISO, J., AIROLDI, E. M., AIT-SI-ALI, S., AKEMATSU, T., AKPORIAYE, E. T., AL-RUBEAI, M., ALBAICETA, G. M., ALBANESE, C., ALBANI, D., ALBERT, M. L., ALDUDO, J., ALGUL, H., ALIREZAEI, M., ALLOZA, I., ALMASAN, A., ALMONTE-BECERIL, M., ALNEMRI, E. S., ALONSO, C., ALTAN-BONNET, N., ALTIERI, D. C., ALVAREZ, S., ALVAREZ-ERVITI, L., ALVES, S., AMADORO, G., AMANO, A., AMANTINI, C., AMBROSIO, S., AMELIO, I., AMER, A. O., AMESSOU, M., AMON, A., AN, Z., ANANIA, F. A., ANDERSEN, S. U., ANDLEY, U. P., ANDREADI, C. K., ANDRIEU-ABADIE, N., ANEL, A., ANN, D. K., ANOOPKUMAR-DUKIE, S., ANTONIOLI, M., AOKI, H., APOSTOLOVA, N., AQUILA, S., AQUILANO, K., ARAKI, K., ARAMA, E., ARANDA, A., ARAYA, J., ARCARO, A., ARIAS, E., ARIMOTO, H., ARIOSA, A. R., ARMSTRONG, J. L., ARNOULD, T., ARSOV, I., ASANUMA, K., ASKANAS, V., ASSELIN, E., ATARASHI, R., ATHERTON, S. S., ATKIN, J.

D., ATTARDI, L. D., AUBERGER, P., AUBURGER, G., AURELIAN, L., AUTELLI, R., AVAGLIANO, L., AVANTAGGIATI, M. L., AVRAHAMI, L., AWALE, S., AZAD, N., BACHETTI, T., BACKER, J. M., BAE, D. H., BAE, J. S., BAE, O. N., BAE, S. H., BAEHRECKE, E. H., BAEK, S. H., BAGHDIGUIAN, S., BAGNIEWSKA-ZADWORNA, A., et al. 2016. Guidelines for the use and interpretation of assays for monitoring autophagy (3rd edition). *Autophagy,* 12**,** 1-222.

KOLB, H. C., FINN, M. G. & SHARPLESS, K. B. 2001. Click Chemistry: Diverse Chemical Function from a Few Good Reactions. *Angew Chem Int Ed Engl,* 40**,** 2004-2021.

KONG, W. & WANG, J. 2003. Hypoxanthine transport in human glioblastoma cells and effect on cell susceptibility to methotrexate. *Pharm Res,* 20**,** 1804-11.

KRALJEVIC PAVELIC, S., CACEV, T. & KRALJ, M. 2008. A dual role of p21waf1/cip1 gene in apoptosis of HEp-2 treated with cisplatin or methotrexate. *Cancer Gene Ther,* 15**,** 576-90.

KRAPP, S., MIMURA, Y., JEFFERIS, R., HUBER, R. & SONDERMANN, P. 2003. Structural analysis of human IgG-Fc glycoforms reveals a correlation between glycosylation and structural integrity. *J Mol Biol,* 325**,** 979-89.

KREMER, J. M. 2004. Toward a better understanding of methotrexate. *Arthritis Rheum,* 50**,** 1370-82.

KREMER, J. M., GALIVAN, J., STRECKFUSS, A. & KAMEN, B. 1986. Methotrexate metabolism analysis in blood and liver of rheumatoid arthritis patients. Association with hepatic folate deficiency and formation of polyglutamates. *Arthritis Rheum,* 29**,** 832-5.

KREMER, J. M., LAWRENCE, D. A., HAMILTON, R. & MCINNES, I. B. 2016. Long-term study of the impact of methotrexate on serum cytokines and lymphocyte subsets in patients with active rheumatoid arthritis: correlation with pharmacokinetic measures. *RMD Open,* 2**,** e000287.

KUMAR, A., LI, K. & CAI, C. 2011. Anaerobic conditions to reduce oxidation of proteins and to accelerate the copper-catalyzed "Click" reaction with a water-soluble bis(triazole) ligand. *Chem Commun (Camb),* 47**,** 3186-8.

KUNDU, S., GHOSH, P., DATTA, S., GHOSH, A., CHATTOPADHYAY, S. & CHATTERJEE, M. 2012. Oxidative stress as a potential biomarker for determining disease activity in patients with rheumatoid arthritis. *Free Radic Res,* 46**,** 1482-9.

KUNKEL, H. G., MULLER-EBERHARD, H. J., FUDENBERG, H. H. & TOMASI, T. B. 1961. Gamma globulin complexes in rheumatoid arthritis and certain other conditions. *J Clin Invest,* 40**,** 117-29.

KUSSMAUL, L. & HIRST, J. 2006. The mechanism of superoxide production by NADH:ubiquinone oxidoreductase (complex I) from bovine heart mitochondria. *Proc Natl Acad Sci U S A,* 103**,** 7607-12.

KUZNETSOV, J. N., LECLERC, G. J., LECLERC, G. M. & BARREDO, J. C. 2011. AMPK and Akt determine apoptotic cell death following perturbations of one-carbon metabolism by regulating ER stress in acute lymphoblastic leukemia. *Mol Cancer Ther,* 10**,** 437-47.

LACKI, J. K., PORAWSKA, W., MACKIEWICZ, U., MACKIEWICZ, S. & MULLER, W. 1996. Changes in agalactosyl IgG levels correlate with radiological progression in early rheumatoid arthritis. *Ann Med,* 28**,** 265-9.

LAHDENPOHJA, N., SAVINAINEN, K. & HURME, M. 1998. Pre-exposure to oxidative stress decreases the nuclear factor-kappa B-dependent transcription in T lymphocytes. *J Immunol,* 160**,** 1354-8.

LAUGHLIN, S. T. & BERTOZZI, C. R. 2007. Metabolic labeling of glycans with azido sugars and subsequent glycan-profiling and visualization via Staudinger ligation. *Nat Protoc,* 2**,** 2930-44.

LAUGHLIN, S. T. & BERTOZZI, C. R. 2009. Imaging the glycome. *Proc Natl Acad Sci U S A,* 106**,** 12-7.

LAWRENCE, S. A., TITUS, S. A., FERGUSON, J., HEINEMAN, A. L., TAYLOR, S. M. & MORAN, R. G. 2014. Mammalian mitochondrial and cytosolic folylpolyglutamate synthetase maintain the subcellular compartmentalization of folates. *J Biol Chem,* 289**,** 29386-96.

LEVINE, R. L., HOOGENRAAD, N. J. & KRETCHMER, N. 1974. A review: biological and clinical aspects of pyrimidine metabolism. *Pediatr Res,* 8**,** 724-34.

LEWIS, K. F., RANDOLPH, V. M., NEMETH, E. & FRISELL, W. R. 1978. Oxidation of one-carbon compounds to formate and carbon dioxide in rat liver mitochondria. *Arch Biochem Biophys,* 185**,** 443-9.

LI, H., LLERA, A., MALCHIODI, E. L. & MARIUZZA, R. A. 1999. The structural basis of T cell activation by superantigens. *Annu Rev Immunol,* 17**,** 435-66.

LI, H. & SIEFF, C. 2016. Characteristic peripheral blood smear findings in disorders of cobalamin metabolism. *Blood,* 128**,** 2584.

LI, H. H., WANG, Y. W., CHEN, R., ZHOU, B., ASHWELL, J. D. & FORNACE, A. J., JR. 2015. Ionizing Radiation Impairs T Cell Activation by Affecting Metabolic Reprogramming. *Int J Biol Sci,* 11**,** 726-36.

LI, J. C. & KAMINSKAS, E. 1984. Accumulation of DNA strand breaks and methotrexate cytotoxicity. *Proc Natl Acad Sci U S A,* 81**,** 5694-8.

LIN, B. F. & SHANE, B. 1994. Expression of Escherichia coli folylpolyglutamate synthetase in the Chinese hamster ovary cell mitochondrion. *J Biol Chem,* 269**,** 9705-13.

LIU, J., WANG, J., FAN, L., CHEN, X., HU, D., DENG, X., POON, H. F., WANG, H., LIU, X. & TAN, W. S. 2015. Galactose supplementation enhance sialylation of recombinant Fc-fusion protein in CHO cell: an insight into the role of galactosylation in sialylation. *World J Microbiol Biotechnol,* 31**,** 1147-56.

LIU, P. Y., JIANG, N., ZHANG, J., WEI, X., LIN, H. H. & YU, X. Q. 2006. The oxidative damage of plasmid DNA by ascorbic acid derivatives in vitro: the first research on the relationship between the structure of ascorbic acid and the oxidative damage of plasmid DNA. *Chem Biodivers,* 3**,** 958-66.

LORICO, A., TOFFOLI, G., BOIOCCHI, M., ERBA, E., BROGGINI, M., RAPPA, G. & D'INCALCI, M. 1988. Accumulation of DNA strand breaks in cells exposed to methotrexate or N10-propargyl-5,8-dideazafolic acid. *Cancer Res,* 48**,** 2036-41.

LULEY-GOEDL, C., SCHMOELZER, K., THOMANN, M., MALIK, S., GREIF, M., RIBITSCH, D., JUNG, C., SOBEK, H., ENGEL, A., MUELLER, R., SCHWAB, H. & NIDETZKY, B. 2016. Two N-terminally truncated variants of human beta-galactoside alpha2,6 sialyltransferase I with distinct properties for in vitro protein glycosylation. *Glycobiology,* 26**,** 1097-1106.

LUM, J. B., INFANTE, A. J., MAKKER, D. M., YANG, F. & BOWMAN, B. H. 1986. Transferrin synthesis by inducer T lymphocytes. *J Clin Invest,* 77**,** 841-9.

MAENAKA, K., VAN DER MERWE, P. A., STUART, D. I., JONES, E. Y. & SONDERMANN, P. 2001. The human low affinity Fcgamma receptors IIa, IIb, and III bind IgG with fast kinetics and distinct thermodynamic properties. *J Biol Chem,* 276**,** 44898-904.

MAHAL, L. K., YAREMA, K. J. & BERTOZZI, C. R. 1997. Engineering chemical reactivity on cell surfaces through oligosaccharide biosynthesis. *Science,* 276**,** 1125-8.

MAJUMDAR, S. & AGGARWAL, B. B. 2001. Methotrexate suppresses NF-kappaB activation through inhibition of IkappaBalpha phosphorylation and degradation. *J Immunol,* 167**,** 2911-20.

MAKRYGIANNAKIS, D., AF KLINT, E., LUNDBERG, I. E., LOFBERG, R., ULFGREN, A. K., KLARESKOG, L. & CATRINA, A. I. 2006. Citrullination is an inflammation-dependent process. *Ann Rheum Dis,* 65**,** 1219-22.

MALHOTRA, R., WORMALD, M. R., RUDD, P. M., FISCHER, P. B., DWEK, R. A. & SIM, R. B. 1995. Glycosylation changes of IgG associated with rheumatoid arthritis can activate complement via the mannose-binding protein. *Nat Med,* 1**,** 237-43.

MARSHALL A. LICHTMAN, T. J. K., URI SELIGSOHN, KENNETH KAUSHANSKY, JOSEF T. PRCHAL Williams Hematology. 8th edition.

MARTIN, S. A., MCCARTHY, A., BARBER, L. J., BURGESS, D. J., PARRY, S., LORD, C. J. & ASHWORTH, A. 2009. Methotrexate induces oxidative DNA damage and is selectively lethal to tumour cells with defects in the DNA mismatch repair gene MSH2. *EMBO Mol Med,* 1**,** 323-37.

MARTINIOVA, L., FIELD, M. S., FINKELSTEIN, J. L., PERRY, C. A. & STOVER, P. J. 2015. Maternal dietary uridine causes, and deoxyuridine prevents, neural tube closure defects in a mouse model of folate-responsive neural tube defects. *Am J Clin Nutr,* 101**,** 860-9.

MATEEN, S., MOIN, S., KHAN, A. Q., ZAFAR, A. & FATIMA, N. 2016. Increased Reactive Oxygen Species Formation and Oxidative Stress in Rheumatoid Arthritis. *PLoS One,* 11**,** e0152925.

MATHEWS, C. K. 2015. Deoxyribonucleotide metabolism, mutagenesis and cancer. *Nat Rev Cancer,* 15**,** 528-39.

MAURICE, M. M., NAKAMURA, H., VAN DER VOORT, E. A., VAN VLIET, A. I., STAAL, F. J., TAK, P. P., BREEDVELD, F. C. & VERWEIJ, C. L. 1997. Evidence for the role of an altered redox state in hyporesponsiveness of synovial T cells in rheumatoid arthritis. *J Immunol,* 158**,** 1458-65.

MAZUR, A. J., NOWAK, D., MANNHERZ, H. G. & MALICKA-BLASZKIEWICZ, M. 2009. Methotrexate induces apoptosis in CaSki and NRK cells and influences the organization of their actin cytoskeleton. *Eur J Pharmacol,* 613**,** 24-33.

MCINNES, I. B. & SCHETT, G. 2007. Cytokines in the pathogenesis of rheumatoid arthritis. *Nat Rev Immunol,* 7**,** 429-42.

MCINNES, I. B. & SCHETT, G. 2011. The pathogenesis of rheumatoid arthritis. *N Engl J Med,* 365**,** 2205-19.

MIRSHAFIEY, A. & MOHSENZADEGAN, M. 2008. The role of reactive oxygen species in immunopathogenesis of rheumatoid arthritis. *Iran J Allergy Asthma Immunol,* 7**,** 195-202.

MITOMA, C. & GREENBERG, D. M. 1952. Studies on the mechanism of the biosynthesis of serine. *J Biol Chem,* 196**,** 599-614.

MIURA, D., FUJIMURA, Y., TACHIBANA, H. & WARIISHI, H. 2010. Highly sensitive matrix-assisted laser desorption ionization-mass spectrometry for high-throughput metabolic profiling. *Anal Chem,* 82**,** 498-504.

MIWA, S. & BRAND, M. D. 2005. The topology of superoxide production by complex III and glycerol 3-phosphate dehydrogenase in Drosophila mitochondria. *Biochim Biophys Acta,* 1709**,** 214-9.

MONTESINOS, M. C., TAKEDACHI, M., THOMPSON, L. F., WILDER, T. F., FERNANDEZ, P. & CRONSTEIN, B. N. 2007. The antiinflammatory mechanism of methotrexate depends on extracellular conversion of adenine nucleotides to adenosine by ecto-5'-nucleotidase: findings in a study of ecto-5'-nucleotidase gene-deficient mice. *Arthritis Rheum,* 56**,** 1440-5.

MONTESINOS, M. C., YAP, J. S., DESAI, A., POSADAS, I., MCCRARY, C. T. & CRONSTEIN, B. N. 2000. Reversal of the antiinflammatory effects of methotrexate by the nonselective adenosine receptor antagonists theophylline and caffeine: evidence that the antiinflammatory effects of methotrexate are mediated via multiple adenosine receptors in rat adjuvant arthritis. *Arthritis Rheum,* 43**,** 656-63.

MOODLEY, D., MODY, G., PATEL, N. & CHUTURGOON, A. A. 2008. Mitochondrial depolarisation and oxidative stress in rheumatoid arthritis patients. *Clin Biochem,* 41**,** 1396-401.

MORABITO, L., MONTESINOS, M. C., SCHREIBMAN, D. M., BALTER, L., THOMPSON, L. F., RESTA, R., CARLIN, G., HUIE, M. A. & CRONSTEIN, B. N. 1998. Methotrexate and sulfasalazine promote adenosine release by a mechanism that requires ecto-5'-nucleotidase-mediated conversion of adenine nucleotides. *J Clin Invest,* 101**,** 295-300.

MORELAND, L. W., PRATT, P. W., MAYES, M. D., POSTLETHWAITE, A., WEISMAN, M. H., SCHNITZER, T., LIGHTFOOT, R., CALABRESE, L., ZELINGER, D. J., WOODY, J. N. & ET AL. 1995. Double-blind, placebo-controlled multicenter trial using chimeric monoclonal anti-CD4 antibody, cM-T412, in rheumatoid arthritis patients receiving concomitant methotrexate. *Arthritis Rheum,* 38**,** 1581-8.

MORGAN, S. L., OSTER, R. A., LEE, J. Y., ALARCON, G. S. & BAGGOTT, J. E. 2004. The effect of folic acid and folinic acid supplements on purine metabolism in methotrexate-treated rheumatoid arthritis. *Arthritis Rheum,* 50**,** 3104-11.

MORPHIS, L. G. & GITLIN, D. 1970. Maturation of the maternofoetal transport system for human gamma-globulin in the mouse. *Nature,* 228**,** 573.

MULLER, F. L., LIU, Y. & VAN REMMEN, H. 2004. Complex III releases superoxide to both sides of the inner mitochondrial membrane. *J Biol Chem,* 279**,** 49064-73.

MURPHY, M. P. 2009. How mitochondria produce reactive oxygen species. *Biochem J,* 417**,** 1-13.

MYINT, K. T., UEHARA, T., AOSHIMA, K. & ODA, Y. 2009. Polar anionic metabolome analysis by nano-LC/MS with a metal chelating agent. *Anal Chem,* 81**,** 7766-72.

NAITO-MATSUI, Y., TAKADA, S., KANO, Y., IYODA, T., SUGAI, M., SHIMIZU, A., INABA, K., NITSCHKE, L., TSUBATA, T., OKA, S., KOZUTSUMI, Y. & TAKEMATSU, H. 2014. Functional evaluation of activation-dependent alterations in the sialoglycan composition of T cells. *J Biol Chem,* 289**,** 1564-79.

NATSUME, A., WAKITANI, M., YAMANE-OHNUKI, N., SHOJI-HOSAKA, E., NIWA, R., UCHIDA, K., SATOH, M. & SHITARA, K. 2006. Fucose removal from complex-type oligosaccharide enhances the antibody-dependent cellular cytotoxicity of single-gene-encoded bispecific antibody comprising of two single-chain antibodies linked to the antibody constant region. *J Biochem,* 140**,** 359-68.

NERADIL, J., PAVLASOVA, G. & VESELSKA, R. 2012. New mechanisms for an old drug; DHFR- and non-DHFR-mediated effects of methotrexate in cancer cells. *Klin Onkol,* 25 Suppl 2**,** 2S87-92.

NESHER, G. & MOORE, T. L. 1990. The in vitro effects of methotrexate on peripheral blood mononuclear cells. Modulation by methyl donors and spermidine. *Arthritis Rheum,* 33**,** 954-9.

NETTLETON, M. Y. & KOCHAN, J. P. 1995. Role of glycosylation sites in the IgE Fc molecule. *Int Arch Allergy Immunol,* 107**,** 328-9.

NEVES, A. A., STOCKMANN, H., WAINMAN, Y. A., KUO, J. C., FAWCETT, S., LEEPER, F. J. & BRINDLE, K. M. 2013. Imaging cell surface glycosylation in vivo using "double click" chemistry. *Bioconjug Chem,* 24**,** 934-41.

NICHOLAS P. B. DUDMAN, P. S. A. M. H. N. T. 1982. Methotrexate Rescue by 5-Methylhydrofolate or 5-Formyl THF in lymphoblast cell lines. *Cancer Research* 42**,** 502-507.

NICOLL, G., NI, J., LIU, D., KLENERMAN, P., MUNDAY, J., DUBOCK, S., MATTEI, M. G. & CROCKER, P. R. 1999. Identification and characterization of a novel siglec, siglec-7, expressed by human natural killer cells and monocytes. *J Biol Chem,* 274**,** 34089-95.

NIELSEN, C. H., ALBERTSEN, L., BENDTZEN, K. & BASLUND, B. 2007. Methotrexate induces poly(ADP-ribose) polymerase-dependent, caspase 3-independent apoptosis in subsets of proliferating CD4+ T cells. *Clin Exp Immunol,* 148**,** 288-95.

NIWA, R., NATSUME, A., UEHARA, A., WAKITANI, M., IIDA, S., UCHIDA, K., SATOH, M. & SHITARA, K. 2005. IgG subclass-independent improvement of antibody-dependent cellular cytotoxicity by fucose removal from Asn297-linked oligosaccharides. *J Immunol Methods,* 306**,** 151-60.

NWE, K. & BRECHBIEL, M. W. 2009. Growing applications of "click chemistry" for bioconjugation in contemporary biomedical research. *Cancer Biother Radiopharm,* 24**,** 289-302.

O'NEILL, L. A. & HARDIE, D. G. 2013. Metabolism of inflammation limited by AMPK and pseudo-starvation. *Nature,* 493**,** 346-55.

OHMI, Y., ISE, W., HARAZONO, A., TAKAKURA, D., FUKUYAMA, H., BABA, Y., NARAZAKI, M., SHODA, H., TAKAHASHI, N., OHKAWA, Y., JI, S., SUGIYAMA, F., FUJIO, K., KUMANOGOH, A., YAMAMOTO, K., KAWASAKI, N., KUROSAKI, T., TAKAHASHI, Y. & FURUKAWA, K. 2016. Sialylation converts arthritogenic IgG into inhibitors of collagen-induced arthritis. *Nat Commun,* 7**,** 11205.

OKAZAKI, A., SHOJI-HOSAKA, E., NAKAMURA, K., WAKITANI, M., UCHIDA, K., KAKITA, S., TSUMOTO, K., KUMAGAI, I. & SHITARA, K. 2004. Fucose depletion from human IgG1 oligosaccharide enhances binding enthalpy and association rate between IgG1 and FcgammaRIIIa. *J Mol Biol,* 336**,** 1239-49.

OKUDA, A., KUBOTA, M., WATANABE, K., SAWADA, M., KOISHI, S., KATAOKA, A., USAMI, I., LIN, Y. W. & FURUSHO, K. 1997. Inhibition of superoxide production and chemotaxis by methotrexate in neutrophils primed by TNF-alpha or LPS. *Eur J Haematol,* 59**,** 142-7.

OLSEN, N. J., CALLAHAN, L. F. & PINCUS, T. 1987. Immunologic studies of rheumatoid arthritis patients treated with methotrexate. *Arthritis Rheum,* 30**,** 481-8.

OLSEN, N. J. & MURRAY, L. M. 1989. Antiproliferative effects of methotrexate on peripheral blood mononuclear cells. *Arthritis Rheum,* 32**,** 378-85.

OLSEN, N. J., SPURLOCK, C. F., 3RD & AUNE, T. M. 2014. Methotrexate induces production of IL-1 and IL-6 in the monocytic cell line U937. *Arthritis Res Ther,* 16**,** R17.

ORBERGER, G., GEYER, R., STIRM, S. & TAUBER, R. 1992. Structure of the N-linked oligosaccharides of the human transferrin receptor. *Eur J Biochem,* 205**,** 257-67.

ORTIZ Z, S. B., SUAREZ-ALMAZOR ME, MOHER D, WELLS GA, TUGWELL P 2009. <Folic and folinic acid for reducing side effects of MTX.pdf>.

P450.KVL.DK. *The Arabidopsis cytochrome P450, Cytochrome B$_5$, P450 Reductase, B-Glucosidase, and Glycosyltransferase Site* [Online]. Available: www.p450.kvl.dk. .

P.WELLER, K. Polychromatic Flow Cytometry and Flow Applications.

PAI, Y. J., LEUNG, K. Y., SAVERY, D., HUTCHIN, T., PRUNTY, H., HEALES, S., BROSNAN, M. E., BROSNAN, J. T., COPP, A. J. & GREENE, N. D. 2015. Glycine decarboxylase deficiency causes neural tube defects and features of non-ketotic hyperglycinemia in mice. *Nat Commun,* 6**,** 6388.

PAILLOT, R., GENESTIER, L., FOURNEL, S., FERRARO, C., MIOSSEC, P. & REVILLARD, J. P. 1998. Activation-dependent lymphocyte apoptosis induced by methotrexate. *Transplant Proc,* 30**,** 2348-50.

PAPACONSTANTINOU, H. T., XIE, C., ZHANG, W., ANSARI, N. H., HELLMICH, M. R., TOWNSEND, C. M., JR. & KO, T. C. 2001. The role of caspases in methotrexate-induced gastrointestinal toxicity. *Surgery,* 130**,** 859-65.

PAREKH, R., ISENBERG, D., ROOK, G., ROITT, I., DWEK, R. & RADEMACHER, T. 1989. A comparative analysis of disease-associated changes in the galactosylation of serum IgG. *J Autoimmun,* 2**,** 101-14.

PASEK, M., DUK, M., PODBIELSKA, M., SOKOLIK, R., SZECHINSKI, J., LISOWSKA, E. & KROTKIEWSKI, H. 2006. Galactosylation of IgG from rheumatoid arthritis (RA) patients--changes during therapy. *Glycoconj J,* 23**,** 463-71.

PATANE, M., CIRIACO, M., CHIMIRRI, S., URSINI, F., NATY, S., GREMBIALE, R. D., GALLELLI, L., DE SARRO, G. & RUSSO, E. 2013. Interactions among Low Dose of Methotrexate and Drugs Used in the Treatment of Rheumatoid Arthritis. *Adv Pharmacol Sci,* 2013**,** 313858.

PAUL, M., HEMSHEKHAR, M., THUSHARA, R. M., SUNDARAM, M. S., NAVEENKUMAR, S. K., NAVEEN, S., DEVARAJA, S., SOMYAJIT, K., WEST, R., BASAPPA, NAYAKA, S. C., ZAKAI, U. I., NAGARAJU, G., RANGAPPA, K. S., KEMPARAJU, K. & GIRISH, K. S. 2015. Methotrexate Promotes Platelet Apoptosis via JNK-Mediated Mitochondrial Damage: Alleviation by N-Acetylcysteine and N-Acetylcysteine Amide. *PLoS One,* 10**,** e0127558.

PETERSON, M. S., INGRAHAM, H. A. & GOULIAN, M. 1983. 2'-deoxyribosyl analogues of UDP-N-acetylglucosamine in cells treated with methotrexate or 5-fluorodeoxyuridine. *J Biol Chem,* 258**,** 10831-4.

PFANNER, N. & NEUPERT, W. 1985. Transport of proteins into mitochondria: a potassium diffusion potential is able to drive the import of ADP/ATP carrier. *EMBO J,* 4**,** 2819-25.

PFANNER, N. & NEUPERT, W. 1986. Transport of F1-ATPase subunit beta into mitochondria depends on both a membrane potential and nucleoside triphosphates. *FEBS Lett,* 209**,** 152-6.

PFEIFLE, R., ROTHE, T., IPSEIZ, N., SCHERER, H. U., CULEMANN, S., HARRE, U., ACKERMANN, J. A., SEEFRIED, M., KLEYER, A., UDERHARDT, S., HAUGG, B., HUEBER, A. J., DAUM, P., HEIDKAMP, G. F., GE, C., BOHM, S., LUX, A., SCHUH, W., MAGORIVSKA, I., NANDAKUMAR, K. S., LONNBLOM, E., BECKER, C., DUDZIAK, D., WUHRER, M., ROMBOUTS, Y., KOELEMAN, C. A., TOES, R., WINKLER, T. H., HOLMDAHL, R., HERRMANN, M., BLUML, S., NIMMERJAHN, F., SCHETT, G. & KRONKE, G. 2016. Regulation of autoantibody activity by the IL-23-TH17 axis determines the onset of autoimmune disease. *Nat Immunol.*

PHILLIPS, D. C., WOOLLARD, K. J. & GRIFFITHS, H. R. 2003. The anti-inflammatory actions of methotrexate are critically dependent upon the production of reactive oxygen species. *Br J Pharmacol,* 138**,** 501-11.

PICKARD, M. & KINSELLA, A. 1996. Influence of both salvage and DNA damage response pathways on resistance to chemotherapeutic antimetabolites. *Biochem Pharmacol,* 52**,** 425-31.

PONCHEL, F., GOEB, V., PARMAR, R., EL-SHERBINY, Y., BOISSINOT, M., EL JAWHARI, J., BURSKA, A., VITAL, E. M., HARRISON, S., CONAGHAN, P. G., HENSOR, E. & EMERY, P. 2014. An immunological biomarker to predict MTX response in early RA. *Ann Rheum Dis,* 73**,** 2047-53.

PORTER, R. K., SCOTT, J. M. & BRAND, M. D. 1992. Choline transport into rat liver mitochondria. Characterization and kinetics of a specific transporter. *J Biol Chem,* 267**,** 14637-46.

POWELL, L. D., SGROI, D., SJOBERG, E. R., STAMENKOVIC, I. & VARKI, A. 1993. Natural ligands of the B cell adhesion molecule CD22 beta carry N-linked oligosaccharides with alpha-2,6-linked sialic acids that are required for recognition. *J Biol Chem,* 268**,** 7019-27.

POWELL, L. D. & VARKI, A. 1995. I-type lectins. *J Biol Chem,* 270**,** 14243-6.

PRESOLSKI, S. I., HONG, V. P. & FINN, M. G. 2011. Copper-Catalyzed Azide-Alkyne Click Chemistry for Bioconjugation. *Curr Protoc Chem Biol,* 3**,** 153-162.

QUEMENEUR, L., BELOEIL, L., MICHALLET, M. C., ANGELOV, G., TOMKOWIAK, M., REVILLARD, J. P. & MARVEL, J. 2004. Restriction of de novo nucleotide biosynthesis interferes with clonal expansion and differentiation into effector and memory CD8 T cells. *J Immunol,* 173**,** 4945-52.

QUEMENEUR, L., GERLAND, L. M., FLACHER, M., FFRENCH, M., REVILLARD, J. P. & GENESTIER, L. 2003. Differential control of cell cycle, proliferation, and survival of primary T lymphocytes by purine and pyrimidine nucleotides. *J Immunol,* 170**,** 4986-95.

RAZI, N. & VARKI, A. 1999. Cryptic sialic acid binding lectins on human blood leukocytes can be unmasked by sialidase treatment or cellular activation. *Glycobiology,* 9**,** 1225-34.

REDDY, M., EIRIKIS, E., DAVIS, C., DAVIS, H. M. & PRABHAKAR, U. 2004. Comparative analysis of lymphocyte activation marker expression and cytokine secretion profile in stimulated human peripheral blood mononuclear cell cultures: an in vitro model to monitor cellular immune function. *J Immunol Methods,* 293**,** 127-42.

REZK, B. M., HAENEN, G. R., VAN DER VIJGH, W. J. & BAST, A. 2003. Tetrahydrofolate and 5-methyltetrahydrofolate are folates with high antioxidant activity. Identification of the antioxidant pharmacophore. *FEBS Lett,* 555**,** 601-5.

RIKSEN, N. P., BARRERA, P., VAN DEN BROEK, P. H., VAN RIEL, P. L., SMITS, P. & RONGEN, G. A. 2006. Methotrexate modulates the kinetics of adenosine in humans in vivo. *Ann Rheum Dis,* 65**,** 465-70.

ROEDERER, M. 2011. Interpretation of cellular proliferation data: avoid the panglossian. *Cytometry A,* 79**,** 95-101.

ROMAO, V. C., LIMA, A., BERNARDES, M., CANHAO, H. & FONSECA, J. E. 2014. Three decades of low-dose methotrexate in rheumatoid arthritis: can we predict toxicity? *Immunol Res,* 60**,** 289-310.

ROOK, G. A., STEELE, J., BREALEY, R., WHYTE, A., ISENBERG, D., SUMAR, N., NELSON, J. L., BODMAN, K. B., YOUNG, A., ROITT, I. M. & ET AL. 1991. Changes in IgG glycoform levels are associated with remission of arthritis during pregnancy. *J Autoimmun,* 4**,** 779-94.

ROSENBLATT, D. S., WHITEHEAD, V. M., MATIASZUK, N. V., POTTIER, A., VUCHICH, M. J. & BEAULIEU, D. 1982. Differential effects of folinic acid and glycine, adenosine, and thymidine as rescue agents in methotrexate-treated human cells in relation to the accumulation of methotrexate polyglutamates. *Mol Pharmacol,* 21**,** 718-22.

ROSENTHAL, G. J., WEIGAND, G. W., GERMOLEC, D. R., BLANK, J. A. & LUSTER, M. I. 1988. Suppression of B cell function by methotrexate and trimetrexate. Evidence for inhibition of purine biosynthesis as a major mechanism of action. *J Immunol,* 141**,** 410-6.

ROSSI, D., MODENA, V., SCIASCIA, S. & ROCCATELLO, D. 2015. Rheumatoid arthritis: Biological therapy other than anti-TNF. *Int Immunopharmacol*.

ROTTENBERG, H. & WU, S. 1998. Quantitative assay by flow cytometry of the mitochondrial membrane potential in intact cells. *Biochim Biophys Acta,* 1404**,** 393-404.

SALLAH, S., HANRAHAN, L. R. & PHILLIPS, D. L. 1999. Intrathecal methotrexate-induced megaloblastic anemia in patients with acute leukemia. *Arch Pathol Lab Med,* 123**,** 774-7.

SAMUELSON, L. E., SCHERER, R. L., VANSAUN, M. N., FAN, K. H., DOZIER, E. A., CARTER, K. J., KOYAMA, T., SHYR, Y., ASCHNER, M., STANWOOD, G. D., BORNHOP, D. J., MATRISIAN, L. M. & MCINTYRE, J. O. 2015. New tools for the quantitative assessment of prodrug delivery and neurotoxicity. *Neurotoxicology,* 47**,** 88-98.

SANT, M. E., LYONS, S. D., PHILLIPS, L. & CHRISTOPHERSON, R. I. 1992. Antifolates induce inhibition of amido phosphoribosyltransferase in leukemia cells. *J Biol Chem,* 267**,** 11038-45.

SATOH, M., IIDA, S. & SHITARA, K. 2006. Non-fucosylated therapeutic antibodies as next-generation therapeutic antibodies. *Expert Opin Biol Ther,* 6**,** 1161-73.

SAWYER, R. C., STOLFI, R. L., MARTIN, D. S. & BALIS, M. E. 1989. Inhibition by methotrexate of the stable incorporation of 5-fluorouracil into murine bone marrow DNA. *Biochem Pharmacol,* 38**,** 2305-11.

SAXON, E. & BERTOZZI, C. R. 2000. Cell surface engineering by a modified Staudinger reaction. *Science,* 287**,** 2007-10.

SAXON, E., LUCHANSKY, S. J., HANG, H. C., YU, C., LEE, S. C. & BERTOZZI, C. R. 2002. Investigating cellular metabolism of synthetic azidosugars with the Staudinger ligation. *J Am Chem Soc,* 124**,** 14893-902.

SCHLEYER, M., SCHMIDT, B. & NEUPERT, W. 1982. Requirement of a membrane potential for the posttranslational transfer of proteins into mitochondria. *Eur J Biochem,* 125**,** 109-16.

SCHNEIDER, E. G., NGUYEN, H. T. & LENNARZ, W. J. 1978. The effect of tunicamycin, an inhibitor of protein glycosylation, on embryonic development in the sea urchin. *J Biol Chem,* 253**,** 2348-55.

SEIDEMAN, P., BECK, O., EKSBORG, S. & WENNBERG, M. 1993. The pharmacokinetics of methotrexate and its 7-hydroxy metabolite in patients with rheumatoid arthritis. *Br J Clin Pharmacol,* 35**,** 409-12.

SENA, L. A., LI, S., JAIRAMAN, A., PRAKRIYA, M., EZPONDA, T., HILDEMAN, D. A., WANG, C. R., SCHUMACKER, P. T., LICHT, J. D., PERLMAN, H., BRYCE, P. J. & CHANDEL, N. S. 2013. Mitochondria are required for antigen-specific T cell activation through reactive oxygen species signaling. *Immunity,* 38**,** 225-36.

SHEA, B., SWINDEN, M. V., GHOGOMU, E. T., ORTIZ, Z., KATCHAMART, W., RADER, T., BOMBARDIER, C., WELLS, G. A. & TUGWELL, P. 2014. Folic acid and folinic acid for reducing side effects in patients receiving methotrexate for rheumatoid arthritis. *J Rheumatol,* 41**,** 1049-60.

SHIBATA-KOYAMA, M., IIDA, S., OKAZAKI, A., MORI, K., KITAJIMA-MIYAMA, K., SAITOU, S., KAKITA, S., KANDA, Y., SHITARA, K., KATO, K. & SATOH, M. 2009. The N-linked oligosaccharide at Fc gamma RIIIa Asn-45: an inhibitory element for high Fc gamma RIIIa binding affinity to IgG glycoforms lacking core fucosylation. *Glycobiology,* 19**,** 126-34.

SHIELDS, R. L., LAI, J., KECK, R., O'CONNELL, L. Y., HONG, K., MENG, Y. G., WEIKERT, S. H. & PRESTA, L. G. 2002. Lack of fucose on human IgG1 N-linked oligosaccharide improves binding to human Fcgamma RIII and antibody-dependent cellular toxicity. *J Biol Chem,* 277**,** 26733-40.

SHINDE, C. G., VENKATESH, M. P., KUMAR, T. M. & SHIVAKUMAR, H. G. 2014. Methotrexate: a gold standard for treatment of rheumatoid arthritis. *J Pain Palliat Care Pharmacother,* 28**,** 351-8.

SIGMUNDSDOTTIR, H., JOHNSTON, A., GUDJONSSON, J. E. & VALDIMARSSON, H. 2004. Differential effects of interleukin 12 and interleukin 10 on superantigen-induced expression of cutaneous lymphocyte-associated antigen (CLA) and alphaEbeta7 integrin (CD103) by CD8+ T cells. *Clin Immunol,* 111**,** 119-25.

SLETTEN, E. M. & BERTOZZI, C. R. 2009. Bioorthogonal chemistry: fishing for selectivity in a sea of functionality. *Angew Chem Int Ed Engl,* 48**,** 6974-98.

SMOLENSKA, Z., KAZNOWSKA, Z., ZAROWNY, D., SIMMONDS, H. A. & SMOLENSKI, R. T. 1999. Effect of methotrexate on blood purine and pyrimidine levels in patients with rheumatoid arthritis. *Rheumatology (Oxford),* 38**,** 997-1002.

SONDERMANN, P., HUBER, R., OOSTHUIZEN, V. & JACOB, U. 2000. The 3.2-A crystal structure of the human IgG1 Fc fragment-Fc gammaRIII complex. *Nature,* 406**,** 267-73.

SONDERMANN, P. & JACOB, U. 1999. Human Fcgamma receptor IIb expressed in Escherichia coli reveals IgG binding capability. *Biol Chem,* 380**,** 717-21.

SORIANO DEL AMO, D., WANG, W., JIANG, H., BESANCENEY, C., YAN, A. C., LEVY, M., LIU, Y., MARLOW, F. L. & WU, P. 2010. Biocompatible copper(I) catalysts for in vivo imaging of glycans. *J Am Chem Soc,* 132**,** 16893-9.

SPEERS, A. E. & CRAVATT, B. F. 2004. Profiling enzyme activities in vivo using click chemistry methods. *Chem Biol,* 11**,** 535-46.

SPURLOCK, C. F., 3RD, AUNE, Z. T., TOSSBERG, J. T., COLLINS, P. L., AUNE, J. P., HUSTON, J. W., 3RD, CROOKE, P. S., OLSEN, N. J. & AUNE, T. M. 2011. Increased sensitivity to apoptosis induced by methotrexate is mediated by JNK. *Arthritis Rheum,* 63**,** 2606-16.

SPURLOCK, C. F., 3RD, GASS, H. M. T., BRYANT, C. J., WELLS, B. C., OLSEN, N. J. & AUNE, T. M. 2015. Methotrexate-mediated inhibition of nuclear factor kappaB activation by distinct pathways in T cells and fibroblast-like synoviocytes. *Rheumatology (Oxford),* 54**,** 178-87.

SPURLOCK, C. F., 3RD, TOSSBERG, J. T., MATLOCK, B. K., OLSEN, N. J. & AUNE, T. M. 2014. Methotrexate inhibits NF-kappaB activity via long intergenic (noncoding) RNA-p21 induction. *Arthritis Rheumatol,* 66**,** 2947-57.

ST-PIERRE, J., BUCKINGHAM, J. A., ROEBUCK, S. J. & BRAND, M. D. 2002. Topology of superoxide production from different sites in the mitochondrial electron transport chain. *J Biol Chem,* 277**,** 44784-90.

STARKOV, A. A., FISKUM, G., CHINOPOULOS, C., LORENZO, B. J., BROWNE, S. E., PATEL, M. S. & BEAL, M. F. 2004. Mitochondrial alpha-ketoglutarate dehydrogenase complex generates reactive oxygen species. *J Neurosci,* 24**,** 7779-88.

STOWE, D. F. & CAMARA, A. K. 2009. Mitochondrial reactive oxygen species production in excitable cells: modulators of mitochondrial and cell function. *Antioxid Redox Signal,* 11**,** 1373-414.

STRAUSS, G., OSEN, W. & DEBATIN, K. M. 2002. Induction of apoptosis and modulation of activation and effector function in T cells by immunosuppressive drugs. *Clin Exp Immunol,* 128**,** 255-66.

STUDYDROID. *Biochemistry: Nucleotide metabolism* [Online]. Available: www.studydroid.com.

SUNDEN, S. L., RENDUCHINTALA, M. S., PARK, E. I., MIKLASZ, S. D. & GARROW, T. A. 1997. Betaine-homocysteine methyltransferase expression in porcine and human tissues and chromosomal localization of the human gene. *Arch Biochem Biophys,* 345**,** 171-4.

SUZAWA, T., HYODO, S., KISHI, T., KASHIWA, H., KARAKAWA, T., KITTAKA, E., SAKANO, T. & USUI, T. 1984. Comparison of phorbol myristate acetate and phytohaemagglutinin as stimulators of in vitro T lymphocyte colony formation of human peripheral blood lymphocytes. I. Surface markers of colony cells. *Immunology,* 53**,** 499-505.

SWAIN, S. L. 1995. T-cell subsets. Who does the polarizing? *Curr Biol,* 5**,** 849-51.

SWAMY, M., PATHAK, S., GRZES, K. M., DAMEROW, S., SINCLAIR, L. V., VAN AALTEN, D. M. & CANTRELL, D. A. 2016. Glucose and glutamine fuel protein O-GlcNAcylation to control T cell self-renewal and malignancy. *Nat Immunol,* 17**,** 712-20.

SWIERKOT, J., MIEDZYBRODZKI, R., SZYMANIEC, S. & SZECHINSKI, J. 2004. Activation dependent apoptosis of peripheral blood mononuclear cells from patients with rheumatoid arthritis treated with methotrexate. *Ann Rheum Dis,* 63**,** 599-600.

TAHERI, M. R., WICKREMASINGHE, R. G. & HOFFBRAND, A. V. 1981. Metabolism of thymine nucleotides synthesized via the 'de novo' mechanism in normal, megaloblastic and methotrexate-treated human cells and in a lymphoblastoid cell line. *Biochem J,* 196**,** 225-35.

TAKAHASHI, N., COHEN-SOLAL, J., GALINHA, A., FRIDMAN, W. H., SAUTES-FRIDMAN, C. & KATO, K. 2002. N-glycosylation profile of recombinant human soluble Fcgamma receptor III. *Glycobiology,* 12**,** 507-15.

TAKAHASHI, N., YAMADA, W., MASUDA, K., ARAKI, H., TSUKAMOTO, Y., GALINHA, A., SAUTES, C., KATO, K. & SHIMADA, I. 1998. N-glycan structures of a recombinant mouse soluble Fcgamma receptor II. *Glycoconj J,* 15**,** 905-14.

TAYLOR, I. W. & TATTERSALL, M. H. 1981. Methotrexate cytotoxicity in cultured human leukemic cells studied by flow cytometry. *Cancer Res,* 41**,** 1549-58.

TEDESCHI, P. M., JOHNSON-FARLEY, N., LIN, H., SHELTON, L. M., OOGA, T., MACKAY, G., VAN DEN BROEK, N., BERTINO, J. R. & VAZQUEZ, A. 2015. Quantification of folate metabolism using transient metabolic flux analysis. *Cancer Metab,* 3**,** 6.

TEDESCHI, P. M., MARKERT, E. K., GOUNDER, M., LIN, H., DVORZHINSKI, D., DOLFI, S. C., CHAN, L. L., QIU, J., DIPAOLA, R. S., HIRSHFIELD, K. M., BOROS, L. G., BERTINO, J. R., OLTVAI, Z. N. & VAZQUEZ, A. 2013. Contribution of serine, folate and glycine metabolism to the ATP, NADPH and purine requirements of cancer cells. *Cell Death Dis,* 4**,** e877.

TIAN, H. & CRONSTEIN, B. N. 2007. Understanding the mechanisms of action of methotrexate: implications for the treatment of rheumatoid arthritis. *Bull NYU Hosp Jt Dis,* 65**,** 168-73.

TIBBETTS, A. S. & APPLING, D. R. 2010. Compartmentalization of Mammalian folate-mediated one-carbon metabolism. *Annu Rev Nutr,* 30**,** 57-81.

TISHLER, M., CASPI, D., FISHEL, B. & YARON, M. 1988. The effects of leucovorin (folinic acid) on methotrexate therapy in rheumatoid arthritis patients. *Arthritis Rheum,* 31**,** 906-8.

TITUS, S. A. & MORAN, R. G. 2000. Retrovirally mediated complementation of the glyB phenotype. Cloning of a human gene encoding the carrier for entry of folates into mitochondria. *J Biol Chem,* 275**,** 36811-7.

TJIATTAS, L., ORTIZ, D. O., DHIVANT, S., MITTON, K., ROGERS, E. & SHEA, T. B. 2004. Folate deficiency and homocysteine induce toxicity in cultured dorsal root ganglion neurons via cytosolic calcium accumulation. *Aging Cell,* 3**,** 71-6.

TOHYAMA, N., TANAKA, S., ONDA, K., SUGIYAMA, K. & HIRANO, T. 2013. Influence of anticancer agents on cell survival, proliferation, and CD4+CD25+Foxp3+ regulatory T cell-frequency in human peripheral-blood mononuclear cells activated by T cell-mitogen. *Int Immunopharmacol,* 15**,** 160-6.

TORRES-ALVAREZ, B., CASTANEDO-CAZARES, J. P., FUENTES-AHUMADA, C. & MONCADA, B. 2007. The effect of methotrexate on the expression of cell adhesion molecules and activation molecule CD69 in psoriasis. *J Eur Acad Dermatol Venereol,* 21**,** 334-9.

TOSCANO, M. A., BIANCO, G. A., ILARREGUI, J. M., CROCI, D. O., CORREALE, J., HERNANDEZ, J. D., ZWIRNER, N. W., POIRIER, F., RILEY, E. M., BAUM, L. G. & RABINOVICH, G. A. 2007. Differential glycosylation of TH1, TH2 and TH-17 effector cells selectively regulates susceptibility to cell death. *Nat Immunol,* 8**,** 825-34.

TRENT, D. F., SEITHER, R. L. & GOLDMAN, I. D. 1991. Compartmentation of intracellular folates. Failure to interconvert tetrahydrofolate cofactors to dihydrofolate in mitochondria of L1210 leukemia cells treated with trimetrexate. *Biochem Pharmacol,* 42**,** 1015-9.

TRETTER, L., TAKACS, K., HEGEDUS, V. & ADAM-VIZI, V. 2007. Characteristics of alpha-glycerophosphate-evoked H2O2 generation in brain mitochondria. *J Neurochem,* 100**,** 650-63.

TRIPPETT, T. M., GARCIA, S., MANOVA, K., MODY, R., COHEN-GOULD, L., FLINTOFF, W. & BERTINO, J. R. 2001. Localization of a human reduced folate carrier protein in the mitochondrial as well as the cell membrane of leukemia cells. *Cancer Res,* 61**,** 1941-7.

TROELSEN, L. N., JACOBSEN, S., ABRAHAMS, J. L., ROYLE, L., RUDD, P. M., NARVESTAD, E., HEEGAARD, N. H. & GARRED, P. 2012. IgG glycosylation changes and MBL2 polymorphisms: associations with markers of systemic inflammation and joint destruction in rheumatoid arthritis. *J Rheumatol,* 39**,** 463-9.

UEHARA, T., YOKOI, A., AOSHIMA, K., TANAKA, S., KADOWAKI, T., TANAKA, M. & ODA, Y. 2009. Quantitative phosphorus metabolomics using nanoflow liquid chromatography-tandem mass spectrometry and culture-derived comprehensive global internal standards. *Anal Chem,* 81**,** 3836-42.

UGA, H., KURAMORI, C., OHTA, A., TSUBOI, Y., TANAKA, H., HATAKEYAMA, M., YAMAGUCHI, Y., TAKAHASHI, T., KIZAKI, M. & HANDA, H. 2006. A new mechanism of methotrexate action revealed by target screening with affinity beads. *Mol Pharmacol,* 70**,** 1832-9.

VAN DER LUBBE, P. A., DIJKMANS, B. A., MARKUSSE, H. M., NASSANDER, U. & BREEDVELD, F. C. 1995. A randomized, double-blind, placebo-controlled study of CD4 monoclonal antibody therapy in early rheumatoid arthritis. *Arthritis Rheum,* 38**,** 1097-106.

VAN EDE, A. E., LAAN, R. F., BLOM, H. J., DE ABREU, R. A. & VAN DE PUTTE, L. B. 1998. Methotrexate in rheumatoid arthritis: an update with focus on mechanisms involved in toxicity. *Semin Arthritis Rheum,* 27**,** 277-92.

VAN ZEBEN, D., ROOK, G. A., HAZES, J. M., ZWINDERMAN, A. H., ZHANG, Y., GHELANI, S., RADEMACHER, T. W. & BREEDVELD, F. C. 1994. Early agalactosylation of IgG is associated with a more progressive disease course in patients with rheumatoid arthritis: results of a follow-up study. *Br J Rheumatol,* 33**,** 36-43.

VARKI, A. & ANGATA, T. 2006. Siglecs--the major subfamily of I-type lectins. *Glycobiology,* 16**,** 1R-27R.

VARKI, A., CUMMINGS, R. D., ESKO, J. D., FREEZE, H. H., STANLEY, P., BERTOZZI, C. R., HART, G. W. & ETZLER, M. E. 1999. *Essentials of Glycobiology*, Cold Spring Harbour Laboratory Press.

VARKI, A. & GAGNEUX, P. 2012. Multifarious roles of sialic acids in immunity. *Ann N Y Acad Sci,* 1253**,** 16-36.

VILLANUEVA-CABELLO, T. M., MOLLICONE, R., CRUZ-MUNOZ, M. E., LOPEZ-GUERRERO, D. V. & MARTINEZ-DUNCKER, I. 2015. Activation of human naive Th cells increases surface expression of GD3 and induces neoexpression of GD2 that colocalize with TCR clusters. *Glycobiology,* 25**,** 1454-64.

VISENTIN, M., ZHAO, R. & GOLDMAN, I. D. 2012. The antifolates. *Hematol Oncol Clin North Am,* 26**,** 629-48, ix.

VISNES, T., AKBARI, M., HAGEN, L., SLUPPHAUG, G. & KROKAN, H. E. 2008. The rate of base excision repair of uracil is controlled by the initiating glycosylase. *DNA Repair (Amst),* 7**,** 1869-81.

VOET, D. 1990. *Biochemistry*, John Wiley & Sons.

VON GUNTEN, S. & BOCHNER, B. S. 2008. Basic and clinical immunology of Siglecs. *Ann N Y Acad Sci,* 1143**,** 61-82.

WAINMAN, Y. A., NEVES, A. A., STAIRS, S., STOCKMANN, H., IRELAND-ZECCHINI, H., BRINDLE, K. M. & LEEPER, F. J. 2013. Dual-sugar imaging using isonitrile and azido-based click chemistries. *Org Biomol Chem,* 11**,** 7297-300.

WALLING, J. 2006. From methotrexate to pemetrexed and beyond. A review of the pharmacodynamic and clinical properties of antifolates. *Invest New Drugs,* 24**,** 37-77.

WANG, F. K., KOCH, J. & STOKSTAD, E. L. 1967. Folate coenzyme pattern, folate linked enzymes and methionine biosynthesis in rat liver mitochondria. *Biochem Z,* 346**,** 458-66.

WANG, R., DILLON, C. P., SHI, L. Z., MILASTA, S., CARTER, R., FINKELSTEIN, D., MCCORMICK, L. L., FITZGERALD, P., CHI, H., MUNGER, J. & GREEN, D. R. 2011a. The transcription factor Myc controls metabolic reprogramming upon T lymphocyte activation. *Immunity,* 35**,** 871-82.

WANG, R. & GREEN, D. R. 2012a. Metabolic checkpoints in activated T cells. *Nat Immunol,* 13**,** 907-15.

WANG, R. & GREEN, D. R. 2012b. Metabolic reprogramming and metabolic dependency in T cells. *Immunol Rev,* 249**,** 14-26.

WANG, W., HONG, S., TRAN, A., JIANG, H., TRIANO, R., LIU, Y., CHEN, X. & WU, P. 2011b. Sulfated ligands for the copper(I)-catalyzed azide-alkyne cycloaddition. *Chem Asian J,* 6**,** 2796-802.

WARD, E. S., ZHOU, J., GHETIE, V. & OBER, R. J. 2003. Evidence to support the cellular mechanism involved in serum IgG homeostasis in humans. *Int Immunol,* 15**,** 187-95.

WEINBLATT, M. E. & FRASER, P. 1989. Elevated mean corpuscular volume as a predictor of hematologic toxicity due to methotrexate therapy. *Arthritis Rheum,* 32**,** 1592-6.

WEINBLATT, M. E., TRENTHAM, D. E., FRASER, P. A., HOLDSWORTH, D. E., FALCHUK, K. R., WEISSMAN, B. N. & COBLYN, J. S. 1988. Long-term prospective trial of low-dose methotrexate in rheumatoid arthritis. *Arthritis Rheum,* 31**,** 167-75.

WESSELS, J. A., HUIZINGA, T. W. & GUCHELAAR, H. J. 2008. Recent insights in the pharmacological actions of methotrexate in the treatment of rheumatoid arthritis. *Rheumatology (Oxford),* 47**,** 249-55.

WHITE, J. C., LOFTFIELD, S. & GOLDMAN, I. D. 1975. The mechanism of action of methotrexate. III. Requirement of free intracellular methotrexate for maximal suppression of (14C)formate incorporation into nucleic acids and protein. *Mol Pharmacol,* 11**,** 287-97.

WHITE, S. J., UNDERHILL, G. H., KAPLAN, M. H. & KANSAS, G. S. 2001. Cutting edge: differential requirements for Stat4 in expression of glycosyltransferases responsible for selectin ligand formation in Th1 cells. *J Immunol,* 167**,** 628-31.

WHITFIELD, J. F., MACMANUS, J. P., BOYNTON, A. L., GILLAN, D. J. & ISAACS, R. J. 1974. Concanavalin A and the initiation of thymic lymphoblast DNA synthesis and proliferation by a calcium-dependent increase in cyclic GMP level. *J Cell Physiol,* 84**,** 445-58.

WHITTLE, S. L. & HUGHES, R. A. 2004. Folate supplementation and methotrexate treatment in rheumatoid arthritis: a review. *Rheumatology (Oxford),* 43**,** 267-71.

WIBOWO, A. S., SINGH, M., REEDER, K. M., CARTER, J. J., KOVACH, A. R., MENG, W., RATNAM, M., ZHANG, F. & DANN, C. E., 3RD 2013. Structures of human folate receptors reveal biological trafficking states and diversity in folate and antifolate recognition. *Proc Natl Acad Sci U S A,* 110**,** 15180-8.

WINTER-VANN, A. M., KAMEN, B. A., BERGO, M. O., YOUNG, S. G., MELNYK, S., JAMES, S. J. & CASEY, P. J. 2003. Targeting Ras signaling through inhibition of carboxyl methylation: an unexpected property of methotrexate. *Proc Natl Acad Sci U S A,* 100**,** 6529-34.

WU, M., GUNNING, W. & RATNAM, M. 1999. Expression of folate receptor type alpha in relation to cell type, malignancy, and differentiation in ovary, uterus, and cervix. *Cancer Epidemiol Biomarkers Prev,* 8**,** 775-82.

XIAO, H., WOODS, E. C., VUKOJICIC, P. & BERTOZZI, C. R. 2016. Precision glycocalyx editing as a strategy for cancer immunotherapy. *Proc Natl Acad Sci U S A,* 113**,** 10304-9.

YAMAGUCHI, T., HIROTA, K., NAGAHAMA, K., OHKAWA, K., TAKAHASHI, T., NOMURA, T. & SAKAGUCHI, S. 2007. Control of immune responses by antigen-specific regulatory T cells expressing the folate receptor. *Immunity,* 27**,** 145-59.

YANAGIMACHI, M., NARUTO, T., HARA, T., KIKUCHI, M., HARA, R., MIYAMAE, T., IMAGAWA, T., MORI, M., KANEKO, T., MORITA, S., GOTO, H. & YOKOTA, S. 2011. Influence of polymorphisms within the methotrexate pathway genes on the toxicity and efficacy of methotrexate in patients with juvenile idiopathic arthritis. *Br J Clin Pharmacol,* 71**,** 237-43.

YANG, Z., FUJII, H., MOHAN, S. V., GORONZY, J. J. & WEYAND, C. M. 2013. Phosphofructokinase deficiency impairs ATP generation, autophagy, and redox balance in rheumatoid arthritis T cells. *J Exp Med,* 210**,** 2119-34.

YOSHIDA, T. & KIKUCHI, G. 1970. Major pathways of glycine and serine catabolism in rat liver. *Arch Biochem Biophys,* 139**,** 380-92.

ZARO, B. W., BATEMAN, L. A. & PRATT, M. R. 2011. Robust in-gel fluorescence detection of mucin-type O-linked glycosylation. *Bioorg Med Chem Lett,* 21**,** 5062-6.

ZHANG, J. Q., NICOLL, G., JONES, C. & CROCKER, P. R. 2000. Siglec-9, a novel sialic acid binding member of the immunoglobulin superfamily expressed broadly on human blood leukocytes. *J Biol Chem,* 275**,** 22121-6.

ZHENG, J. & RAMIREZ, V. D. 2000. Inhibition of mitochondrial proton F0F1-ATPase/ATP synthase by polyphenolic phytochemicals. *Br J Pharmacol,* 130**,** 1115-23.

ZHENG, T., ROUHANIFARD, S. H., JALLOH, A. S. & WU, P. 2012. Click Triazoles for Bioconjugation. *Top Heterocycl Chem,* 28**,** 163-183.

ZHENG, Y., COLLINS, S. L., LUTZ, M. A., ALLEN, A. N., KOLE, T. P., ZAREK, P. E. & POWELL, J. D. 2007. A role for mammalian target of rapamycin in regulating T cell activation versus anergy. *J Immunol,* 178**,** 2163-70.

ZHU, J., YAMANE, H. & PAUL, W. E. 2010. Differentiation of effector CD4 T cell populations (*). *Annu Rev Immunol,* 28**,** 445-89.

ZHUO, Y. & BELLIS, S. L. 2011. Emerging role of alpha2,6-sialic acid as a negative regulator of galectin binding and function. *J Biol Chem,* 286**,** 5935-41.